Optimization of an innovative thermal energy storage technology at low temperatures when coupled to multi-source energy architectures

Letizia Roccamena

N°d'ordre NNT : 2017LYSET010

THESE de DOCTORAT DE L'UNIVERSITE DE LYON
opérée au sein de
l'Ecole Nationale des Travaux Publics de l'Etat

Ecole Doctorale N° accréditation
MEGA (Mécanique, Energétique, Génie Civil, Acoustique)

Spécialité / discipline de doctorat : Génie Civil

Soutenue publiquement le 15/12/2017, par :
Letizia Roccamena

Optimization of an innovative thermal energy storage technology at low temperatures when coupled to multi-source energy architectures

Devant le jury composé de :

Dumortier, Dominique	Professeur	ENTPE - LGCB	Président
Paksoy, Halime	Professeur	Cukurova University	Rapporteure
Perino, Marco	Professeur	Politecnico di Torino	Rapporteur
Draoui, Abdeslam	Professeur	FST de Tanger	Examinateur
Corgier, David	Ingénieur	MANASLU ING	Examinateur
Rosenstein, Frédéric	Ingénieur	ADEME	Examinateur
El Mankibi, Mohamed	Directeur de Recherche	ENTPE – LTDS	Directeur de thèse
Stathopoulos, Nikolaos	Docteur	Chalmers University of Technology	Co-encadrant

N°d'ordre NNT : 2017LYSET010

THESE de DOCTORAT DE L'UNIVERSITE DE LYON
opérée au sein de
l'Ecole Nationale des Travaux Publics de l'Etat

Ecole Doctorale N° accréditation
MEGA (Mécanique, Energétique, Génie Civil, Acoustique)

Spécialité / discipline de doctorat : Génie Civil

Soutenue publiquement le 15/12/2017, par :
Letizia Roccamena

Optimisation d'une technique avancée de stockage d'énergie thermique couplée à des architectures énergétiques multi-sources

Devant le jury composé de :

Dumortier, Dominique	Professeur	ENTPE - LGCB	Président
Paksoy, Halime	Professeur	Cukurova University	Rapporteure
Perino, Marco	Professeur	Politecnico di Torino	Rapporteur
Draoui, Abdeslam	Professeur	FST de Tanger	Examinateur
Corgier, David	Ingénieur	MANASLU ING	Examinateur
Rosenstein, Frédéric	Ingénieur	ADEME	Examinateur
El Mankibi, Mohamed	Directeur de Recherche	ENTPE – LTDS	Directeur de thèse
Stathopoulos, Nikolaos	Docteur	Chalmers University of Technology	Co-encadrant

Optimisation d'une technique avancée de stockage d'énergie thermique couplée à des architectures énergétiques multi-sources

1. Introduction

1.1 Problématique et contexte de la thèse

Le changement climatique dû à l'activité humaine, la raréfaction des ressources fossiles, les chocs pétroliers, l'augmentation de la population mondiale et urbaine sont les principales forces motrices derrière les efforts au niveau international, national et local pour une meilleure gestion de la production et de la consommation d'énergie. Ces efforts visent à la fois à la diminution des consommations d'énergie mais aussi à l'augmentation de l'utilisation des énergies renouvelables.

Le secteur du bâtiment peut largement contribuer à ces égards, étant donné qu'il il constitue à travers le monde l'un des principaux contributeurs en ce qui concerne la consommation d'énergie et les émissions de gaz à effet de serre. Une gestion efficace du bâtiment doit surmonter deux difficultés considérables : l'intermittence des énergies renouvelables et les variations quotidiennes ou saisonnières de la consommation d'énergie. Le stockage de l'énergie a été recherché et utilisé dans un grand nombre d'applications grâce aux avantages que cette technologie offre. En effet, le stockage d'énergie ne réduit pas seulement le déséquilibre entre l'offre et la demande, mais améliore également la performance des systèmes, contribue à la sécurité de l'approvisionnement en énergie, à l'élaboration des stratégies de contrôle avancées (associé à des smart grids) et l'augmentation de l'inertie. Toutefois, la mise à disposition de résultats expérimentaux et d'outils d'évaluation robustes pour cette technologie reste nécessaire pour disposer d'une analyse globale sur le plan environnemental.

Le but de ce projet est d'optimiser une technologie innovante de stockage d'énergie thermique basée sur un échangeur eau – matériaux à changement de phase (MCP). Ce système est couplé à l'architecture énergétique multi-sources d'un îlot composé de trois bâtiments à énergie positive situé à Lyon : l'îlot HIKARI.

1.2 L'îlot HIKARI

L'îlot HIKARI est le premier îlot à énergie positive (BEPOS) d'Europe. Situé dans le quartier Confluence de la ville de Lyon, il inclut trois bâtiments à usage multiples : bureaux, logement et commerce. La cible du bilan d'énergie positif est atteinte à l'aide de plusieurs systèmes de production et de stockage d'énergie innovants:

- Un système de stockage d'eau glacée qui utilise du matériel à changement de phase,
- Des panneaux photovoltaïques, en toiture et en façade
- Un système de domotique intégré aux logements,
- Un système de GTB appelé le BEMS pour Building Energy Management System,
- Un système de stockage d'énergie électrique à batterie Lithium,
- Des luminaires LED pour les surfaces de bureaux et les parties communs.

L'architecture énergétique du projet est présentée dans le schéma suivant :

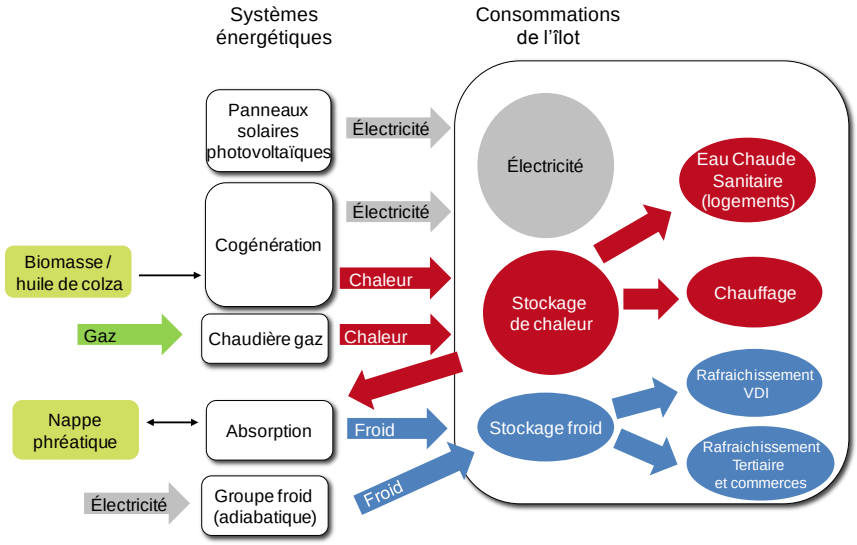

Figure 1- Architecture énergétique de l'Ilot HIKARI.

1.3 Le système de référence

L'îlot HIKARI bénéficie d'un système de stockage de froid sous forme de réservoirs remplis de matériaux à changement de phase fournis par JX Nippon Oil. Le MCP en question (ECOJOULE 108) est une paraffine avec une température de changement de phase de 8°C. Il est encapsulé dans des sachets plastiques et le modèle standard enferme une quantité de 100g de paraffine, avec une taille d'environ 274mm x 40mm (25 à 30 mm de diamètre) (figure 2).

Figure 2- Brique de MCP ECOJOULE 108.

Plusieurs briques de MCP sont ensuite introduites dans un boîtier en plastique (figure 3), à l'intérieur d'un réservoir d'eau. Les dimensions extérieures du panier sont 465 x 345 x 280mm (562mm en diagonale).

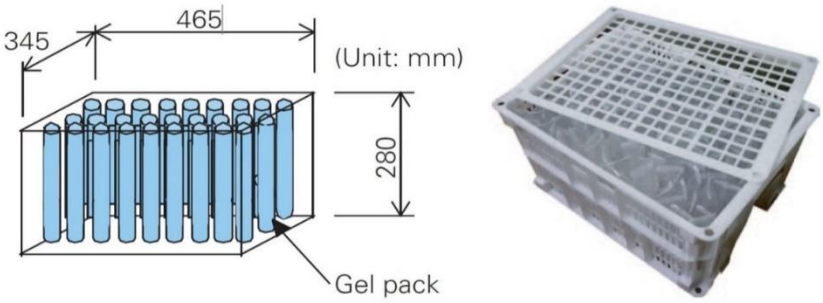

Figure 3 - Boîtier en plastique.

Enfin, plusieurs paniers peuvent être empilés en fonction des besoins de stockage du système étudié (figure 4).

Figure 4- Empilement des boîtiers de MCP

Le système de stockage d'énergie thermique à basse température de l'îlot HIKARI exploite la capacité des matériaux à changement de phase d'absorber et libérer une grande quantité d'énergie thermique pendant leur transition de phase et il est utilisé pour améliorer la performance du chiller à absorption de l'îlot HIKARI.

1.4 La démarche du travail de thèse

La technologie de ce système a été conçue expressément pour l'îlot HIKARI, donc un travail d'optimisation était nécessaire afin d'améliorer son rendement dans des futures applications. L'objectif du projet de ce travail de thèse est de développer une méthodologie et des outils numériques et expérimentaux pour la prise en compte et l'optimisation de cette technologie couplé avec des techniques de stockage énergétiques évoluées.

La démarche scientifique est basée sur une approche à la fois numérique et expérimentale. Un modèle numérique a été réalisé en utilisant l'environnement MATLAB Simulink et en suite il a été validé en trois étapes : dans un premier temps, par un modèle CFD (Computational Fluid Dynamics) conçu en utilisant le logiciel ANSYS Fluent (pour une validation numérique de la cohérence du modèle), dans un second temps les données expérimentales in-situ de l'ilot HIKARI ont été utilisées pour la validation du comportement in-situ. Finalement, un prototype expérimental dédié et représentatif du système du système de stockage, conçu et réalisé dans des conditions de laboratoire à l'ENTPE, a été utilisé pour une validation laboratoire.

Une fois validé, le modèle a ensuite été couplé au modèle des bâtiments de l'îlot HIKARI, afin d'optimiser le rendement énergétique de cette technologie en utilisant la technique des algorithmes génétiques.

2. Le développement du modèle numérique

2.1 L'approche numérique de modélisation

L'approche adopté pour la modélisation du comportement du matériau à changement de phase est basée sur la discrétisation du medium considéré en un nombre suffisant volume et à l'application de l'équation du bilan thermique pour chaque élément. Ceci est réalisé par une discrétisation nodale du volume considéré, en supposant que la valeur de température est la même pour le volume qui correspond à chaque nœud (figure 5). Nous nous retrouvons ici avec plusieurs couches étudiés (eau, plastique, MCP), différentes couches sont donc considérés afin de représenter les différentes échanges. Plusieurs flux de chaleur sont donc pris en compte, compris conduction, convection, et advection.

L'équation du bilan thermique est ainsi formulée pour chaque nœud et résolue à chaque pas de temps pour calculer l'évolution de la température au niveau des nœuds considérés.

En résumant cette approche, trois étapes principales peuvent être identifiées:

• discrétisation de la couche nodale considérée.

• formulation du bilan thermique pour chaque nœud tenant compte de tous les flux énergétiques présent.

• transformation des équations obtenues en équations matricielles et leur résolution à chaque pas de temps.

Dans le cas du projet HIKARI, nous avons décidé d'étudier l'élément principale de stockage de chaleur (brique de gel) et ensuite extrapoler son comportement pour reproduire le comportement du système complet. Deux couches ont été ainsi considérées: celle du fluide caloporteur (eau) et celle du matériau de stockage de chaleur (MCP) en négligeant la résistance thermique du plastique vu sa très faible épaisseur. La couche 'eau' est représentée par un nœud et la couche 'MCP' est discrétisée plusieurs nœuds. La discrétisation est faite en longueur et en épaisseur (axiale), comme représentée sur la figure 5. Les résistances thermiques ont été formulées entre les différents nœuds (figure 6), en aboutissant à l'écriture du bilan thermique pour chaque couche.

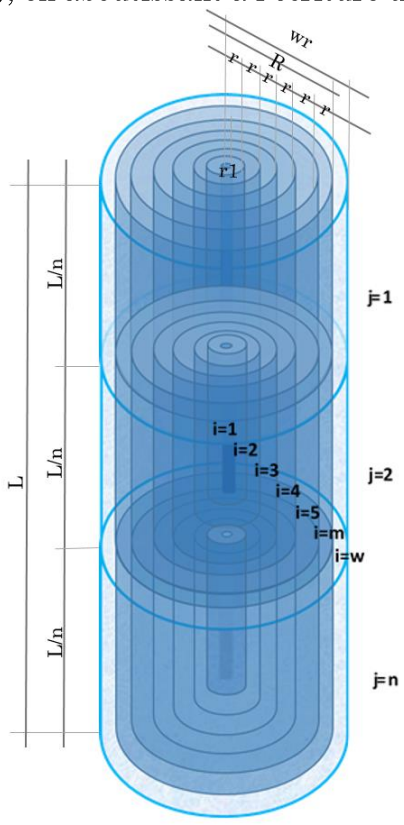

Figure 5 – Discrétisation en longueur et en épaisseur du composant MCP

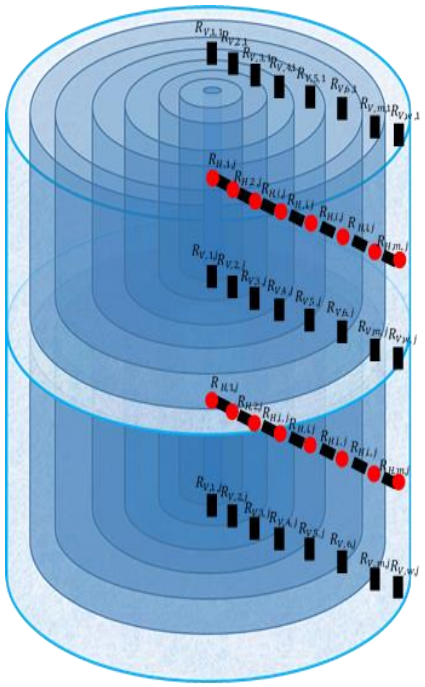

Figure 6 – Formulation des résistances thermiques entre les nœuds considérés

L'aboutissement de ce travail a permis de disposer d'un outil numérique qui reproduit le comportement du système de stockage de froid en réduisant considérablement le temps de calcul. Le modèle développé offre également la possibilité de modifier plusieurs paramètres du dispositif étudié (propriétés du MCP, géométrie du module, etc.), ce qui est nécessaire pour la suite du projet et notamment le travail d'optimisation du système.

Pour prendre en compte le changement de phase dans la simulation, la méthode de la capacité apparente a été choisi. Cette méthode consiste en la représentation du changement de phase du moyen de stockage de chaleur (la paraffine ici) par une augmentation apparente des valeurs de sa capacité thermique pour des certaines variations de température, en correspondance avec l'absorption et la sortie de la chaleur latente.

Afin de réaliser le modèle avec la méthode de la capacité thermique apparente décrit ci-dessus, notre choix s'est porté sur l'environnement Matlab/Simulink.

2.2 Les résultats

En résolvant les équations présentées dans la section précédente sous l'environnement MATLAB Simulink, on a obtenu un outil numérique capable de reproduire le comportement du système de stockage de froid de l'îlot HIKARI alliant précision et rapidité.

Une fois le modèle réalisé, on a simulé des exchanges thermiques entre le stick de MCP et les flux d'eau en considérant différentes discrétisations spatiales (nombre de couches horizontales et verticales dans lequel couper le modèle pour étudier les équations du bilan énergétique) afin de analyser la robustesse et la cohérence du modèle.

Des exemples de valeurs de température dans le même nœud qui se trouve dans la dernière couche d'eau (i = w, j = n) en utilisant différentes discrétisations sont montrés dans les figures 7 et 8 :

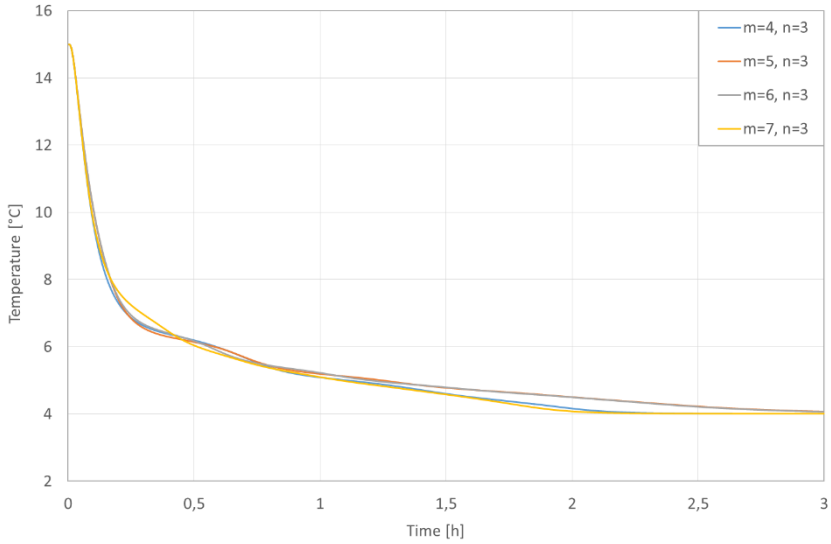

Figure 7 - Valeurs de la température en fonction du temps du nœud (i = w, j = n) en modifiant le nombre de couches horizontales.

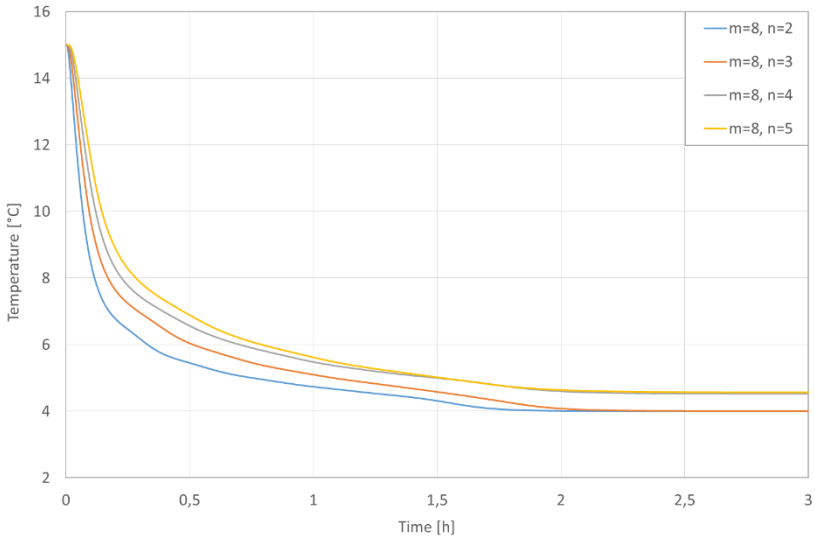

Figure 8 - Valeurs de la température en fonction du temps du nœud (i = w, j = n) en modifiant le nombre de couches verticales.

Le décalage temporel entre les changements de température dans la figure 9 est dû aussi à la différence de position de chaque nœud à niveau de la longueur du stick ; si, par exemple, le centre du nœud n = 5 se trouve à une distance de 2,5 cm dès l'extrémité inferieure du stick de gel, le centre du nœud n = 2 sera à une distance de 6,25 cm. Il sera donc normal que l'échange thermique atteindra avant pour ce deuxième point, vue la direction du flux d'eau.

3. La calibration numérique

3.1 La simulation CFD

La CFD (Computational Fluid Dynamics), est un outil numérique de modélisation dédiée à la mécanique des fluides (liquides, gaz), des propriétés de ces écoulements (température, vitesse, ...) et des interactions avec leur environnement (échange thermiques, réactions chimiques, forces aérodynamiques, aéroacoustique).

L'approche CFD est caractérisée par la génération, sur l'ensemble du domaine fluide étudié, d'un maillage dont chaque volume de contrôle est utilisé pour résoudre les équations de conservation (équations de Navier–Stokes) et modéliser la turbulence.

Un calcul de mécanique des fluides, ou plus précisément un calcul de dynamique des fluides, se divise en trois étapes:

1) Pre–processing	- Construire la géométrie 3D - Générer le maillage de calcul
2) Calcul	- Prescrire les conditions aux parois (températures, débits d'air, …) - Tester et optimiser la convergence des calculs - Calculer
3) Post–processing	- Sortir les tableaux de résultats - Visualiser et analyser les résultats

On utilisera les résultats obtenus avec cet outil pour valider le modèle réalisé avec l'approche du bilan thermique.

3.2 La comparaison des résultats

Le modèle réalisé sous ANSYS Fluent présente les mêmes caractéristiques géométrique que celles utilisées pour le modèle MATLAB Simulink : un cylindre à base circulaire contourné par un cylindre d'eau. On a aussi ajouté, comme dans le vrai système, 30 centimètres d'eau avant et après le cylindre de MCP.

On a considéré que ça serait utile de trouver ainsi les vraies valeurs de température de l'eau à l'entrée du système, qui seront surement différents de la température fixe qu'on a considéré jusqu'à ce moment comme valeur d'entrée (2°C).

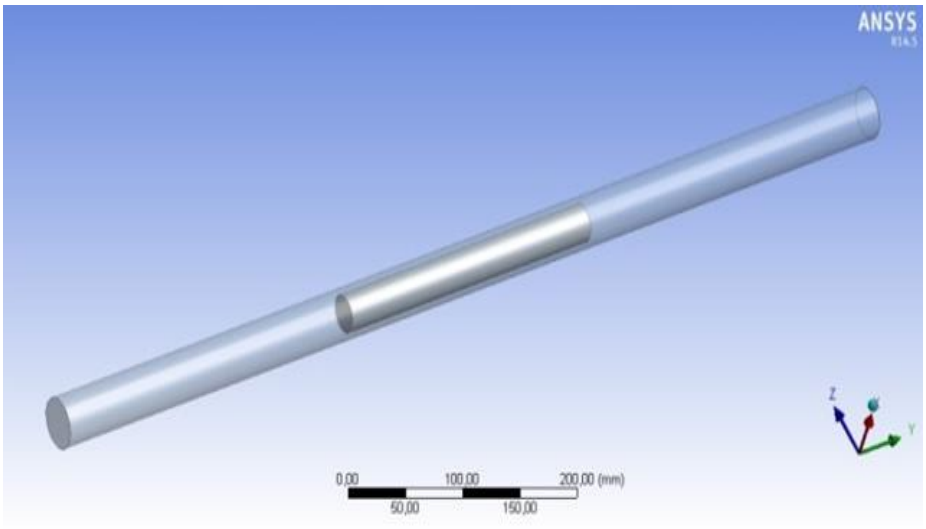

Figure 9 – Modèle CFD cylindrique du stick de MCP contourné par l'eau réalisé par ANSYS Fluent.

Pour avoir des résultats compatibles à niveau du comportement du MCP, on a inséré sur ANSYS Fluent les mêmes valeurs de C_p qu'on a utilisé pour le modèle de MATLAB Simulink. Au même temps, pour avoir les mêmes données d'entrée sur MATLAB, on a substitué la valeur fixe de la température T_{inlet} (température de l'eau qui entre dans le système), avec la courbe des valeurs de température de l'eau à l'entrée, obtenue avec ANSYS Fluent. De cette manière on peut tenir en compte les 30 cm d'eau qu'il y a à l'entrée du système.

On a inséré les mêmes données utilisés pour le modèle MATLAB (propriétés des matériaux, propriétés géométriques, pas de temps, températures, etc…) et on a essayé de comparer les résultats obtenus avec les deux logiciels en insèrent dans le système 3 différents débits d'entrée de l'eau (0.00015 kg/s, 0.0003 kg/s and 0.00045 kg/s).

Un exemple de comparaison obtenue en analysant le point montré dans les figures 10 et 11 en utilisant le débit de 0.0003 kg/s est montré dans les Figures 12 (charge) et 13 (décharge):

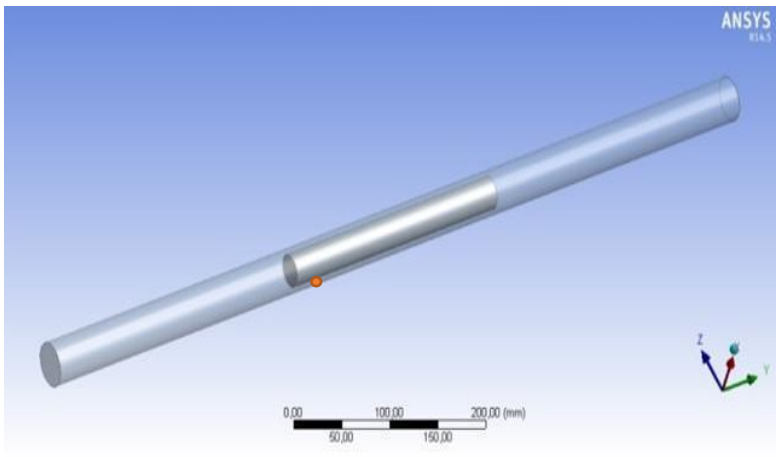

Figure 7 – Position du point i = 8, j = 2 dans le modèle ANSYS Fluent.

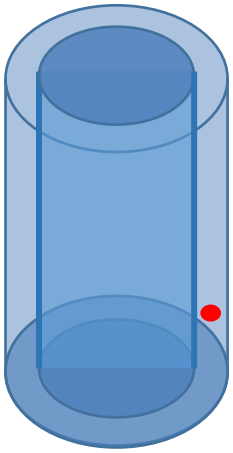

Figure 11 - Position du point analysé dans le cylindre d'eau du modèle.

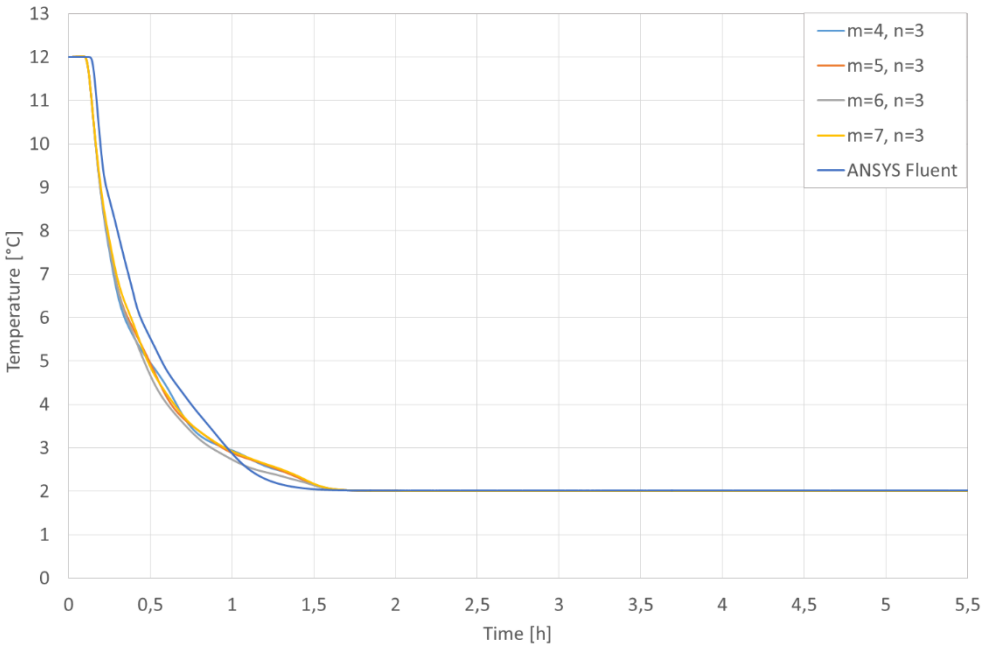

Figure 12 - Valeurs de la température en fonction du temps pour le nœud (i = w, j = n) et pour son équivalent dans le modèle ANSYS Fluent pendant la phase de charge du système.

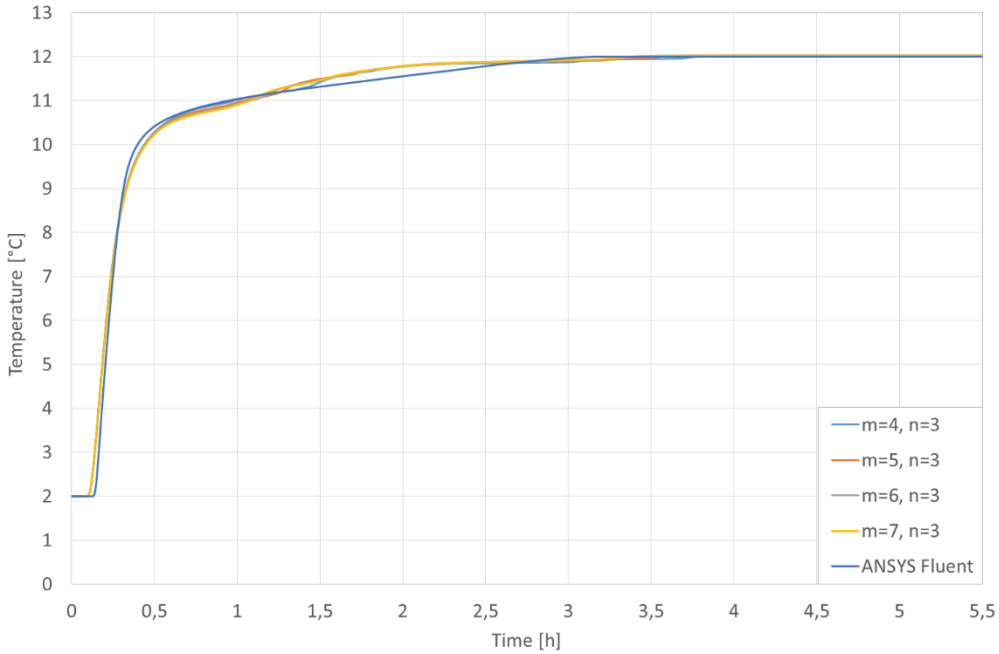

Figure 13 – Valeurs de la température en fonction du temps pour le nœud (i = w, j = n) et pour son équivalent dans le modèle ANSYS Fluent pendant la phase de décharge du système.

Pour tester la précision du MATLAB Model par rapport aux résultats obtenus avec le modèle ANSYS Fluent, deux critères ont été utilisés :

- La Normalized Mean Bias Error (NMBE)

$$\boldsymbol{NMBE} = \frac{\sum_{i=1}^{n}\left(\boldsymbol{y_{simulated,i}} - \boldsymbol{y_{measured,i}}\right)}{\boldsymbol{\bar{y}_{measured}} \times (\boldsymbol{n} - \boldsymbol{p})} \times 100$$

- Le Coefficient of Variation of the Root Mean Squared Error (CV(RMSE))

$$\boldsymbol{CV(RMSE)} = \frac{1}{\boldsymbol{\bar{y}_{measured}}} \times \sqrt{\frac{\sum_{i=1}^{n}\left(\boldsymbol{y_{simulated,i}} - \boldsymbol{y_{measured,i}}\right)^2}{(\boldsymbol{n} - \boldsymbol{p} - 1)}} \times 100$$

Selon la guide ASHRAE, un modèle peut être considéré calibré s'il produit une valeur de NMBE compris entre ± 10% et de CV(RMSE) compris entre ± 30%.

Les résultats obtenus ont montré que le modèle MATLAB Simulink avec le comportement le plus proche au modèle ANSYS c'est celui-là avec une discrétisation axiale de 8 cylindres concentriques (7 cylindres de MCP et 1 d'eau extérieur) et une discrétisation verticale de 3 nœuds (m = 8, n = 3).

4. La comparaison avec les données in situ

Une première calibration expérimentale a été réalisée entre les données obtenues avec le modèle MATLAB Simulink et les données expérimentales in situ enregistrées dans l'îlot HIKARI.

Grace au monitoring prévu dans le cadre du projet, il est possible de disposer de données expérimentales riches en informations sur les performances en exploitation de ces procédés de stockage pour valider une méthodologie adaptée de modélisation de ce type de composant.

Les données ont été enregistrées pendant une durée de 25 jours et elles représentent la variation de température dans le temps pour 14 points dans chaque bac. Chaque point représente le bord supérieur et/ou inferieur de chaque panier empilé dans une file.

La donnée expérimentale qui on a utilisée pour la comparaison avec les données numériques est la moyenne (appelée "in situ" dans la figure 15) des valeurs de température des bords inferieurs des paniers les plus bas de la file centrale et la file la plus proche au bord gauche de chaque bac (voir Figure 14).

Pour obtenir les températures correspondantes aux points choisis, on a du "recréer" l'empilement des paniers dans notre modèle. Pour avoir ça on a connecté le modèle de plusieurs sticks entre eux en utilisant l'output de chaque un comme input pour le suivant. Dans cette manière on a pu modéliser l'exchange thermique entre les différents paniers empilés l'un sur l'autre.

Les résultats sont montrés dans la figure 15 :

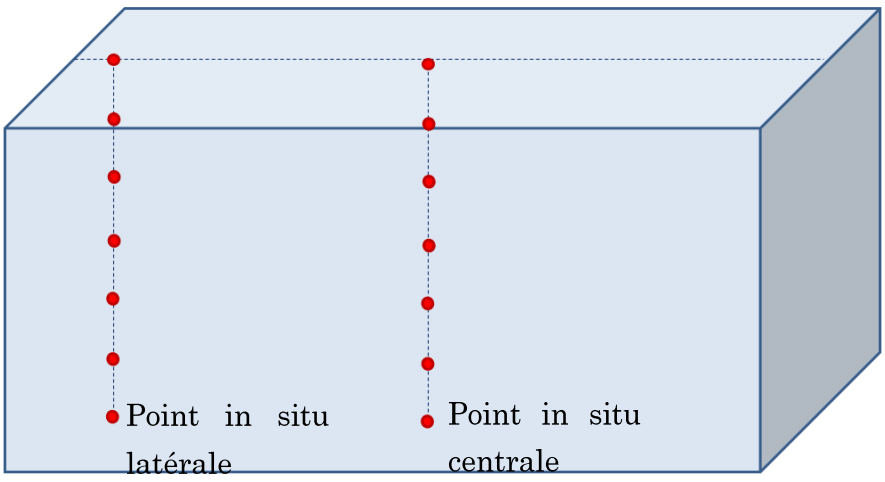

Figure 14 – Position des points analysés dans chaque bac, dont la moyenne représente la valeur "in situ" (Figure 15).

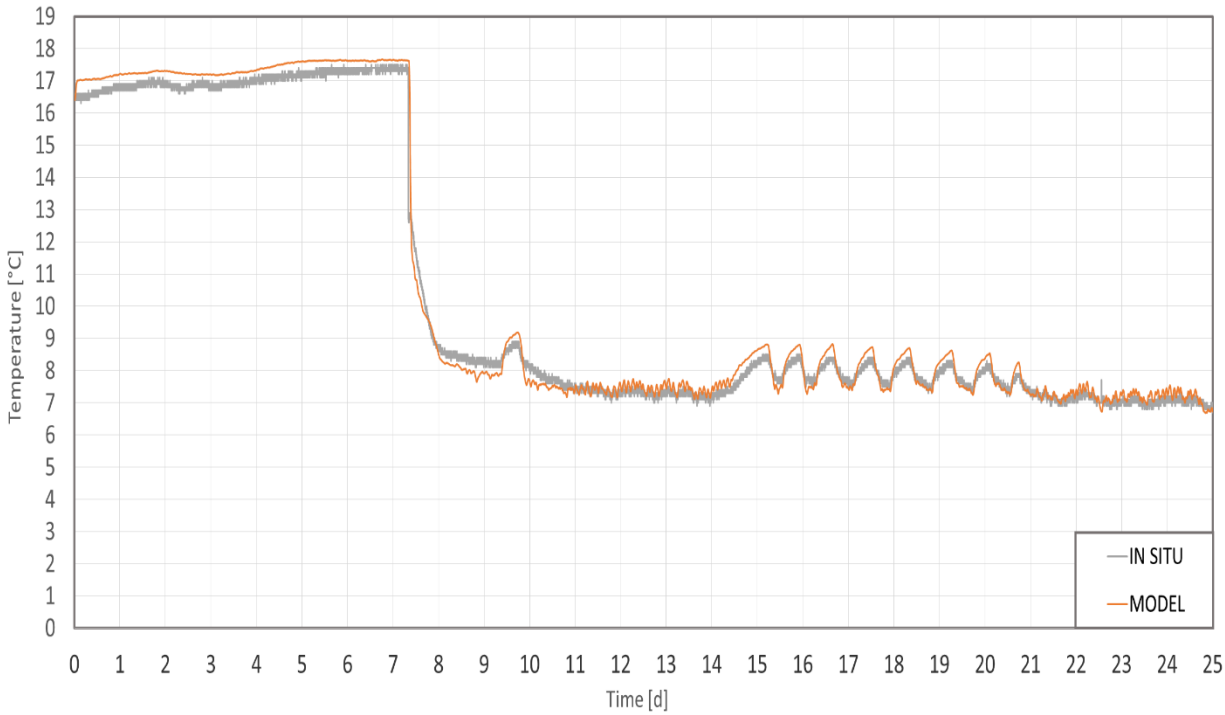

Figure 15 – Moyenne des valeurs de température reportées pour les points montrés dans la figure 15 et valeurs de la température en fonction du temps obtenues avec le modèle MATLAB Simulink.

En utilisant le même critère montré dans le chapitre précèdent, on a calculé les valeurs du NMBE et du CV(RMSE) entre les données in situ et les résultats obtenu en utilisant notre modèle en obtenant des valeurs très favorables :

- Normalized Mean Bias Error : 1,86%
- Coefficient of Variance of Root Mean Square Error: 4,02%

5. La calibration expérimentale

5.1 La conception du prototype expérimental

Malgré les bons résultats obtenus en comparant les données in situ et les résultats obtenus en utilisant notre modèle, ce n'était pas possible de considérer cette comparaison comme une validation expérimentale complète. En fait, il était impossible de modifier le scenario opérationnel du système de référence en changeant des paramètres comme le débit d'eau d'entrée ou la quantité de MCP. Un prototype expérimental du système de stockage de froid de l'îlot HIKARI a été fabriqué dans les locaux d l'ENTPE afin d'obtenir des données expérimentales fiables ; ces données ont été utilisées pour la deuxième étape de validation du modèle numérique.

Pour obtenir des résultats comparables avec ceux de l'ilot HIKARI, on a considéré un bac qui contient un panier remplis de sticks MCP identiques à ceux qu'il y a dans le système

de référence. L'eau (froide ou chaude, en fonction de la phase qu'on veut étudier) passe par le panier en sortant par un robinet installé au-dessus du bac.

Un deuxième bac est connecté avec un refroidisseur afin de pouvoir faire refroidir l'eau qu'il contient jusqu'à la température désirée et de l'envoyer après vers l'autre bac, où il y a le panier remplis de MCP. Le schéma de prototype est reporté dans la Figure 16:

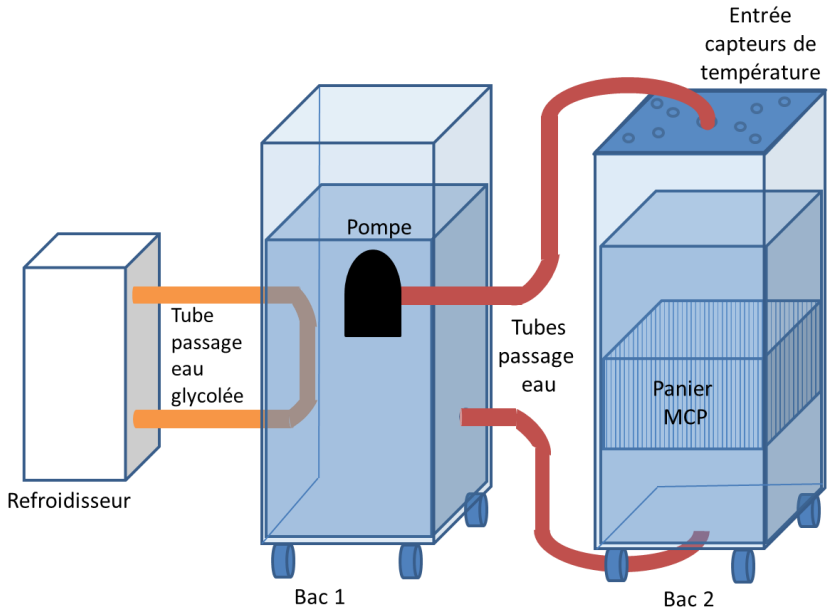

Figure 16: Schéma du prototype expérimental.

L'eau glycolée refroidit l'eau du premier bac en circulant dans un tube qui traverse le bac, en forme de serpentine. Le premier bac servira comme " zone tampon ", parce que, à travers sa connexion avec refroidisseur, sera possible de chauffer ou refroidir l'eau qu'il contient jusqu'à la température souhaité. Pour contrôler que l'eau contenue dans le bac soit à la température souhaitée, on insérera des capteurs de température Pt100 (Figure 17) à différents hauteurs.

Figure 17 – Les capteurs de température Pt100.

Une fois que la température du bac 1 arrivera à la valeur établie, on pourra faire passer l'eau du premier bac vers le deuxième bac (à travers un robinet présent en haute du bac 2), en démarrant la pompe présente dans le premier bac (Figure 18).

Avec cette opération on peut obtenir un exchange thermique entre le flux d'eau et le matériel à changement de phase présent dans le bac 2, qui on peut étudier en utilisant des capteurs de température présents dans plusieurs points d'intérêts, correspondants à ceux des nœuds du modèle de MATLAB Simulink, pour faire la première comparaison (Figures 18 et 19).

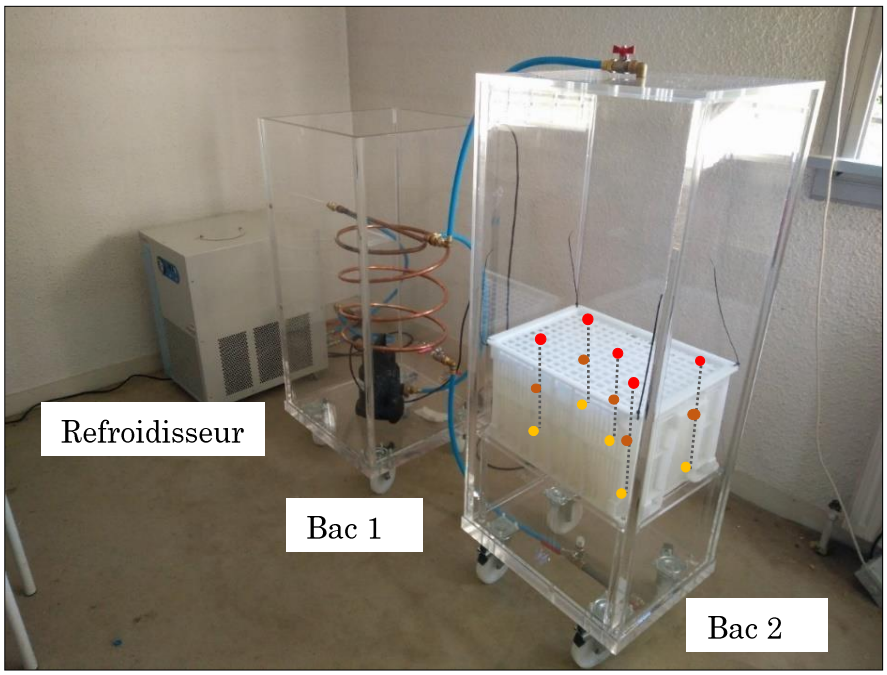

Figure 18 – Le bac 1 et le bac 2 avec les positions des capteurs de température.

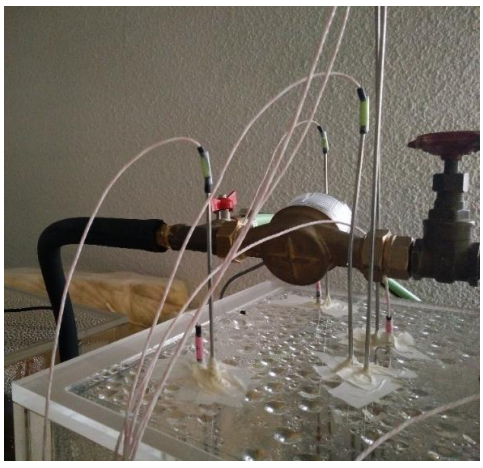

Figure 19 – Les capteurs de température insérés dans le bac 2.

Pour étudier l'exchange vertical entre deux sticks on a pensé d'ajouter un panier dans le bac 2 juste au-dessus du panier déjà présent, comme on peut voir dans la Figure 20.

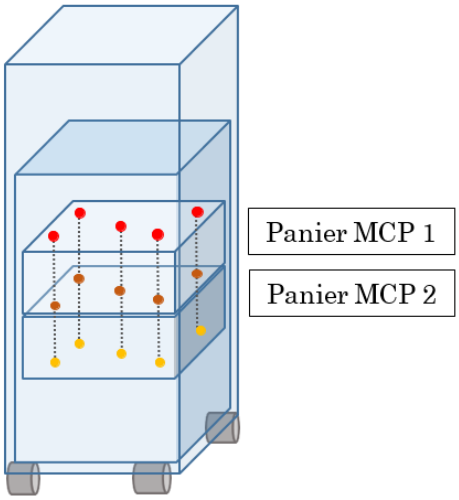

Figure 20– Schéma du bac 2 avec les deux paniers empilés et la position des capteurs de température.

5.2 Le protocole de simulation

Une fois le prototype construit, on a établi un protocole d'expérimentation pour analyser si le comportement de notre modèle coïncide avec celui du prototype, même en changeant le débit de l'eau en entrée et ensuite en ajoutant un stick au-dessus du stick modélisé.

Le débit sera changé en réglant le robinet présent en haut du bac 2, qui est directement connecté à la pompe présente dans le bac 1. Pour pouvoir effectuer cette analyse on a établis un protocole expérimentale composé de 6 scenarios basés sur la répétition de 4 actions avec 3 différents débits et un nombre diffèrent de paniers de MCP (1 ou 2).

5.3 La comparaison des résultats

Les résultats obtenus avec cette comparaison, en utilisant les critères montrés dans le paragraphe 3.2 (NMBE et CV(RMSE)) montrent que le comportement du modèle MATLAB Simulink est très proche à celui du prototype expérimental dans tous les 6 scenarios du protocole.

Dans les prochains graphiques on peut trouver deux exemples de comparaisons entre les données expérimentales obtenues en faisant la moyenne des valeurs registrés par les capteurs installés au-dessous des paniers de MCP et les résultats numériques du modèle MATLAB Simulink pour le nœud (i = w, j = n).

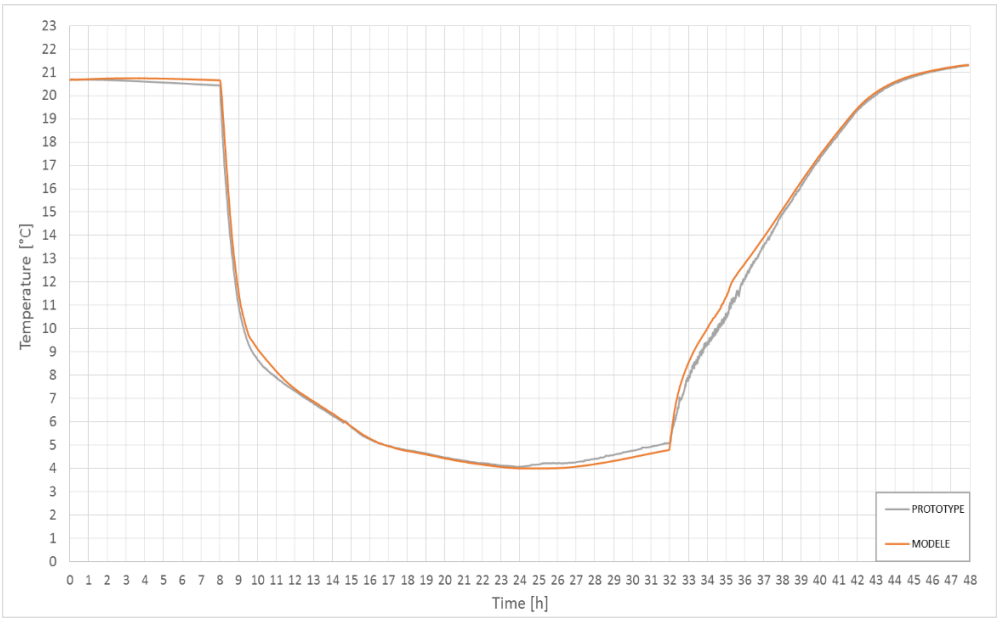

Figure 21– Valeurs de la température en fonction du temps pour le nœud (i = w, j = n) et pour son équivalent dans le prototype expérimentale en utilisant un seul panier de MCP avec un débit d'entrée d'eau de 3l/m.

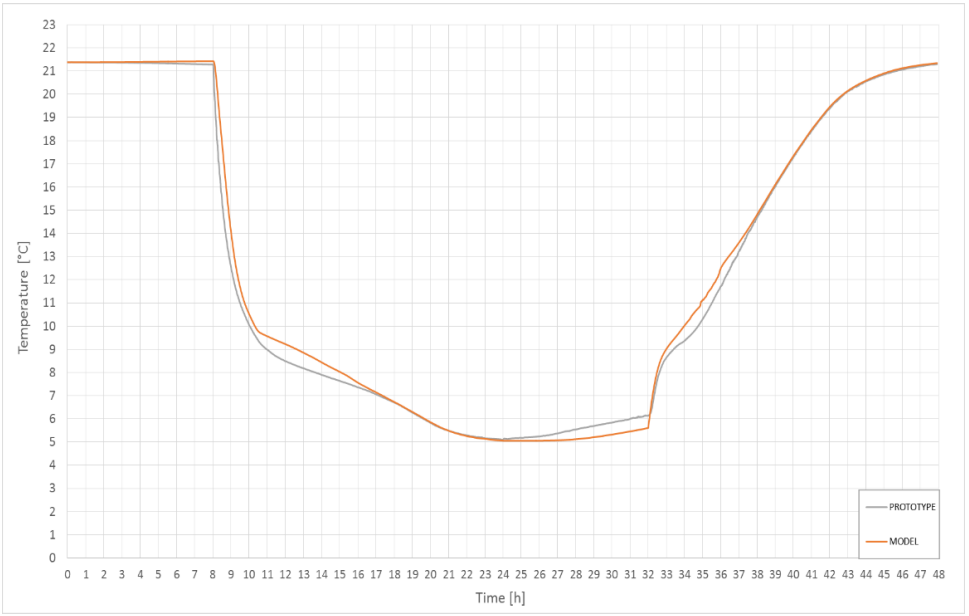

Figure 22– Valeurs de la température en fonction du temps pour le nœud (i = w, j = n) et pour son équivalent dans le prototype expérimentale en utilisant deux paniers de MCP avec un débit d'entrée d'eau de 3l/m.

6. Optimisation

Une fois validé, le modèle du système de stockage a été couplé au modèle MATLAB Simulink des autres systèmes de l'îlot HIKARI (réalisé par le partenaire du projet, MANASLU), afin de pouvoir optimiser le système quand il est couplé à des autres architectures énergétiques en utilisant la technique des algorithmes génétiques.

Cette technique, inspirée de la génétique, part d'un ensemble de solutions possibles initialisé aléatoirement. Les individus sont représentés par leurs variables de conception et certaines solutions de la première population sont utilisées pour former, à partir d'opérateurs génétiques (croisement, mutation, etc.), une nouvelle population en faisant en sorte que la nouvelle population soit meilleure que la précédente. Les solutions qui serviront à former de nouvelles solutions sont sélectionnées aléatoirement d'après leur mérite (représenté par une ou plus " fonction objectif" qui devraient être minimisées ou maximisées) jusqu'à ce qu'un critère de convergence soit satisfait (typiquement un nombre de générations fixé ou une valeur cible atteinte par la fonction objectif).

Dans notre cas, trois " fonctions objectifs " ont été choisi, afin d'être minimisés en modifiant des variables du système de référence :

- OBJ 1 : La somme des différences entre la température d'entrée de l'eau froide et de l'eau chaude du chiller à absorption pour chaque pas de temps (°C)
- OBJ 2: Les besoins énergétiques du bâtiment (kWh)
- OBJ 3 : Le nombre de cour cycles du Groupe Frigorifique auxiliaire (-)

Les variables à modifier étaient :

- Le diamètre des sticks de MCP (m) [0,013 ; 0.015] ;
- La longueur des sticks de MCP (m) [0.2 ; 0.3]
- Le point de fusion du MCP (°C) [8 ; 12]
- Le point de congélation du PCM (°C) [9 ; 13]

En raison du manque des lignes guide sur le choix exacte d'individus à définir pour chaque population et du nombre de générations à créer, on a effectué plusieurs tentatives, jusqu'à quand on a trouvé de valeurs capables de nous fournir de résultats rapides et fiables.

Les meilleures valeurs attribuables aux caractéristiques du système de stockage thermique à basse température de l'îlot HIKARI sont:

- Le diamètre des sticks de MCP : 0.014m
- La longueur des sticks de MCP : 0.2 m
- Le point de fusion du MCP : 8°C
- Le point de congélation du PCM : 13°C

7. Conclusions

Le travail réalisé a donné des résultats encourageants : un modèle numérique qui reproduise le fonctionnement d'un échangeur eau/MCP a été développé et il pourra être utilisé pour l'optimisation de la technique de stockage thermique où il est utilisé.

Les comparaisons avec les données numériques et expérimentales montrent, en fait, que l'approche adoptée pour la conception du modèle donne des résultats qui se rapprochent visiblement au vrai comportement du système. Il peut donc être utilisé pour la résolution de problèmes d'optimisation multicritère comme celui montré dans ce travail de thèse.

L'analyse des résultats de ces simulations a notamment abouti sur des recommandations de dimensionnement et d'usage pour l'Ilot HIKARI et des bâtiments futurs intégrant la technologie de stockage étudiée. Cependant, vu la versatilité du modèle et du prototype expérimentale réalisé dans le cadre de ce travail, il sera possible de les réutiliser pour l'analyse d'autre technologies de stockage thermique dans le future.

ABSTRACT

One of the most promising technics used in building applications for energy efficiency purposes is the thermal energy storage (TES). It consists of stocking thermal energy by heating a material capable to release, when cooled, the thermal energy stored at a later time. Despite the thorough research on TES techniques of the last years, the release to market of cost effective technologies is quite recent. For this reason it appears necessary, nowadays, to develop accurate and fast numerical tools for the optimization of this technic.

The aim of this study is to optimize the energetic behavior of an innovative TES technology consisting on a water/PCM exchanger that is part of the multi-energy production and storage systems of HIKARI, a positive energy district located in Lyon and consisting of three buildings combining commercial, residential and office usage. The HIKARI's low temperature heat storage system exploits the PCM ability to absorb and release a large amount of thermal energy during its phase transition and it is used for improving the performance of the HIKARI's absorption chiller.

In order to optimize this innovative technic, a numerical model reproducing the functioning of the reference system was created using the software MATLAB Simulink.

As the HIKARI's reference thermal storage system was still inoperative when the model was developed, it was impossible to make an experimental validation. For this reason a second numerical model was developed using a different software (ANSYS Fluent) that is based on a different numerical method, in order to make a numerical validation.

Once the in situ data obtained from the reference system monitoring, a first experimental validation was obtained by comparing these results with the results obtained from the MATLAB Simulink numerical model. However, it was considered impossible to obtain a complete experimental validation only considering the data obtained from the in situ monitoring, because it could only provide data registered during its working cycles (that always occur with fixed water flow rate, PCM quantity and temperature range).

For this reason, the design and implementation of an innovative experimental prototype reproducing the behavior of the reference PCM-Water heat exchanger has been considered necessary, because it gave us the opportunity to validate and calibrate the numerical model and carry out a large amount of operating scenarios.

Once the model numerically and experimentally validated, the optimization of the HIKARI's cold storage system technology has been obtained using Genetic Algorithms (GAs). After several attempts, due to lack of guidelines about the correct and optimal adaptation of the Genetic Algorithms, we have been able to find the best values to allocate to four characteristics of the cold storage system, in order to minimize two predefined objective functions linked to its functioning.

This study showed that it is possible to solve a Multi-Objective optimization problem using the Genetic Algorithms applied to a low temperature heat storage integrated to a complex multi energy system.

The results obtained through the numerical and experimental validations showed that our choices and assumption, adopted during the conception phase of the numerical model, provided valid results.

Due to its versatility, the model will be able to be used in the future in order to test other scenarios or other types of Phase Change Materials, same as the experimental prototype developed for its validation.

This work was supported by the French Agency for Environment and Energy Management (ADEME) and it was part of the project "Optimisation of innovative energy storage technologies when coupled to multi-sources energy architectures" based on the monitoring and optimization study of the positive energy district HIKARI.

ACKNOWLEDGEMENTS

First, I want to thank Mohamed El Mankibi for his continuous support, endless patience, motivation, and immense knowledge. He believed in me even when I did not believe in myself. I could not have imagined having a better director for my PhD study.

Thanks to Nikolaos Stathopoulos for his great help, his numerous corrections and advice on all the aspects of this work. Thanks a lot to Florian Simon for being a very helpful and accessible person during these 3 years. Special thanks to Nadia Bekkouche and Stéphane Cointet for their great help and advice on all aspects of the experimental part of the study.

I am also grateful to Professors Halime Paksoy and Marco Perino for accepting to review this work and participate in the defense jury. My sincere gratitude also goes to David Corgier, Frédéric Rosenstein and Professors Draoui and Dumortier for their willingness to participate in the jury.

Thanks are also due to all members of the LTDS and LGCB laboratories for their support and all the joyous moments I spent around them.

Special thanks to Jean-Félix for the love and support he gave me during the last two years, and to his grandparents Arlette and Félix for caring for me like a family.

I want to express my sincere gratitude to my mother, father and brother for their faith in me and for their huge support throughout my life. They always respected and encouraged my dreams and never made me feel alone.

Lastly, I would like to thank my grandmother Maria, for being the most independent, strong and inspiring woman I had the privilege to know.

I acknowledge the financial support from the French Agency for Environment and Energy Management (ADEME) and the fruitful collaboration with the members of the HIKARI project.

CONTENTS

LIST OF FIGURES

LIST OF TABLES

CHAPTER 1

GENERAL INTRODUCTION

1) GENERAL INTRODUCTION

1.1 GLOBAL CONTEXT OF THE WORK: NZEBS AS PART OF THE SOLUTION

Paris Agreement, signed in November 2016, represents an important milestone in the global effort to resolve the climate change problem. In fact, in order to reach the ambitious goal to limit the global temperature increase, appropriate financial flows and new energy-effective technologies must be put in place (IEA, 2016).

In this context, the building sector plays a key role, as it is one of the major contributors worldwide concerning energy consumption and greenhouse gas emissions (Ghorbani et al., 2017) (Turner et al., 2017). It has been estimated, in fact, that 40% of the global energy consumption is used in the building sector of developed countries to provide heating, ventilating and air conditioning (HVAC) and domestic hot water. In addition, global warming associated with this energy consumption is one of the most worrying problems facing the world today (IEA, 2014).

We can define this datum as no more sustainable, neither from the economic stand-point nor from the environmental one (Cao et al., 2016) (Nchelatebe Nkwetta and Haghighat, 2014), especially because it could be possible to obviate this situation thanks to the correct use of the technology available today (Hachem-Vermette et al., 2016) (Ferreira and Almeida, 2015).

Consequently, great importance is given to the targets of the EU Energy Performance of Buildings Directive (EPBD) and to the thermal regulations in most of concerned countries. In the Directive, a Zero Energy Building was defined as a building using 0 kWh/(m².year)of non-renewable energy. Following the good-sense and understanding that zero energy buildings are not cost efficient yet, the concept of Nearly-Zero Energy Building (NZEB) was defined as "technically and reasonably achievable". In fact, these buildings need more than 0 kWh/(m².year) but less than the national limit value of non-renewable primary energy, using a combination of the best practice energy efficiency measures and renewable energy technologies.

Indeed, the proper design and operation of buildings, buildings energy systems and districts have been clearly identified as key elements to decrease energy consumption and facilitate integration of renewable energy systems. Hence, the aim of the European Thermal regulations and the recommendations of political and environmental decision makers are to produce NZEBs by 2020 for all new construction. At a larger scale, Nearly-Zero Energy Districts (NZEDs) such as university campuses, office parks and rural communities, can also be created through the synergistic integration of several buildings, especially those with complementary usage patterns, and distribute electricity generators using a smart micro-grid. Renewable Energy supported Smart Micro-Grids (RESMGs)

can enable NZEDs by allowing the synergistic integration of hybrid renewable energy electric generation technologies too large for a single building, such as combinations of PV farms, wind turbines, and bio-fuelled electric generators. The same fundamental design and control strategies used for NZEBs are appropriate for buildings integrated into a larger NZED except building level electricity generation and energy storage technologies that may in part be replaced by district level generation technologies and complementary electricity usage through a smart micro-grid. Regarding the thermal energy demand and generation, analogous considerations can be applied.

1.2 ENERGETIC AND ECOLOGICAL CONTEXT IN FRANCE: TOWARD A NEW PARADIGM

Until 1973, oil constituted the main means of energy production in France, in order to support the industrial development and the declining use of coal. Between that year and the late '80s, the oil price chocks led to a better control of energy consumption and oriented its production to other sources. First the nuclear sector became the dominant producer – it is still so nowadays. An increase of renewable sources production could be observed after the '90s, mostly from hydraulic energy but also from photovoltaic and wind energy (INSEE, 2012).

The Kyoto Protocol was implemented through the 'Climate Plan 2004-2012' (Ministère de la Transition écologique et solidaire, 2006) aiming at a 10% reduction of CO_2 emission as well as aiming to raise awareness within society and among public and private actors etc. It was reinforced by the commitments established by the First and Second Grenelle Acts (Ministère de la Transition écologique et solidaire, 2009, 2012), whose main commitments include the generalization of standards of low consumption in new housing and public buildings, the renovation of housing and building heating, transportation measures favoring low polluting means, the development of renewable energy, as well as other actions in the health, agricultural and biodiversity domains.

In August 2015, the French Law on Energy Transition for Green Growth (Loi Transition Energétique relative à la Croissance Verte - LTECV) was published. This new low required all economic agents to position themselves with regard to taking environmental, social and governance criteria into consideration in a 'climate' approach in their core businesses. The LTECV implementation decree, published on 29 December 2015, echoes the Paris climate agreement, that sets out a global action plan to put the world on track to avoid dangerous climate change by limiting global warming to well below 2 °C.

France has given itself legislative tools to combat climate change more effectively and strengthen its energy independence by a better balance in its sources of energy supply. This legislation aims to reduce greenhouse gas emissions by 40% in 2030 relative to 1990,

raise the share of renewable energies in end-user energy consumption to more than 30% by 2030 and reduce the share of nuclear energy to 50% of electricity production by 2025 (Ministère de la Transition écologique et solidaire, 2015).

The document "Contribution à l'élaboration de Visions énergétiques 2030-2050 (2013)", wrote by the French Agency for Environment and Energy Management (ADEME), helped in laying the foundations for the achieving of LTECV objectives. In this document some predictions are made about the France's future energy needs on the basis of economic, social and demographic possible changes. As shown in figure 1.1, according to their predictions, the energy used in buildings should almost halve in the next 35 years.

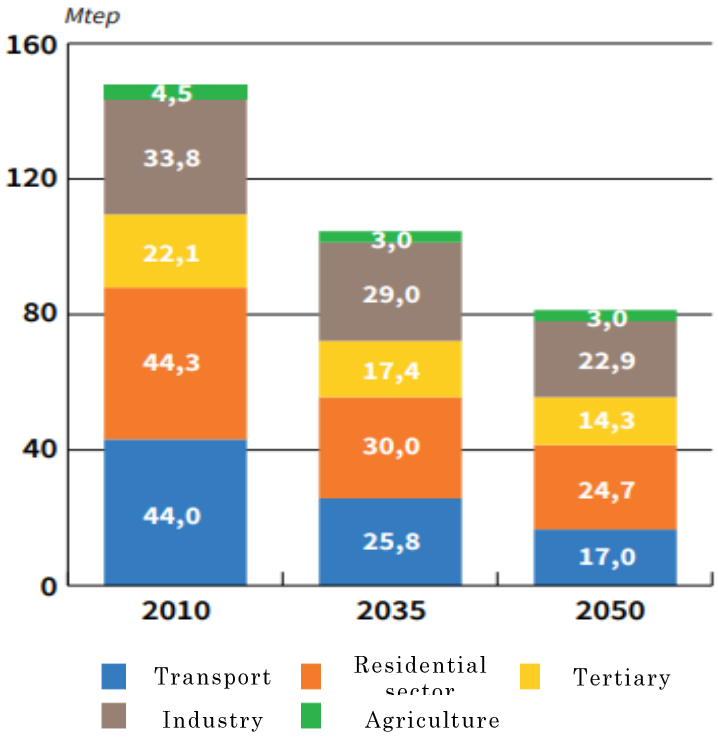

Figure 1. 1- France's energy needs in 2010 and predictions for 2035 and 2050 (ADEME, 2017).

In view of these facts, European and French policies are considering imposing zero or even positive energy buildings regulations in the near future. The need for more efficient energy buildings seems essential, and one of the technologies useful for achieving this objective is the replacement of conventional energy sources with renewable and waste ones being a highly promising perspective.

Although a large number of studies have been carried out on this topic (IEA, 2014) implementing renewable sources in the building presents some drawbacks, the main difficulty being the variability and intermittence of their availability (especially concerning wind and solar energy). In view of this, Thermal Energy Storage (TES) is

considered as one of the most promising technologies which can be used, as it can enable greater and more efficient use of these fluctuating energy sources by matching the energy supply with the demand. In fact, it consists in stocking thermal energy by heating a material (the "storage medium") capable to release the thermal energy stored at a later time.

1.3 SCIENTIFIC CONTEXT AND OBJECTIVE OF THE WORK

According to the alarming situation described above, many complex questions exist related to the design and analysis of intelligent building components and Renewable Energy Systems for NZEBs and NZEDs. Developing robust answers to these questions requires an interdisciplinary and multi-level approach targeting architecture design (building shape, floor plan arrangement, fenestration and shadings elements), components (thermal insulation of building envelope, walls and systems), occupants (behaviour and exigencies), renewable energy production and energy storage. The answers must include technology development and innovation in the form of new tools, methods (numerical and experimental), and technologies that take into account the complexity of the next generation of buildings appropriate for the French and European expectations. Thus researchers have to fill technology gaps and advance the state-of-the-art by developing and exploiting by enhancing the existing models and providing design and operating toolkits based on revolutionary methodologies and rich in-situ monitoring.

In order take part to the establishment of this new paradigm, this PhD thesis aims manly to optimize the energetic behaviour of an innovative thermal energy storage system (water – Phase Change Material exchanger) at low temperatures integrated to an innovative - Positive Energy District.

This storage system was particularly created for the HIKARI project, the first positive energy, mixed use building group located in Lyon, France, and due to its novelty it was found necessary to optimize its technology, in order to make it more cost-effective and efficient for future use.

Because of the high costs of experimental tests in the real conditions of buildings, numerical simulation, developed analytical methods and different modelling are needed to predict the behaviour and results of thermal energy storage usage in buildings in order to optimize this technique and to make it more efficient and cost-effective. For this reason innovative numerical and experimental tools were developed along this thesis, in order to achieve this success.

To reach this target, several sub-objectives have been dressed and achieved:

A numerical model that took into account the non-linear phenomena induced by the next generation of building systems. The goal was to develop a numerical model that had to be fast (simulation time) and more accurate, and took the induced complexity (natural convection, Latent Heat Storage, model coupling, etc.) into account.

An original experimental prototype capable to describe the complexes phase change phenomenon completed by in-situ monitoring. Indeed, this kind of experimental approaches are strongly needed to develop the necessary knowledge, tools and networks useful for achieving reliable in-situ dynamic testing and data analysis methods that can be used to characterise the actual performance of Phase Change Materials based exchangers.

Genetic algorithm multi-criteria optimisation approaches and tools in order to manage the interactions between a multi-energy source building's HVAC systems.

1.4 METHODOLOGY: NUMERICAL AND MULTI-SCALE EXPERIMENTAL BASED APPROACH

In order to optimize the technology of the HIKARI's thermal energy storage at low temperatures and achieve our objectives a numerical and laboratory and in-situ scale approached has been led (figure 1.2). Thus prior literature review about the thermal energy storage functioning, the thermo-physical behaviour of the materials employed and the simulation, optimization techniques and existing similar technologies has been made.

This review has proven the inadequacy of existing numerical models and convinced us to use Genetic Algorithms as optimization method. We started by realizing a numerical model using the heat balance approach and the apparent heat capacity method and we developed it using the MATLAB Simulink environment.

As the in situ data of the reference system were not yet available, the model was firstly calibrated comparing its results with those obtained through a second model realized using the Computational Fluid Dynamics method and developed using the software ANSYS Fluent.

Once the HIKARI buildings inaugurated (September 2015), the building monitoring process started so we started with a comparison between the results obtained through the model and the data registered by the temperature sensors as first in-situ validation. However, it was considered impossible to obtain a complete experimental validation using the only in situ data because, given the complexity of the reference system, it was very difficult and even impossible to recreate particular conditions, like varying inlet water flow rate or changing the number of plastic cases filled with PCM. For this reason, an experimental prototype with validation purposes was designed and developed.

The objective of this experimental prototype construction was, on the one hand, to reproduce the behaviour of the reference storage system in a small-scale and with the opportunity to modify the boundary conditions, changing for example the inlet water flow rate or the type of PCM, and on the other hand to provide coherent and accurate measurement of water temperature evolution during the heat exchange between water and PCM.

Once numerically calibrated and experimentally validated, the model was coupled to the numerical model of the set of cooling systems of the HIKARI district, in order to reproduce the mutual interaction between all these systems (including the absorption chiller connected to the storage system). After that, the Genetic Algorithms method has been used in order to find the best values to allocate to four characteristic parameters of the reference cold storage system, for minimizing the HIKARI's energy consumption linked to its functioning.

The scheme of this approach is shown in figure 1.2:

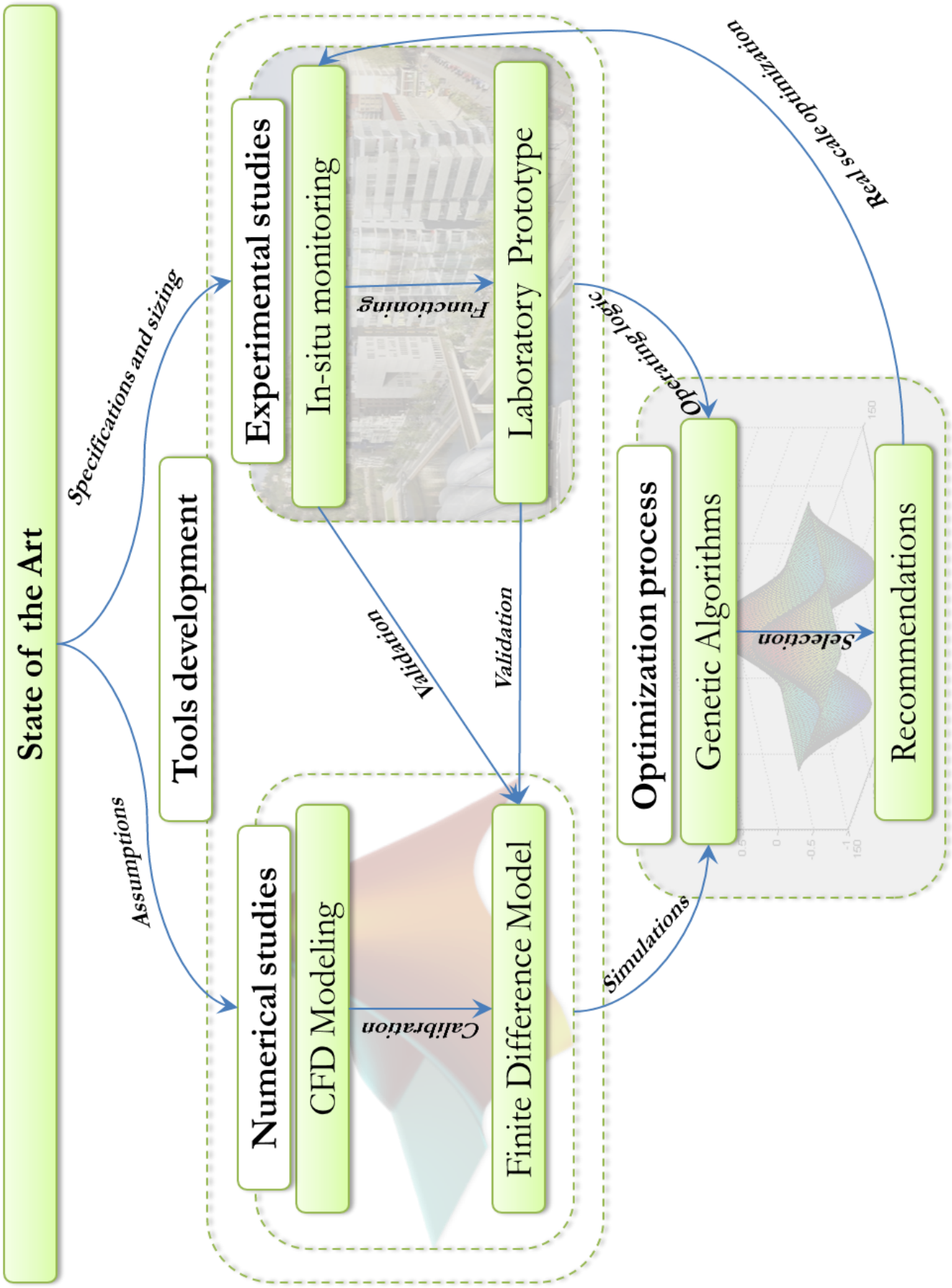

Figure 1. 2 - Scheme of the methodology followed along this thesis.

1.5 CHAPTER CONTENTS

The thesis is divided into 6 chapters including introduction, presenting the various elements that had to be linked together in order to achieve the established goals.

This first chapter briefly presents the energy and built environment context in France and the need to find new technologies able to replace conventional energy sources with renewable and waste ones in view of the energetic and economical goals imposed by the entry into force of the Paris Agreement in November 2016.

The second chapter presents the literature review and the reference project HIKARI. It deals mainly with the thermal energy storage. It focuses on thermal energy storage processes and targets phase change materials by demonstrating existing applications in buildings, enhancement techniques as well as limitations and barriers to their use. The second part of the chapter describes the multi-energy source buildings, and present the case study of the first positive energy building group in France (HIKARI).

The third chapter presents the numerical part of the study. In the first part of this chapter the reference thermal energy storage system is presented, while in the second part the simulation approach for the development of the finite difference method model is described.

The fourth chapter presents the model's numerical calibration obtained through the development of a second numerical model realized using the Computational Fluid Dynamics method.

The first part of chapter five presents the HIKARI monitoring system and the first experimental calibration of the numerical model obtained using the in situ monitoring data of the reference system. The second part shows the modelling and development of an experimental prototype realized for the experimental validation of the model but mainly useful for the validation of other kinds of phase change materials in the future.The important choices concerning design are explained including geometry, instrumentation and data acquisition.

Chapter six presents the optimization study of the heat exchanger integrates to HIKARI HVAC system. In the first part of the chapter, the coupling of the numerically calibrated and experimentally validated model to the numerical model of the set of cooling systems of the HIKARI district is explained, while in the second part the results of the Genetic Algorithms optimisation results are shown.

Finally, the last section of this thesis presents the conclusions of the study and discusses the outlooks that can be tackled in the future.

CHAPTER 2

THERMAL ENERGY STORAGE AND MULTI-SOURCE ENERGY BUILDINGS: HIKARI AS REFERENCE PROJECT

2) THERMAL ENERGY STORAGE AND MULTI-SOURCE ENERGY BUILDINGS: HIKARI AS REFERENCE PROJECT

2.1 INTRODUCTION

As detailed in the previous chapter the French energy context clearly raised the need to improve energy-effective technologies and induced the challenge of this PhD thesis work: optimize an innovative thermal energy storage technology making it more cost-effective and efficient for future use.

In order to achieve this objective, we started analyzing the effects of thermal energy storage technologies in terms of consumption shifting and more efficient management of the built environment.

At first, the field of application of such technology is presented, along with its different forms. Furthermore, phase change materials are discussed as one of the most frequent ways to achieve thermal storage (classification, properties, containment, applications, enhancement techniques and limitations).

Some existing studies using PCM based active and passive systems are shown, in order to acquire useful information regarding their development and utilization in the building and take advantage of learned lessons for establishing assumptions for our numerical models described chapter 3 and 4 and in order to design and assess our experimental prototype (see chapter 5).

Finally, the benefits and limitations of multi-source energy systems are presented and in particular the HIKARI project is described, focusing on the novelty of the systems parts of its multi-energy source systems.

2.2 THERMAL ENERGY STORAGE

Thermal energy storage (TES) is a technology that can enable greater and more efficient use of these fluctuating energy sources by matching the energy supply with the demand, as it consists of stocking thermal energy by heating a material (the "storage medium") capable to release the thermal energy stored at a later time. In this way, this technology can help balance energy consumption and reduce peak demand, CO_2 emissions and costs, while increasing overall efficiency of energy systems (IEA-ETSAP and IRENA, 2013) (Alva et al., 2017). In view of this, TES is considered the most promising technologies, as it can play a key role in energy efficient buildings by stocking thermal energy in order to reduce indoor air temperature fluctuation or reinstituting it to the system (building, district, and town) at a later period with an hourly, daily or even seasonal time lag.

TES can be achieved through three major methods: sensible heat storage, latent heat storage and chemical heat storage.

2.2.1 Sensible heat storage

Sensible heat storage (SHS) occurs when the temperature of the medium changes within a fixed range and when it does not change phase. The storage medium can be a liquid (such as water, the most common use) or a solid (such as bricks, concrete or steel.

SHS presents a lower energy efficiency and storage capacity compared to latent heat storage, even if it is usually simpler and less expensive.

The amount of heat stored in the storage medium can be calculated by the following equation:

$$Q = Cp\ m\ (T_2 - T_1)$$ *Equation 2.1*

where Q is the amount of stored sensible heat (J), m is the storage mass (kg), Cp is the specific heat of the storage medium at constant pressure (J/kg · K), and T_1 and T_2 are the temperatures before and after stocking/destocking. As it can be noticed, the ability to store sensible heat for a given material strongly depends on the value of its energy density, that is the heat capacity per unit volume or $\rho\ Cp$. For this reason, a material to be useful in a TES application, it must be inexpensive and have good thermal conductivity (Fernandez et al., 2010).

In buildings, SHS applications can be found in wall insulation, inertia increasing techniques, solar or gas water heaters, load levelling, night cooling etc.

2.2.2 Latent heat storage

Latent heat storage (LHS) occurs when the storage medium undergoes a phase change, from solid to liquid or liquid to gas or solid to gas, and vice versa. This phase transformation requires additional energy thus it reduces the storage efficiency so solid–gas and liquid-gas based LHS materials have not gained more attention for their commercial application (Salunkhe and Krishna, 2017).

The stored latent heat for a given mass of a substance can be calculated by the following equation:

$$Q_l = \Delta H_l\ m$$ *Equation 2.0.2*

Where Q_l is the amount of stored latent heat during the phase change of the substance (J), m is the mass of the substance (kg) and ΔH_l is the change in enthalpy for the substance (J/kg).

One major advantage of LHS systems is its relatively large heat storage capacities, compared with sensible heat storage, due to the high enthalpy change during phase change.

Concerning the built environment, LHS technology can be introduced into the building structure (wall, ceiling, façade) or in separate heat and cold storage devices usually related to HVAC systems. The first category constitutes the passive elements of the building, whereas the second one constitutes the active components, that can be used on demand.

A scheme of the difference between the heat stored during the same temperature range using sensible and latent storage systems is shown in figure 2.1:

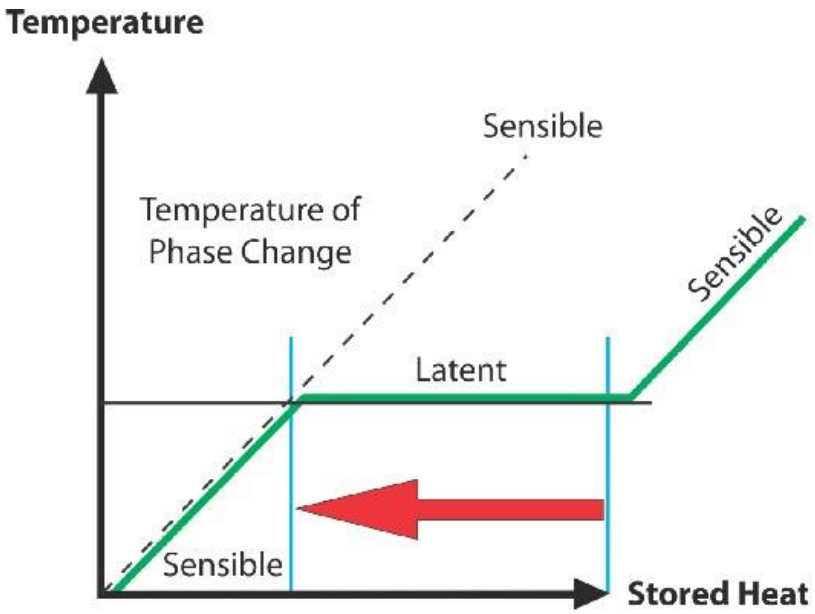

Figure 2. 1 - Scheme of the temperature variation with stored heat evolution using sensible and latent storage systems (savENRG™).

However, even if they present a higher storage capacity and a narrower temperature operating range if compared to SHS systems, the application of these storage media called Phase Change Materials (PCMs) is still very limited in the building sector (Cascone and Perino, 2015). One of the obstacles to the diffusion of PCMs is the lack of information regarding their thermo-physical properties, that will be discussed in the next paragraphs.

2.2.3 Chemical heat storage

Chemical heat storage relies on the reversible chemical reactions, during which the energy is absorbed or released by breaking or reforming chemical bonds (Yan et al., 2015). It is an emerging field presenting the advantages of high energy density, with compact and long term storage potential. On the other hand, it is more expensive and technically complex to implement compared with sensible and latent heat storage technology.

Chemical heat storage can be divided into thermochemical processes and sorption processes: the first ones are based on the energy released and absorbed during the breaking and the formation of molecular bonds for completely reversible chemical reactions, while sorption systems involve adsorption and absorption processes.

During thermochemical processes, thermal energy can be absorbed when the endothermic dissociation of a material (C) takes place, this constituting the charging procedure. This process leads to the formation of two separate components (A and B), which have different properties and can be stored at ambient temperatures for long periods with few or no thermal losses.

Finally, the discharging process occurs when the reversed procedure is performed and the components A and B are mixed through an exothermic reaction that leads to the reformation of the initial material C. The described procedures can be represented by the following equation:

$$C + heat \rightleftarrows A + B \qquad \textit{Equation 2.3}$$

Where C is the thermochemical material and A and B are the reactants.

With regard to sorption processes, adsorption takes place when a molecular or atomic layer is shaped, following the accumulation of an adsorptive on the surface of an adsorbent, while absorption consists in the formation of a solution which is occurring when a substance is distributed into a liquid or solid. The following table resumes the main parameters of the three TES methods, as well as their advantages and disadvantages (Abedin and Rosen, 2011):

Table 2. 1 – Comparison of different types of TES based on various performance parameters (Abedin and Rosen, 2011).

Performance Parameter	Type of Thermal Energy Storage		
	Sensible TES	**Latent TES**	**Chemical TES (Sorption and Thermochemical)**
Temperature range	Up to: 110 °C (water tanks) 50 °C (aquifers and ground storage) 400 °C (concrete)	20–40 °C (paraffin) 30–80 °C (salt hydrates)	20–200 °C
Storage density	Low (with high temperature interval): 0.2 GJ/m^3 (for typical water tanks)	Moderate (with low temperature interval): 0.3–0.5 GJ/m^3	Normally high: 0.5–3 GJ/m^3

Lifetime	Long	Often limited due to storage material cycling	Depends on reactant degradation and side reactions
Technology status	Available commercially	Available commercially for some temperatures and materials	Generally not available, but undergoing
Advantages	Low cost Reliable Simple application with available materials	Medium storage density Small volumes Short distance transport possibility	High storage density Low heat losses (storage at ambient temperatures) Long storage period Long distance transport possibility Highly compact energy storage
Disadvantages	Significant heat loss over time (depending on level of insulation) Large volume needed	Low heat conductivity Corrosivity of materials Significant heat losses (depending on level of insulation)	High capital costs Technically complex

2.3 PHASE CHANGE MATERIALS

Phase change materials (PCMs) have been proven useful within the building sector due to their high latent heat storage capacity. In fact, choosing the PCM material in such a way that its phase change temperature is exactly located across the working temperature range at which the any system operates, they can store a large amount of energy in a small volume and mass compared to sensible energy systems (Palomba et al., 2017).

2.3.1 Classification

A complete review of different types of phase change material, their characteristics and classification, merits and demerits as well as experimental techniques undertaken to investigate the behavior of PCMs in both melting and solidification phases has been reported by different authors (Abhat, 1983), (Cabeza et al. 2011), (Kenisarin and Mahkamov 2007), (Verma et al. 2008).

PCMs are divided in three categories: organic, inorganic, and eutectics (Beatens et al., 2010) (Tyagi and Buddhi, 2005). Even if PCMs were previously used to be divided into two

main groups (the organic and the inorganic compounds) it is now common to consider eutectics (that are actually a mix of two or more components) as a specific group.

A classification table for different types of PCMs is given in Fig. 2.2:

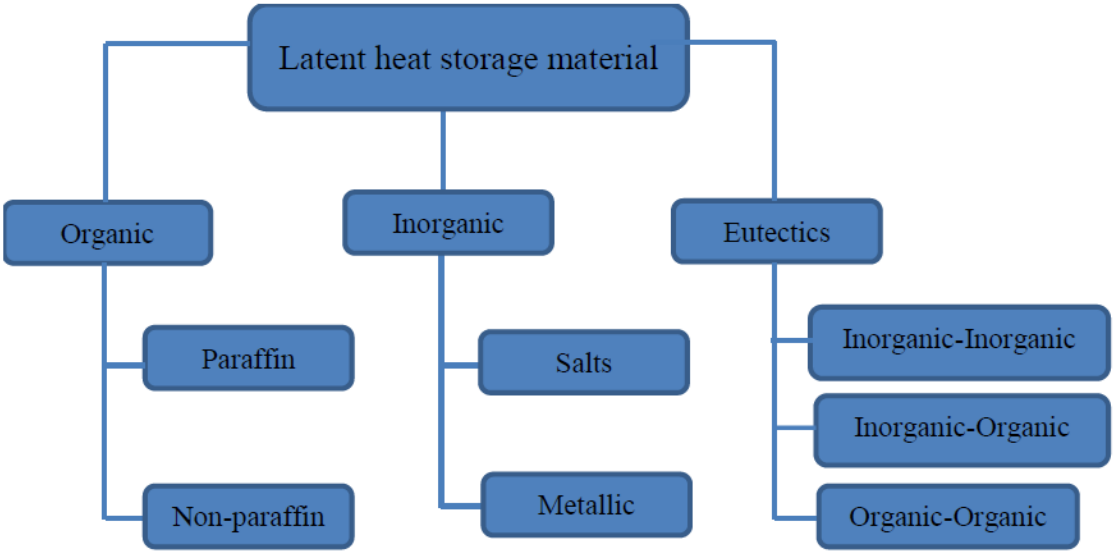

Figure 2. 2 - Classification of PCMs (IEA, Annex 23, 2014).

A great number of materials have been used and studied as PCMs in TES applications, including hydrated salts, paraffin waxes, fatty acids and eutectics of organic and non-organic compounds.

Figure 2.3 illustrates a classification of PCMs according to their melting temperature range and melting enthalpy.

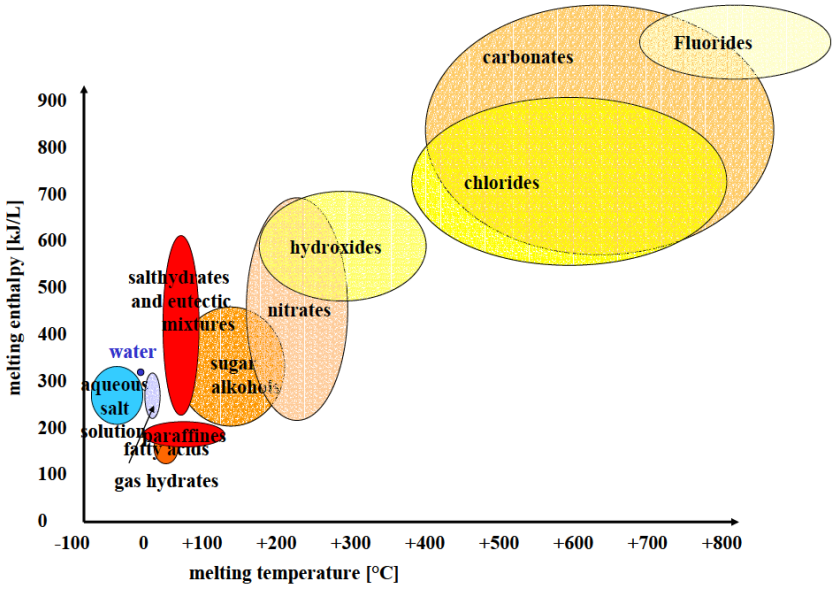

Figure 2. 3 - Classification of PCMs according to their meting temperature range and enthalpy (IEA, Annex 17, 2005).

2.3.2 Problematic phenomena

Even though the LHS is one of the most promising technics used in building applications for energy efficiency purposes, several problematic phenomena related to PCMs thermo-physical properties have been identified and studied over the years. This section presents the most common ones.

2.3.2.1 The subcooling phenomenon

Subcooling (or supercooling) occurs when the PCM remains in liquid form even when its temperature decreases below the solidification threshold value (T_f).

Solidification starts with a nucleation effect that requires the formation of initial crystals (the nucleus) and the propagation of these crystals. For some PCMs (particularly salt hydrates and some eutetics) if the nucleation rate is too low, it results in the reduction of the nucleus. Accordingly, the PCM remains in a liquid phase even though its temperature is lower than T_f. As a result, the beginning of solidification is delayed and the PCM temperature rises back to T_f (figure 2.4).

Subcooling can have a disrupting effect on the performance of the PCM unit and must be taken into account in the design phase of TES applications. A solution to minimize this phenomenon lies in the addition of suitable nucleating agents to the PCM.

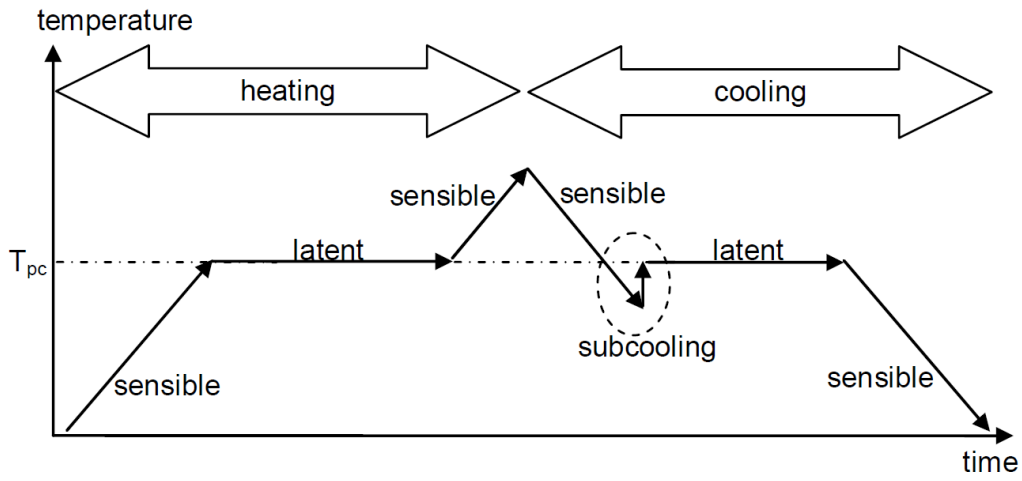

Figure 2. 4 – Subcooling effect during solidification (Cabeza et al. 2008).

2.3.2.2 The segregation phenomenon

The segregation phenomenon is observed on salt hydrates PCMs and it occurs due to the congruent melting of most salt hydrates with the formation of the lower salt hydrate. The effect is irreversible and the storage density decreases with cycling (Cabeza et al. 2011) which, as a consequence, decreases the thermal properties and performance of the

PCM itself. Solutions can be found in the inclusion of materials that can alter the properties of the salt hydrate by preventing the heavier phases from sinking to the bottom.

2.3.2.3 Thermal life cycle

Thermal life cycle refers to the number of cyclic phase change repetitions (melting-solidification) before the PCM thermal properties begin to alter (decrease). For example, in the case of paraffin, the thermal life varies between 3000 and 10000 cycles (Hadjieva et al., 1992).

2.3.2.4 Incompatibility with storage containers: Corrosion or volume change

Some PCMs may not be compatible with the chosen storage solution. This concerns corrosion and volume changes that could both lead to the degradation of the container and the leakage of the PCM, rendering the application unusable in the long term.

2.3.2.5 Flammability and odor

PCM based materials or applications meant to be implemented in buildings have to respect building legislation related to fire risks and the occupants' olfactory comfort.

Some PCMs present high combustibility values and require special treatment before usage in a real life application, such as the incorporation of fire retardant additives and conducting fire risk tests. However these procedures are bound to increase / raise the final price of the PCM and of its implementation in the building. Furthermore, some PCMs are not odorless and the inhalation of PCM vapor may cause irritation, both facts being unacceptable by the occupant. Air-tight containment is thus required to overcome these problems.

2.3.3 PCM containment

Because of the frequent change of the PCMs from solid to liquid during their heat storage process, they need to be kept in some kind of containers or matrices (Konuklu et al., 2015). PCM containment is a very important issue in an LHS unit, as it has to supply at the PCM low thermal conductivity (providing a high exchange surface to volume ratio or having a small storage thickness) and at the same time avoid the problematic phenomena illustrated in the previous paragraph.

The existing PCM containement approaches (Kuznik et al., 2010) are described in the following paragraphs.

2.3.3.1 Macroencapsulation

Macroencapsulation means inclusion of PCM in a macroscopic containment (usually larger than 1 cm in diameter) such as tubes, pouches, spheres, panels or other containers. In microencapsulation, solid or liquid particles are encapsulated in a thin, high molecular weight polymeric film (Saffari et al., 2017). Macro-encapsulation offers the advantages of small leakage risks and of little affection of the building's structure but it presents poor thermal conductivity and in some cases complicated integration into the building materials. Some examples of macro-encapsulation are shown in figure 2.5.

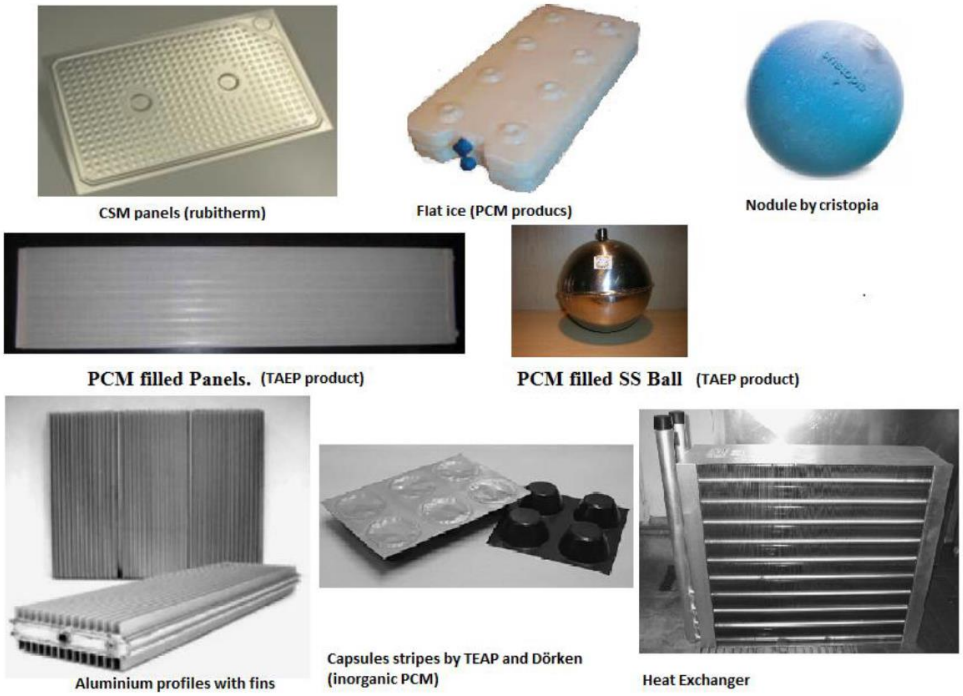

Figure 2. 5 - Examples of macro-encapsulation (IEA, Annex 23, 2014).

2.3.3.2 Microencapsulation

Microencapsulation is the technique of coating individual particles or droplets with a continuous film to produce capsules in a micrometer to millimeter in size, known as a microcapsule (Tyagi et al., 2010). The particles are then incorporated in any matrix that is compatible with the film, in order to form a homogenous compound in macro scale. This containment method is the most used (Cabeza et al., 2011) because it increases heat transfer as it presents a high surface to volume ratio and improves cycling stability as the phase separation is restricted to microscopic distances.

2.3.3.3 Impregnation of porous building materials

Porous building materials can be enriched with the addition of PCM in two ways: through the direct incorporation and the immersion.

2.3.3.3.1 Direct incorporation

Direct incorporation consists in adding liquid or powered PCM to building constructions materials (gypsum, concrete or plaster) during production. It is the most economical method, but at the same time it presents leakage and incompatibility with some construction materials.

2.3.3.3.2 Immersion

This technique is based on the sinking of porous building components such as gypsum board, brick, concrete block, wood and plaster into liquid PCM. The PCM is then absorbed into the component's pores by capillary effect. The main risk using this method could be leakage.

2.3.3.4 Shape stabilized PCM

Shape-stabilized PCM is a composite material composed of a liquid mixture of PCM with a support material, usually high density polyethylene (HDPE) or styrene-butadiene-styrene (SBS). The mixture is then cooled below the glass transition temperature of the supporting material, leading to a solid component that can have up to 80% PCM mass proportion. The observed low thermal conductivity can be increased by adding materials such as ex-foliated graphite into the mixture composition.

2.4 PCM APPLICATION IN BUILDINGS

Several reviews have been carried out in the field of PCM applications in buildings in the last years. The first review was done by Zalba et al. (2003), who investigated the history of the use of phase change materials for thermal storage. The year after, Khudhair and Farid (2004) reviewed the previous studies focusing on the application of PCMs in buildings. Zhu et al. (2009) provided a review of the effects of PCM applications on the thermal performance and dynamic characteristics of buildings, while Cabeza et al. (2011) provided the information about the characterization, requirements, problems and appropriate solutions associated with the use of PCMs in buildings, in order to resolve technical problems linked to the use of this technology and to find new types of more efficient PCMs.

The PCM applications in buildings can be divided into two large categories: active and passive ones (figure 2.6). They will be described in the following paragraphs.

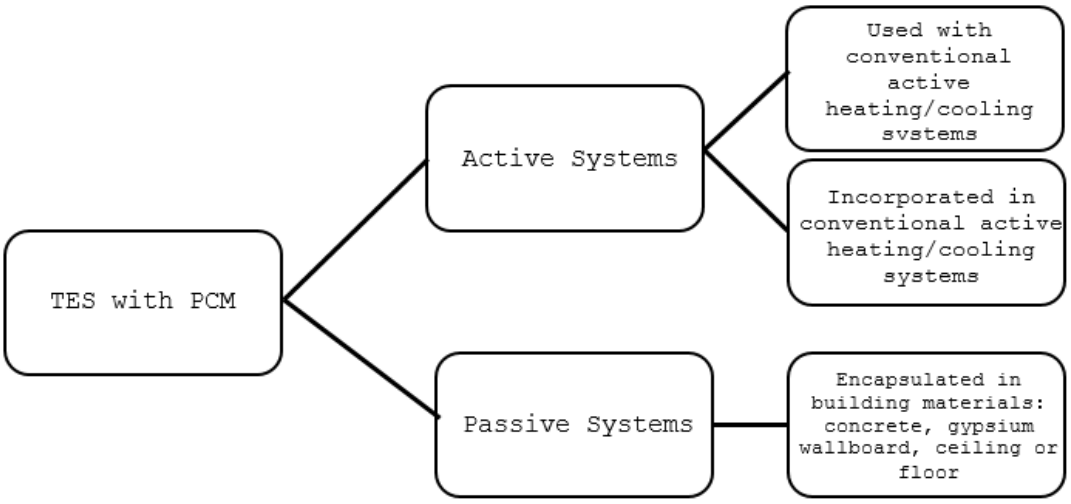

Figure 2. 6 - Active and passive system for TES with PCM (Iten et al., 2016).

2.4.1 Active systems

When an active system is present in a building, the thermal storage is activated by a supplementary mechanical system (fan, pump, etc), enhancing heat transfer performance and allowing stocking or destocking heat/cold on demand. These thermal storage systems can operate on specific time slots, being able to correlate the needs with the energy supplies and apply in such a way peak power reduction strategies.

In some active systems the heat transfer and storage are obtained using the same medium, whereas in others heat transfer is performed by a first medium (usually air or water) while the heat storage is obtained through the use of a PCM. The use of PCMs for thermal energy storage in buildings backs to before 1980. The first studies on this material for heating and cooling applications were carried out by Telkes (1978) and Lane (1981).

One of the active applications, is the integration of PCMs in building HVAC systems for peak power reduction needs and for improving its thermal efficiency, as it enhances the cooling (or heating) performance of mechanical ventilation units. Their integration in HVAC systems can be mainly performed in two ways: incorporating either a heat exchanger or a PCM panel board in the HVAC system either PCM.

The encapsulated PCM is contained in a heat exchanger while a fluid (air or water) is used as the heat transfer medium. Design considerations include heat transfer optimization between the heat transfer fluid and the PCM. Concerning the PCM panel boards, this

consists in the use of passive PCM technology with the advantage of the coupling with an active mechanical system.

Another active system is the thermally activated ceiling gypsum panel, developed allowing heat gains of up to 40 W/m^2 and an increase of the thermal mass of light weight buildings. An incorporated water capillary tube system allows the active control of the thermal storage.

PCM actives applications can also be found in radiant floor panels. Granulated PCM was employed together with integrated pipes for heating and cooling. The results demonstrated the benefits of this application.

2.4.1.1 Examples of active systems

In this paragraph two case studies of experimental active systems are described among others, showing the technologies, the monitoring techniques and the results obtained.

2.4.1.1.1 Zalba et al. system

Zalba et al. (2004) developed a system in order to test the performance of PCM in a cooling system that allows storage of outdoor coolness during the night, to supply it to the indoor environment during the day.

The proposed unit (see figure 2.7) is a closed air circuit consisting of a fan for circulating the air, a device for heating and cooling the air at the desired temperature, a flow meter and the thermal energy storage system. The last one consists of flat plate rectangular encapsulation vesicles made with methacrylate to allow visualization of the phase change.

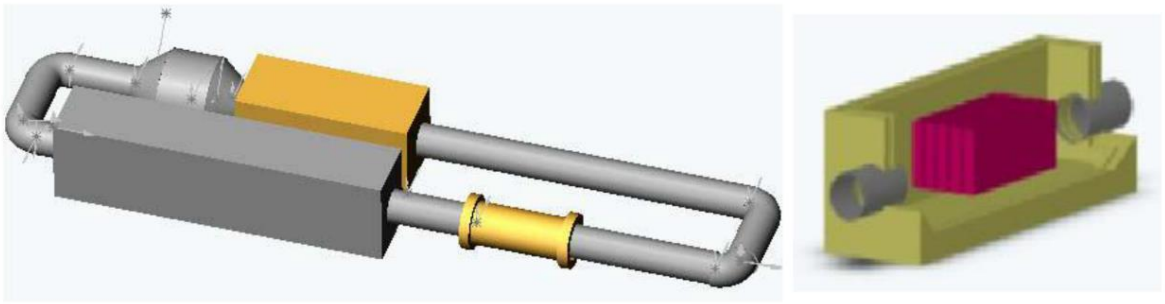

Figure 2. 7 – Zalba's et al. experimental set up (left) and heat exchanger unit (right).

Two PCMs were selected:

- A molecular alloy consisting of 34% C_{16} and 66% C_{18}, with a latent heat of 152 kJ / kg and a melting range between 19.5 °C and 22.2 °C.

- The RT25 Rubitherm paraffin, with a latent heat of 164 kJ/kg and a melting range between 18.8°C and 24.1 °C.

Inlet and outlet air temperatures were measured using five calibrated Pt100 sensors at the entrance and exit of the unit. Air flow was measured using a calibrated flow meter and customized software was used for data acquisition and evaluation.

The two following figures show the experimental results for Zalba's et al. proposed unit. Figure 2.13 illustrates the exchanged heat and figure 2.14 the exchanged energy, both for the melting and solidification processes.

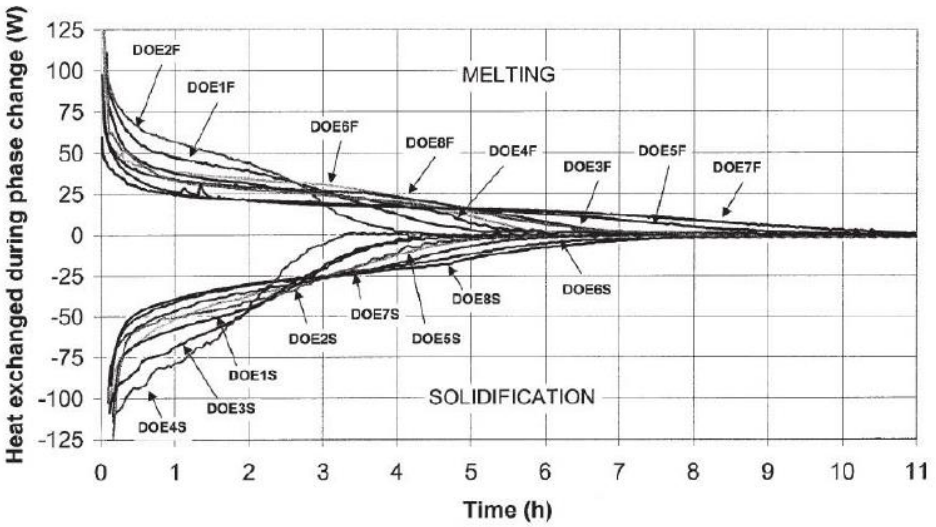

Figure 2. 8 – Zalba's et al. unit's heat transfer during phase change for different configurations.

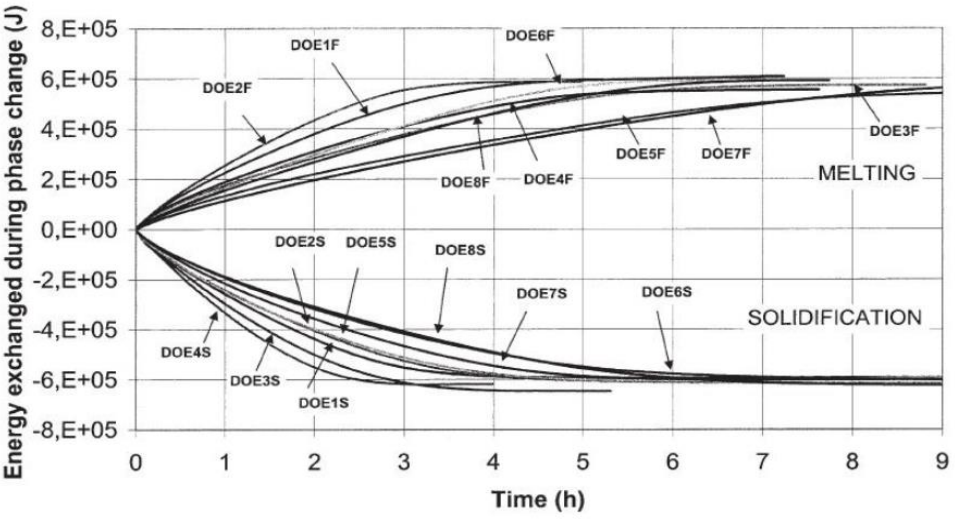

Figure 2. 9 – Zalba's et al. unit's heat exchange during phase change for different configurations.

Studies performed on the designed system showed that for the solidification and the melting processes the most influential factors are the thickness of the encapsulate container, the inlet temperature of the air, the air flow, and the interaction thickness /

temperature. The researchers also performed a viability analysis that showed that this kind of system can be developed in a real installation, regarding technical feasibility as well as economic advantages (when compared to existing cooling systems).

2.4.1.1.2 Stathopoulos et al. system

Stathopoulos et al. developed a PCM– Air heat exchanger, conceived for load shifting purposes, in order to investigate its behavior and to possess the necessary tools for the development of advanced control strategies taking into account various factors: peak power reduction, thermal comfort and indoor air quality.

The PCM-Air heat exchanger was designed and fabricated using Microtek 37D paraffin as the heat storage medium. The heat exchanger was designed so that it could be integrated into a HVAC system, for example in a ventilation plenum, a false ceiling or the ceiling over a corridor.

The paraffin presented a melting/solidification temperature range around 37 °C, a dilatation of 10% between phases and a latent heat of fusion of 230 kJ/kg and it was macro-encapsulated in aluminum containers, which are then assembled parallel one to another fins have been introduced between them to increase the heat exchange. Three of the containers were equipped with additional pierced components that were used to introduce temperature sensors at variable depths inside the PCM, in three different parts of the plates: inlet, middle and outlet areas. Polystyrene panels enclose the PCM containers in order to thermally insulate it from the surrounding environment. Finally, wooden boards are used to assemble and ensure the stability of the structure (see figure 2.10).The unit was coupled to an experimental platform and then characterized for various airflow rates.

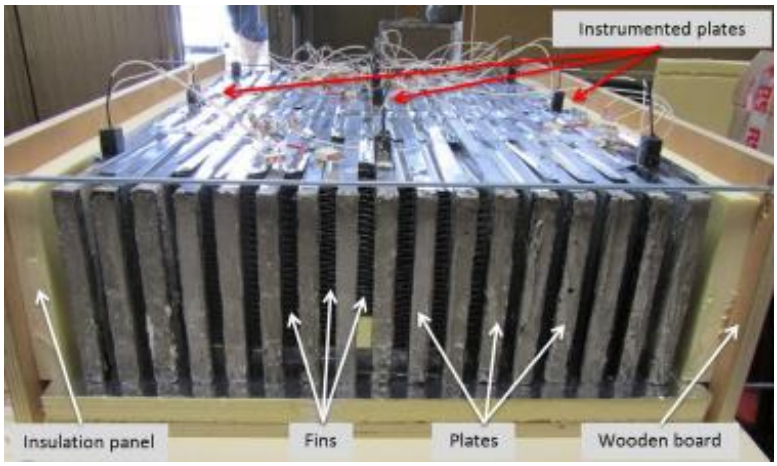

Figure 2. 10 - Stathopoulos et al. Air-PCM exchanger during fabrication.

A data acquisition system was used to collect all the measured data in order to study the fusion and the solidification of the PCM, the heat losses and the progression of the charging/discharging process of the heat exchanger (El Mankibi et al., 2015). The measurements include temperature and relative humidity of air at the inlet and outlet of the heat exchanger, and the airflow rate after the heat exchanger. Concerning the heat exchanger, 3 plates were instrumented with temperature sensors (PT100 class A) at three specific points: inlet, middle and outlet part of the plate. Two sensors were installed for each point: one inside the PCM, allowing a direct measurement of the PCM temperature and one on the exterior plate surface. The three-instrumented plates were at the beginning, middle and the end of the heat exchanger. Finally, temperature sensors were also installed on the exterior surface of each plate at the outlet part of the exchanger.

These sensors (PT100 class A) were used to verify the airflow uniformity and monitor the charging/discharging process.

The heat exchanger was designed to be integrated in the mechanical ventilation system of an experimental test cell Hybcell (see figure 2.11). The dimensions of the heat exchanger are 1.05 m long, 0.75 m wide and 0.25 m high with a capacity of 31.8 kg PCM.

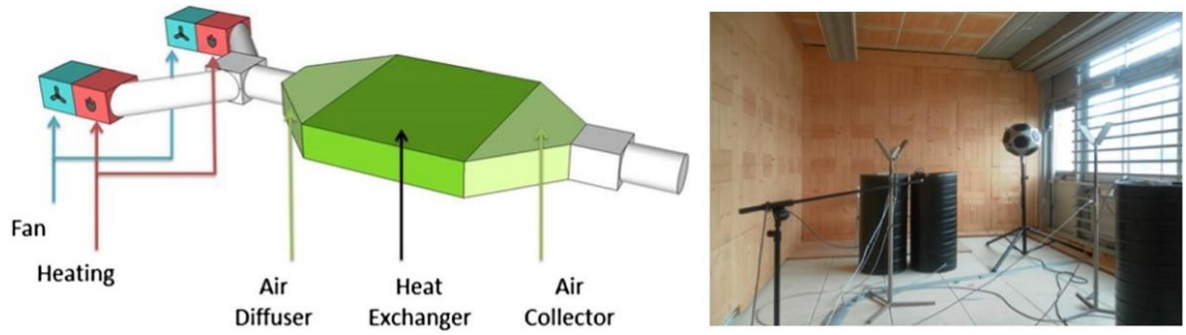

Figure 2. 11 - Stathopoulos et al. experimental platform and Hybcell test cell.

Results showed that the proposed system managed to perform peak load shifting while maintaining comfortable indoor conditions. Nevertheless, the needed charging/discharging time was superior to the peak period, this observation leading to the need for an optimization study for the heat exchanger.

2.4.2 Passive systems

In passive systems PCM is incorporated into specific components of the building. The integration of passive LHTES systems with PCMs could increase the thermal storage capacity of the buildings and help to avoid overheating problems during the summer due to internal loads or solar radiation (Soares et al., 2013).

In passive systems, PCM can be integrated in many parts of the building, such as:

- gypsum boards and wallboards (in order to increase the thermal mass of lightweight of the buildings and to lower indoor temperature fluctuations)
- floor and ceiling panels (aiming to absorb heat (solar related, in roofs for example) and diminish indoor temperature variation)
- glazing and shading shutters (for absorbing part of the solar heat and reducing the indoor air temperature fluctuation)
- concrete (in order to increase heat storage in heavy construction materials by combining their high density with the augmented latent heat PCM capacity)
- bricks (less analyzed in literature).

2.4.2.1 Examples of studies on passive systems technologies

In this paragraph two case studies of experimental passive systems are described, showing the technologies, the monitoring techniques and the results obtained.

2.4.2.1.1 Goia et al. study (2013)

The DGU_PCM prototype is a double glazed unit (8/15/6 mm) made of two clear glass panes, whose 15 mm cavity was filled with about 13 kg of a commercial grade paraffin wax (RT35 paraffin) whose density in the solid state was about 0.88 kg/l.

A thermal characterization of the paraffin wax was performed by means of a DSC analysis, showing a value nominal melting temperature of about 34 °C with a phase change range of about 10 °C. In order to test the benefits that a PCM glazing system could provide, a measurement campaign was launched comparing the results obtained through the monitoring of DGU_PCM to those obtained analyzing a traditional double glass unit (Double Glass Unit Clear Glass, DGU_CG, made of two panes of clear glass – 8/15/6 mm – with a cavity filled with air). In figure 2.12 it is shown the tested PCM glazing system and it is possible to see the two glazing systems (the prototype and the reference) assembled on the test cell facility used during the experimental campaign.

Figure 2. 12 - The Goia and al. test cell and the two glazing systems (DGU_PCM and DGU_CG).

An extensive experimental campaign was performed, with the aim of evaluating the visual appearance of DGU_PCM for various boundary conditions, investigating the thermo-physical behaviour of DGU_PCM and later assessing the thermal comfort performance under actual operating configurations, analysing the energy performance of the proposed technology, collecting data for the calibration and validation of a numerical model of PCM glazing system configurations.

The measurement campaign lasted more than six months and the thermo-physical behaviour of the PCM glazing system was continuously monitored, under different weather conditions and in different seasons. The results are shown in figure 2.13. Its performances were monitored under real working conditions and compared with those of a conventional double glass unit (DGU_CG), attention was focused on thermal comfort implications. It has emerged that the PCM glazing is in general able to provide good performance.

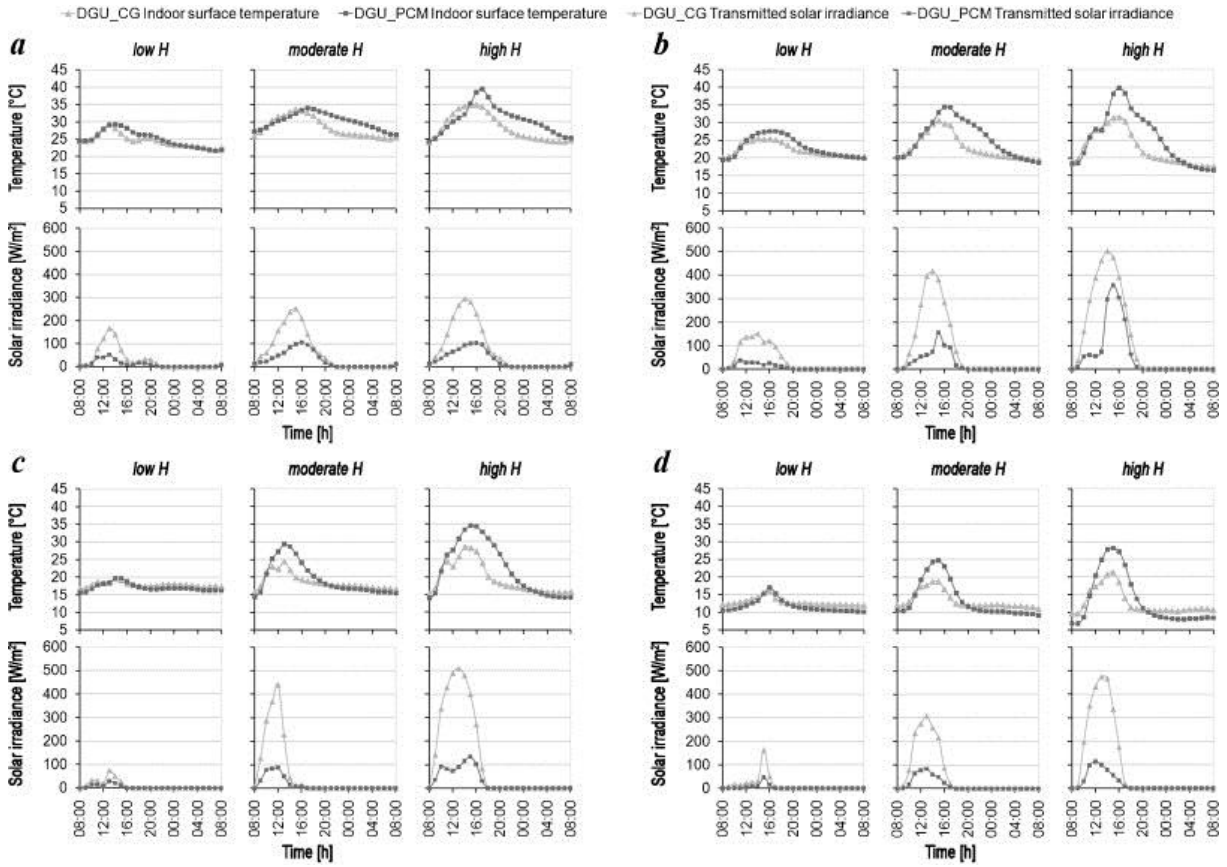

Figure 2. 13 - Goia et al. summer (a), mid-season (warm period) (b), mid-season (cold period) (c), and winter (d) – surface temperatures (ϑ_{surf}^{PCM} and ϑ_{surf}^{CG}) and transmitted irradiances (I_t^{PCM} and I_t^{CG}).

The thermal conditions of the indoor environment achieved adopting the DGU_PCM façade have resulted to be considerably improved, compared to a DGU_CG façade, for most of the time during the various seasons. In general, it has been observed that the higher the outdoor solar irradiance, the greater the benefits offered by DGU_PCM. This is due to

the shading and energy buffering effects that are provided by the paraffin layer. On cloudy days (low incident solar irradiation), the performance of the two technologies is similar, in relation to thermal comfort.

The indoor surface temperatures of PCM glazing were usually higher than that of the DGU_CG unit for most of the analysed boundary conditions. This is always a positive feature for thermal comfort during mid-seasons and winter, while it can have a negative effect on comfort in summer. Nevertheless, as far as the latter season is concerned, it should be pointed out that such conditions only occurs during the night or when the PCM melts completely during the hours in which the façade is subject to direct solar radiation (a fact that should be avoided through a proper choice of the melting temperature).

2.4.2.1.2 Cellat et al. prototype (2015)

In this study, Cellat et al. focus on thermal and mechanical effects due to the direct addition of bio-based fatty acids to specific concrete mixtures.

In the first part of this work, two binary mixtures of CA–LA and CA–MA were developed as PCMs candidate for building applications. Fatty acids were chosen as PCM because of their significantly lower flammability and non-fossil fuel origins. Once the thermal storage capacities were measured for both the binary mixtures with a differential scanning calorimeter it was found out that both PCMs were thermally and chemically stable. In addiction, the durabilities of PCM mixtures determined by the thermal gravimetric analysis indicated that degradation started at 120 °C, so both could be used for passive solar energy storage in buildings.

In order to test the benefits of PCM integration in concrete it was effectuated a comparison of the temperature evolution for different samples of fresh concrete with and without the developed PCMs.

Temperature levels of fresh concrete samples in semi-adiabatic containers were monitored during 24 h at constant temperature of 22 °C in a climate chamber in order to determine the effect of PCMs on the concrete hardening process. To achieve semi-adiabatic measurements, the samples were placed in insulated polystyrene containers with volume of 0.200 L. Temperatures were measured by a T-type thermocouple with an accuracy of ±0.5 °C, which was inserted into the fresh concrete and recorded by a data logger (Agilent 34970A) at 10 s intervals.

The results are shown in figure 2.14:

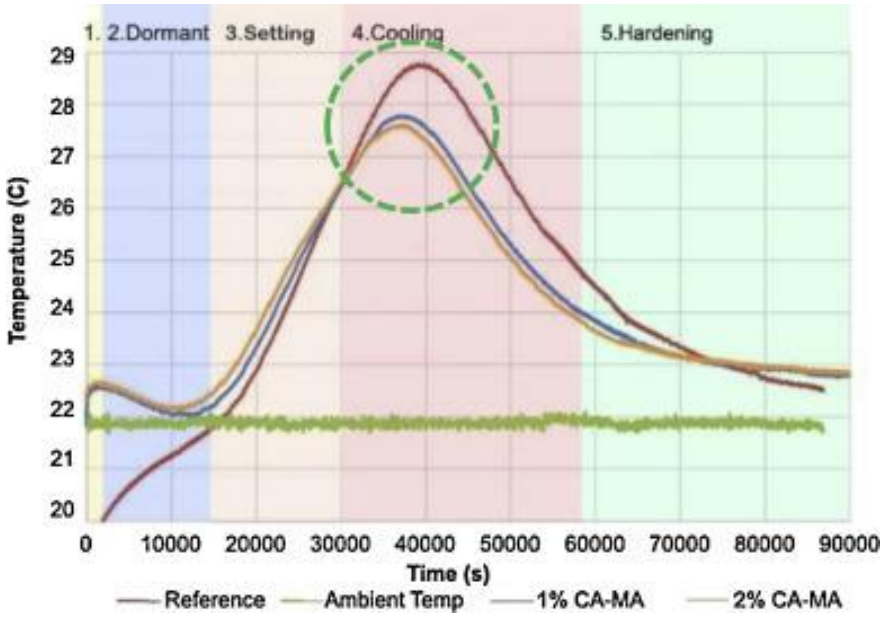

Figure 2. 14 - Cellat et al. temperature evolution due to heat of hydration in fresh concrete mixtures with and without PCM.

In the dormant and setting stages, all samples exhibited a similar trend in temperature increases. After 26 °C PCM started to melt and absorb the hydration heat. After this point, shown with the circle on the graph, temperature of the reference sample without PCM reached a maximum value of about 1 °C higher than the samples with PCM. During the cooling stage, temperatures of samples with PCM were below the reference and remained constant at around 23 °C when the PCM started to freeze. On the other hand, hardening time of concrete sample with PCM was shorter than that of the reference sample – and as a result – these samples started the cooling stage earlier. This would mean that temperature increase due to hydration and the setting time can be lowered by adding PCMs into fresh concretes.

Temperature evolution measurements in fresh concrete indicated temperature increase due to hydration and the setting time could be lowered by adding even small amounts of PCMs into fresh concretes.

2.5 MULTI-ENERGY SOURCE SYSTEMS

The characteristic of multi-energy source buildings is to reduce the primary energy consumption by producing the needed energy directly on site. Lately, the study of their functioning has been intensified due to their potential to reduce the building energy consumption and to eventually arrive to a zero or even a positive energy building (Catalina et al., 2011).

Several examples of multi-source building studies are found in the literature: just as the study of the couple solar thermal panels-geothermal heat pump by an extended experimental and simulation campaign conducted by Trillat-Berdal et al. (2006) or the combined cogeneration with solar energy (thermal and photovoltaic) with the wind energy analyzed by Sontage and Lange (2003), the combination of wood boiler, condensing boiler, heat pump and solar energy (both thermal and photovoltaic) studied by Fabrizio et al. (2010) and the integrated renewable system composed of solar water heating, solar photovoltaic, ground source heat pump, electric chiller and gas fired boiler analyzed by Lee et al. (2012).

The benefits of multiple sources of energy on the same construction are different from case to case (i.e. for certain climate areas installing solar thermal panels is not economic rentable but a geothermal heat pump will be a good decision). For this reason, an important but in the same time difficult task would be to identify alternative multi-source system configurations that could minimize the energy consumption and the investment payback time.

Multi-source systems for the fulfillment of electric, thermal and cooling demand of a building can be based on different technologies (e.g. solar photovoltaic, solar heating, cogeneration, heat pump, absorption chiller) which use renewable, partially renewable and fossil energy sources and this can brings some difficulties. In fact, the allocation strategy which allows the division of the energy demands among the various technologies and the proper sizing of each technology are deeply interrelated, as while a wiser energy demand allocation strategy can lead to significant reductions in primary energy consumption, the definition itself of an optimal allocation strategy strongly depends on the actual sizing of the employed technologies. Thus the problem of optimizing the sizing of each technology cannot be separated from the definition of an optimal control strategy.

An example of multi-energy source system is shown in the next paragraph.

2.5.1 THE HIKARI PROJECT

2.5.1.1 The design

On September 17, 2015 the first positive energy, mixed use building group in France was inaugurated in Lyon. The project, called HIKARI ("natural light" in Japanese), ran more than five years ahead of the goal of the European Union to have energy-neutral new build dwellings by the start of 2019 and it is the result of a cooperation between city of Lyon, the Japanese New Energy and Industrial Technology Development Organisation (Nedo), Toshiba and Bouygues Immobilier.

This ambitious project is composed of 3 buildings for a total floor area of approx. 12 000 m^2:

• HIGASHI (East), an office building with shops on the ground floor,

• MINAMI (South), in the middle of the plot, an apartment building with 36 dwellings and shops on the ground floor,

• NISHI (West), 3060 m^2 with 5 storeys of offices and 4 top-end penthouse apartments on the 2 upper storeys and shops on the ground floor (see figure 2.15 and table 2.2)

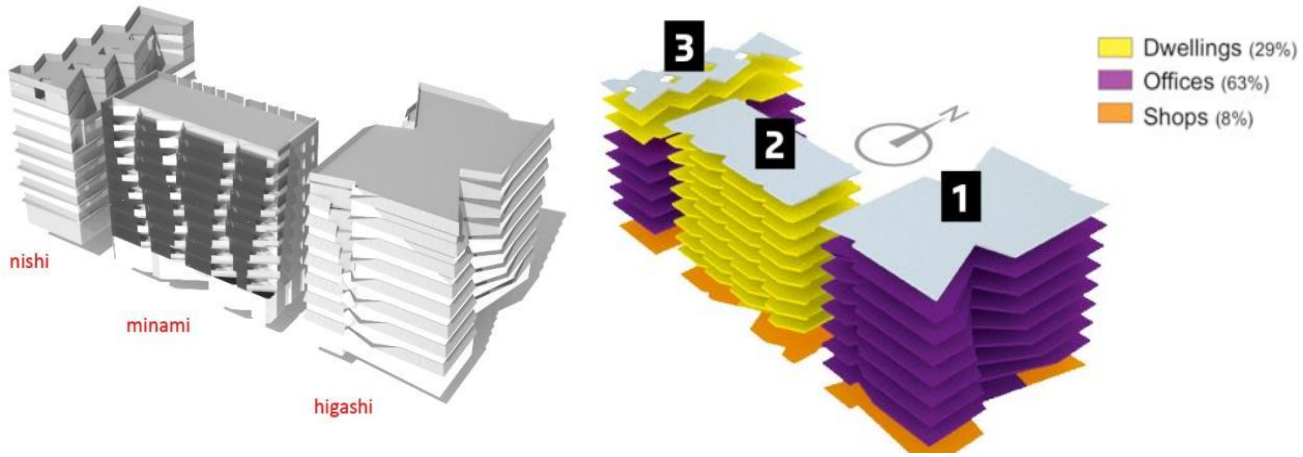

Figure 2. 15 - The three buildings of the HIKARI project.

Table 2. 2 - Floor area of the HIKARI project.

Building name	Offices	Dwellings	Shops	Total
HIGASHI	5 434 m^2	-	567 m^2	6 001 m^2
MINAMI	-	2 959 m^2	289 m^2	3 248 m^2
NISHI	2 338 m^2	570 m^2	153 m^2	3 061 m^2
Total	7 772 m^2	3 529 m^2	1 009 m^2	12 320 m^2

The main objective of HIKARI initiative is to establish a large scale (district level) in-situ multi-usage buildings (residential, office and commercial) with multi-energy architecture and storage solutions. On one hand, HIKARI goal is to provide recommendations on energy production and storage management and optimization strategies with integration of

occupants' behaviours. On the other hand, the HIKARI building and system monitoring will serve to adjust and calibrate latent storage systems models with real operating conditions.

The design work was focused on an architectural solution to improve natural lighting access and to reduce artificial lighting energy consumption, especially in the office area. The building were designed by the Japanese architect Kengo Kuma, who created specific cuttings in each façade based on the sun path (see Figure 2.16) in order to improve natural lighting and to link the inner space of the building with the outer space.

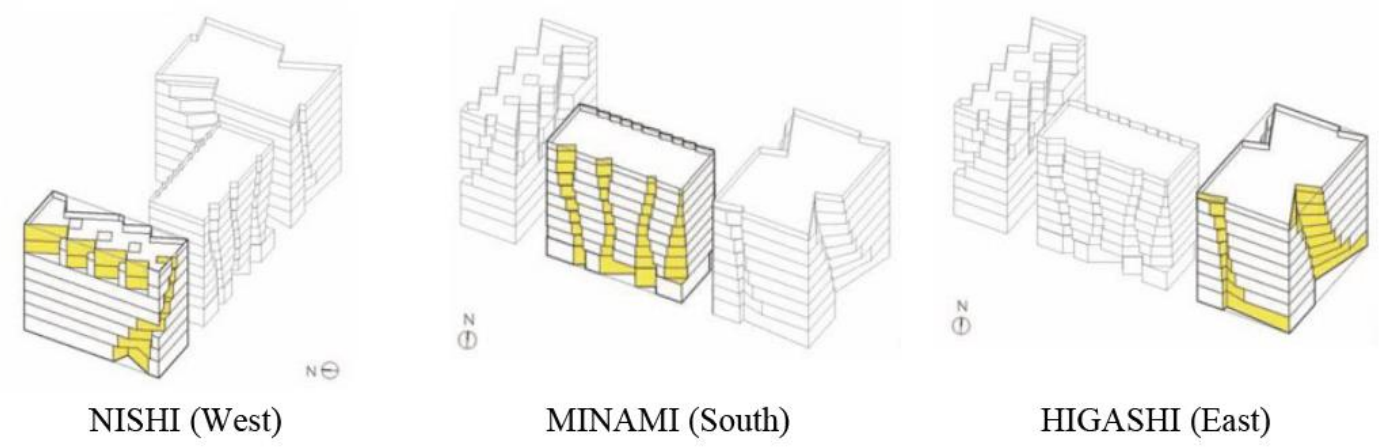

Figure 2. 16 - Cuttings in each façade in order to improve natural light.

The large glazing areas of office places and a see-though PV façade for dwellings also increase this transparency and create a pleasant and convenient ambiance for the users of buildings (see figure 2.17).

Figure 2. 17 - Southern façade of the HIKARI building.

2.5.1.2 The systems

The selection of the developer in charge of the design and construction of the building was set at a very ambitious level: make the P-plot building a positive energy building conforming to the global scale of the plot, including specific energy consumption for dwellings, office area and retail shops.

The design a positive energy building requires to strongly focus on energy systems in order to produce on site and with renewable energy sources the energy necessary to operate the building.

The energy balance was defined using dynamic calculation over a one-year period with realistic technical hypothesis. The proposed method of calculation is the following:

$$Ep_{consumption}\ (Office + Dwellings + Commercial)\ /\ year \leq\ (Ep_{produced\ locally})\ /\ year$$

Where:

$Ep_{consumption}$ = Primary Energy consumption,

$Ep_{produced\ locally}$ = Primary Energy generated onsite

It should be noted that the primary energy factors of conversion are specific ones, as defined in the frame of the P-Plot competition:

Biomass: 0.2

Electricity: 3.2

In order to provide electricity, heat and cold to the building, the design team decided to use 3 kinds of renewable energy sources available on site:

- solar
- biomass
- geothermal

With 3 main energy systems which are:

- solar PV modules
- a cogeneration system (CHP)
- an absorption chiller

A scheme of the HIKARI energy system design is shown in figure 2.18.

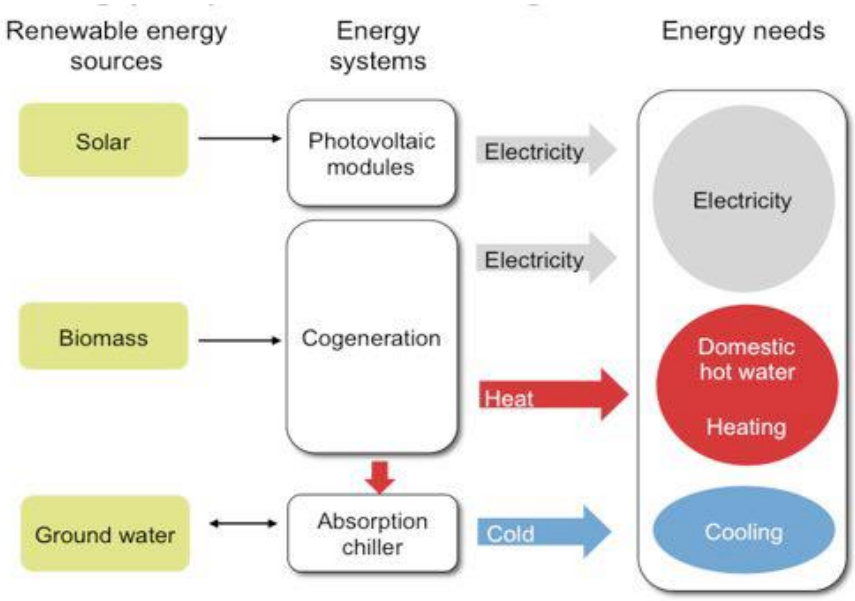

Figure 2. 18 - Overview of the energy system design.

The technical details of these energy systems, which have been designed in partnership with Toshiba as a supplier of most of them, are given below.

2.5.1.2.1 PV systems

The HIKARI building is equipped with 2 kinds of PV systems:

A see-through PV façade on the MINAMI building,

A rooftop PV system on the roof of each of the 3 buildings.

The see-through PV façade as a power of 21 kWp and is used as balcony for the dwellings of the MINAMI building and is highly visible from the street and from the inside of the flat (Figure 2.19).

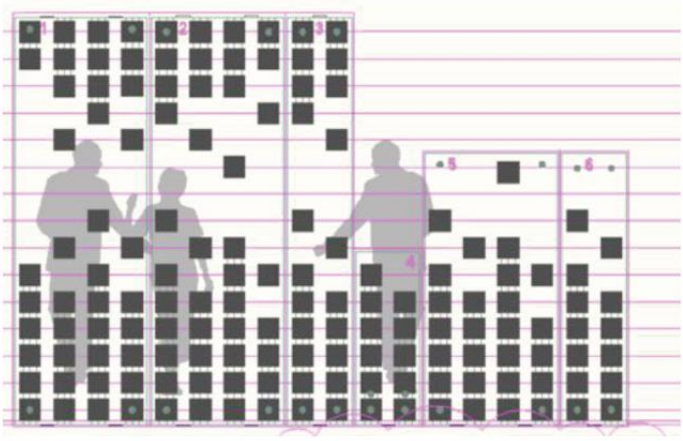

Figure 2. 19 - Custom-made PV modules used as balcony of dwellings.

Therefore, the design team paid a special attention to its design and to safety issues.

Cells: 1120 x Neo Solar Power NP6 multi crystalline cells (5" – 3.8 W)

PV modules: AGC SunEwat / thickness of 21.6 mm / 9 different layouts

Inverters: 3 x SMA Tripower – 18.5 kVA in total

Expected yield: 15 MWh/year

The rooftop PV system has a power of 168 kWp and covers almost all the roof area of the 3 buildings (HIGASHI, MINAMI and NISHI) and has also an esthetical role as it has been design to give a homogenous appearance of the roof surface which is visible from surrounding hills.

PV modules: 700 x Panasonic HIT-N240 (240 Wp)

Inverters: 13 x SMA Tripower – 143 kVA in total

Expected yield: 182 MWh/year

2.5.1.2.2 Cogeneration system

The heat and the domestic hot water of the HIKARI building is generated by a 75 kW CHP unit from COGENGreen, which will be fired by rapeseed oil that is stored in a 90 m3 tank (see Figure 2.20). The power generated by the CHP is simply consumed within the building (self-consumption).

Type: COGENGreen ecoGEN-75SH

Fuel: vegetable oil (rapeseed)

Electric outpour/Heat rating: 75 kW/98 kW

Fuel consumption: 21 l/h

Total efficiency: 85.2%

Expected yield: 275 MWh/year

Figure 2. 20 - CHP unit of COGENGreen.

2.5.1.2.3 Absorption chiller

The cold necessary to cool office places is generated by an absorption chiller, which uses heat from ground water and from the CHP (see Figure 2.21).

Type: YAZAKI WFC-SC30

Heat medium input: 70 kW

Heat flow rate: 7.8 m^3/h (72-64.2°C)

Cooling capacity: 46 kW (8.4-6°C)

Chilled water flow rate: 16.5 m^3/h

Figure 2. 21 - Absorption chiller from Yazaki.

2.5.1.2.4 Ventilation

The 3 buildings all use mechanical air extract systems. In addition, HIGASHI has a specific design to increase natural ventilation at night in order to cool down this building. On each floor the façade has fresh air inlets located on the corners of the building. Also, 2 chimneys located in the middle of the floor generate airflow to extract the heated air (see figure 2.22). The 2x7 chimneys are grouped on the roof of the HIGASHI building and are equipped with a system to open/close them automatically.

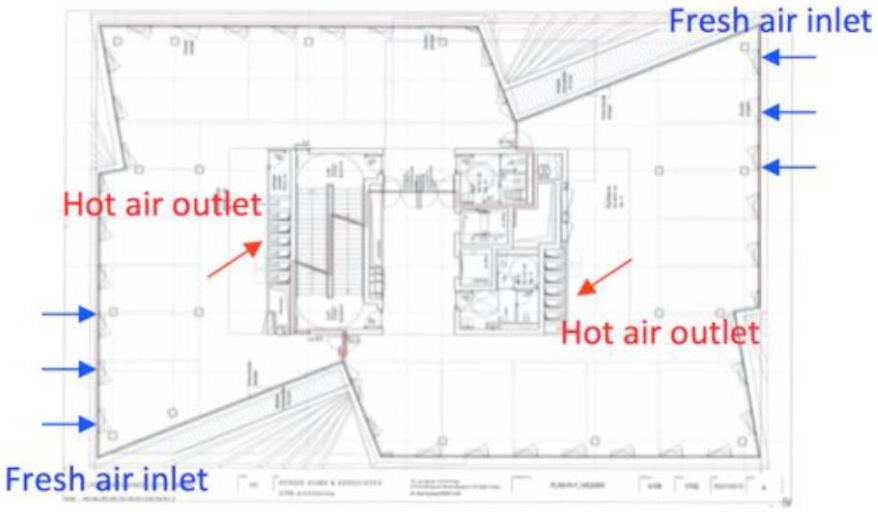

Figure 2. 22 - Natural ventilation flow in the HIGASHI building.

2.5.1.2.5 Storage

The design team undertook many simulations in order to demonstrate that the use of thermal storage could drastically reduce the size of energy production systems. Thus, without thermal storage, energy production systems have to be sized on peak loads but with a storage capacity they can be sized close to the average load (see figure 2.23).

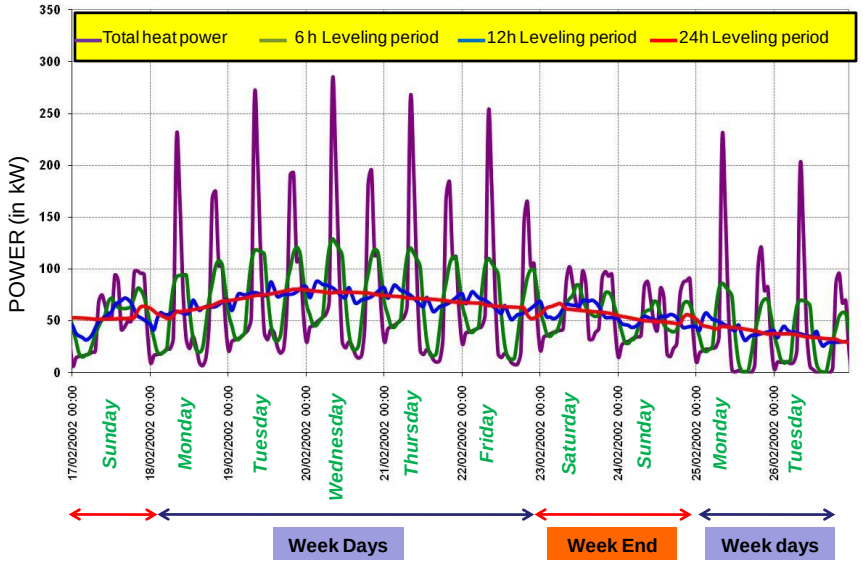

Figure 2. 23 - Heat storage levelling impact on heating power demand for one winter week.

These simulations lead to decide to equip HIKARI with an 8 hour heat storage made of 65 m^3 of water (figures 2.24).

Figure 2. 24 - Water tanks used as heat storage before (left) and after (right) full insulation.

Also, in addition to the heat storage, HIKARI is equipped with a cold storage made of 60 m^3 of phase change material (PCM) stored on tanks in the basement (described in paragraph 3.2). The HIKARI's cold storage system exploits the PCM ability to absorb and release a large amount of thermal energy during its phase transition (Shamsi, 2017) and it is used for optimising and improving the performance of the HIKARI's absorption chiller.

As this system was particularly created for the HIKARI project, it was considered necessary to optimize its technology, in order make it more cost-effective and efficient for future use.

2.6 LIMITATIONS AND LEARNED LESSONS FOR THE STUDY

In spite of the fact that thermal energy storage has been a main topic in research for the last 30 years – and phase change materials (PCM) in particular - the release to market of efficient technologies for the cold storage systems using these materials is quite recent (Nchelatebe Nkwetta et al., 2014), due to the elevated price of the material and its implementation in the building and the PCM thermo-physical properties explained in previous chapters.

Because of the high costs of experimental tests in the real conditions of buildings, numerical simulation, developed analytical methods and different modelings are needed to predict the behavior and results of PCM usage in buildings (Kasaeian et al., 2017) in order to optimize this technique and to make it more efficient and cost-effective.

This work present the multi-objective optimization of an active thermal energy storage system at low temperatures containing PCM that is part of e multi-energy source building. For this purpose, a model has been developed and has been implemented in the MATLAB environment (see paragraph 3.3).

As explained in previous paragraphs, the difficulties that we encountered in this work were linked to the limits in reproduce the particular behavior of PCMs and to identify the system configurations that could minimize the energy consumption of the multi-energy source building HIKARI (described in paragraph 2.5).

The literature review summarized in this chapter largely helped to establish numerical model assumptions and also oriented preliminary laboratory tests (DSC). The design and development of our experimental prototype also took into account the listed case study especially the monitoring system and the density of sensors.

CHAPTER 3

DEVELOPMENT OF THE NUMERICAL MODEL

3) DEVELOPMENT OF THE NUMERICAL MODEL

3.1 INTRODUCTION

Since the aim of this thesis was the optimization of the technology of the innovative HIKARI's thermal energy storage at low temperatures, we needed to develop a numerical model reproducing its functioning.

In order to develop the numerical model, we started analysing the functioning of the reference system and its connection to the HIKARI HVAC system. The description of the technology can be found in the first paragraph of this chapter.

In the second part of the chapter, the development of the numerical model is shown. It was realised using the heat balance approach and the apparent heat capacity method and developed using the MATLAB Simulink environment.

Once numerically and experimentally validated, this model would allow us to optimize the system's technology applying the Genetic Algorithms.

3.2 THE REFERENCE SYSTEM

The HIKARI's low temperature heat storage system relies on the PCM ability to store and release a large amount of thermal energy during its transition phases and it is used for optimising and improving the performance of the HIKARI's absorption chiller. Through the presence of the latent heat storage system, in fact, it is possible to reduce the difference between the chiller's cold and hot inlet water temperature and the short cycling.

Its operating philosophy is explained in the next paragraph.

3.2.1 Description of the reference thermal energy storage system

The reference thermal energy storage system at low temperatures is part of the complex heating, ventilation, and air conditioning (HVAC) system of the HIKARI building group.

The scheme of this system is shown in figure 3.1. The cooling system includes an absorption chiller, an adiabatic dry cooler, a vapor-compression refrigeration system and a storage system, while the heating system includes a cogeneration unit feed with rapeseed oil, a gas boiler (that is connected to the absorption chiller) and a storage system.

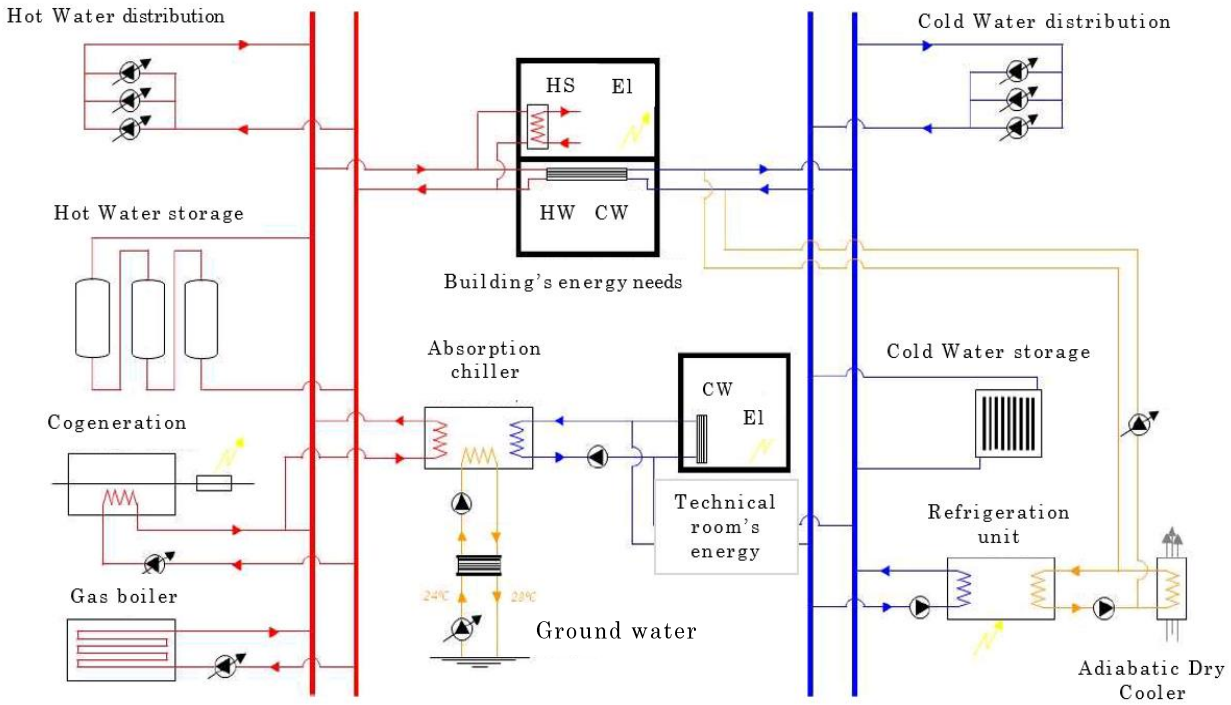

Figure 3. 1 - Scheme of the HVAC system of HIKARI.

The PCM based thermal storage system at low temperatures (defined as "cold water storage system in the above figure) is connected to an absorption chiller (46kW) that provides the water during the charging and discharging phases. This heat exchanger is used in order to improve the performance of the chiller and reduce the short-cycling.

Concerning its technology, the the water-PCM heat exchanger consists of 60 m^3 of phase change material (PCM) (subject to a phase change between 9 and 11°C) processed into a gelatinous form and enclosed in impermeable cylindrical stick packages (Figure 3.2). A quantity of 100g of PCM (paraffin Ecojoule®) is enclosed in each cylindrical stick package and its dimensions are approximately 274mm x 40mm in size, 25 to 30mm in diameter.

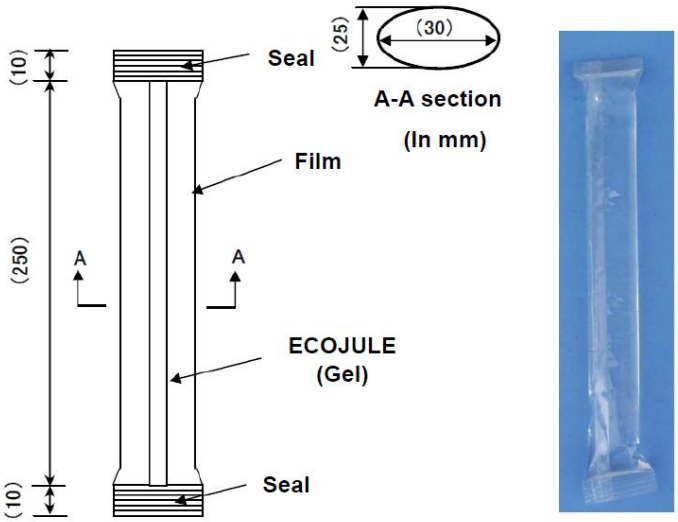

Figure 3. 2 - Latent Heat Thermal Storage material package (gel pack).

The sticks are inserted in plastic cases (Figure 3.3) whose dimensions are 465 x 345 x 280mm. Each case is filled with 156 PCM sticks.

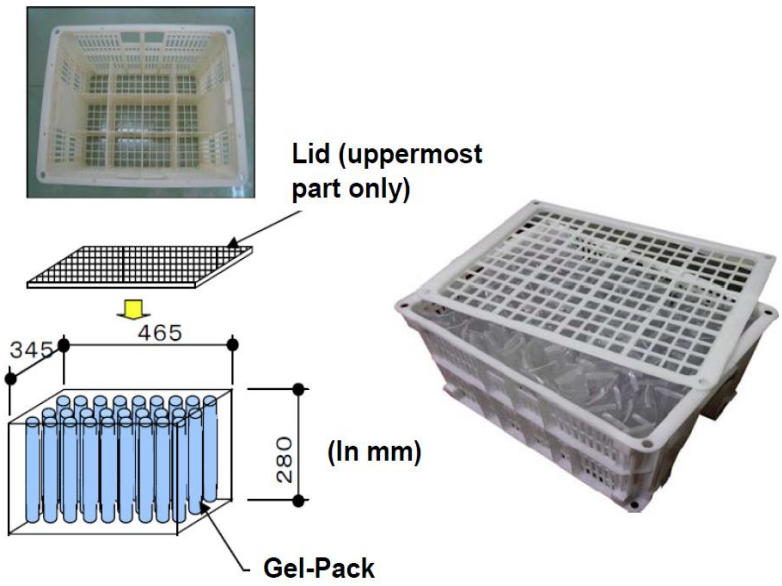

Figure 3. 3 - Plastic case filled with gel packs.

Once filled with the gels sticks, the plastic cases are positioned in four insulated thermal storage tanks (Figure 3.4).

Figure 3. 4 - Typical installation of the plastic cases into every isolated tank.

A flow of water runs into each tank, entering the system through tubes situated on the top of the tank, passing from small openings with a flow rate of 3 l/minute. The plastic cases have large apertures so as not to impede the water flow that runs into the tank when they are stacked in it. After passing through the gel sticks layer (PCM), the water exits the system passing through openings present in other tubes located at the bottom of the tanks (Figure 3.5).

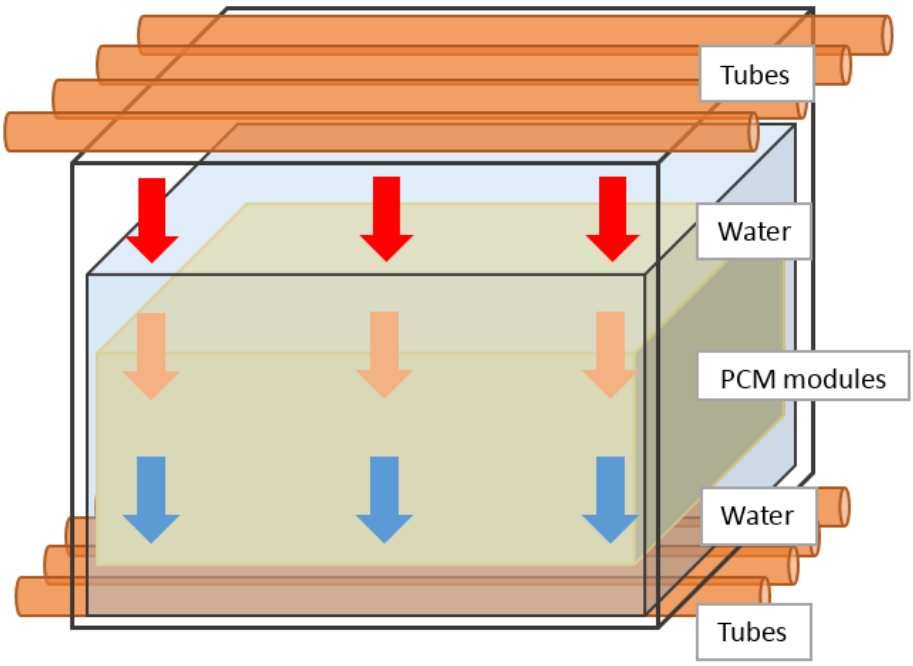

Figure 3. 5 – Scheme of one of the four tanks making up the system.

Once the temperature of the water into the four tanks is 6°C, the system is considered "100 % charged", and the water that it contains is sent to the absorption chiller, reducing the difference between the chiller's cold and hot inlet water temperature. After the heat exchange, the water flow comes back to the storage tank and it continues this cycle until the tank's temperature reaches 10°C. In that moment the system is considered "discharged" and it is no longer available until it is charged again.

The scheme of the operation is shown in figure 3.6:

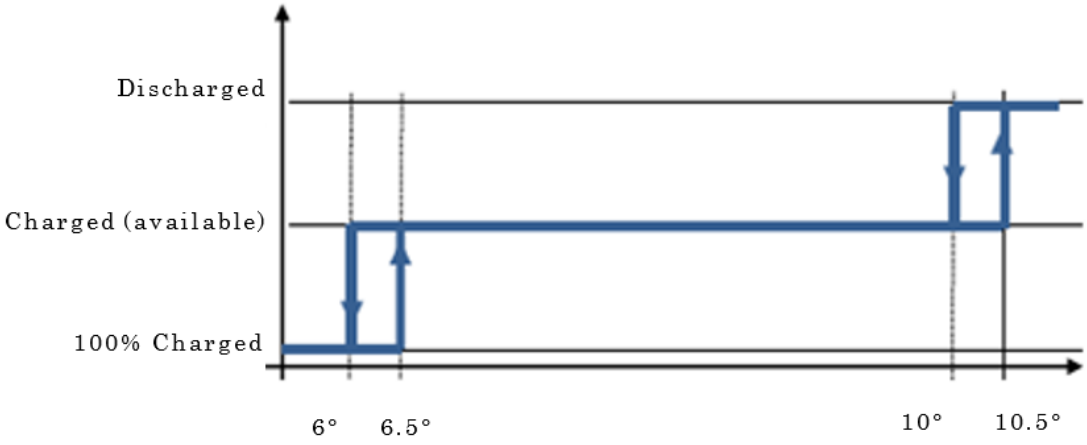

Figure 3. 6 - Scheme of the functioning of the thermal storage system at low temperatures.

An example of the temperature and water flow evolution into each tank is shown in figure 3.7:

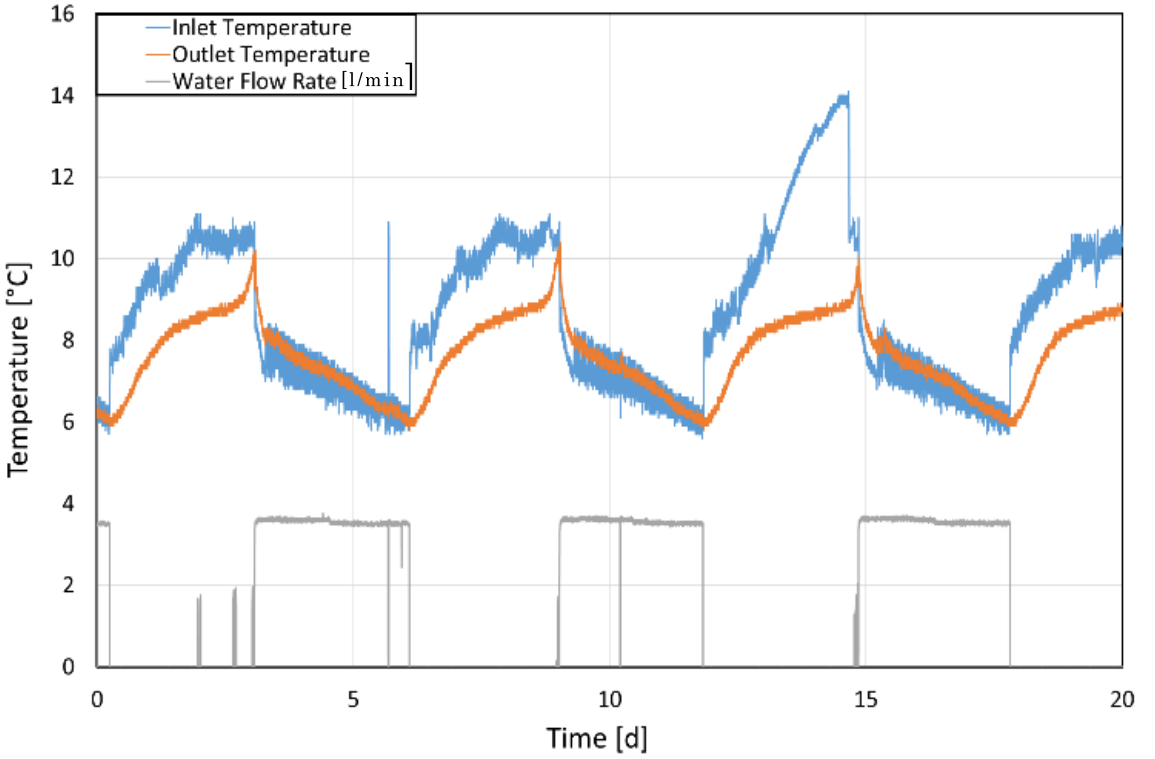

Figure 3. 7 - Example of temperatures recorded by the sensors and the inlet water flow rate in each tank.

When the system is in its discharged phase (the temperature of the water in the four tanks is equal or greater than 10°C) a vapor-compression refrigeration system (VCRS) substitutes its operation, improving the performance of the absorption chiller and reducing

the difference between the chiller's cold and hot inlet water temperature and its short-cycling.

The scheme of the mutual working between the absorption chiller, the storage system and the VCRS, that depends on the power needs and the storage system state, is shown in figures 3.8, 3.9 and 3.10:

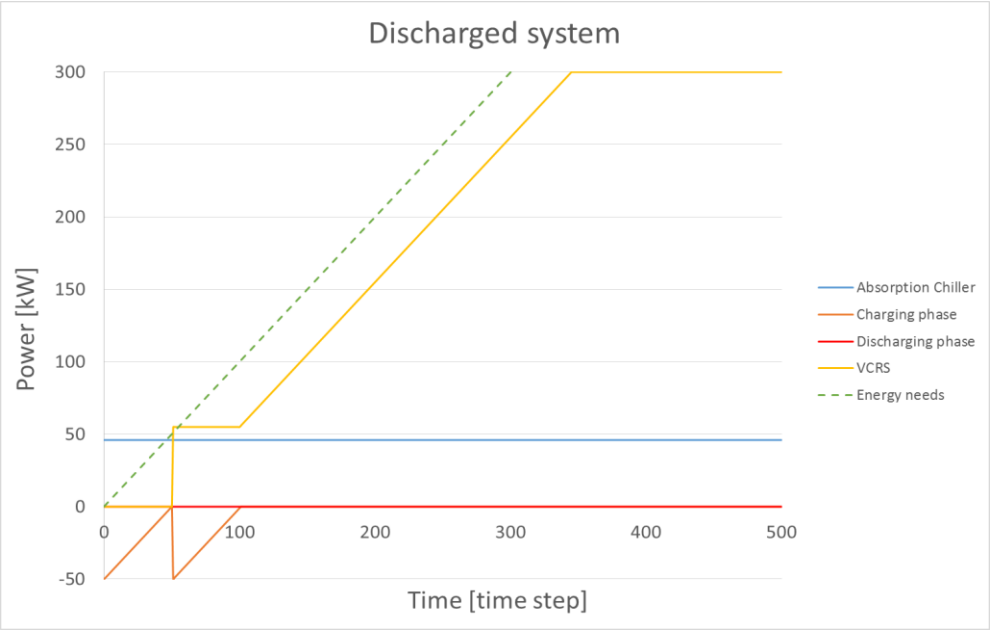

Figure 3. 8 – Example of the mutual working between the absorption chiller, the storage system and the VCRS when the storage system's temperature is equal to or greater than 10°C.

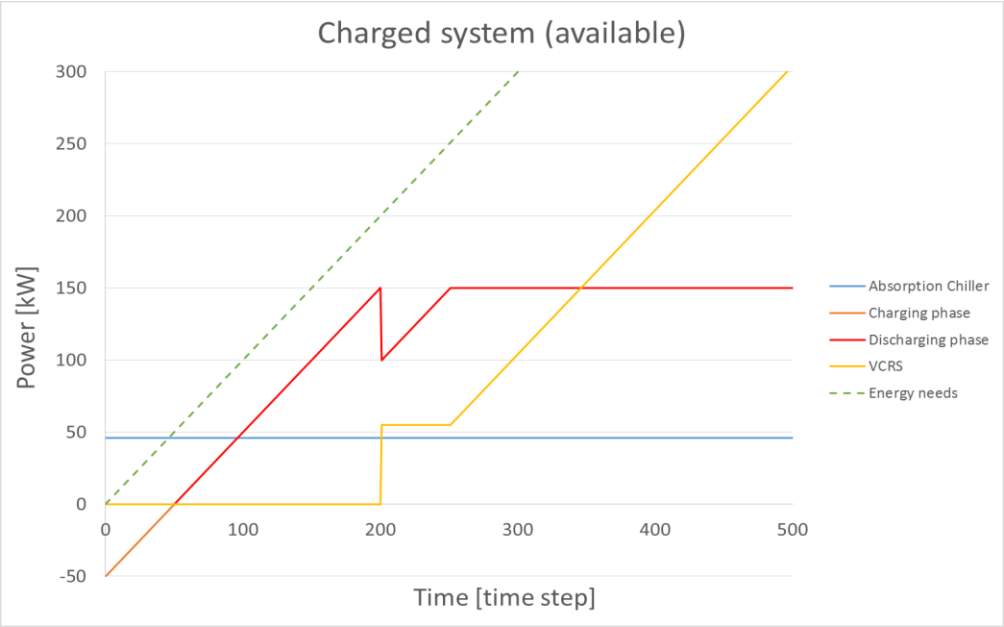

Figure 3. 9 – Example of the mutual working between the absorption chiller, the storage system and the VCRS when the storage system's temperature is between 5 and 10°C.

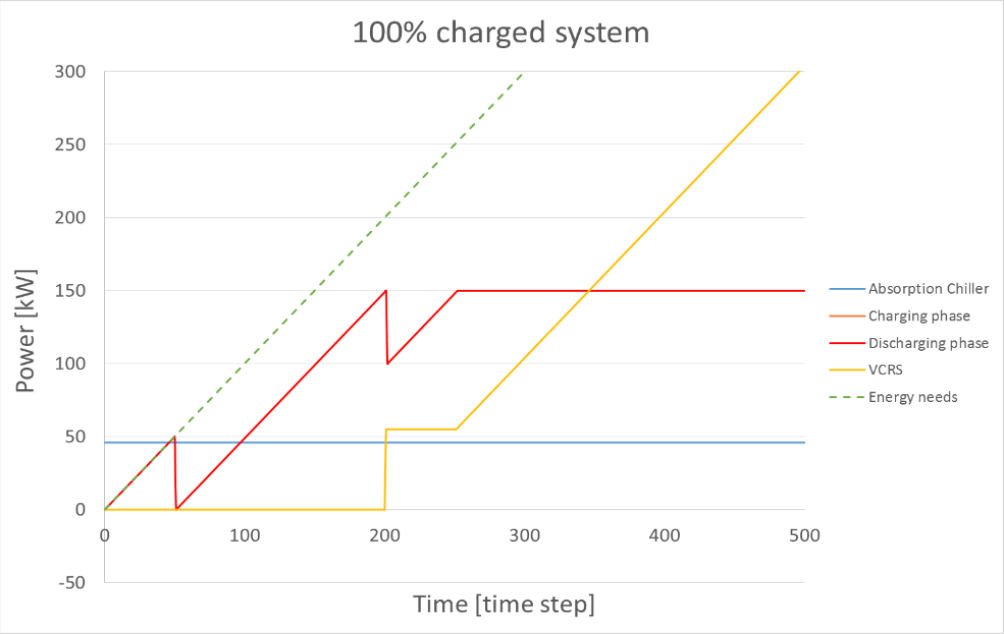

Figure 3. 10 - Example of the mutual working between the absorption chiller, the storage system and the VCRS when the storage system's temperature is 6°C.

3.3 NUMERICAL MODELLING

This paragraph exposes the design and development of the numerical model reproducing the behaviour of the heat exchanger for cooling purposes described in the previous paragraph.

It presents all the procedure followed for the model development: the heat transferring phenomena considered, layer selection, nodal discretization, heat balance equation formulation, matrix writing and solution.

This model will be numerically and experimentally validated and then integrated into the HIKARI's HVAC model in order to optimize the actual version of this storage system, so as to improve the productivity and reduce the losses during its mutual working with the absorption chiller.

3.3.1 State of the art of the numerical modelling

Contrary to experimental studies, numerical simulations can analyse physical phenomena quickly and cheaply. Furthermore, validated models can be used in parametric studies having a greater versatility compared to experimental prototypes. For this reason, numerical simulation is largely used for reproducing complex physical phenomena, such as the nonlinear behaviour and the variation of thermo-physical properties of PCMs.

Fundamentally, the developed models are based on the formulation of a series of energy related equations and their solution using analytical or numerical methods.

In PCMs case, the boundary separating two different phases develops and moves in the matter during the process. Transport properties vary considerably between phases, which result in totally different rates of energy, mass and momentum transport from one phase to another. In these problems (called Stefan problems), the position of the moving boundary cannot be identified in advance, but has to be determined as an important constituent of the solution.

Because of the complexity of Stefan problems, the analytical methods are very rarely used (Liu et al., 2014). They are utilized in one-dimensional problems with mostly simple initial and boundary conditions and constant thermal properties. Therefore, approximate numerical solutions are usually used to handle this class of problems.

The numerical methods for resolving these problems can be generally divided into:

1) Fixed grid methods

These methods consist of fixed space grids where the boundary is tracked by the use of an auxiliary function (Voller et al., 1990). This method introduces enthalpy apart from the use of temperature as a dependent variable, and as it is continuous only in time (and temperature only in space) the governing equation is the same for the two phases and can be solved over the whole space as a fixed domain.

The two mainly fixed-grid methods that have been proposed are enthalpy-based methods and the effective heat capacity method (AL-Saadi and Zhai, 2013).

2) Deforming grid methods

These methods allow the grid nodes move along with the moving boundary layer and thus the exact location of the moving boundary is evaluated on a grid at each step, allowing to avoid the constraints of the fixed grid formulation (Alexiades et al., 1993). The basic idea is to cluster more grid points in the regions with large solution variations, singularities or oscillations.

3) Hybrid method

These methods utilize the features of the previous numerical methods. They use a fixed background grid and employ local front tracking schemes to follow the movement of the boundary (Voller et al.,2006).

3.3.2 The heat balance approach

In order to obtain the dynamic model, the heat balance approach was chosen. It is based on the division of the analysed system into a defined number of volume elements (it is a fixed grid method) and the subsequent application of the energy balance equations for each of them. The heat balance equations are formed for every volume element and solved at each time step to calculate the temperature evolution at the considered nodes.

This approach assumes that the temperature value is the same for each volume element. When the system is composed of two or more different materials (as in our case in which there are water and PCM) different layers are considered, in order to better study the behaviour of each material.

In our case, the first step was to analyse all the relevant energy flows present in the system, in order to write the energy balance equations (in our case conduction, convection and advection transfers were considered).

Once the energy balance equations were written, the finite difference method was employed, in order to approximate the partial differential equations.

Finally, the equations were solved at each time step and for each volume through the software MATLAB Simulink.

This method was chosen as it was previously used and provided good results for similar configurations (Stathopoulos and El Mankibi, 2016).

3.3.3 The apparent heat capacity method

The problem of the phase change of the heat storage medium was resolved using the "apparent heat capacity method". It consists in representing the phase change through an apparent increase of the material's heat capacity value for a certain temperature range ; this increase represents the corresponding latent heat absorption/release.

In case of uniform process, we can define the apparent heat capacity (Cp) as:

$$C_{p,app} = \begin{cases} C_{p,s}\ (for\ the\ solid\ phase, where\ \ T < T_s) \\ C_p(T)\ (for\ the\ phase\ change, where\ T_s < T < T_l) \\ C_{p,l}\ \ (for\ the\ liquid\ phase, where\ \ T > T_l) \end{cases}$$

In order to obtain the C_p values of our PCM, we had to make a Differential Scanning Calorimetry (DSC) test, that will be explained in the next paragraph.

3.3.3.1 The DSC method

The heat capacity values of the PCM were obtained using the Differential Scanning Calorimetry (DSC) method. The DSC is a measuring technique based on the comparison of a sample material (in this case paraffin) with a reference material (with known properties) while undergoing a heating or cooling process. More particularly, known masses of the sample and of the reference material are heated at a constant rate while a temperature control system measures the temperature difference between the two pans

and adjusts this difference to zero by controlling a differential component of the total heating power.

The measurement of this differential power and the knowledge of the heat capacity value of the reference material allow the calculation of the heat capacity of the sample material.

Once the DSC test is made, the computation of the specific heat capacity of the specimen along the tested temperatures $C_p(T)$ (J/g·K) is made according to the formula:

$$C_p(T) = \frac{(DSC(T)_s)}{\varphi} \qquad \textit{Equation 3.1}$$

Where $DSC(T)_s$ is the heat flow across the specimen at temperature T from the thermogram (m·W/m·g), and φ is the heating rate (°C/s) (Kheradmand et al., 2015).

In our case, measurements were effectuated at the Laboratory of Tribology and Systems Dynamics (LTDS) of the Ecole Centrale of Lyon and they were made on a 0.01 g sample, at a heating/cooling rate of 0.05 °C/min and between -5 and 20 °C.

Results are illustrated in figures 3.11 and 3.12.

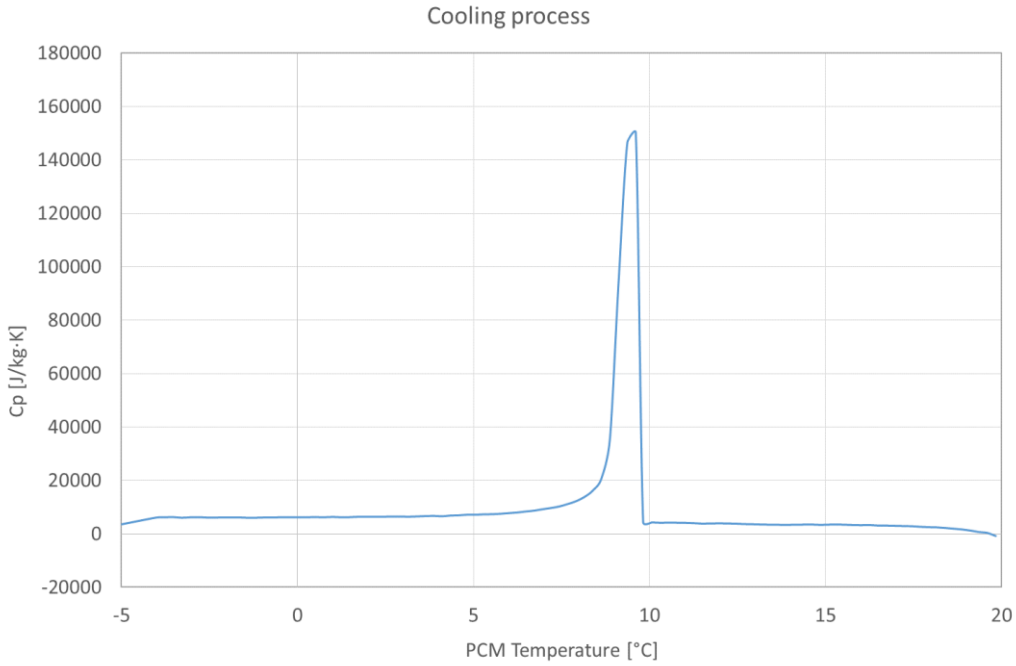

Figure 3. 11 - DSC obtained heat capacity curves for cooling process.

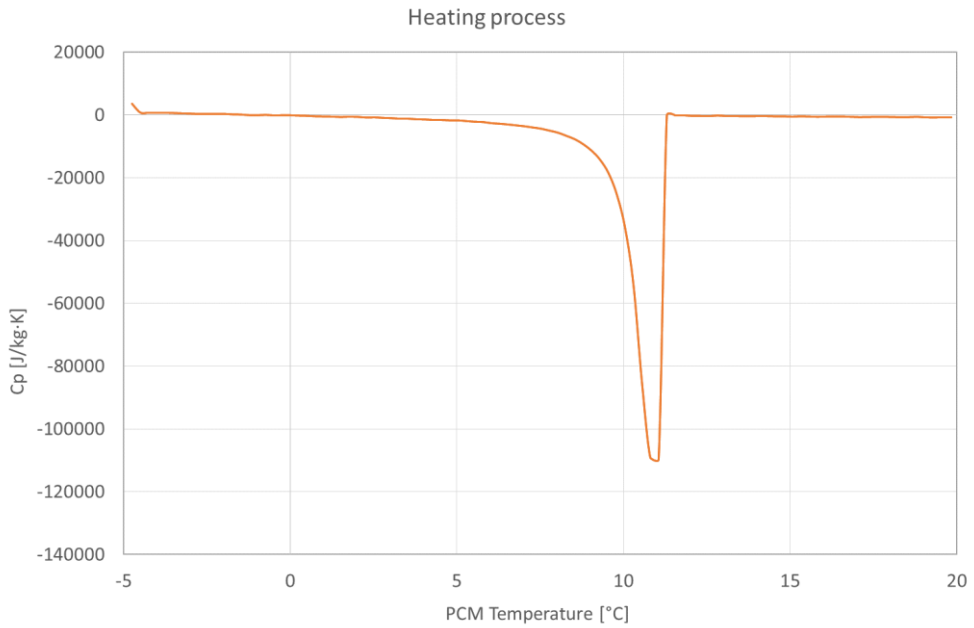

Figure 3. 12 - DSC obtained heat capacity curves for heating process.

The graphics show that a single peak appear on the temperature curve of the PCM for both the charging and discharging phase. In figure 3.12 we can see that, during the charging phase (the cooling process), the peak is reached at about 9.5 °C, while in the discharging one it is reached at about 11 °C. These peaks correspond to the freezing and melting point of the PCM respectively.

3.3.4 Developing environment selection

In order to develop our numerical model, we had to choose a software able to let us create a fast and accurate model, capable of reproducing the heat exchange between water and PCM and of being coupled to the HIKARI's HVAC model for the subsequent optimization phase. Thus, a three dimensional numerical model was created in MATLAB Simulink environment, using the heat balance approach and the apparent heat capacity method.

3.3.4.1 MATLAB Simulink

The MATLAB Simulink environment was chosen because of these reasons:

- The HIKARI's HVAC model, that would later be used for the optimization of the thermal storage system's technology, was also developed under the same environment ; thus, the coupling between the two models was facilitated.
- It offers a powerful optimization toolbox.
- We could insert our own heat balance equations in a matrix form, giving us the opportunity to automate the modification of several parameters during the simulations.

- We could use the MATLAB Simulink's block S-Function (example in figure 3.13) , that interacts with the Simulink environment by requesting input variables and supplying output results, extending the capabilities of the Simulink environment by automatically loading and computing a subroutine written in various programming languages (MATLAB®, C, C++, or Fortran).

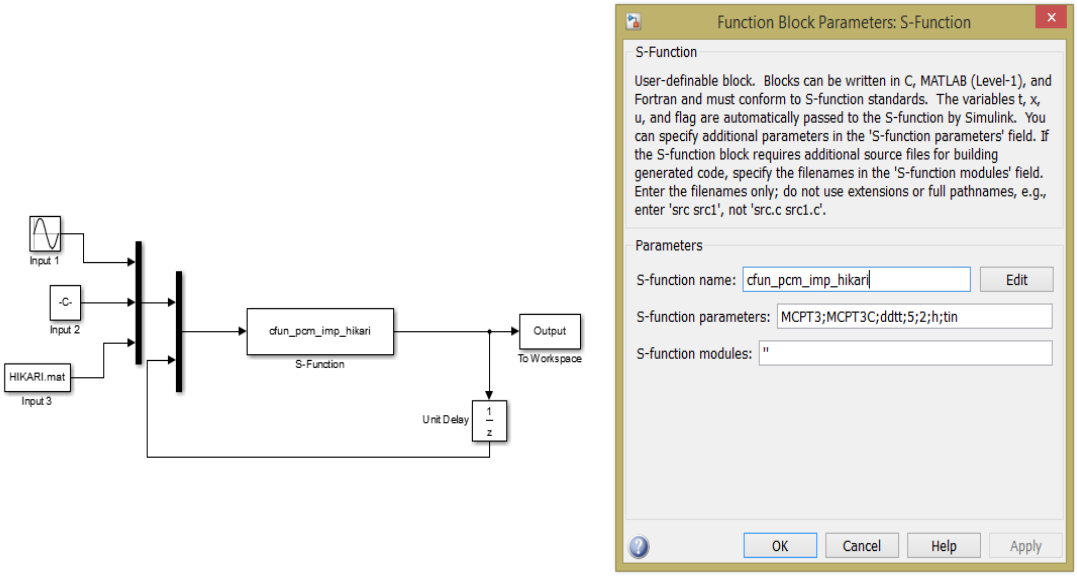

Figure 3. 13 - S-function block under Simulink environment (left) and parameters definition block (right).

3.3.4.2 TRNSYS

The energy simulation software TRNSYS proposed a numeric model developed to simulate heat transfer in phase change materials (PCM) plunged in water tank storage. This model, based on the enthalpy approach, takes into account the conduction and the convection into PCM as well as at the interface between PCM and water of the storage (Bony et Citherlet, 2008). This model has been implemented in an existing TRNSYS type of water tank storage (type 60) and it allows the simulation of a water storage tank filled with PCM modules made of different materials and different shapes such as cylinders, plates or spheres bed.

In return, all the modifications must be made punctually and upon the user's request. It means that an automation of the modification of several parameters simultaneously and in series cannot be realized with this software.

For this reason it was chosen to realize the model using the MATLAB Simulink environment.

3.3.5 The nodal discretisation of the model and the application of the heat balance approach

It was chosen to model the heat exchange between the PCM and the water flow by reproducing the thermal exchange between a single PCM gel sticks and the water.

As the thickness of the enclosing plastic film of the gel sticks is minor (0.5 mm), the thermal resistance of this layer is considered negligible. Thus, two layers were considered of the discretization: PCM and water.

Each layer was then discretized lengthwise into n equal regions (nodes) of length L/n, where L is the total length of the PCM/water exchanger (length of the PCM stick). The PCM layer was further discretized crosswise in m nodes which correspond to m concentric cylinders with a thickness of r = R/m where R is the radius of the gel stick contained in a cylinder of water (i = w node) (Figure 3.14).

The discretization into multiple nodes offers the possibility of a more thorough treatment of the medium where the phase change occurs. Subscript letter j signifies the nodal lengthwise position for each layer (j = 1 to n) and the subscript i signifies the nodal crosswise position in the PCM layer (i = 1 to m).

The thermal resistances (represented with black rectangles) are formulated between nodes (represented with red dots) (Figure 3. 15).

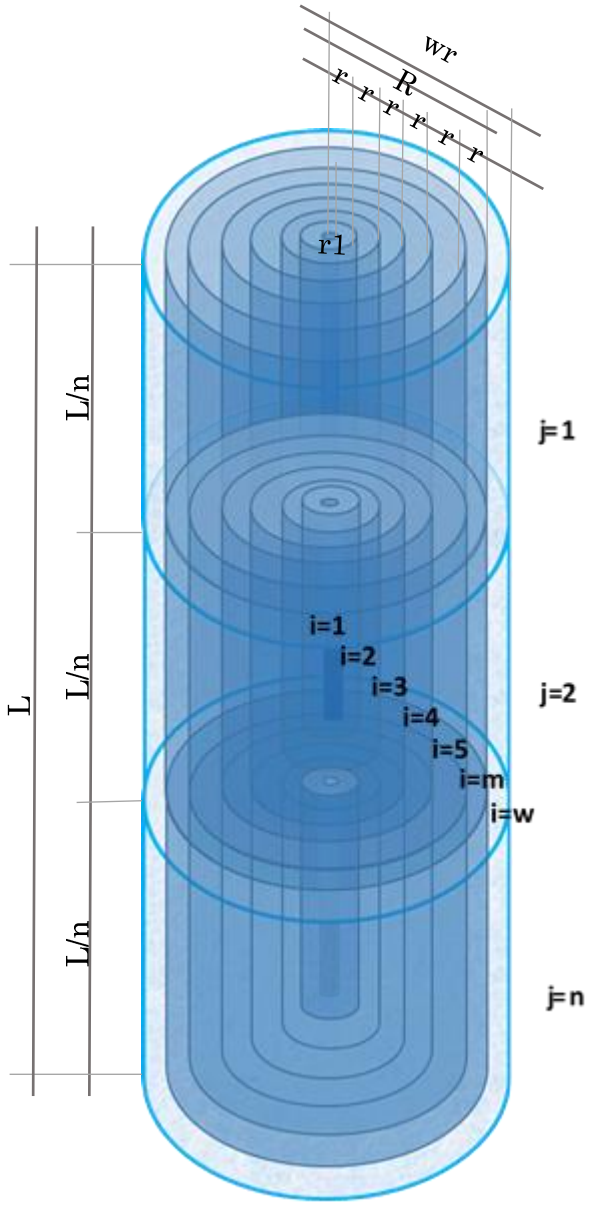

Figure 3. 14 - Scheme of the discretization of the model.

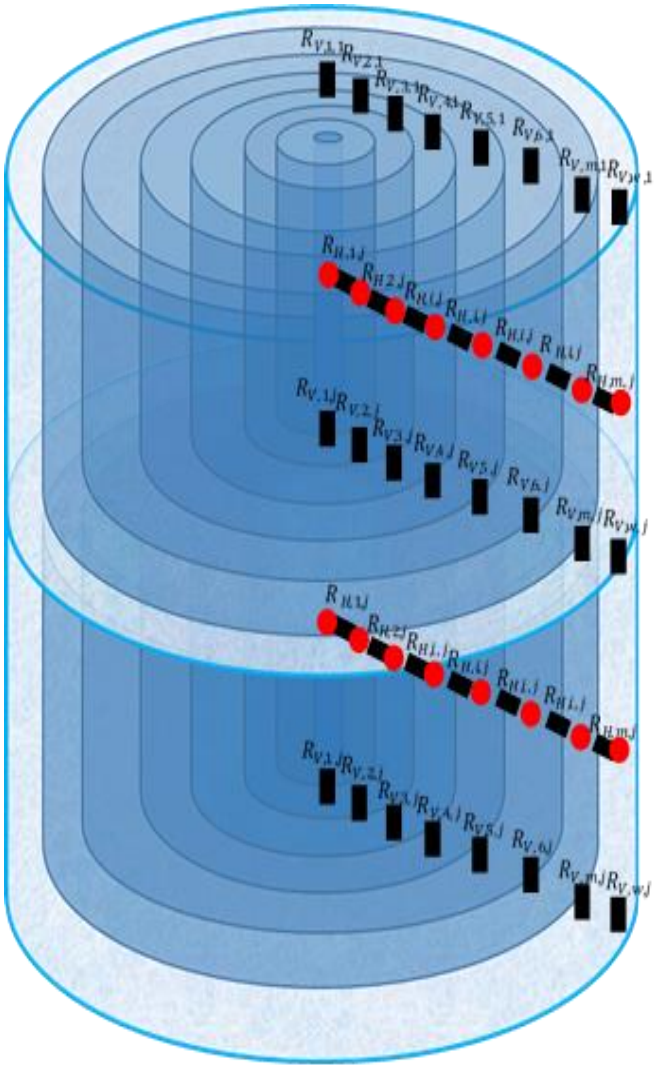

Figure 3. 15 -Overview of the resistances between the control volumes.

3.3.6 Writing of the energy balance equations and transformation to matrix

In order to write the energy balance equations we considered conduction in PCM, convection between water and PCM and advection in water as the possible transfer phenomena that could take place in each node, so the equations could be written as follows:

$$\begin{Bmatrix} Temperature \\ change\ rate \\ in\ node \end{Bmatrix} = \begin{Bmatrix} Conduction \\ transfers \\ in\ node \end{Bmatrix} + \begin{Bmatrix} Convective \\ transfers \\ in\ node \end{Bmatrix} + \begin{Bmatrix} Advection \\ transfers \\ in\ node \end{Bmatrix}$$

Equation 3.2

The energy balance equation was written for each node, taking into account that the heat entering into that node is equal to the heat exiting that position.

The temperature change rate (or storage of heat in the node) can be expressed as follows:

$$\left\{\begin{matrix}Temperature\\change\ rate\\in\ node\end{matrix}\right\} = \rho CpVdT \qquad \textit{Equation 3.3}$$

Where:

ρ :	Density of the node's medium	[kg/m^3]
Cp :	Specific heat capacity of the node's medium	[J/kg·K]
V:	Volume of the node	[m^3]
T :	Temperature of the node	[°C]
t :	Time	[s]

The conduction term concerns the PCM nodes. It is given by the following equation:

$$\left\{\begin{matrix}\text{Conduction}\\\text{transfers}\\\text{in node}\end{matrix}\right\} = \frac{T_{i-1} - 2 \cdot T_i + T_{i+1}}{R} \qquad \textit{Equation 3.4}$$

Where:

T_i :	Node temperature at node i	[°C]
T_{i-1} : :	Node temperature at node i–1	[°C]
T_{i+1}	Node temperature at node i+1	[°C]
$R = \frac{L/n}{S \cdot \lambda}$	Thermal resistance between neighbouring nodes	[W/K]
L/n:	Length of node	[m]
S :	Contact surface between neighbouring PCM nodes	[m²]
λ :	Conductivity of the node's material	[W/m · K]

The advection term concerns the water layer and represents the heat transported into a water node i from a neighbouring water node i–1 and from the water node i to a neighbouring water node i+1. In its explicit form, the advection term is given by the following equation:

$$\left\{\begin{matrix}\text{Advection}\\\text{transfers}\\\text{in node}\end{matrix}\right\} = \dot{m}\, Cp\, (T_{i-1} - 2 \cdot T_i + T_{i+1}) \qquad \textit{Equation 3.5}$$

Where

T_i :	Node temperature at node i	[°C]
T_{i-1} :	Node temperature at node i-1	[°C]
T_{i+1}	Node temperature at node i+1	[°C]
Cp :	Specific heat capacity of the node's medium	[J/kg·K]
$\dot{m}$:	Waterflow rate	[kg/s]

The convection term concerns the water layer and the most external nodes of the PCM layer, adjacent to the water layer. It is given by the following equation:

$$\left\{\begin{matrix}\text{Convective}\\ \text{transfers}\\ \text{in node}\end{matrix}\right\} = \frac{(\Delta T_{w-p})}{R} \qquad \textit{Equation 3.6}$$

Where

ΔT_{w-p} :	Temperature difference between adjacent water and PCM nodes	[°C]
$R = \frac{1}{S \cdot h}$	Thermal resistance between neighbouring nodes	[W/K]
S :	Contact surface between water and PCM nodes	[m²]
h :	Heat transfer coefficient	[W/m²·K]

The average temperature

$$\overline{T_{i,J}} = \frac{({T_{i,j}}^{t} + {T_{i,j}}^{t-dt})}{2} \qquad \textit{Equation 3.7}$$

is introduced as the temperature variation is considered to be linear and the heat balance equation is formulated for each layer. The finite difference method is used to approximate the temperature derivative terms and the final form of the equations leads to a matrix formulation for each layer (Stathopoulos et al., 2015).

3.3.6.1 Model assumptions

The objective of the numerical modelling was to reproduce the behaviour of the reference system in order to obtain model able to calculate the temperature of the water after its

heat exchange with the PCM modules. In order to develop an accurate and fast model, some assumptions had to be made.

First of all, the water flow is considered the same for all the sticks: it was calculated by dividing the water flow that crosses each tank for the total number of gel sticks.

The model considers convection transfers between the water and the PCM layers, conduction transfers between the PCM layers and advection transfer between adjacent water nodes. It does not take into account convection inside the PCM during the melting and the liquid phases, irradiation and, as anticipated in paragraph 3.3.5, the thermal resistance of the enclosing plastic film of the gel sticks.

For the calculation of the temperature change rate in j = n nodes we considered a convection transfer between PCM nodes and the average temperature of the adjacent water node at the previous time step ($\overline{T_{w,n}}^{t-dt}$). It was necessary as we could not obtain the temperature of the water node $\overline{T_{w,n}}$ before calculating it, but we needed a water temperature value for the convection transfer calculation.

We used the same assumption for the advection transfer calculation between the j = n water node and the adjacent water node.

Another assumption that we made was for the i = 1 node: we consider a unidirectional conduction transfer from it to the i = 2 node (without considering an exchange between another internal node). This assumption was made for simplifying the calculation. In order to reduce the effect of this assumption, we assigned a fixed radius of 0.001 m (r1) to the i = 1 node.

3.3.6.2 The heat transfer coefficient calculation

The convective heat transfer coefficient was calculated taking into account the packing density of the gel sticks into the water tanks $\left(\frac{D_h}{R_{c,out}}\right)$. The relation between the packing density of the gel sticks and the Nusselt number (Nu) value is shown in figure 3.16:

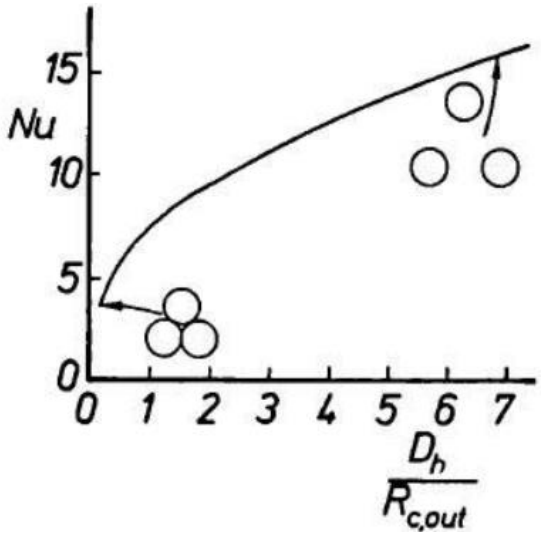

Figure 3. 14 – Nusselt number values curve with reference to the packing density of the gel sticks for laminar flow (Bubbico et al., 2014).

We can therefore determine the Nusselt number using the formula:

$$Nu = 3.66 + 4.12 \cdot \left(\frac{D_h}{R_{c,out}} - 0.205\right)^{0.569}$$ *Equation 3.8*

Once calculated, we obtained the convective heat transfer coefficient using the formula

$$h = \frac{Nu \cdot \lambda}{R_{c,out}}$$ *Equation 3.9*

(with $R_{c,out}$ = external radius of the gel stick and λ = *water conductivity).*

The obtained value has been 160 W/m² · K.

The following section presents the energy balance equation writing for each node of the water and PCM layers.

3.3.6.3 Water layer

The application of the heat balance equation for the water nodes results in the following equation:

$$\frac{\rho_w . Cp_w . V_w}{dt} \cdot 2. \left(\overline{T_{w,J}} - T_{w,j}^{t-dt}\right) = \dot{m} \cdot Cp_w \cdot \left(\overline{T_{w,J-1}} - 2 \cdot \overline{T_{w,J}} + \overline{T_{w,J+1}}\right) + \left(\frac{h \cdot 2 \cdot \pi \cdot mr \cdot L}{n} + \frac{2 \cdot \pi \cdot k \cdot (L/n)}{\ln \frac{(mr)}{(mr - r/2)}}\right) \cdot \left(\overline{T_{m,J}} - \overline{T_{w,J}}\right);$$ *Equation 3.10*

Where:

ρ_w :	Water density	[kg/m^3]
Cp_w : :	Specific heat capacity of the water	[J/kg ·K]
$V_{w,j}$:	Volume of the water node	[m^3]
dt :	Time step	[s]
$\overline{T_{w,J}}$:	Average temperature of the water node	[°C]
$\overline{T_{m,J}}$:	Average temperature of the adjacent PCM node	[°C]
ṁ :	Water flow rate	[kg/s]
h :	Heat transfer coefficient	[W/m² ·K]
λ:	Water conductivity	[W/m ·K]
r :	Radius of the gel stick	[m]
mr:	Radius of the gel stick	[m]

L:	Length of the gel stick	[m]
m:	Number of nodes of the crosswise discretization	
n:	Number of nodes of the lengthwise discretization	

If we consider:

$R_{V,w,j} = \frac{1}{\dot{m} \cdot Cp_w}$ Thermal resistance between neighboring water nodes [W/K]

$R_{H,m,j} = \frac{1}{h \cdot 2 \cdot \pi \cdot mr \cdot (L/n)} + \frac{\ln \frac{(mr)}{(mr - r/2)}}{2\pi \cdot \lambda \cdot (L/n)}$ Thermal resistance between water and PCM nodes [W/K]

Then we can re-write the equation 3.10 as:

$$\frac{\rho_w . Cp_w . V_w}{dt} \cdot \left(\overline{T_{w,J}} - T_{w,j}^{t-dt}\right) = \frac{\left(\overline{T_{w,J-1}} - 2\overline{T_{w,J}} + \overline{T_{w,J+1}}\right)}{2 . R_{V,w,j}} + \frac{\left(\overline{T_{m,J}} - \overline{T_{w,J}}\right)}{2 . R_{H,m,j}}; \quad \textit{Equation 3.11}$$

Out of which $T_{w,j}^{t-dt}$ can be expressed as function of $\overline{T_{w,J-1}} + \overline{T_{w,J+1}}$ and $\overline{T_{w,J}}$:

$$T_{w,j}^{t-dt} = \overline{T_{w,J}} \cdot \left[1 + \left(\frac{dt}{\rho_w . Cp_w . V_w}\right) \cdot \left(\frac{2}{2 . R_{V,w,j}} + \frac{1}{2 . R_{H,m,j}}\right)\right] - \quad \textit{Equation 3.12}$$

$$\frac{dt}{2 . \rho_w . Cp_w . V_w \cdot R_{V,w,j}} \cdot \left(\overline{T_{w,J-1}} + \overline{T_{w,J+1}}\right) + \frac{dt}{2 . \rho_w . Cp_w . V_w \cdot R_{H,m,j}} \cdot \left(\overline{T_{m,J}}\right);$$

Setting:

$a_w = 1 + 2 \cdot b_w + c_w$

$b_w = \frac{dt}{2 . \rho_w . Cp_w . V_w \cdot R_{V,w,j}}$

$c_w = \frac{dt}{2 . \rho_w . Cp_w . V_w \cdot R_{H,m,j}}$

The final equation is obtained:

$$T_{w,1}^{t-dt} = a_w \cdot \overline{T_{w,1}} - b_w\left(\overline{T_{w,inlet}} + \overline{T_{w,J+1}}\right) - c_w \cdot \left(\overline{T_{m,1}}\right) \qquad \text{for node j = 1} \qquad \textit{Equation 3.13}$$

$$T_{w,j}^{t-dt} = a_w \cdot \overline{T_{w,J}} - b_w\left(\overline{T_{w,J-1}} + \overline{T_{w,J+1}}\right) - c_w \cdot \left(\overline{T_{m,J}}\right) \qquad \textit{Equation 3.14}$$

$$T_{w,n}^{t-dt} = a_w \cdot \overline{T_{w,n}} - b_w\left(\overline{T_{w,J-1}} + \overline{T_{w,n}^{\,t-dt}}\right) - c_w \cdot \left(\overline{T_{m,n}}\right) \qquad \text{for node j = n} \qquad \textit{Equation 3.15}$$

Equations 3.13, 3.14 and 3.15 can then be written in a matrix equation, representing nodes 1 to n:

$$\begin{bmatrix} T_{w,1}^{t-dt} \\ \vdots \\ T_{w,j}^{t-dt} \\ \vdots \\ T_{w,n}^{t-dt} \end{bmatrix} = \begin{bmatrix} a_w & -b_w & 0 & \dots & 0 \\ -b_w & \ddots & \ddots & \ddots & \vdots \\ 0 & \ddots & a_w & \ddots & 0 \\ \vdots & \ddots & \ddots & \ddots & -b_w \\ 0 & \cdots & 0 & -b_w & a_w \end{bmatrix} \times \begin{bmatrix} \overline{T_{w,1}} \\ \vdots \\ \overline{T_{w,J}} \\ \vdots \\ \overline{T_{w,n}} \end{bmatrix} + \begin{bmatrix} -c_w & 0 & \cdots & \cdots & 0 \\ 0 & \ddots & \ddots & & \vdots \\ \vdots & \ddots & \ddots & \ddots & \vdots \\ \vdots & & \ddots & \ddots & 0 \\ 0 & \cdots & \cdots & 0 & -c_w \end{bmatrix} \times \begin{bmatrix} \overline{T_{m,1}} \\ \vdots \\ \overline{T_{m,J}} \\ \vdots \\ \overline{T_{m,n}} \end{bmatrix} + \begin{bmatrix} -b_w \cdot \overline{T_{w,inlet}} \\ 0 \\ \vdots \\ 0 \\ 0 \end{bmatrix} + \begin{bmatrix} 0 \\ \vdots \\ \vdots \\ 0 \\ -b_w \cdot \overline{T_{w,inlet}} \end{bmatrix}$$

3.3.6.4 PCM layer

3.3.6.4.1 First PCM node (i=1)

The application of the heat balance equation for the i = 1 PCM nodes (Figure) results in the following equation:

$$\frac{\rho_p . Cp_p . V_p}{dt} \cdot \left(\overline{T_{1,J}} - T_{1,j}^{t-dt}\right) = \frac{n \cdot \lambda \cdot \pi \cdot (r1)^2}{L} \cdot \left(\overline{T_{1,J-1}} - 2\overline{T_{1,J}} + \overline{T_{1,J+1}}\right) + \frac{2\pi \cdot \lambda \cdot (L/n)}{\ln\frac{(r/2)}{(r1)}} \cdot \left(\overline{T_{2,J}} - \overline{T_{1,J}}\right); \qquad \textit{Equation 3.16}$$

Where:

ρ_p :	PCM density	[kg/m^3]
Cp_p : :	Specific heat capacity of the PCM	[J/kg ·K]
$V_{p,j}$:	Volume of the PCM node	[m^3]
dt :	Time step	[s]
$\overline{T_{i,J}}$:	Average temperature of the adjacent PCM node	[°C]
λ:	Water conductivity	[W/m ·K]
r :	Radius of the PCM stick	[m]
L:	Length of the gel stick	[m]
m:	Number of nodes of the crosswise discretization	
n:	Number of nodes of the lengthwise discretization	

If we consider:

$$R_{V,1,j} = \frac{\mathrm{L}}{n \cdot \lambda \cdot \pi \cdot (r1)^2}$$ Thermal resistance between neighboring PCM nodes [W/K]

$$R_{H,1,j} = \frac{\ln\frac{(r/2)}{(r1)}}{2\pi \cdot \lambda \cdot (L/n)}$$ Thermal resistance between i = 1 and i = 2 PCM nodes [W/K]

Then we can re-write the equation 3.16 as:

$$\frac{\rho_p . Cp_p . V_p}{dt} . \left(\overline{T_{1,J}} - T_{1,j}^{t-dt}\right) = \frac{\left(\overline{T_{1,J-1}} - 2\overline{T_{1,J}} + \overline{T_{1,J+1}}\right)}{R_{V,1,j}} + \frac{(\overline{T_{2,J}} - \overline{T_{1,J}})}{R_{H,1,j}};$$ *Equation 3.17*

Out of which $T_{1,j}^{t-dt}$ can be expressed as function of $\overline{T_{1,J-1}} + \overline{T_{1,J+1}}$ and $\overline{T_{2,J}}$:

$$T_{1,j}^{t-dt} = \overline{T_{1,J}} \cdot \left[1 + \left(\frac{dt}{\rho_p . Cp_p . V_p}\right)\left(\frac{2}{R_{V,1,j}} + \frac{1}{R_{H,1,j}}\right)\right] - \frac{dt}{\rho_p . Cp_p . V_p \cdot R_{V,1,j}}\left(\overline{T_{1,J-1}} + \overline{T_{1,J+1}}\right) - \frac{dt}{\rho_p . Cp_p . V_p \cdot R_{H,1,j}} \cdot \left(\overline{T_{2,J}}\right);$$ *Equation 3.18*

In this way the convection transfer between the j = 1 PCM node and the inlet water flow and the j = n PCM node and the bottom water layer $\overline{T_{w,n}}^{t-dt}$ is not considered. For this reason we introduce a new resistance for the j = 1 and j = n PCM nodes that takes into account this transfer:

$$R_{V,1,1} = \frac{1}{h \cdot \pi \cdot (r1)^2} + \frac{\mathrm{L}}{2 \cdot n \cdot \lambda \cdot \pi \cdot (r1)^2}$$

Setting:

$$a_{p\_1} = 1 + b_p + c_p + d_p$$

$$a_p = 1 + 2 \cdot b_p + c_p$$

$$b_p = \frac{dt}{\rho_p . Cp_p . V_p \cdot R_{V,1,j}}$$

$$c_p = \frac{dt}{\rho_p . Cp_p . V_p \cdot R_{H,1,j}}$$

$$d_p = \frac{dt}{\rho_p . Cp_p . V_p \cdot R_{H,1,1}}$$

The final equation is obtained:

$$T_{1,1}^{t-dt} = a_w \cdot \overline{T_{1,1}} - b_p \cdot \left(\overline{T_{1,J+1}}\right) - c_p \cdot \left(\overline{T_{2,1}}\right) - d_p \cdot \left(\overline{T_{inlet}}\right) \qquad \text{for node j} = 1 \qquad \textit{Equation 3.19}$$

$$T_{1,j}^{t-dt} = a_w \cdot \overline{T_{1,J}} - b_p\left(\overline{T_{1,J-1}} + \overline{T_{1,J+1}}\right) - c_p \cdot \left(\overline{T_{2,J}}\right) \qquad \textit{Equation 3.20}$$

$$T_{1,n}^{t-dt} = a_w \cdot \overline{T_{1,n}} - b_p\left(\overline{T_{1,J-1}}\right) - c_p \cdot \left(\overline{T_{2,n}}\right) - d_p \cdot \left(\overline{T_{1,n}^{\,t-dt}}\right) \qquad \text{for node j} = \text{n} \qquad \textit{Equation 3.21}$$

Equations 3.19, 3.20 and 3.21 can then be written in a matrix equation, representing nodes 1 to n:

$$\begin{bmatrix} T_{1,1}^{t-dt} \\ \vdots \\ T_{1,j}^{t-dt} \\ \vdots \\ T_{1,n}^{t-dt} \end{bmatrix} = \begin{bmatrix} a_{p\_1} & -b_p & 0 & \dots & 0 \\ -b_p & \ddots & \ddots & \ddots & \vdots \\ 0 & \ddots & a_p & \ddots & 0 \\ \vdots & \ddots & \ddots & \ddots & -b_p \\ 0 & \cdots & 0 & -b_p & a_{p\_1} \end{bmatrix} \times \begin{bmatrix} \overline{T_{1,1}} \\ \vdots \\ \overline{T_{1,J}} \\ \vdots \\ \overline{T_{1,n}} \end{bmatrix} + \begin{bmatrix} -c_p & 0 & \cdots & \cdots & 0 \\ 0 & \ddots & \ddots & & \vdots \\ \vdots & \ddots & \ddots & \ddots & \vdots \\ \vdots & & \ddots & \ddots & 0 \\ 0 & \cdots & \cdots & 0 & -c_p \end{bmatrix} \times \begin{bmatrix} \overline{T_{2,1}} \\ \vdots \\ \overline{T_{2,J}} \\ \vdots \\ \overline{T_{2,n}} \end{bmatrix}$$

$$+ \begin{bmatrix} -d_p \cdot \overline{T_{w,inlet}} \\ 0 \\ \vdots \\ \vdots \\ 0 \end{bmatrix} + \begin{bmatrix} 0 \\ \vdots \\ \vdots \\ 0 \\ -d_p \cdot \overline{T_{w,n}^{\,t-dt}} \end{bmatrix}$$

3.3.6.4.2 Second PCM node (i=2)

The application of the heat balance equation for the i = 2 PCM nodes results in the following equation:

$$\frac{\rho_p . Cp_p . V_p}{dt} \cdot \left(\overline{T_{2,J}} - T_{2,j}^{t-dt}\right) = \frac{n \cdot \lambda \cdot \pi \cdot [r^2 - (r1)^2]}{L} \cdot \left(\overline{T_{2,J+1}} - 2\overline{T_{2,J}} + \overline{T_{2,J-1}}\right) +$$

$$\frac{2\pi \cdot \lambda \cdot (L/n)}{\ln \frac{(r/2)}{(r1)}} \cdot \left(\overline{T_{1,J}} - \overline{T_{2,J}}\right) + \frac{2\pi \cdot \lambda \cdot (L/n)}{\ln \frac{(3r/2)}{(r/2)}} \cdot \left(\overline{T_{3,J}} - \overline{T_{2,J}}\right); \qquad \textit{Equation 3.22}$$

Where:

ρ_p :	PCM density	[kg/m^3]
Cp_p : :	Specific heat capacity of the PCM	[J/kg ·K]
$V_{p,j}$:	Volume of the PCM node	[m^3]
dt :	Time step	[s]
$\overline{T_{i,J}}$:	Average temperature of the adjacent PCM node	[°C]
λ:	Water conductivity	[W/m ·K]
r :	Radius of the PCM stick	[m]
L:	Length of the gel stick	[m]
m:	Number of nodes of the crosswise discretization	
n:	Number of nodes of the lengthwise discretization	

If we consider:

$$R_{V,2,j} = \frac{L}{n \cdot \lambda \cdot \pi \cdot [r^2 - (r1)^2]}$$ Thermal resistance between neighboring PCM nodes [W/K]

$$R_{H,1,j} = \frac{\ln \frac{(r/2)}{(r1)}}{2\pi \cdot \lambda \cdot (L/n)}$$ Thermal resistance between i = 1 and i = 2 PCM nodes [W/K]

$$R_{H,2,j} = \frac{\ln \frac{(3r/2)}{(r/2)}}{2\pi \cdot \lambda \cdot (L/n)}$$ Thermal resistance between i = 2 and i = 3 PCM nodes [W/K]

Then we can re-write the equation 3.22 as:

$$\frac{\rho_p . Cp_p . V_p}{dt} . \left(\overline{T_{2,J}} - T_{2,j}^{t-dt}\right) = \frac{\left(\overline{T_{2,J+1}} - 2\overline{T_{2,J}} + \overline{T_{2,J-1}}\right)}{R_{V,2,j}} + \frac{\left(\overline{T_{1,J}} - \overline{T_{2,J}}\right)}{R_{H,1,j}} + \frac{\left(\overline{T_{3,J}} - \overline{T_{2,J}}\right)}{R_{H,2,j}}$$ *Equation 3.23*

Out of which $T_{2,j}^{t-dt}$ can be expressed as function of $\overline{T_{2,J-1}} + \overline{T_{2,J+1}}$, $\overline{T_{1,J}}$ and $\overline{T_{3,J}}$:

$$T_{2,j}^{t-dt} = \overline{T_{2,J}} \cdot \left[1 + \left(\frac{dt}{\rho_p . Cp_p . V_p}\right)\left(\frac{2}{R_{V,2,j}} + \frac{1}{R_{H,2,j}} + \frac{1}{R_{H,1,j}}\right)\right] - \frac{dt}{\rho_p . Cp_p . V_p \cdot R_{V,2,j}}\left(\overline{T_{2,J-1}} + \overline{T_{2,J+1}}\right) - \frac{dt}{\rho_p . Cp_p . V_p \cdot R_{H,1,j}} \cdot \left(\overline{T_{1,J}}\right) - \frac{dt}{\rho_p . Cp_p . V_p \cdot R_{H,2,j}} \cdot \left(\overline{T_{3,J}}\right)$$ *Equation 3.24*

Introducing the thermal resistance between the j = 1 and j = n PCM nodes and water:

$$R_{V,2,1} = \frac{1}{h \cdot \pi \cdot [r^2 - (r1)^2]} + \frac{\mathrm{L}}{2 \cdot n \cdot \lambda \cdot \pi \cdot [r^2 - (r1)^2]}$$

We set:

$$e_{p\_1} = 1 + f_p + g_p + h_p + i_p$$

$$e_p = 1 + 2 \cdot f_p + g_p + h_p$$

$$f_p = \frac{dt}{\rho_p . Cp_p . V_p \cdot R_{V,2,j}}$$

$$g_p = \frac{dt}{\rho_p . Cp_p . V_p \cdot R_{H,1,j}}$$

$$h_p = \frac{dt}{\rho_p . Cp_p . V_p \cdot R_{H,2,j}}$$

$$i_p = \frac{dt}{\rho_p . Cp_p . V_p \cdot R_{V,2,1}}$$

The final equation is obtained:

$$T_{2,1}^{t-dt} = e_w \cdot \overline{T_{2,1}} - f_p\left(\overline{T_{2,J+1}}\right) - g_p \cdot \left(\overline{T_{1,1}}\right) - h_p \cdot \left(\overline{T_{3,1}}\right) - i_p \cdot \left(\overline{T_{w,inlet}}\right) \quad \text{for node j = 1} \qquad \textit{Equation 3.25}$$

$$T_{2,j}^{t-dt} = e_w \cdot \overline{T_{2,J}} - f_p\left(\overline{T_{2,J-1}} + \overline{T_{2,J+1}}\right) - g_p \cdot \left(\overline{T_{1,J}}\right) - h_p \cdot \left(\overline{T_{3,J}}\right) \qquad \textit{Equation 3.26}$$

$$T_{2,n}^{t-dt} = e_w \cdot \overline{T_{2,n}} - f_p\left(\overline{T_{2,J-1}}\right) - g_p \cdot \left(\overline{T_{1,n}}\right) - h_p \cdot \left(\overline{T_{3,n}}\right) - i_p \cdot \left(\overline{T_{w,n}^{\,t-dt}}\right) \quad \text{for node j = n} \qquad \textit{Equation 3.27}$$

Equations 3.25, 3.26 and 3.27 can then be written in a matrix equation, representing nodes 1 to n:

$$\begin{bmatrix} T_{2,1}^{t-dt} \\ \vdots \\ T_{2,j}^{t-dt} \\ \vdots \\ T_{2,n}^{t-dt} \end{bmatrix} = \begin{bmatrix} e_{p\_1} & -f_p & 0 & \dots & 0 \\ -f_p & \ddots & \ddots & \ddots & \vdots \\ 0 & \ddots & e_p & \ddots & 0 \\ \vdots & \ddots & \ddots & \ddots & -f_p \\ 0 & \cdots & 0 & -f_p & e_{p\_1} \end{bmatrix} \times \begin{bmatrix} \overline{T_{2,1}} \\ \vdots \\ \overline{T_{2,J}} \\ \vdots \\ \overline{T_{2,n}} \end{bmatrix} + \begin{bmatrix} -g_p & 0 & \cdots & \cdots & 0 \\ 0 & \ddots & \ddots & & \vdots \\ \vdots & \ddots & \ddots & \ddots & \vdots \\ \vdots & & \ddots & \ddots & 0 \\ 0 & \cdots & \cdots & 0 & -g_p \end{bmatrix} \times \begin{bmatrix} \overline{T_{1,1}} \\ \vdots \\ \overline{T_{1,J}} \\ \vdots \\ \overline{T_{1,n}} \end{bmatrix} +$$

$$\begin{bmatrix} -h_p & 0 & \cdots & \cdots & 0 \\ 0 & \ddots & \ddots & & \vdots \\ \vdots & \ddots & \ddots & \ddots & \vdots \\ \vdots & & \ddots & \ddots & 0 \\ 0 & \cdots & \cdots & 0 & -h_p \end{bmatrix} \times \begin{bmatrix} \overline{T_{3,1}} \\ \vdots \\ \overline{T_{3,J}} \\ \vdots \\ \overline{T_{3,n}} \end{bmatrix} + \begin{bmatrix} -i_p \cdot \overline{T_{w,inlet}} \\ 0 \\ \vdots \\ 0 \end{bmatrix} + \begin{bmatrix} 0 \\ \vdots \\ \vdots \\ 0 \\ -i_p \cdot \overline{T_{w,n}^{t-dt}} \end{bmatrix}$$

3.3.6.4.3 Last PCM nodes (i=m)

The application of the heat balance equation for the i = 2 PCM nodes results in the following equation:

$$\frac{\rho_p . Cp_p . V_p}{dt} \cdot \left(\overline{T_{m,J}} - T_{m,j}^{t-dt}\right) = \frac{n \cdot \lambda \cdot \pi \cdot \left((mr)^2 - [(m-1)r]^2\right)}{L} \cdot \left(\overline{T_{m,J-1}} - 2\overline{T_{m,J}} + T_{m,j+1}\right) +$$

$$\frac{2\pi \cdot \lambda \cdot \left(\frac{L}{n}\right)}{\ln \frac{(mr - r/2)}{\left(mr - \frac{3r}{2}\right)}} \cdot \left(\overline{T_{m-1,J}} - \overline{T_{m,J}}\right) + \left(\frac{h \cdot 2 \cdot \pi \cdot (m-1)r \cdot L}{n} + \frac{2\pi \cdot \lambda \cdot \left(\frac{L}{n}\right)}{\ln \frac{(mr)}{\left(mr - \frac{r}{2}\right)}} \right) \cdot \left(\overline{T_{w,J}} - \overline{T_{m,J}}\right);$$

Equation 3.28

Where:

ρ_w :	Water density	[kg/m^3]
Cp_w : :	Specific heat capacity of the water	[J/kg ·K]
$V_{w,j}$:	Volume of the water node	[m^3]
dt :	Time step	[s]
$\overline{T_{w,J}}$:	Average temperature of the water node	[°C]
$\overline{T_{m,J}}$:	Average temperature of the adjacent PCM node	[°C]
ṁ :	Water flow rate	[kg/s]
h :	Heat transfer coefficient	[W/m² ·K]
λ:	Water conductivity	[W/m ·K]
r :	Radius of the gel stick	[m]
mr:	Radius of the gel stick	[m]
L:	Length of the gel stick	[m]
m:	Number of nodes of the crosswise discretization	

n: Number of nodes of the lengthwise discretization

If we consider:

$$R_{V,m,j} = \frac{\mathrm{L}}{n \cdot \lambda \cdot \pi \cdot \{(mr)^2 - [(m-1)r]^2\}}$$ Thermal resistance between neighboring PCM nodes [W/K]

$$R_{H,i-1,j} = \frac{\ln \frac{(mr - r/2)}{(mr - 3r/2)}}{2\pi \cdot \lambda \cdot (L/n)}$$ Thermal resistance between neighboring PCM nodes [W/K]

$$R_{H,m,j} = \frac{1}{h \cdot 2 \cdot \pi \cdot mr \cdot (L/n)} + \frac{\ln \frac{(mr)}{(mr - r/2)}}{2\pi \cdot \lambda \cdot (L/n)}$$ Thermal resistance between water and PCM nodes [W/K]

Then we can re-write the equation 3.28 as:

$$\frac{\rho_p . Cp_p . V_p}{dt} . \left(\overline{T_{m,J}} - T_{m,j}^{t-dt}\right) = \frac{\left(\overline{T_{m,J-1}} - 2\overline{T_{m,J}} + T_{m,j+1}\right)}{R_{V,m,j}} + \frac{\left(\overline{T_{m-1,J}} - \overline{T_{m,J}}\right)}{R_{H,m-1,j}} + \frac{\left(\overline{T_{w,J}} - \overline{T_{m,J}}\right)}{R_{H,m,j}}$$

Equation 3.29

Out of which $T_{m,j}^{t-dt}$ can be expressed as function of $\overline{T_{m,J-1}} + \overline{T_{m,J+1}}$, $\overline{T_{m-1,J}}$ and $\overline{T_{w,J}}$:

$$T_{m,j}^{t-dt} = \overline{T_{m,J}} \cdot \left[1 + \left(\frac{dt}{\rho_p . Cp_p . V_p}\right)\left(\frac{2}{R_{V,m,j}} + \frac{1}{R_{H,m,j}} + \frac{1}{R_{H,3,j}}\right)\right] - \frac{dt}{\rho_p . Cp_p . V_p \cdot R_{V,m,j}}\left(\overline{T_{m,J-1}} + \overline{T_{m,J+1}}\right) - \frac{dt}{\rho_p . Cp_p . V_p \cdot R_{H,m-1,j}} \cdot \left(\overline{T_{m-1,J}}\right) - \frac{dt}{\rho_p . Cp_p . V_p \cdot R_{H,m,j}} \cdot \left(\overline{T_{w,J}}\right);$$

Equation 3.30

Introducing the thermal resistance between the j = 1 and j = n PCM nodes and water:

$$R_{V,m,1} = \frac{1}{h \cdot \pi \cdot \{(mr)^2 - [(m-1)r]^2\}} + \frac{\mathrm{L}}{2 \cdot n \cdot \lambda \cdot \pi \cdot \{(mr)^2 - [(m-1)r]^2\}}$$

We set:

$$o_{p\_1} = 1 + p_p + q_p + r_p + s_p$$

$$o_p = 1 + 2 \cdot p_p + q_p + r_p$$

$$p_p = \frac{dt}{\rho_p . Cp_p . V_p \cdot R_{V,m,j}}$$

$$q_p = \frac{dt}{\rho_p . Cp_p . V_p \cdot R_{H,m-1,j}}$$

$$r_p = \frac{dt}{\rho_p . Cp_p . V_p \cdot R_{H,m,j}}$$

$$s_p = \frac{dt}{\rho_p . Cp_p . V_p \cdot R_{V,m,1}}$$

The final equation is obtained:

$$T_{m,1}^{t-dt} = o_p \cdot \overline{(T_{m,J})} - p_p \cdot \overline{(T_{m,J+1})} - q_p \cdot \overline{(T_{m-1,J})} - r_p \cdot \overline{(T_{w,J})} - s_p \cdot \overline{(T_{w,inlet})} \quad \text{for node j = 1} \quad \textit{Equation 3.31}$$

$$T_{m,j}^{t-dt} = o_w \cdot \overline{T_{m,J}} - p_p\overline{(T_{m,J-1} + T_{m,J+1})} - q_p \cdot \overline{(T_{m-1,J})} - r_p \cdot \overline{(T_{w,J})} \quad \textit{Equation 3.32}$$

$$T_{m,n}^{t-dt} = o_w \cdot \overline{T_{m,n}} - p_p\overline{(T_{m,J-1})} - q_p \cdot \overline{(T_{m-1,n})} - r_p \cdot \overline{(T_{w,n})} - s_p \cdot \overline{\left(T_{w,n}{}^{t-dt}\right)} \quad \text{for node j = n} \quad \textit{Equation 3.33}$$

Equations 3.31, 3.32 and 3.33 can then be written in a matrix equation, representing nodes 1 to n:

$$\begin{bmatrix} T_{m,1}^{t-dt} \\ \vdots \\ T_{m,j}^{t-dt} \\ \vdots \\ T_{m,n}^{t-dt} \end{bmatrix} = \begin{bmatrix} o_{p_1} & -p_p & 0 & \dots & 0 \\ -p_p & \ddots & \ddots & \ddots & \vdots \\ 0 & \ddots & o_p & \ddots & 0 \\ \vdots & \ddots & \ddots & \ddots & -p_p \\ 0 & \cdots & 0 & -p_p & o_{p_n} \end{bmatrix} \times \begin{bmatrix} \overline{T_{m,1}} \\ \vdots \\ \overline{T_{m,J}} \\ \vdots \\ \overline{T_{m,n}} \end{bmatrix} + \begin{bmatrix} -q_p & 0 & \cdots & \cdots & 0 \\ 0 & \ddots & \ddots & & \vdots \\ \vdots & \ddots & \ddots & \ddots & \vdots \\ \vdots & & \ddots & \ddots & 0 \\ 0 & \cdots & \cdots & 0 & -q_p \end{bmatrix} \times \begin{bmatrix} \overline{T_{3,1}} \\ \vdots \\ \overline{T_{3,J}} \\ \vdots \\ \overline{T_{3,n}} \end{bmatrix} +$$

$$\begin{bmatrix} -r_p & 0 & \cdots & \cdots & 0 \\ 0 & \ddots & \ddots & & \vdots \\ \vdots & \ddots & \ddots & \ddots & \vdots \\ \vdots & & \ddots & \ddots & 0 \\ 0 & \cdots & \cdots & 0 & -r_p \end{bmatrix} \times \begin{bmatrix} \overline{T_{w,1}} \\ \vdots \\ \overline{T_{w,J}} \\ \vdots \\ \overline{T_{w,n}} \end{bmatrix} + \begin{bmatrix} -s_p \cdot \overline{T_{w,inlet}} \\ 0 \\ \vdots \\ \vdots \\ 0 \end{bmatrix} + \begin{bmatrix} 0 \\ \vdots \\ \vdots \\ 0 \\ -s_p \cdot \overline{T_{w,n}^{\,t-dt}} \end{bmatrix}$$

3.3.6.4.4 Other PCM nodes

The application of the heat balance equation for the PCM nodes results in the following equation:

$$\frac{\rho_p.Cp_p.V_p}{dt} \cdot \left(\overline{T_{\iota,J}} - T_{i,j}^{t-dt}\right) = \frac{2\pi \cdot \lambda \cdot (L/n)}{\ln \frac{(ir-3r/2)}{(ir-5r/2)}} \cdot \left(\overline{T_{\iota-1,J}} - \overline{T_{\iota,J}}\right) + \frac{2\pi \cdot \lambda \cdot (L/n)}{\ln \frac{(ir-r/2)}{(ir-3r/2)}} \cdot \left(\overline{T_{\iota+1,J}} - \overline{T_{\iota,J}}\right) +$$

$$\frac{n \cdot \lambda \cdot \pi \cdot \left\{[(i-1)r]^2 - [(i-2)r]^2\right\}}{L} \cdot \left(\overline{T_{\iota,J+1}} - 2\overline{T_{\iota,J}} + \overline{T_{\iota,J-1}}\right) ;$$

Equation 3.34

Where:

ρ_p :	PCM density	[kg/m^3]
Cp_p : :	Specific heat capacity of the PCM	[J/kg ·K]
$V_{p,j}$:	Volume of the PCM node	[m^3]
dt :	Time step	[s]
$\overline{T_{\iota,J}}$:	Average temperature of the adjacent PCM node	[°C]
λ:	Water conductivity	[W/m ·K]
r :	Radius of the PCM stick	[m]
L:	Length of the gel stick	[m]
m:	Number of nodes of the crosswise discretization	
n:	Number of nodes of the lengthwise discretization	

If we consider:

$$R_{V,i,j} = \frac{\mathrm{L}}{n \cdot \lambda \cdot \pi \cdot \{[(i-1)r]^2 - [(i-2)r]^2\}}$$ Thermal resistance between neighboring PCM nodes [W/K]

$$R_{H,i-1,j} = \frac{\ln \frac{(ir - 3r/2)}{(ir - 5r/2)}}{2\pi \cdot \lambda \cdot (L/n)}$$ Thermal resistance between neighboring PCM nodes [W/K]

$$R_{H,i,j} = \frac{\ln \frac{(ir - r/2)}{(ir - 3r/2)}}{2\pi \cdot k \cdot (L/n)}$$ Thermal resistance between water and PCM nodes [W/K]

Then we can re-write the equation 3.34 as:

$$\frac{\rho_p . Cp_p . V_p}{dt} . \left(\overline{T_{\iota,J}} - T_{i,j}^{t-dt}\right) = \frac{\left(\overline{T_{\iota-1,J}} - \overline{T_{\iota,J}}\right)}{R_{H,i-1,j}} + \frac{\left(\overline{T_{\iota+1,J}} - \overline{T_{\iota,J}}\right)}{R_{H,i,j}} + \frac{\left(\overline{T_{\iota,J+1}} - 2\overline{T_{\iota,J}} + \overline{T_{\iota,J-1}}\right)}{R_{V,i,j}}$$ *Equation 3.35*

Out of which $T_{i,j}^{t-dt}$ can be expressed as function of $\overline{T_{\iota,J-1}} + \overline{T_{\iota,J+1}}$, $\overline{T_{\iota-1,J}}$ and $\overline{T_{\iota+1,J}}$

$$T_{i,j}^{t-dt} = \overline{T_{3,J}} \cdot \left[1 + \left(\frac{dt}{\rho_p . Cp_p . V_p}\right)\left(\frac{2}{R_{V,i,j}} + \frac{1}{R_{H,i,j}} + \frac{1}{R_{H,i-1,j}}\right)\right] - \frac{dt}{\rho_p . Cp_p . V_p \cdot R_{H,i-1,j}} \cdot \left(\overline{T_{\iota-1,J}}\right) - \frac{dt}{\rho_p . Cp_p . V_p \cdot R_{H,i,j}} \cdot \left(\overline{T_{\iota+1,J}}\right) - \frac{dt}{\rho_p . Cp_p . V_p \cdot R_{V,i,j}} \left(\overline{T_{\iota,J-1}} + \overline{T_{\iota,J+1}}\right)$$ *Equation 3.36*

Introducing the thermal resistance between the j = 1 and j = n PCM nodes and water:

$$R_{V,i,1} = \frac{1}{h \cdot \pi \cdot \{[(i-1)r]^2 - [(i-2)r]^2\}} + \frac{\mathrm{L}}{2 \cdot n \cdot \lambda \cdot \pi \cdot \{[(i-1)r]^2 - [(i-2)r]^2\}}$$

We set:

$$j_{p\_1} = 1 + k_p + l_p + m_p + n_p$$

$$j_p = 1 + 2 \cdot k_p + l_p + m_p$$

$$k_p = \frac{dt}{\rho_p . Cp_p . V_p \cdot R_{V,i,j}}$$

$$l_p = \frac{dt}{\rho_p . Cp_p . V_p \cdot R_{H,i-1,j}}$$

$$m_p = \frac{dt}{\rho_p . Cp_p . V_p \cdot R_{H,i+1,j}}$$

$$n_p = \frac{dt}{\rho_p . Cp_p . V_p \cdot R_{V,i+1,1}}$$

The final equation is obtained:

$$T_{i,1}^{t-dt} = j_p \cdot \overline{(T_{i,J})} - k_p \cdot (\overline{T_{i,J+1}}) - l_p \cdot (\overline{T_{i-1,1}}) - m_p \cdot (\overline{T_{i+1,1}}) - n_p \cdot (\overline{T_{inlet}}) \quad \text{for node j = 1} \quad \textit{Equation 3.37}$$

$$T_{i,n}^{t-dt} = j_w \cdot \overline{T_{i,n}} - k_p \cdot \left(\overline{T_{i,J-1}} + \overline{T_{i,n}}^{t-dt}\right) - l_p \cdot (\overline{T_{i-1,n}}) - m_p \cdot (\overline{T_{i+1,n}}) \quad \textit{Equation 3.38}$$

$$T_{i,j}^{t-dt} = j_w \cdot \overline{T_{i,J}} - k_p \cdot (\overline{T_{i,J-1}}) - l_p \cdot (\overline{T_{i-1,J}}) - m_p \cdot (\overline{T_{i+1,J}}) - n_p \cdot \left(\overline{T_{w,n}}^{t-dt}\right) \quad \text{for node j = n} \quad \textit{Equation 3.39}$$

Equations 3.37, 3.38 and 3.39 can then be written in a matrix equation, representing nodes 1 to n:

$$\begin{bmatrix} T_{i,1}^{t-dt} \\ \vdots \\ T_{i,j}^{t-dt} \\ \vdots \\ T_{i,n}^{t-dt} \end{bmatrix} = \begin{bmatrix} j_{p_1} & -k_p & 0 & \dots & 0 \\ -k_p & \ddots & \ddots & \ddots & \vdots \\ 0 & \ddots & j_p & \ddots & 0 \\ \vdots & \ddots & \ddots & \ddots & -k_p \\ 0 & \cdots & 0 & -k_p & j_{p_n} \end{bmatrix} \times \begin{bmatrix} \overline{T_{i,1}} \\ \vdots \\ \overline{T_{i,J}} \\ \vdots \\ \overline{T_{i,n}} \end{bmatrix} + \begin{bmatrix} -l_p & 0 & \cdots & \cdots & 0 \\ 0 & \ddots & \ddots & & \vdots \\ \vdots & \ddots & \ddots & \ddots & \vdots \\ \vdots & & \ddots & \ddots & 0 \\ 0 & \cdots & \cdots & 0 & -l_p \end{bmatrix} \times \begin{bmatrix} \overline{T_{i-1,1}} \\ \vdots \\ \overline{T_{i-1,J}} \\ \vdots \\ \overline{T_{i-1,n}} \end{bmatrix} +$$

$$\begin{bmatrix} -m_p & 0 & \cdots & \cdots & 0 \\ 0 & \ddots & \ddots & & \vdots \\ \vdots & \ddots & \ddots & \ddots & \vdots \\ \vdots & & \ddots & \ddots & 0 \\ 0 & \cdots & \cdots & 0 & -m_p \end{bmatrix} \times \begin{bmatrix} \overline{T_{i+1,1}} \\ \vdots \\ \overline{T_{i+1,J}} \\ \vdots \\ \overline{T_{i+1,n}} \end{bmatrix} + \begin{bmatrix} -n_p \cdot \overline{T_{w,inlet}} \\ 0 \\ \vdots \\ \vdots \\ 0 \end{bmatrix} + \begin{bmatrix} 0 \\ \vdots \\ \vdots \\ 0 \\ -n_p \cdot \overline{T_{w,n}}^{t-dt} \end{bmatrix}$$

3.3.6.4.5 Numerical resolution

Finally, the matrix equations obtained from each layer were assembled into the centralized matrix equation:

$$\overline{T} = A - 1\,(T^{t-dt} - B) \quad \textit{Equation 3.40}$$

Where:

$\overline{T}$ is a n*(m+2) column matrix containing average temperature values for the water and PCM layers,

A is a n*(m+1) x n*(m+1) matrix containing thermal resistance coefficients,

T^{t-dt} is a n*(m+1) column matrix containing temperature values for the three layers at the previous time step

B is a n*(m+1) column matrix containing initial temperature values for the layers.

C is a n*(m+1) column matrix containing i = w, j = n water node temperature at the previous time step

($\overline{T_{w,n}^{\,t-dt}}$).

Finally, water and PCM temperatures at each node and at each time step were calculated using inlet water temperature, neighbouring nodes temperature and temperatures calculated at the previous time step with the final equation:

$$T^{t} = 2 \cdot \overline{T} - T^{t-dt} \qquad \textit{Equation 3.41}$$

In the end, the use of the heat balance approach and the finite difference method as presented in the previous subsections was reduced to the solution of the matrix equation shown in the following figure.

$$
\begin{bmatrix} T_{w,1}^{t-dt} \\ \vdots \\ T_{w,j}^{t-dt} \\ \vdots \\ T_{w,n}^{t-dt} \\ T_{1,1}^{t-dt} \\ \vdots \\ T_{1,j}^{t-dt} \\ \vdots \\ T_{1,n}^{t-dt} \\ T_{2,1}^{t-dt} \\ \vdots \\ T_{2,j}^{t-dt} \\ \vdots \\ T_{2,n}^{t-dt} \\ T_{i,1}^{t-dt} \\ \vdots \\ T_{i,j}^{t-dt} \\ \vdots \\ T_{i,n}^{t-dt} \\ T_{m,1}^{t-dt} \\ \vdots \\ T_{m,j}^{t-dt} \\ \vdots \\ T_{m,n}^{t-dt} \end{bmatrix} =
\underbrace{\begin{bmatrix}
a_{w\_1} & -b_w & 0 & \cdots & 0 & 0 & \cdots & \cdots & \cdots & 0 & 0 & \cdots & \cdots & \cdots & 0 & 0 & \cdots & \cdots & \cdots & 0 & -c_w & 0 & \cdots & \cdots & 0 \\
-b_w & \ddots & \ddots & \ddots & \vdots & \vdots & \ddots & \ddots & \ddots & \vdots & \vdots & \ddots & \ddots & \ddots & \vdots & \vdots & \ddots & \ddots & \ddots & \vdots & 0 & \ddots & \ddots & \ddots & \vdots \\
0 & \ddots & a_w & \ddots & 0 & \vdots & \ddots & \ddots & \ddots & \vdots & \vdots & \ddots & \ddots & \ddots & \vdots & \vdots & \ddots & \ddots & \ddots & \vdots & \vdots & \ddots & \ddots & \ddots & \vdots \\
\vdots & \ddots & \ddots & \ddots & -b_w & \vdots & \ddots & \ddots & \ddots & \vdots & \vdots & \ddots & \ddots & \ddots & \vdots & \vdots & \ddots & \ddots & \ddots & \vdots & \vdots & \ddots & \ddots & \ddots & 0 \\
0 & \cdots & 0 & -b_w & a_{w\_1} & 0 & \cdots & \cdots & \cdots & 0 & 0 & \cdots & \cdots & \cdots & 0 & 0 & \cdots & \cdots & \cdots & 0 & 0 & \cdots & \cdots & 0 & -c_w \\
0 & \cdots & \cdots & \cdots & 0 & a_{p\_1} & -b_p & 0 & \cdots & 0 & -c_p & 0 & \cdots & \cdots & 0 & 0 & \cdots & \cdots & \cdots & 0 & 0 & \cdots & \cdots & \cdots & 0 \\
\vdots & \ddots & \ddots & \ddots & \vdots & -b_p & \ddots & \ddots & \ddots & \vdots & 0 & \ddots & \ddots & \ddots & \vdots & \vdots & \ddots & \ddots & \ddots & \vdots & \vdots & \ddots & \ddots & \ddots & \vdots \\
\vdots & \ddots & \ddots & \ddots & \vdots & 0 & \ddots & a_p & \ddots & 0 & \vdots & \ddots & \ddots & \ddots & \vdots & \vdots & \ddots & \ddots & \ddots & \vdots & \vdots & \ddots & \ddots & \ddots & \vdots \\
\vdots & \ddots & \ddots & \ddots & \vdots & \vdots & \ddots & \ddots & \ddots & -b_p & \vdots & \ddots & \ddots & \ddots & 0 & \vdots & \ddots & \ddots & \ddots & \vdots & \vdots & \ddots & \ddots & \ddots & \vdots \\
0 & \cdots & \cdots & \cdots & 0 & 0 & \cdots & 0 & -b_p & a_{p\_1} & 0 & \cdots & \cdots & 0 & -c_p & 0 & \cdots & \cdots & \cdots & 0 & 0 & \cdots & \cdots & \cdots & 0 \\
0 & \cdots & \cdots & \cdots & 0 & -g_p & 0 & \cdots & \cdots & 0 & e_{p\_1} & -f_p & 0 & \cdots & 0 & -h_p & 0 & \cdots & \cdots & 0 & 0 & \cdots & \cdots & \cdots & 0 \\
\vdots & \ddots & \ddots & \ddots & \vdots & 0 & \ddots & \ddots & \ddots & \vdots & -f_p & \ddots & \ddots & \ddots & \vdots & 0 & \ddots & \ddots & \ddots & \vdots & \vdots & \ddots & \ddots & \ddots & \vdots \\
\vdots & \ddots & \ddots & \ddots & \vdots & \vdots & \ddots & \ddots & \ddots & \vdots & 0 & \ddots & e_p & \ddots & 0 & \vdots & \ddots & \ddots & \ddots & \vdots & \vdots & \ddots & \ddots & \ddots & \vdots \\
\vdots & \ddots & \ddots & \ddots & \vdots & \vdots & \ddots & \ddots & \ddots & 0 & \vdots & \ddots & \ddots & \ddots & -f_p & \vdots & \ddots & \ddots & \ddots & 0 & \vdots & \ddots & \ddots & \ddots & \vdots \\
0 & \cdots & \cdots & \cdots & 0 & 0 & \cdots & \cdots & 0 & -g_p & 0 & \cdots & 0 & -f_p & e_{p\_1} & 0 & \cdots & \cdots & 0 & -h_p & 0 & \cdots & \cdots & \cdots & 0 \\
0 & \cdots & \cdots & \cdots & 0 & 0 & \cdots & \cdots & \cdots & 0 & -l_p & 0 & \cdots & \cdots & 0 & j_{p\_1} & -k_p & 0 & \cdots & 0 & -m_p & 0 & \cdots & \cdots & 0 \\
\vdots & \ddots & \ddots & \ddots & \vdots & \vdots & \ddots & \ddots & \ddots & \vdots & 0 & \ddots & \ddots & \ddots & \vdots & -k_p & \ddots & \ddots & \ddots & \vdots & 0 & \ddots & \ddots & \ddots & \vdots \\
\vdots & \ddots & \ddots & \ddots & \vdots & \vdots & \ddots & \ddots & \ddots & \vdots & \vdots & \ddots & \ddots & \ddots & \vdots & 0 & \ddots & j_p & \ddots & 0 & \vdots & \ddots & \ddots & \ddots & \vdots \\
\vdots & \ddots & \ddots & \ddots & \vdots & \vdots & \ddots & \ddots & \ddots & \vdots & \vdots & \ddots & \ddots & \ddots & 0 & \vdots & \ddots & \ddots & \ddots & -k_p & \vdots & \ddots & \ddots & \ddots & \vdots \\
0 & \cdots & \cdots & \cdots & 0 & 0 & \cdots & \cdots & \cdots & 0 & 0 & \cdots & \cdots & 0 & -l_p & 0 & \cdots & 0 & -k_p & j_{p\_1} & 0 & \cdots & \cdots & \cdots & -m_p \\
-r_p & 0 & \cdots & \cdots & 0 & 0 & \cdots & \cdots & \cdots & 0 & 0 & \cdots & \cdots & \cdots & 0 & -q_p & 0 & \cdots & \cdots & 0 & o_{p\_1} & -p_p & 0 & \cdots & 0 \\
0 & \ddots & \ddots & \ddots & \vdots & \vdots & \ddots & \ddots & \ddots & \vdots & \vdots & \ddots & \ddots & \ddots & \vdots & 0 & \ddots & \ddots & \ddots & \vdots & -p_p & \ddots & \ddots & \ddots & \vdots \\
\vdots & \ddots & \ddots & \ddots & \vdots & \vdots & \ddots & \ddots & \ddots & \vdots & \vdots & \ddots & \ddots & \ddots & \vdots & \vdots & \ddots & \ddots & \ddots & \vdots & 0 & \ddots & o_p & \ddots & 0 \\
\vdots & \ddots & \ddots & \ddots & 0 & \vdots & \ddots & \ddots & \ddots & \vdots & \vdots & \ddots & \ddots & \ddots & \vdots & \vdots & \ddots & \ddots & \ddots & 0 & \vdots & \ddots & \ddots & \ddots & -p_p \\
0 & \cdots & \cdots & 0 & -r_p & 0 & \cdots & \cdots & \cdots & 0 & 0 & \cdots & \cdots & \cdots & 0 & 0 & \cdots & \cdots & 0 & -q_p & 0 & \cdots & 0 & -p_p & o_{p\_1}
\end{bmatrix}}_{A}
\times
\begin{bmatrix} \overline{T_{w,1}} \\ \vdots \\ \overline{T_{w,J}} \\ \vdots \\ \overline{T_{w,n}} \\ \overline{T_{1,1}} \\ \vdots \\ \overline{T_{1,J}} \\ \vdots \\ \overline{T_{1,n}} \\ \overline{T_{2,1}} \\ \vdots \\ \overline{T_{2,J}} \\ \vdots \\ \overline{T_{2,n}} \\ \overline{T_{i,1}} \\ \vdots \\ \overline{T_{i,J}} \\ \vdots \\ \overline{T_{i,n}} \\ \overline{T_{m,1}} \\ \vdots \\ \overline{T_{m,J}} \\ \vdots \\ \overline{T_{m,n}} \end{bmatrix}
+
\underbrace{\begin{bmatrix} -b_w \cdot \overline{T_{w,inlet}} \\ 0 \\ \vdots \\ 0 \\ -d_p \cdot \overline{T_{w,inlet}} \\ 0 \\ \vdots \\ 0 \\ -i_p \cdot \overline{T_{w,inlet}} \\ 0 \\ \vdots \\ 0 \\ -n_p \cdot \overline{T_{w,inlet}} \\ 0 \\ \vdots \\ 0 \\ -s_p \cdot \overline{T_{w,inlet}} \\ 0 \\ \vdots \\ 0 \end{bmatrix}}_{B}
+
\underbrace{\begin{bmatrix} 0 \\ \vdots \\ 0 \\ -b_p \cdot \overline{T_{w,n}^{t-dt}} \\ 0 \\ \vdots \\ 0 \\ -d_p \cdot \overline{T_{w,n}^{t-dt}} \\ 0 \\ \vdots \\ 0 \\ -i_p \cdot \overline{T_{w,n}^{t-dt}} \\ 0 \\ \vdots \\ 0 \\ -n_p \cdot \overline{T_{w,n}^{t-dt}} \\ 0 \\ \vdots \\ 0 \\ -s_p \cdot \overline{T_{w,n}^{t-dt}} \end{bmatrix}}_{C}
$$

3.4 ROBUSTNESS AND COHERENCE TEST

Once the MATLAB Simulink model created, a simulation scenario was established, in order to start to run the simulations. The scenario corresponds to a thermal cycle of the unit: charging and discharging period.

It was decided to send to the water-PCM stick exchanger a vertical water flow rate of 0.0003 kg/s (exactly the same water flow rate of the reference system for each PCM stick) at 4 °C during 3 hours.

The initial temperature of the exchanger was set at 15°C and the acquisition time step at 10 seconds.

The same scenario was adopted for each simulation, changing only the nodes discretization crosswise and lengthwise.

An example of the temperature evolution obtained for the same point through the comparison between models differently crosswise and lengthwise discretized is shown in figures 3.17 and 3.18.

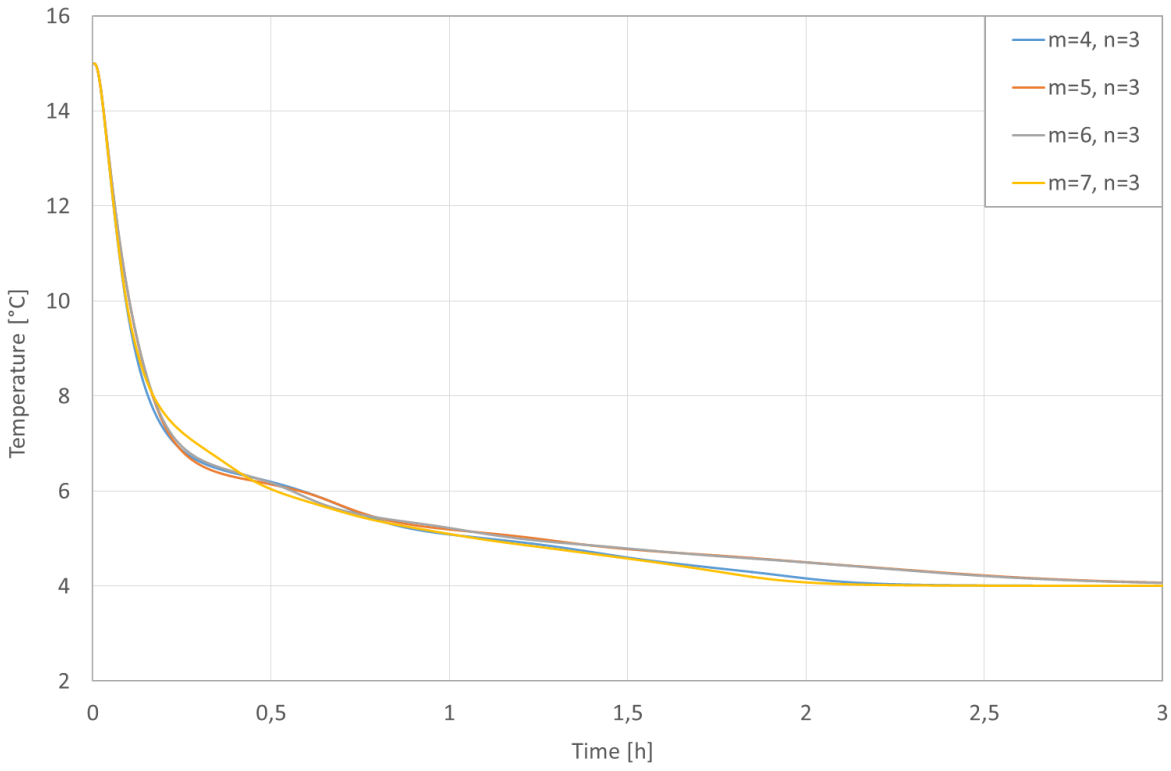

Figure 3. 15 - Example of difference between the temperature curves obtained in the same control volume (i = w, j = n) with various models lengthwise discretized in 3 nodes and crosswise discretized between 4 and 7 nodes.

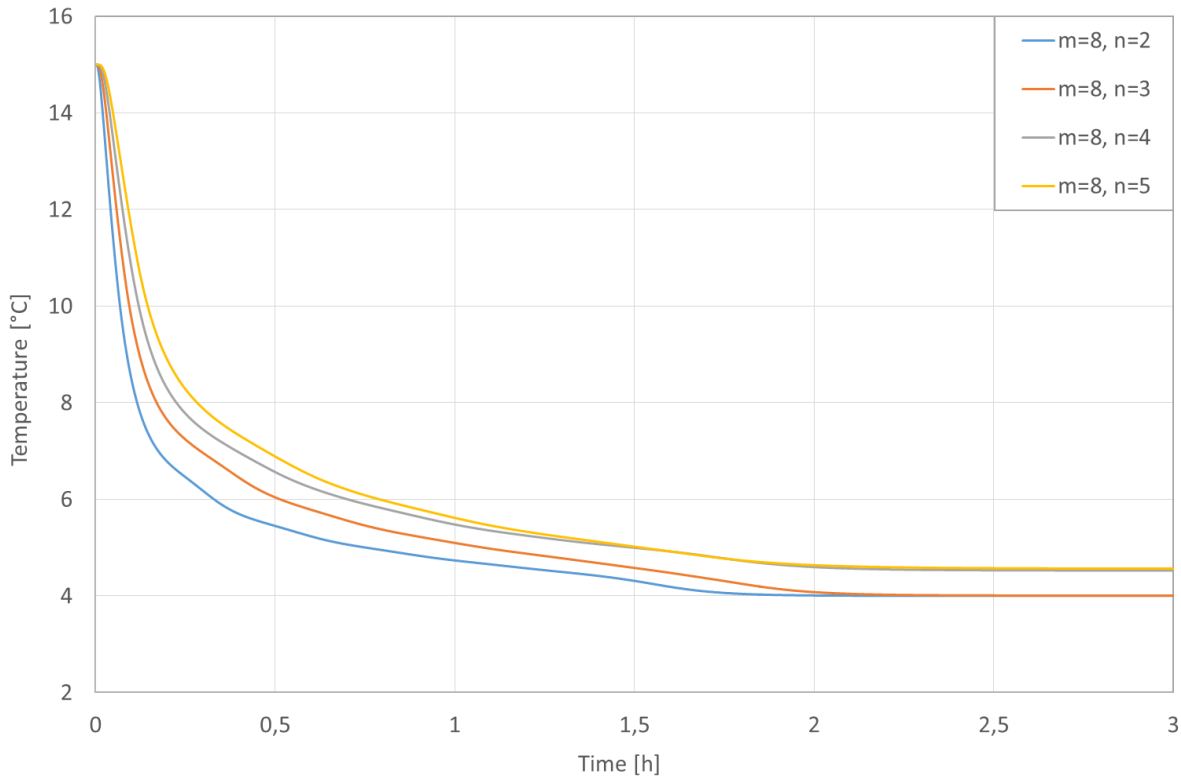

Figure 3. 16 - Example of difference between the temperature curves obtained in the same control volume (i = w, j = n) with various models crosswise discretized in 8 nodes and lengthwise discretized between 2 and 5 nodes.

The temperature curves of the figure 3.17 correspond to the points indicated with red circles in figure 3.19, while those of the figure 3.18 are indicated in figure 3.20.

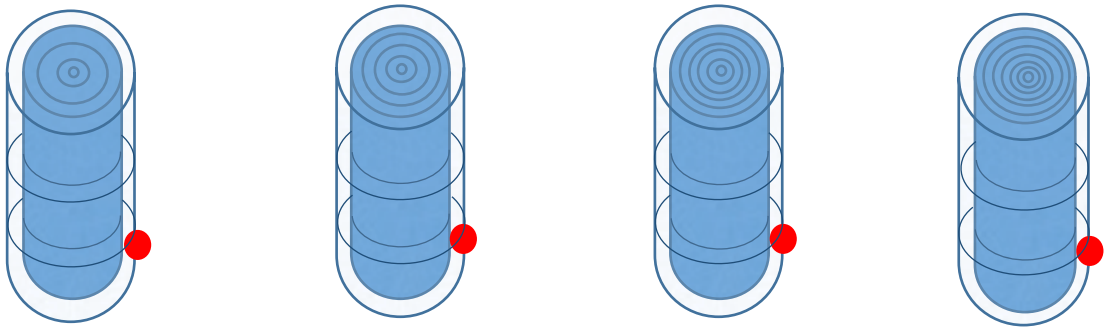

Figure 3. 17 - Position of the points analyzed in figure 3.17 in accordance to the different discretizations.

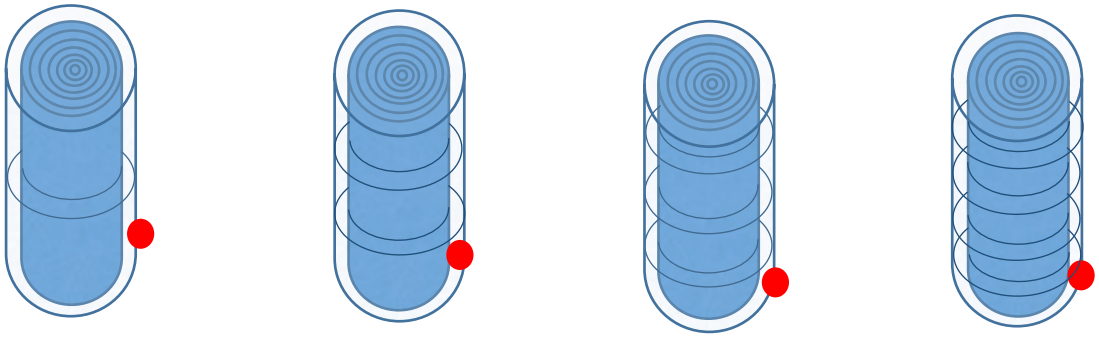

Figure 3. 20 - Position of the points analyzed in figure 3.18 in accordance to the different discretizations.

As it can be noticed, every discretization caused a different temperature evolution curve in each node. This is due to the volume difference between all the different discretization configurations and, in the case shown in figure 3.18, to the different position of the analysed node in relation to the total length of the stick (as it can be observed in figure 3.20).

Once these first results obtained, it appeared necessary to make a comparison between them and the in situ monitored values, in order to calibrate the model and validate it.

However, as the HIKARI's reference thermal storage system was still inoperative when we developed the model, it was impossible to make an experimental validation. For this reason we developed a second numerical model, using a different simulation method – the Computational Fluid Dynamics–, in order to make a first numerical comparison. The model is explained in the next chapter.

3.5 CONCLUSIONS

The design and functioning of the HIKARI's thermal energy storage system at low temperature are described in this chapter, as well as the conception and modelling phases of the numerical model that was developed in order to reproduce its behaviour.

As the objective of this work was to develop a numerical tool useful for the optimization of this innovative technology, it was necessary to create a fast and accurate model that we could couple to the HIKARI's HVEC systems model.

In order to create the model, it was chosen to use the heat balance approach, that is based on the division of the analysed system into a defined number of volume elements and the subsequent application of the energy balance equations for each of them. The problem of the phase change of the heat storage medium was resolved using the apparent heat capacity method, that consists in representing the phase change through an apparent increase of the material's heat capacity value for a certain temperature range.

Once all the energy balance equations written, considering all the relevant energy flows present in the system (in our case conduction, convection and advection), they were transformed in matrix form and finally solved using the software MATLAB Simulink.

The results obtained show that the choice of this approach provided a model with coherent and robust results, even if reliable experimental data are necessary for its validation.

CHAPTER 4

NUMERICAL CALIBRATION

4) NUMERICAL CALIBRATION

4.1 INTRODUCTION

As explained in the previous chapter, the HIKARI's reference thermal storage system was still inoperative when we developed the model, so it was impossible to make an experimental validation.

For this reason we developed a second numerical model using the Computational Fluid Dynamics method, in order numerically calibrate the finite difference method model described in the previous chapter.

The model was developed using the software ANSYS Fluent and its design and development are showed in this chapter. Once the model created, the numerical validation was realized, comparing the results obtained through the different software and analysing their difference using two different criteria.

4.2 NUMERICAL MODELLING

This paragraph exposes the design and development of a numerical model developed using Computational Fluid Dynamics (CFD).

As the objective of this work was to develop a fast and numerical too, accurate which is a great challenge, that we could couple to the HIKARI's HVEC systems model (see chapter 6), the CFD model described in this chapter could be used only for validation purposes, because of its slow computational speed. For instance, for simulating the same phenomenon, the time needed is more than 100 times greater than the time needed using the MATLAB Simulink model.

4.2.1 Computational Fluid Dynamics

The Computational Fluid Dynamics is a branch of fluid mechanics that provides numerical approximation to the equations that govern fluid motion: the three fundamental principles of mass, momentum, and energy conservation (Tannehill, Anderson et al., 1997).

The application of the CFD for the analysis of the fluid problems requires initially the writing of the mathematical equations describing the fluid flow ; these are usually a set of partial differential equations (typically the Navier–Stokes equations, the mass and energy conservation equations, and the turbulence equations) that are then discretized to produce a numerical analogue of the equations. The domain is then divided into small grids or elements. Finally, the initial conditions and the boundary conditions of the specific problem are used to solve these equations (Ashgriz and Mostaghimi, 2000).

In order to solve the governing equations of the fluid motion, the finite volume method was chosen. It is a discretization method for the approximation of a single or a system of conservation laws: partial differential equations that describe the relations between partial derivatives of unknown fields such as temperature, concentration or pressure, with respect to variables within the domain (space, time, etc...) under consideration.

The specificity of the finite volume method with respect to the finite difference method, which we used for our reference model, is that the discretization is performed on the local balance equations, rather than the partial differential equations: the fluxes on boundaries of the control volumes are discretized, rather than the continuous differential operator.

4.2.2 Choice and usage of ANSYS Fluent environment

For the development of this second model, the software ANSYS Fluent was used. This software is based on the finite volume method and Navier-Stokes equations are solved numerically thanks to the discretisation of the domain into a finite set of control volumes and the sequent writing of the general conservation equations for mass, momentum, energy, etc.

Thanks to the interfaces of this software, it is possible to obtain a graphic model of the analysed system, to choose the precision of its division into control volumes and to define the material properties and the boundary condition of the system. Subsequently all the partial difference equations can be discretized into a system of algebraic equations and solved numerically, in order to render the solution field.

As previously mentioned, it was chosen to use this program only for the numerical validation and not for the optimization, because of it is time consuming and because the change of some properties cannot be automatized. For reproducing the temperature evolution of the system during 330 minutes, for example, it needed about 120 minutes while the MATLAB Simulink model needed less than 1 minute.

4.2.3 Numerical model development

As shown in figure 4.1, Ansys Fluent gives the opportunity to define geometry, meshing configuration, solving methods and post-treatment tools.

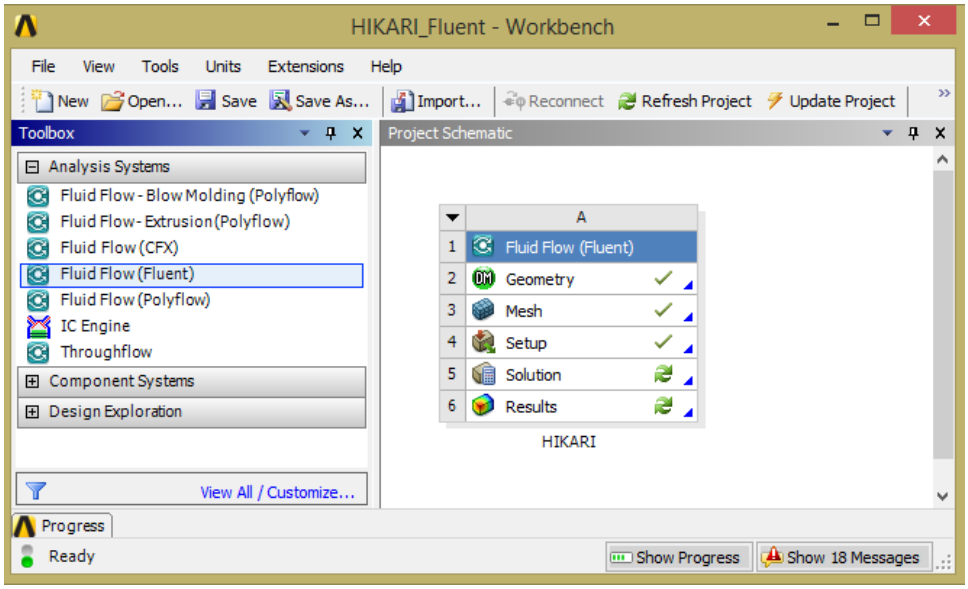

Figure 4. 1 - ANSYS Fluent main screen.

We started by using the Geometry interface in order to create a configuration that should respect the geometry and the proprieties of the PCM water model developed through MATLAB Simulink.

A water layer of 30 cm was nevertheless added on the top and on the bottom of the stick, in order to respect the geometry of the real system (as it can be found in paragraph 3.2) figure 4.2 shows the adopted geometrical configuration.

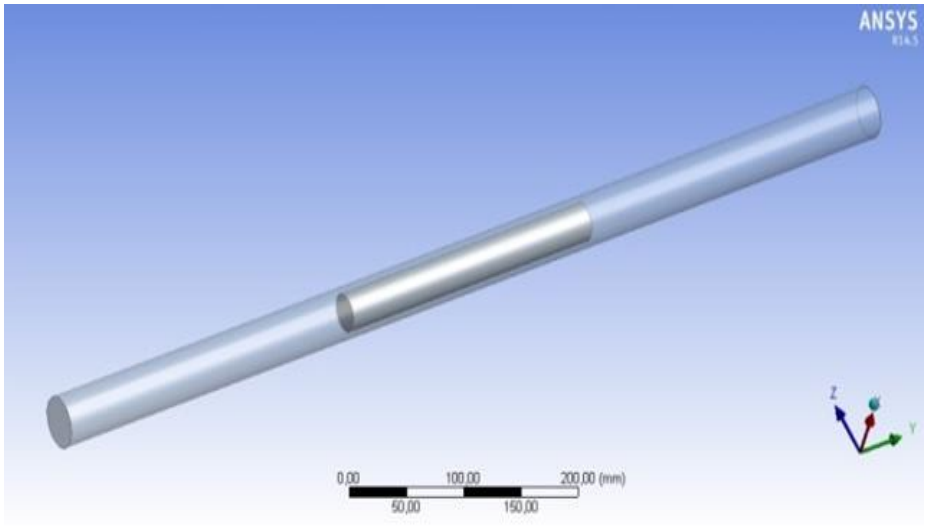

Figure 4. 2 - CFD model of the system realized through the software ANSYS Fluent.

After its design phase, the meshing of the model was chosen using the Mesh interface (figure 4.3).

The minimum edge length was set to 0.088781 m with a minimum of 5 layers.

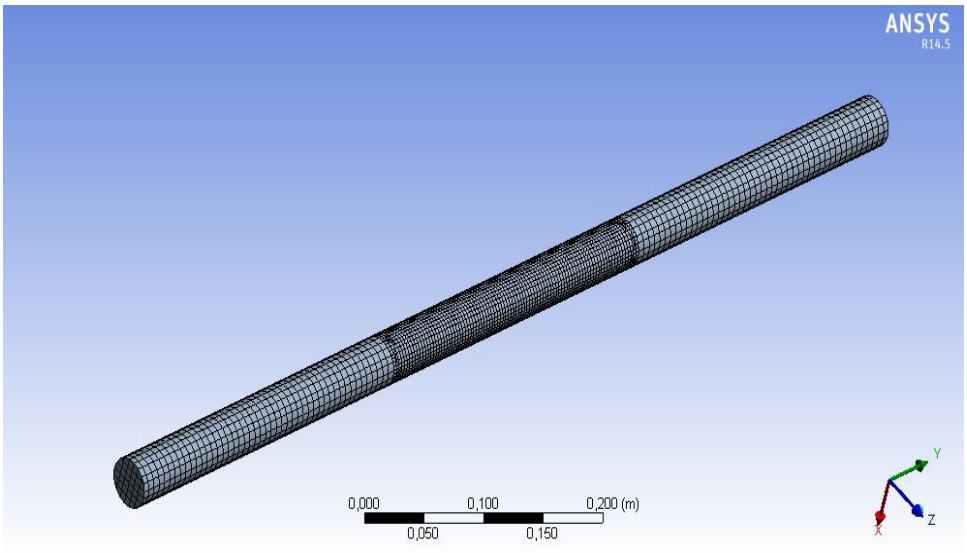

Figure 4. 3 -Meshing of the model realized through the Mesh interface.

Finally, through the Setup ANSYS Fluent interface, the proprieties of the materials were added (figure 4.4).

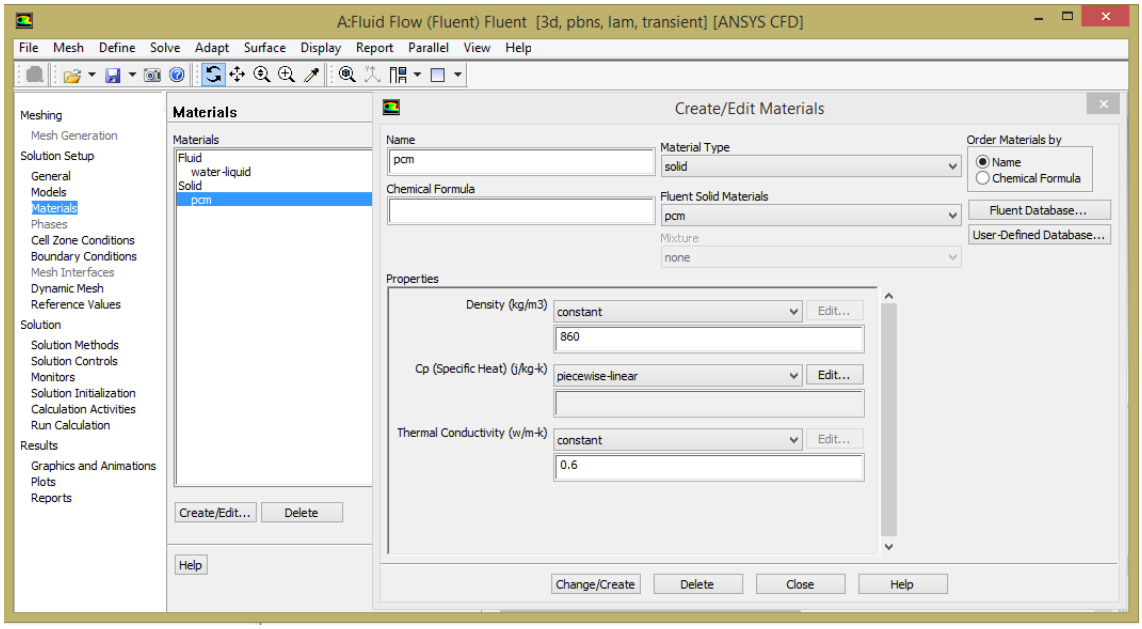

Figure 4. 4 -The ANSYS Fluent Setup interface.

In order to make a valid comparison, we inserted the heat capacity values of the PCM obtained through the DSC method (see paragraph 3.3.4).

Once the model and the materials properties defined, a simulation scenario was established, in order to run the simulations.

The protocol is composed of 3 scenarios, with varying water flow rate (0.00015 kg/s, 0.0003 kg/s and 0.00045 kg/s); every scenario consists of 2 steps:

1) The initial temperature of the exchanger is set at 12°C and the acquisition time step at 10 seconds. A water flow rate at 2°C is sent to the system during 330 minutes.

2) The initial temperature of the exchanger is set at 2°C and the acquisition time step at 10 seconds. A water flow rate at 12°C is sent to the system during 330 minutes.

These water flow rates were chosen because 0.0003 kg/s is the real flow rate that crosses a single PCM stick in the HIKARI reference system, while 0.00015 kg/s and 0.00045 kg/s are respectively the half and the double of its value.

The results obtained after the simulations are finally shown in the Solution interface, that provides temperature evolution curves for each point of the system and shows through an animation how the heat exchange occurs (a video captured frame is shown in figure 4.5).

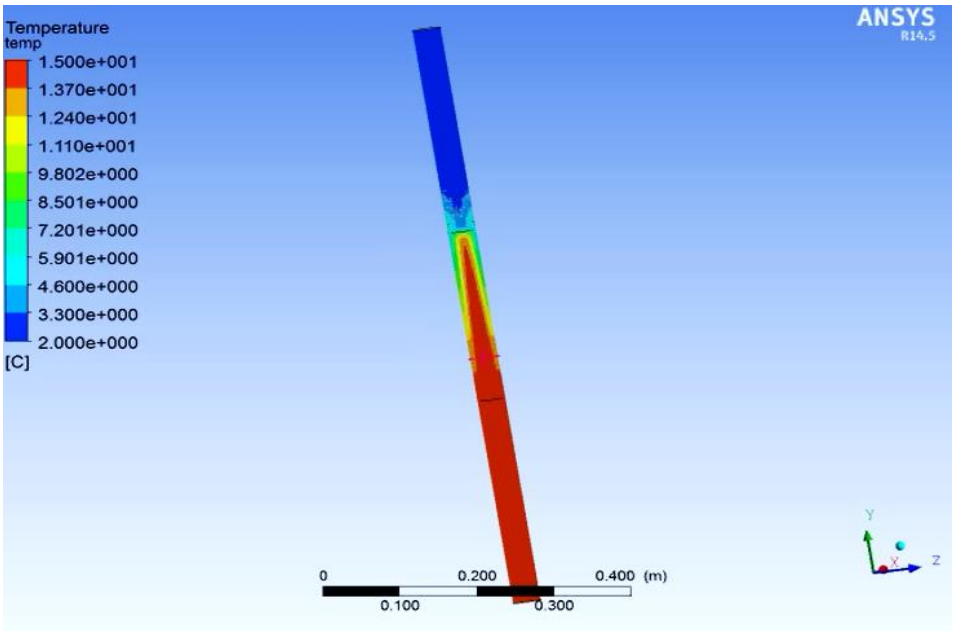

Figure 4. 5 - Frame of the system's temperature evolution video.

4.3 ROBUSTNESS AND COHERENCE TEST

Once all the simulations were run, we compared the temperature results obtained through the developed MATLAB Simulink model and the ANSYS Fluent one for the same points.

Examples of the temperature evolution in the same point (i = w, j = 3) for different discretizations (see paragraph 3.3.5 for discretisation description) during the first and the second step of the 0.00045 kg/s water flow rate scenario are shown in figures 4.6 and 4.7:

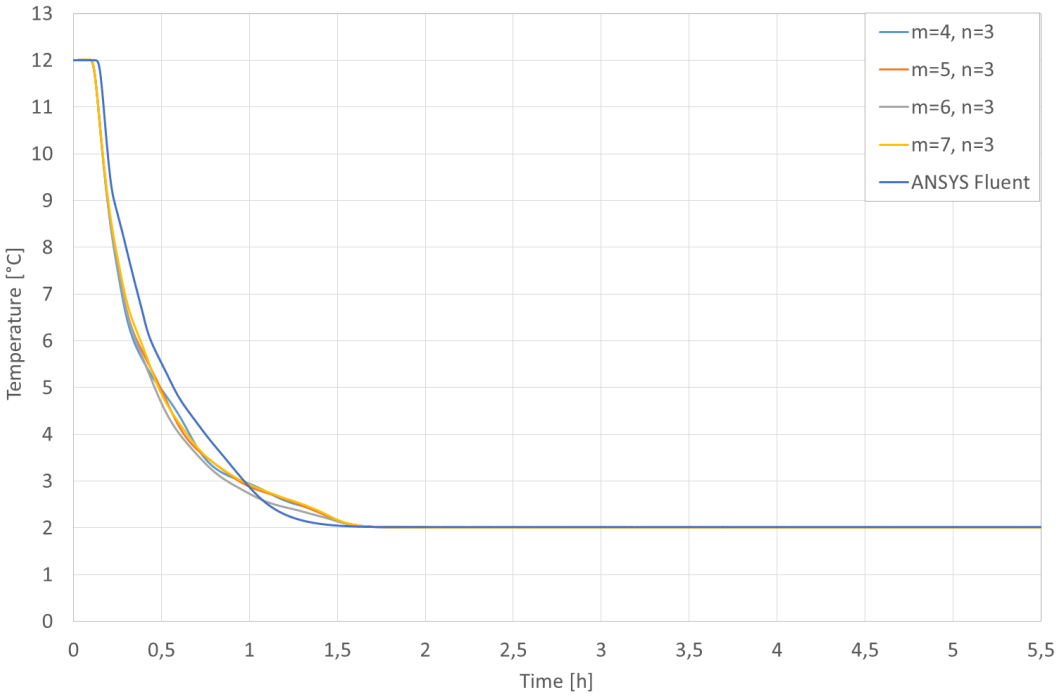

Figure 4. 6 - Comparison of the temperature curves obtained with the two different software in the first step of the 0.00045 kg/s water flow rate for the same point obtained using different crosswise discretization and the same lengthwise discretization (n = 3).

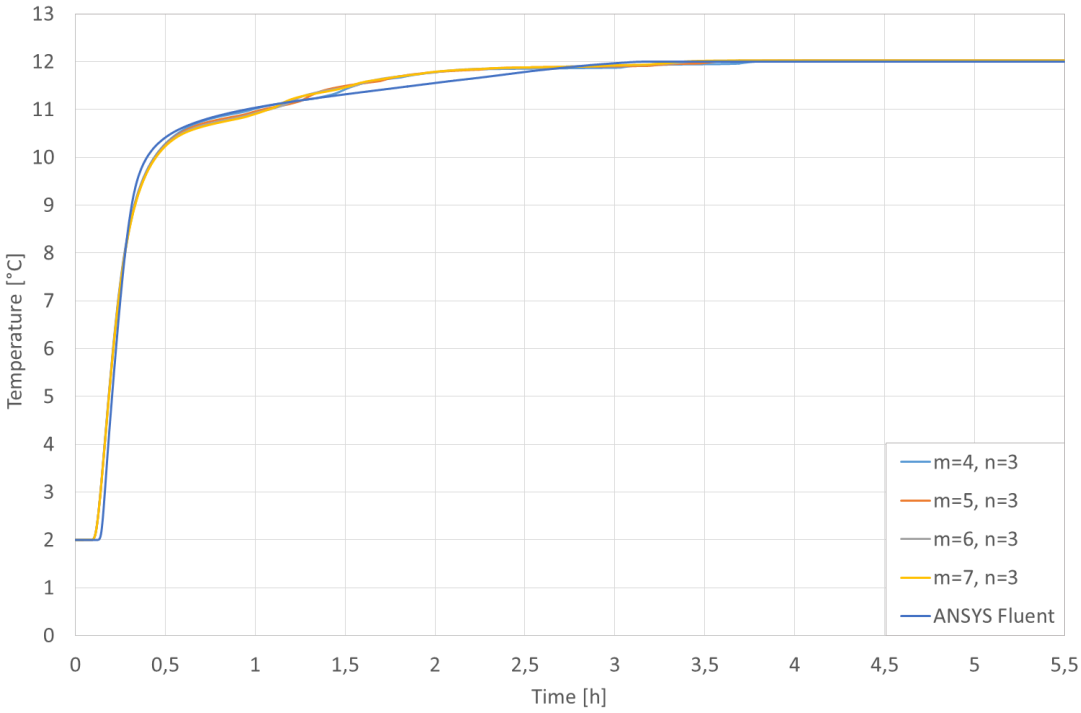

Figure 4. 7 – Comparison of the temperature curves obtained with the two different software in the second step of the 0.00045 kg/s water flow rate for the same point obtained using different crosswise discretization and the same lengthwise discretization (n = 3).

The temperature evolution curves in figures 4.6 and 4.7 show the values obtained through different crosswise discretisation for the same water node (i = w, j = 3) shown in figure 4.8, that corresponds to the point shown in figure 4.9 in the ANSYS Fluent model:

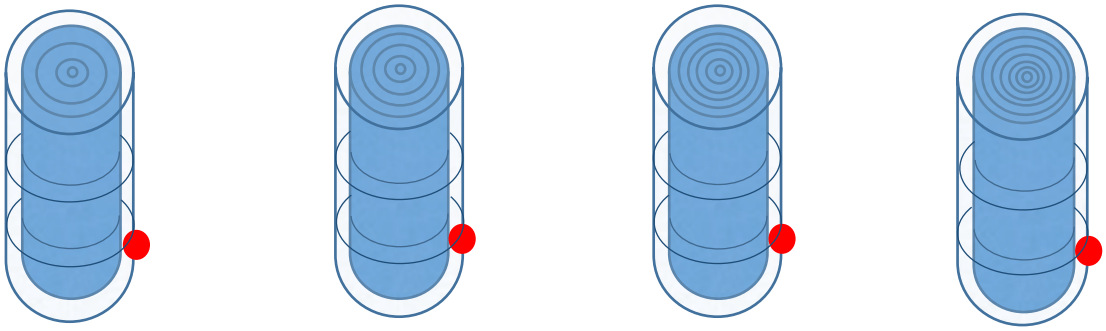

Figure 4. 8 – Position of the analysed point in accordance to the different discretization created through the MATLAB Simulink model.

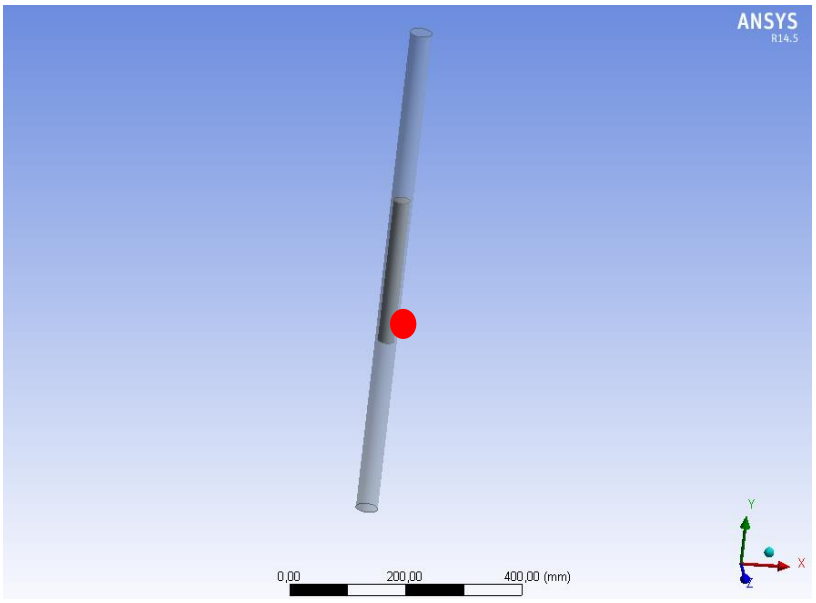

Figure 4. 9 – Position of the analysed point in the ANSYS Fluent model.

All the comparisons were made for each point considering the previously developed discretizations. For the same scenario, examples of comparisons obtained with other discretization of the MATLAB Simulink model are shown in the following figures:

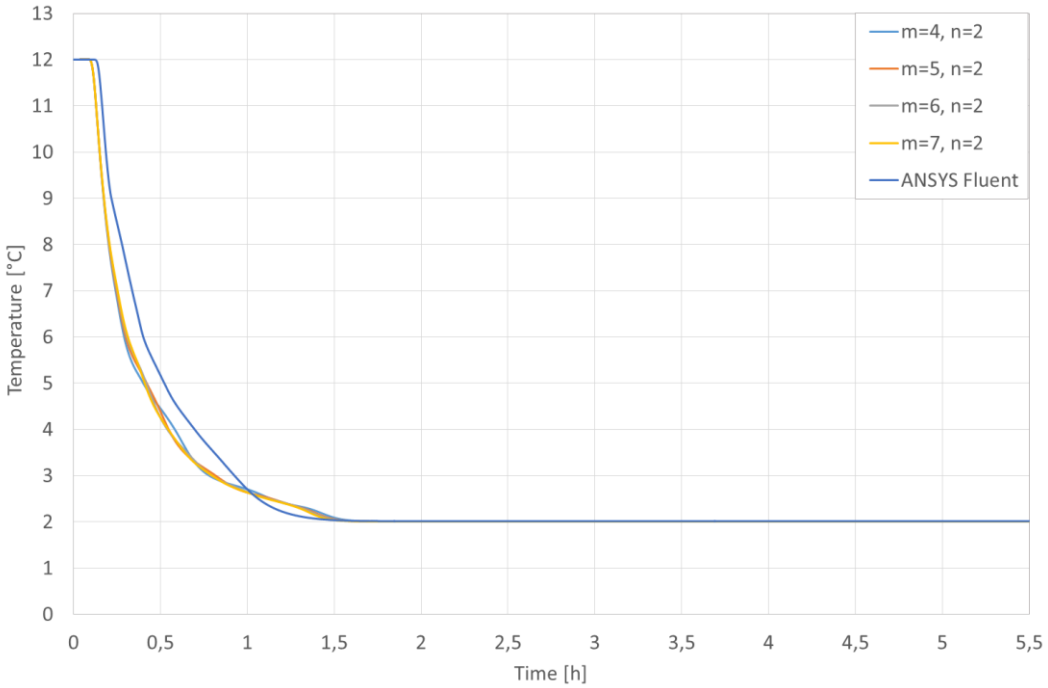

Figure 4. 10 – Comparison of the temperature curves obtained with the two different software in the first step of the 0.00045 kg/s water flow rate for the same point obtained using different crosswise discretization and the same lengthwise discretization (n = 2).

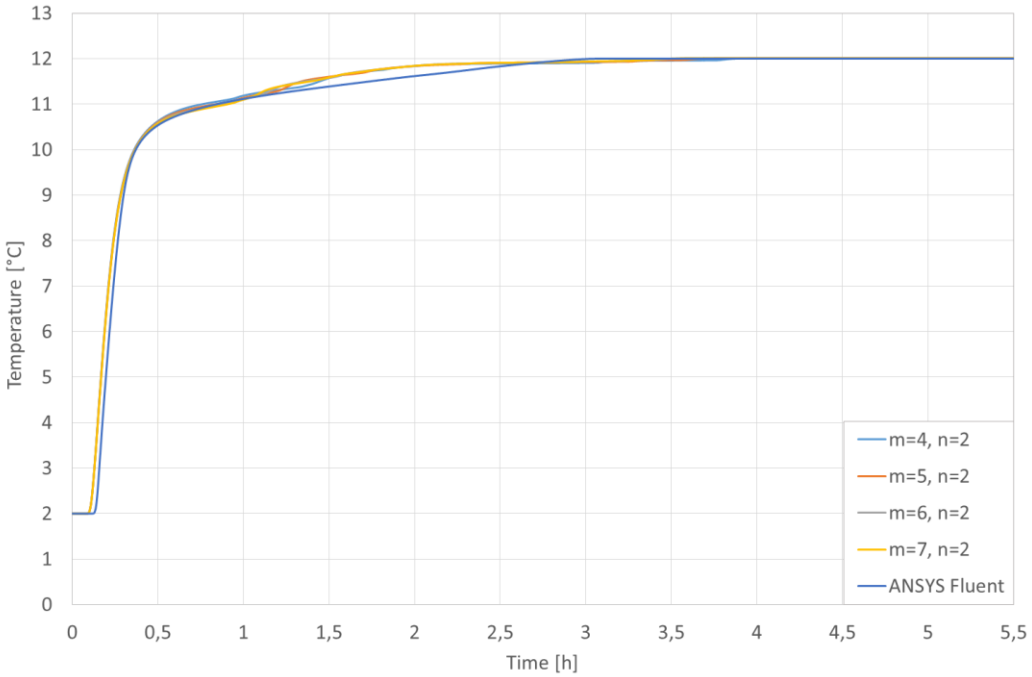

Figure 4. 12 - Comparison of the temperature curves obtained with the two different software in the second step of the 0.00045 kg/s water flow rate for the same point obtained using different crosswise discretization and the same lengthwise discretization (n = 2).

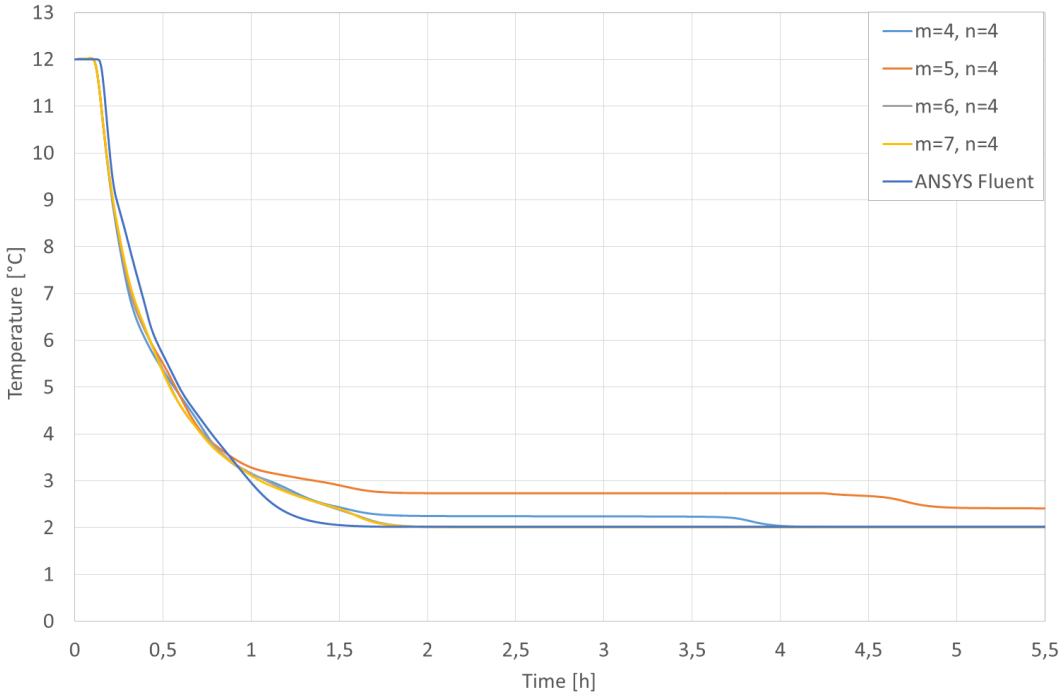

Figure 4. 11 - Comparison of the temperature curves obtained with the two different software in the first step of the 0.00045 kg/s water flow rate for the same point obtained using different crosswise discretization and the same lengthwise discretization (n = 4).

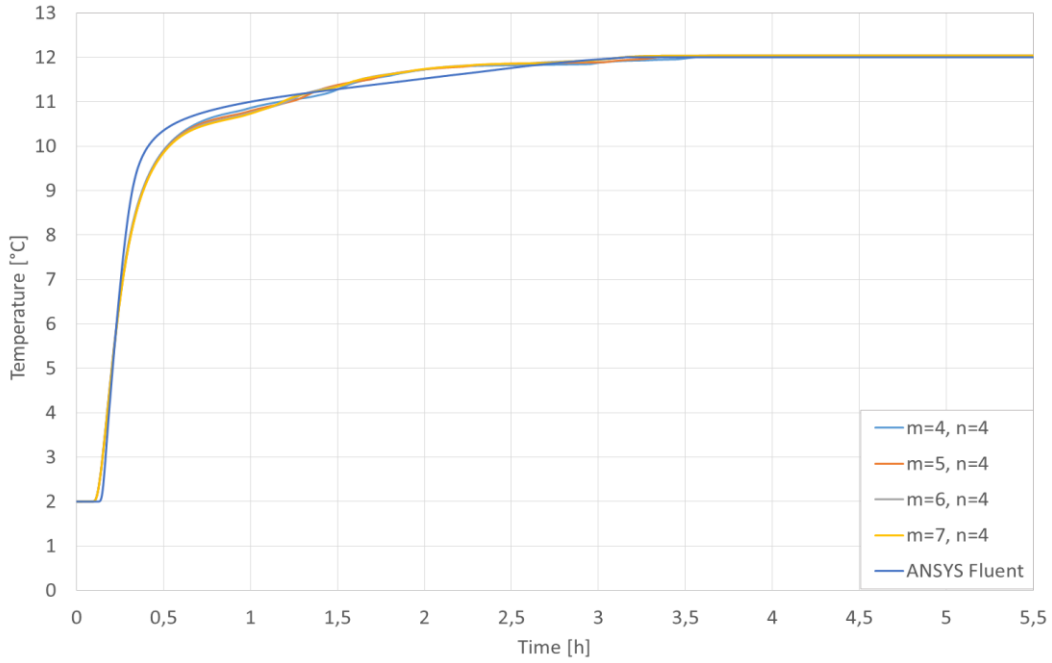

Figure 4. 14 - Comparison of the temperature curves obtained with the two different software in the second step of the 0.00045 kg/s water flow rate for the same point obtained using different crosswise discretization and the same lengthwise discretization (n = 4).

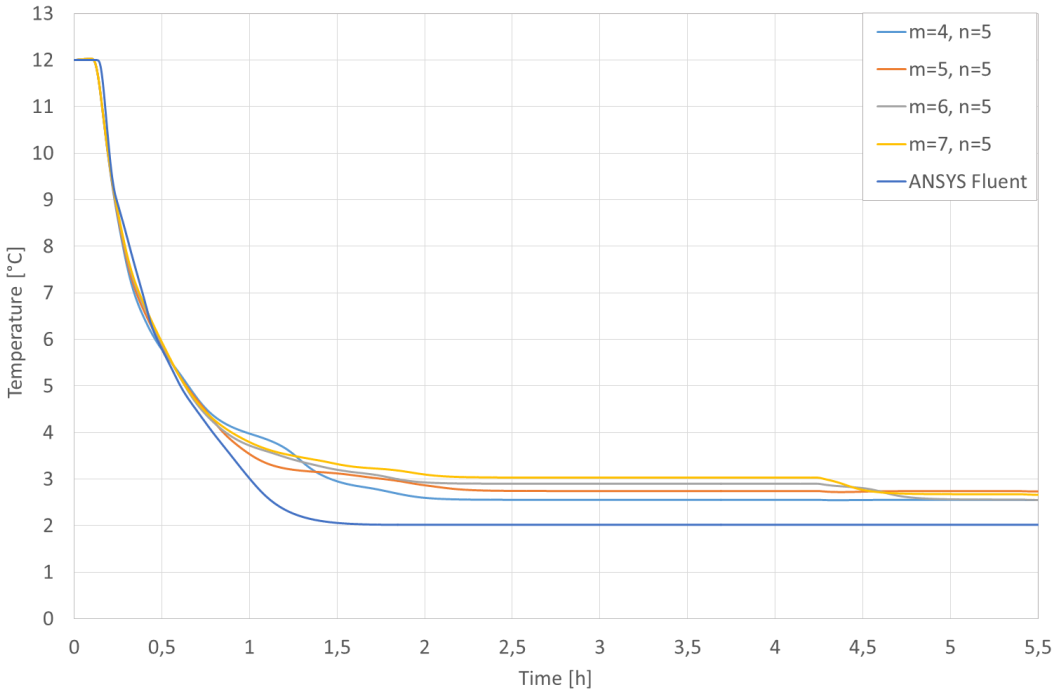

Figure 4. 13 - Comparison of the temperature curves obtained with the two different software in the first step of the 0.00045 kg/s water flow rate for the same point obtained using different crosswise discretization and the same lengthwise discretization (n = 5).

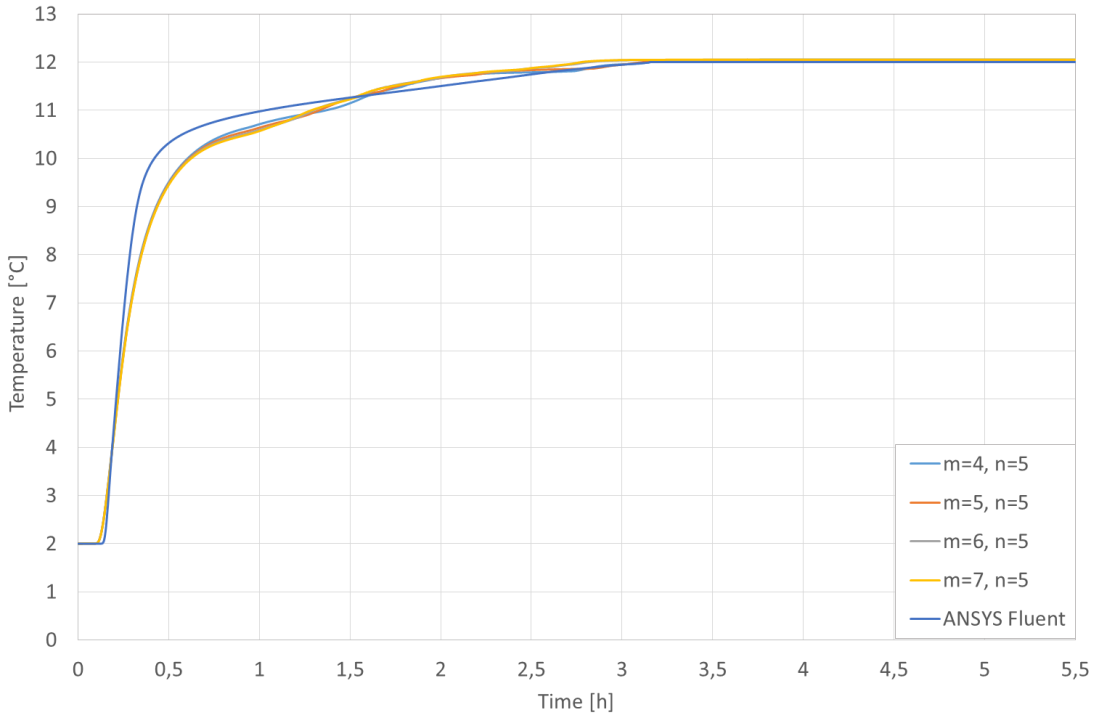

Figure 4. 15 - Comparison of the temperature curves obtained with the two different software in the second step of the 0.00045 kg/s water flow rate for the same point obtained using different crosswise discretization and the same lengthwise discretization (n = 5).

As it can be noticed, in all the figures shown above there is a little time difference between the two software at the moment in which the water starts being chilled (or heated). In fact, for all the scenarios the ANSYS Fluent model starts being chilled (and heated) some minutes after the MATLAB Simulink one, with a difference of the order of 5 minutes. This time delay could be due to the difference between the dimension of the meshing in the two software and to the different solving methods.

Another interesting phenomenon that can be observed is that the MATLAB Simulink model provides some not acceptable results according to physics when it is lengthwise discretized in 4 or more nodes. In fact, one of the assumption made during the modelling phase was that the PCM-water system was considered adiabatic, as all the tanks of the reference system were thermally insulated: for this reason, if a continue water flow rate at 2°C is sent to the system, the whole system should stabilise at 2°C after some time, as there is no heat exchange with the external ambient. Instead, some of the results obtained through particular discretizations, never reach the temperature of 2°C. This could be due to a particular rapport between the length and the thickness of the nodes that does not let the software adequately solve the heat balance equations for those discretizations.

4.4 NUMERICAL CALIBRATION

After different comparisons between the ANSYS Fluent model and the MATLAB Simulink model's results for the same node, we carried out an error analysis between the results obtained through the two software.

In order to test the accuracy of the MATLAB Model two criteria were calculated:

- The Normalized Mean Bias Error (NMBE)

$$\boldsymbol{NMBE} = \frac{\sum_{i=1}^{n}\left(\boldsymbol{y_{simulated,i}} - \boldsymbol{y_{measured,i}}\right)}{\bar{\boldsymbol{y}}_{\boldsymbol{measured}} \times (\boldsymbol{n} - \boldsymbol{p})} \times 100$$

- The Coefficient of Variation of the Root Mean Squared Error (CV(RMSE))

$$\boldsymbol{CV(RMSE)} = \frac{1}{\bar{\boldsymbol{y}}_{\boldsymbol{measured}}} \times \sqrt{\frac{\sum_{i=1}^{n}\left(\boldsymbol{y_{simulated,i}} - \boldsymbol{y_{measured,i}}\right)^2}{(\boldsymbol{n} - \boldsymbol{p} - 1)}} \times 100$$

Typically and according to ASHRAE, models are declared to be calibrated if they produce NMBEs within ± 10% and CV(RMSE)s within ± 30% (ASHRAE guideline 14 – Measurement of Energy and Demand Savings).

We considered the ANSYS Fluent model results as the reference values, and we calculated the variation of the MATLAB Simulink model results from them for each discretization and for the different water flow rate.

After different comparison between the ANSYS Fluent model and all the MATLAB Simulink model's results for the same nodes, it was noticed that some discretization provided a time difference between the two software's results, even if the behaviour could be considered really similar.

In particular, it was noticed that when the model was lengthwise discretized in 4 or more nodes, the time delay was greater. It could be caused by some input errors that caused the delay between the curves or by some assumptions made in the energy balance equations that were incorrect.

However, after the NMBE and the CV(RMSE) were calculated between the ANSYS Fluent model and all the MATLAB Simulink model for different scenarios and discretizations, it was noticed that the discretization that provided the best results was the one with 8 nodes crosswise (7 concentric cylinder and a water layer) and 3 nodes lengthwise (m = 7, n = 3).

In table 4.1 the NMBE and the CV(RMSE) values for this discretization are showed, while figures 4.16, s.17 and 4.18 illustrate the difference between the results obtained with the two software for the point (i = w, j = 3) when the flow rates is 0.00015, 0.0003 and 0.00045 kg/s.

Table 4. 1 - NMBE and the CV(RMSE) values for the comparison between the results obtained through the software ANSYS Fluent and the discretization (m = 7, n = 2) of the MATLAB Simulink model.

Scenario	Statistical Index	Values [%]
1) Flow rate : 0.00015 kg/s	MBE	-0.26
	CV(RMSE)	17
2) Flow rate : 0.0003 kg/s	MBE	-0.18
	CV(RMSE)	12
3) Flow rate : 0.00045 kg/s	MBE	-0.21
	CV(RMSE)	13

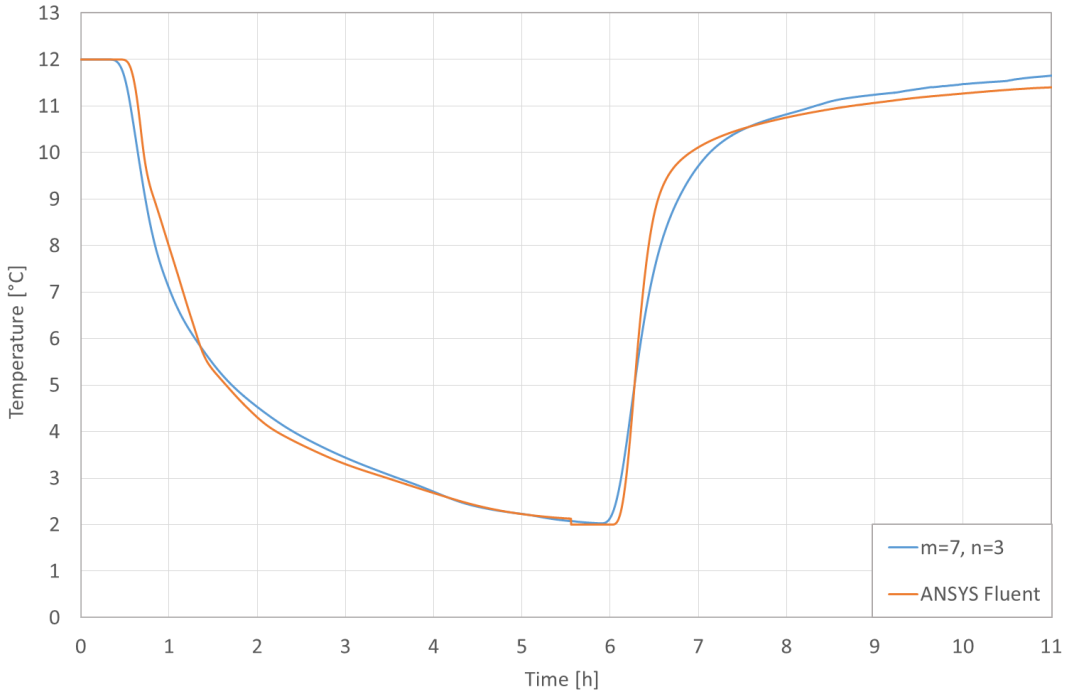

Figure 4. 16 - Comparison of the temperature curves for the same point between the results obtained through the software ANSYS Fluent and the discretization (m = 7, n = 2) of the MATLAB Simulink model for 0.00015 kg/s flow rate.

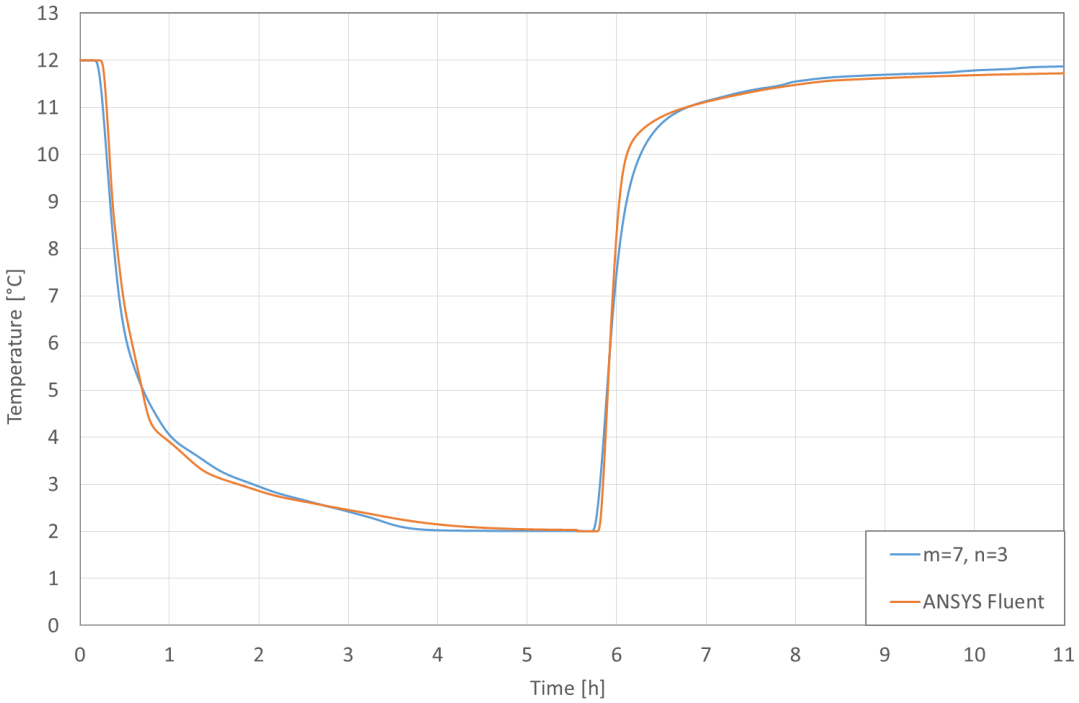

Figure 4. 17 - Comparison of the temperature curves for the same point between the results obtained through the software ANSYS Fluent and the discretization (m = 7, n = 2) of the MATLAB Simulink model for 0.0003 kg/s flow rate.

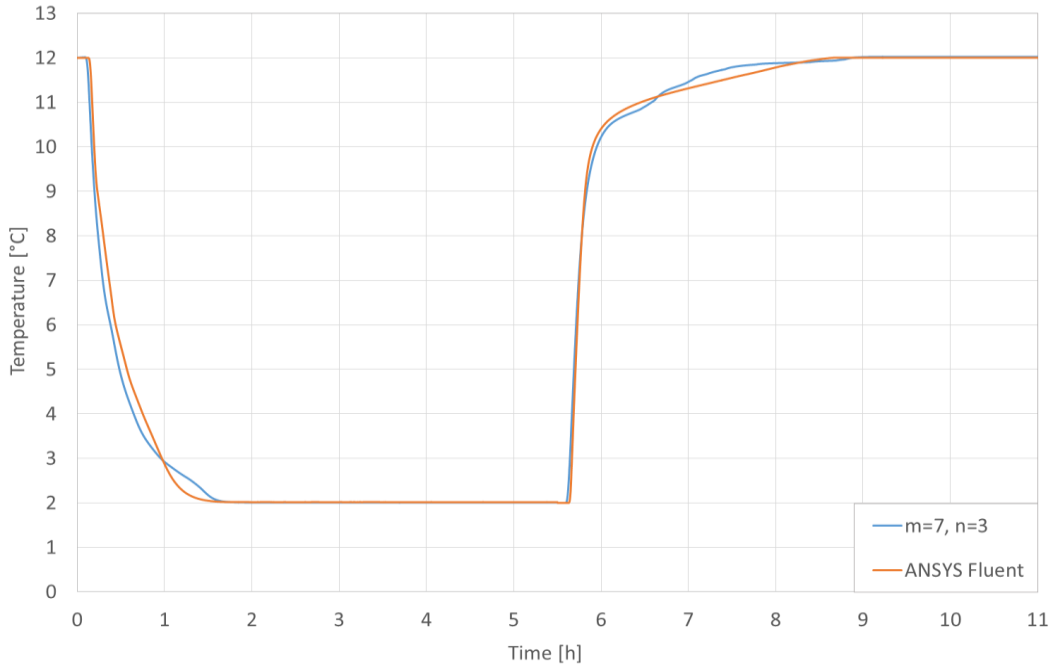

Figure 4. 18 - Comparison of the temperature curves for the same point between the results obtained through the software ANSYS Fluent and the discretization (m = 7, n = 2) of the MATLAB Simulink model for 0.00045 kg/s flow rate.

4.5 CONCLUSIONS

As the HIKARI's reference thermal storage system was still inoperative when the model described in the previous chapter was developed, it was necessary to realize a second numerical model, in order to make a first numerical validation. This second model was developed through the software ANSYS Fluent, that uses Computational Fluid Dynamics.

The first part of the chapter focuses on the conception and development of this model, while the second part is about the numerical calibration of the model developed in the previous chapter.

Even if their behaviour could be considered really similar, some discretization provided a time difference between the two software's results, so it was necessary to conduct an experimental validation in order to have a clearer view on eventual inaccurate assumptions or input errors.

CHAPTER 5

EXPERIMENTAL VALIDATION

5) EXPERIMENTAL VALIDATION

5.1 INTRODUCTION

In order to experimentally validate the numerical model described in chapter 3, both the in situ data obtained through the monitoring of the reference system and an original water – PCM heat exchanger prototype were used.

Indeed, it was considered impossible to obtain a complete experimental validation using the only in situ data because, given the complexity of the reference system, it was very difficult and even impossible to recreate particular conditions, like varying inlet water flow rate or changing the number of plastic cases filled with PCM. For this reason, an experimental prototype with validation purposes was designed, developed, instrumented and carachterized.

The difficulty of this work was to try to reproduce the logic of the behaviour of a 240 m^3 latent heat thermal storage system containing 60 m^3 of PCM using a small-scale prototype and to use the experimentally generated data for a complete experimental validation of a numerical model.

A matter of importance that merits mentioning is the capability of the prototype to test other behaviors. Indeed, due to its versatility the prototype will be able to be used in order to test other scenarios or other kinds of Phase Change Materials, once the numerical model validated. As a matter of fact, interest has already been demonstrated by a visiting PhD student from Hunan (China) and a H2020 project team.

5.2 HIKARI IN SITU MONITORING

Once the HIKARI buildings inaugurated (September 2015), the monitoring process started in order to evaluate the building's and equipments' performance, so as to reach the positive energy balance target.

The energy consumption of the buildings is measured and recorded, including the following building environment conditions, with different sensors:

Meteorological conditions: wind velocity, hygrometry, air temperature,

Solar irradiation with external irradiance sensors (global and diffuse),

Heating and cooling power and energy meters (production and distribution loops),

Electrical power and energy measurement system for pumps, fans and technical equipment,

Electrical power and energy consumption for light, plugs and other specific equipment for each floor and each apartment,

Domestic hot water and tap water consumption for each apartment,

Indoor air temperature in each room of each apartment and offices area.

The measured data are compared every month with the expected simulated data for the same weather conditions to detect any failure or decay between actual and planned performance of equipment and systems.

Measured indoor temperature in every zone is used as input file to finalize the model calibration with the objective to match calculated and measured heating and cooling power profiles.

The last step is the analysis of equipment performances and specific energy model calibration, which have been specifically developed in the frame of the HIKARI project. This is carried out to evaluate onsite the actual performances of:

The heat storage system (see paragraph 1.2)

The PCM storage system (see paragraph 3.2)

The energy storage efficiency could be demonstrated only if the control strategy was implemented correctly. Consequently, a commissioning work has been achieved to operate dynamical measurement to validated programmed control strategies.

5.2.1 The reference system monitoring obtained data

In the specific case of the HIKARI's cold storage system, 14 temperature sensors were inserted in each insulated tank of the system in 14 points of interest represented in the section of the tank 1 shown in figure 5.1 and the scheme shown in figure 5.2.

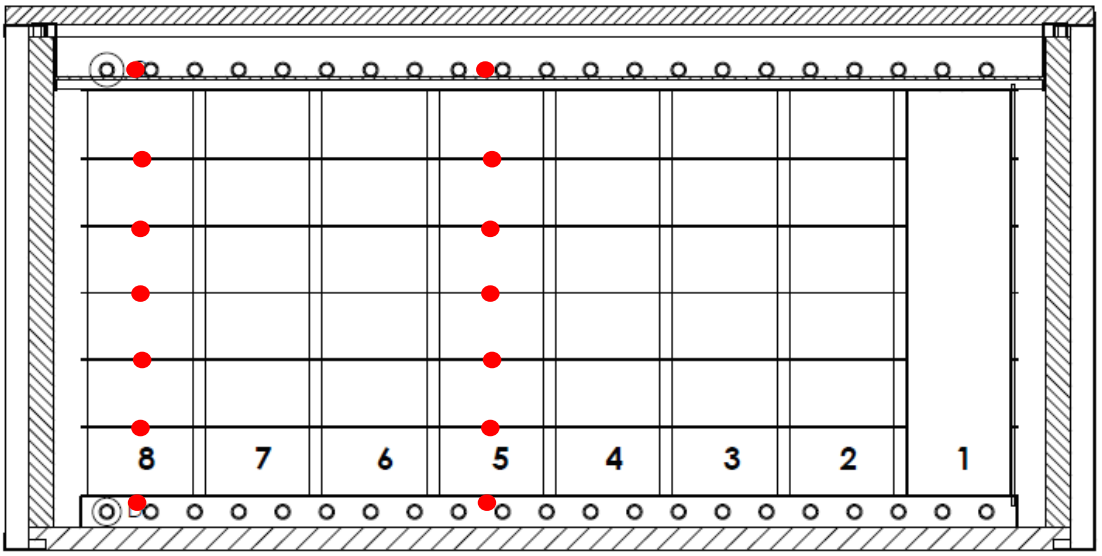

Figure 5. 1 - Section of the tank 1 showing the positions of the temperature sensors.

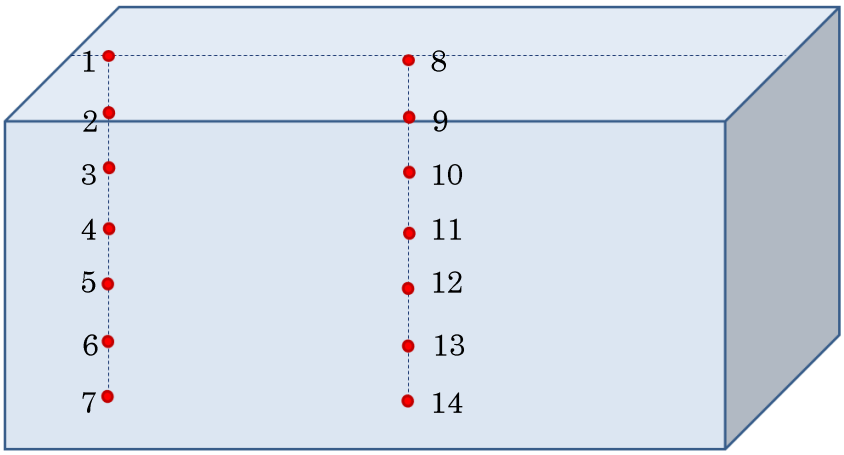

Figure 5. 2 - Scheme of the positions of the temperature sensors in each tank.

As it can be noticed, the temperature sensors were inserted at the top and the bottom of the set of plastic cases filled with the PCM modules and between all the plastic cases. The central and an external column of plastic cases were chosen in order to test the impact of the external leakage and the homogeneity of the vertical heat transfer. The temperature values were registered with a time step of 60 seconds.

An example of the temperature recorded for the tank 1 by the 14 sensors is shown in figure 5.3:

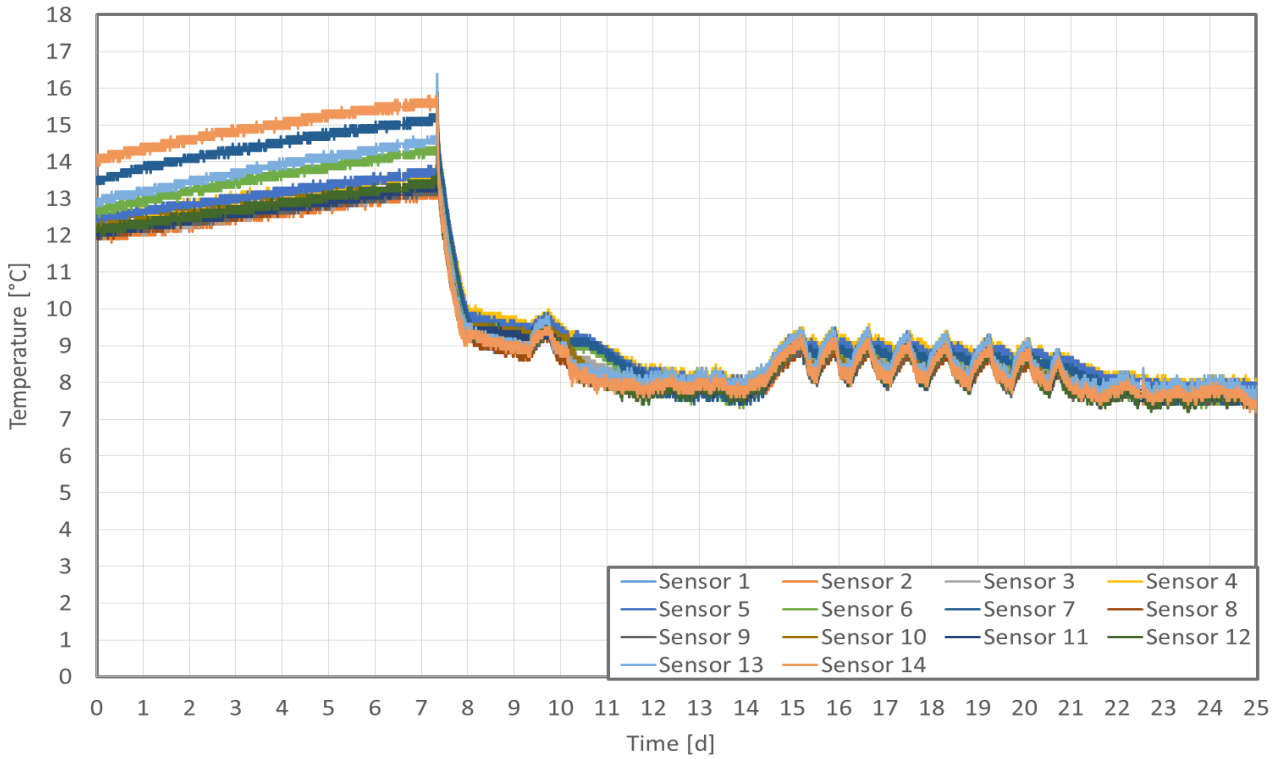

Figure 5. 3 - Example of the temperature recorded by the 14 sensors of the tank 1.

5.3 IN SITU CALIBRATION

Once the in situ data obtained, we started with a comparison between the results obtained through the model and the data registered by the last sensor of the central column of the tank (the number 14 shown in figure 5.2) which correspond to the output value of our model.

A challenging and overcame problem during this part of the work was that the company responsible for the in situ data treatment found out that the flowmeters at the bottom of the tanks could not report the actual water flow rate during the charging phase. In fact, as during this phase the water flow rate was very low, the flowmeters were not accurate enough to measure it and they recorded this value as 0 l/m during the whole time. For this reason and only in this case, we had to correct water flow rate values as input data for our model.

Hence, we resolved this problem adding a constraint at the MATLAB Simulink model, setting a minimum value of 0.3 l/m when the input file showed a value of 0 l/m. We choose this flow rate based on a calibration methodology using a dichotomy method (attempts made setting greater and lower values). This one was considered the best one because it was noticed that inserting it as a lower value, the results obtained from the numerical model were more similar to those obtained through the in situ monitoring.

As for the numerical validation (Paragraph 4.4), we calculated the Normalized Mean Bias Error (NMBE) and the Coefficient of Variation of the Root Mean Squared Error (CV(RMSE)) between the reference results (the data obtained through the in situ monitoring) and the model results, in order to make a first experimental validation.

Once the comparison made between the in situ data and the model results for different discretization, we found out that, even in this case, the discretization that provided the best values was the one that is discretized in 8 nodes crosswise and 3 nodes lengthwise (see paragraph 4.4).

The graphic showing the difference between the in situ data recorded by the sensor 14 and the model results for this discretization is shown in figure 5.4, while the results of the NMBE and CV(RMSE) criteria are shown in table 5.1:

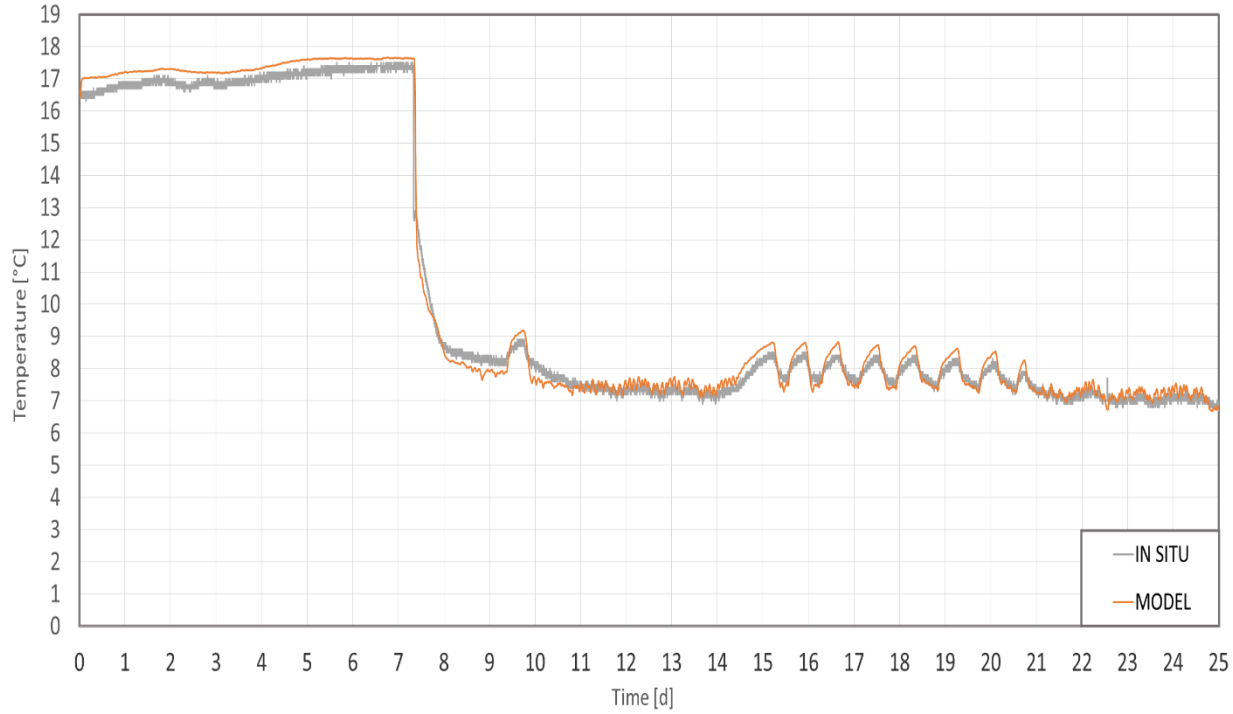

Figure 5. 4 – Comparison of the temperature curves recorded by the sensor 14 and the model results.

Table 5. 1 – Results of the NMBE and CV(RMSE) criteria.

Normalized Mean Bias Error	1,86%
Coefficient of Variance of Root Mean Square Error	4,02%

According to the ASHRAE guideline 14 – Measurement of Energy and Demand Savings (ref), models are assumed to be calibrated if they produce MBEs within ±10% and CV (RMSE)s within ±30%, so the model can be considered validated.

5.4 DESIGN OF THE EXPERIMENTAL PROTOTYPE

5.4.1 Design considerations

As explained in paragraph 5.1, it was not possible to consider the comparison between the model results and the in situ data as a complete experimental validation, as it was impossible to recreate different conditions, such as different inlet water flow rates or quantity of PCM sticks.

For this reason, an original experimental prototype reproducing the HIKARI cold storage system has been developed in the ENTPE Laboratory of Tribology and Systems Dynamics

(LTDS), in order to obtain valid experimental data useful for the experimental validation of the numerical model described in chapter 3.

Several review articles describe existing experimental prototypes of latent heat thermal storage systems: Stathopoulos et al., 2016, Borderon et al., 2015, Lopez-Navarro et al., 2014, Nagano et al., 2006.

Another challenge of this work was to succeed to reproduce the logic of the behavior of a 240 m^3 latent heat thermal storage system containing 60 m^3 of PCM using a small-scale prototype in order to produce the necessary data for a complete experimental validation of a numerical model.

In order to make the comparison useful for the experimental validation, the prototype had to provide the temperature of the water flow before, during and after the passage through the plastic case filled with the PCM sticks.

Even if the construction of this prototype was necessary for the experimental validation of the numerical model developed in this work, our objective was also to develop a test bed useful for the validation of other kinds of phase change materials in the future. For this reason, we wanted to make a prototype easy to dissemble and reassemble (in case of transport) but at the same time able to make the PCM changing quickly its phase and to record all the temperature changes with a very good precision.

For this reason, we planned to use 15 Pt100 sensors with an accuracy of +/- 0.03°C, in order to acquire every temperature value with the least amount of deficit. The sensors were inserted in aluminium tubes (length of 0.9 m and diameter of 1 mm), allowing to protect them from interaction with water and to position them at various depths inside the tank (Figure 5.6). For providing the chilled water to the PCM modules, we used a recirculating chiller able to reach set point temperatures from -10 to +30 °C and with a cooling capacity up to 2000 W.

5.4.2 Initial proposal

The first concept of the prototype consisted of an isolated tank filled with water and containing a plastic case containing PCM sticks equal to those present in the HIKARI reference system (described in paragraph 3.2).

According to this project, water should pass through the plastic case and go out through some small holes present in the tubes that crossed the top and bottom of the tank.

The scheme of this first version is shown in figure 5.5:

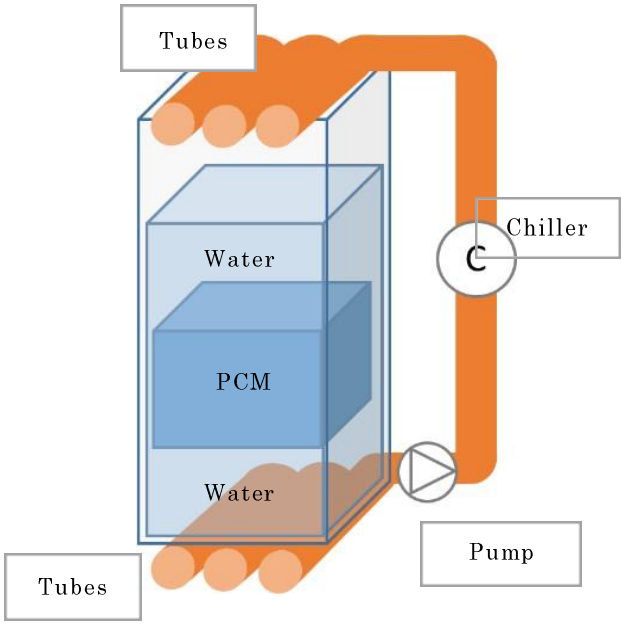

Figure 5. 5 – Scheme of the first version of the laboratory prototype.

The problem that we could have encountered with a similar prototype is that it would not offer the possibility to chill directly the fluid that passed through the tubes connected to the chiller: in fact, the latter is compatible only with brine and in order to represent the real reference system with its real properties water had to be used.

Other design limitations could be that the chiller was not powerful enough to chill the water once it went out from the exchanger and that the presence of the tubes on the top of the tank made difficult to position the temperature sensors.

In order to find a solution for these problems, we added a second tank connected with the chiller. This second tank is used as a buffer zone where the temperature of the water can be regulated until it reaches the set point temperature. Once reached, the water is sent to the other tank through a submersible pump (max. flow rate 108.3 l/m), where it crosses the PCM modules layer and makes the heat exchange happen.

The water injected in the tank filled with the plastic case enters through a single tap positioned in the middle of a lid: in this way it is possible, at the same time, to control the water flow rate and to position the 15 temperature sensors (Figure 5.6) in specific locations all around the tap (as showed in figure 5.7).

Figure 5. 7 - PT100 temperature sensor.

Figure 5. 6 - Disposition of the temperature sensors on the lid of the tank.

The sensors were installed in several points of the inlet, intermediate and outlet part of the prototype, in order to provide an overview of the water temperature evolution at these three key positions.

The final version of the prototype is shown in the scheme below. It consists of three main parts: the chiller, the first tank (containing water as the heat transferring fluid and the pump) and the second tank (containing the PCM case and water).

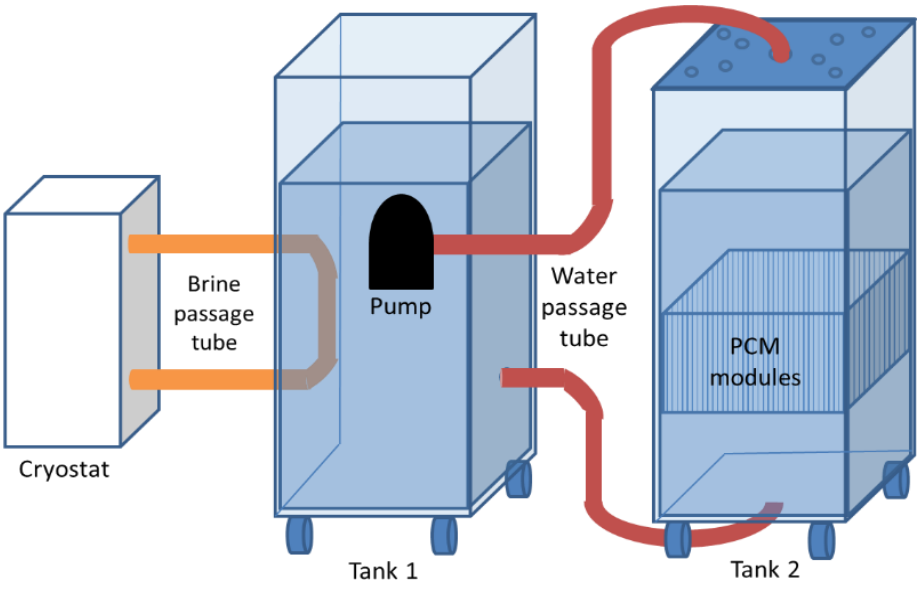

Figure 5. 8 - Scheme of the final version of the prototype.

Some pictures of the prototype can be found in the Annex A.

5.6 CONFIGURATION, MONITORIN AND DATA ACQUISITION OF THE SYSTEM

LabVIEW programming language and environment was used for data acquisition and control of the components of the experimental test bed. A graphical interface (Figure 5.9) was created through this software, by which it was possible to acquire the temperature values registered by all the sensors at each time step and at the end of the entire cycles and to switch on and off the pump whenever it was needed.

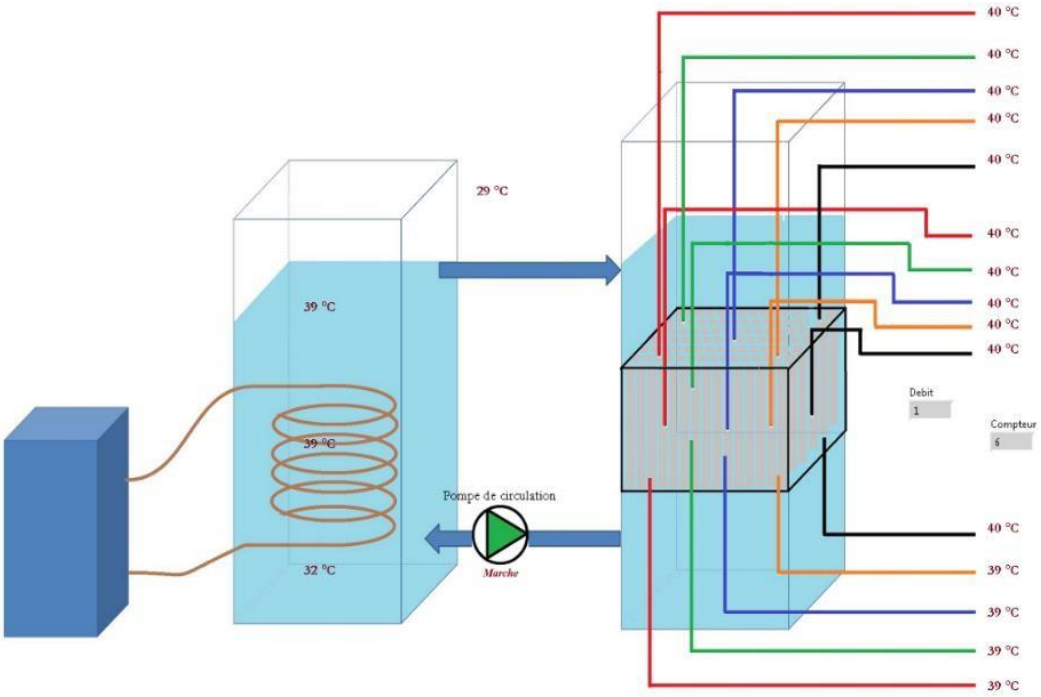

Figure 5. 9 – Graphical interface created through LabVIEW.

The data logger is composed of 3 National Instruments Cards that are inserted in a Compact Daq modular system (figure 5.10) and connected to a PC through a USB port. The developed LabVIEW interface performs data acquisition at any desired time step.

Figure 5. 10 – Compact Daq modular system.

In a first step, only one PCM module has been inserted in tank 2, in order to test the PCM-water heat exchange prevision of the model along the length of a single gel stick.

The dots (red, brown and yellow) shown in figure 13 illustrate the position of the temperature sensors before, during and after the heat exchange with the PCM sticks contained in the plastic case.

As the discretization that provided us the best values both for the numerical and in situ validation was that with a lengthwise discretization in 3 nodes, we choose the position of the sensors because of their correspondence with the nodes analyzed in the numerical model, in order to make the comparison (figure 5.11).

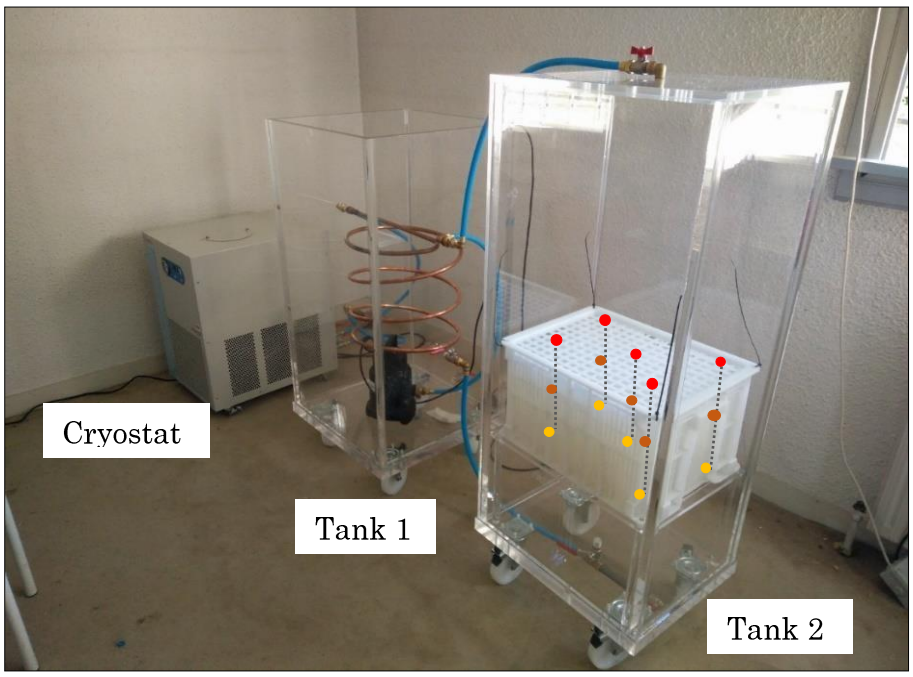

Figure 5. 11 - Positions of the 15 points analyzed using the temperature sensors for scenarios 1, 2 and 3.

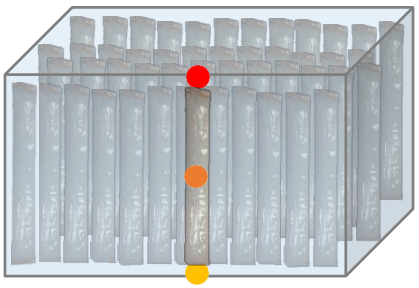

Figure 5. 13 - Position of the temperature sensors in relation to the PCM sticks contained in the plastic case.

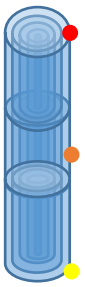

Figure 5. 12 - Position of the temperature sensors in relation to the discretization used for the modelling of a PCM stick.

In a second step another PCM module has been inserted on the first one in tank 2 (figure 5.14), in order to test if the model is able to simulate the heat exchange module-module beside the module-water flow one. In this second case the PT100 temperature sensors have been placed at 15 different points corresponding to the points analyzed in the model of a double PCM gel stick-water heat exchange (figures 5.15 and 5.16).

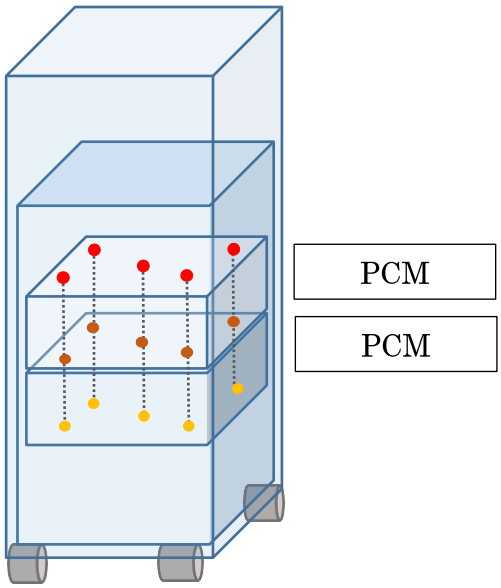

Figure 5. 14 - Positions of the 15 points analysed using the temperature sensors for scenarios 1, 2 and 3.

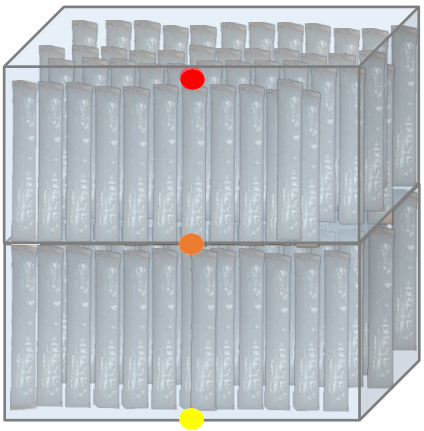

Figure 5. 16 - Position of the temperature sensors in relation to the PCM sticks contained in the plastic case.

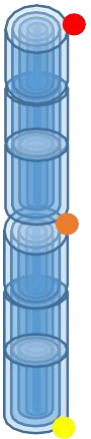

Figure 5. 15 - Position of the temperature sensors in relation to the discretization of the finite difference method model of a PCM stick.

5.5 EXPERIMENTAL PROTOCOL

Once the prototype built, an experimental protocol has been established, in order to test the "goodness of fit" between the numerical model prediction and the experimental data in different scenarios. The objective of this protocol is to recreate particular situations that cannot be obtained using only thein situ data, that are registered in the operating scenario of the system.

In particular, we wanted to overcome two obligations imposed by the real functioning of the system: the constant water flow rate and temperature range.

The water flow rates were chosen considering the flow rate for every plastic case of the reference system during the charge period (3 l/m).

It was decided to test the heat exchange when the flow rate between the two tanks is the half (1.5 l/m) and the double (6 l/m) of that value in order to verify the validity of the numerical model when it is used in different contexts.

As regards the temperature range, we know that the reference storage system works between 6 and 10°C. Our objective was to make the prototype work with water temperatures ranging from 3 to 20°C.

For this reason, the protocol is composed of 6 scenarios, with varying water flow rate (1.5, 3 and 4.5 l/min) and different PCM quantity (1 or 2 plastic cases), as summarized in Table 5.2 ; every scenario consists of 4 steps:

1) The cryostat is set to -2°C and the pump that regulates the water flow between the two tanks is off. The water of tank one is chilled during 8 hours.

2) The cryostat is still set to -2°C, but the pump that regulates the water flow between the two tanks is on. The heat exchange between the PCM modules and the water flow happens and it reproduces the charging phase of the system during 16 hours.

3) The cryostat is set to 20°C and the pump that regulates the water flow between the two tanks is off. The water of tank one is heated during 8 hours.

4) The cryostat is still set to 20°C, but the pump that regulates the water flow between the two tanks is on. The heat exchange between the PCM modules and the water flow occurs and it reproduces the discharging phase of the system during 16 hours.

Table 5. 2 – Scheme of the experimental protocol.

Scenario	Steps	Duration of the steps [h]
1 Plastic case Flow rate : 1,5 l/min	Cryostat set to -2 °C / Pump off	8
	Cryostat set to -2 °C / Pump on	16
	Cryostat set to 20 °C / Pump off	8
	Cryostat set to 20 °C / Pump on	16
1 Plastic case Flow rate : 3 l/min	Cryostat set to -2 °C / Pump off	8
	Cryostat set to -2 °C / Pump on	16
	Cryostat set to 20 °C / Pump off	8
	Cryostat set to 20 °C / Pump on	16
1 Plastic case Flow rate : 4,5 l/min	Cryostat set to -2 °C / Pump off	8
	Cryostat set to -2 °C / Pump on	16
	Cryostat set to 20 °C / Pump off	8
	Cryostat set to 20 °C / Pump on	16
2 Plastic cases Flow rate : 1,5 l/min	Cryostat set to -2 °C / Pump off	8
	Cryostat set to -2 °C / Pump on	16
	Cryostat set to 20 °C / Pump off	8
	Cryostat set to 20 °C / Pump on	16
2 Plastic cases Flow rate : 3 l/min	Cryostat set to -2 °C / Pump off	8
	Cryostat set to -2 °C / Pump on	16
	Cryostat set to 20 °C / Pump off	8
	Cryostat set to 20 °C / Pump on	16
6) 2 Plastic cases Flow rate : 4,5 l/min	Cryostat set to -2 °C / Pump off	8
	Cryostat set to -2 °C / Pump on	16
	Cryostat set to 20 °C / Pump off	8
	Cryostat set to 20 °C / Pump on	16

5.7 ROBUSTNESS AND COHERENCE TEST

For every scenario, the temperature evolution was registered. The curves showing the data measured by the 15 sensors positioned in tank during a charging and discharging cycles for all the scenarios are shown in the following figures. The non-linear evolution of the temperature is observed during the phase change of the PCM.

The position of each sensor is shown in figure 5.17:

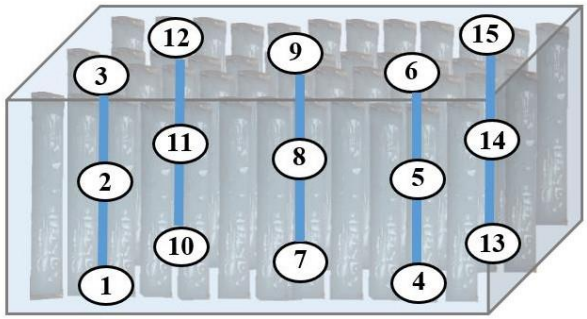

Figure 5. 17 - Position of the temperature sensors.

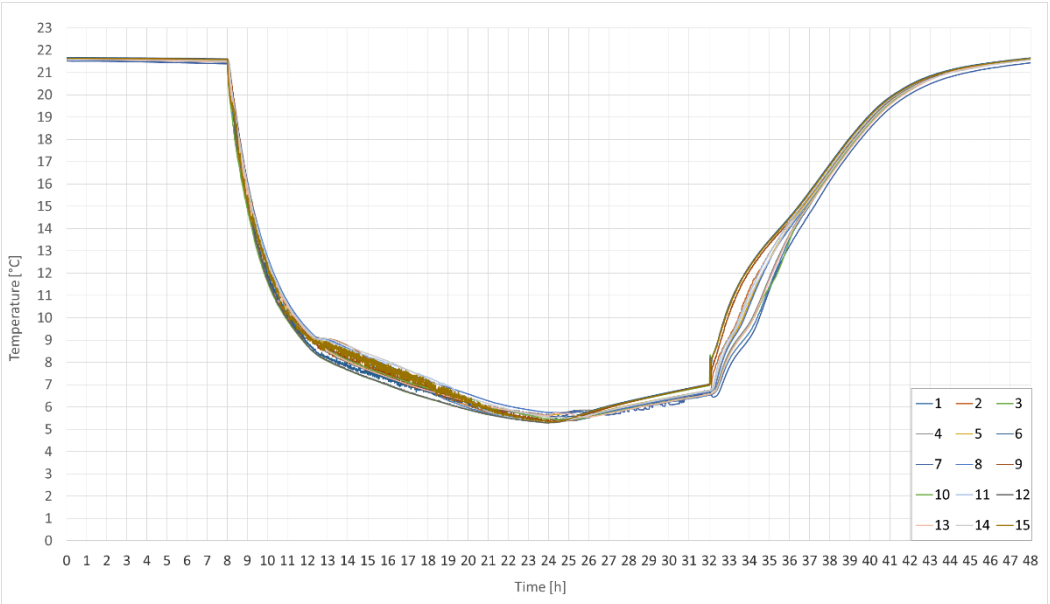

Figure 5. 18 - Water temperature recorded by all the sensors put in the tank 2 in the scenario 1 (one plastic case, flow rate: 1.5 l/min).

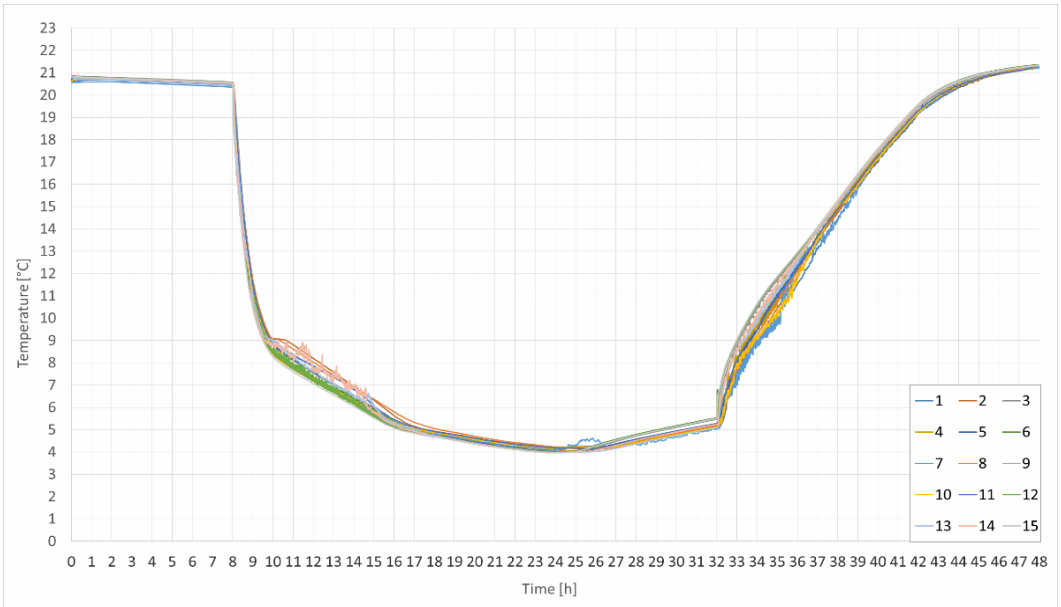

Figure 5. 19 – Water temperature recorded by all the sensors put in the tank 2 in the scenario 2 (one plastic case, flow rate: 3 l/min).

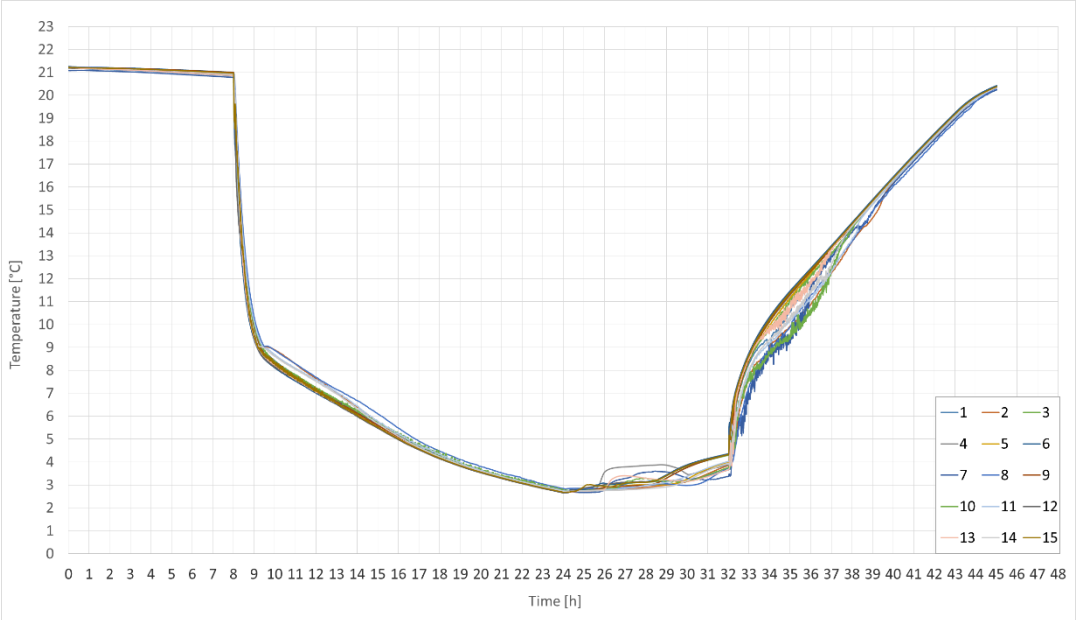

Figure 5. 20 – Water temperature recorded by all the sensors put in the tank 2 in the scenario 3 (one plastic case, flow rate: 4.5 l/min).

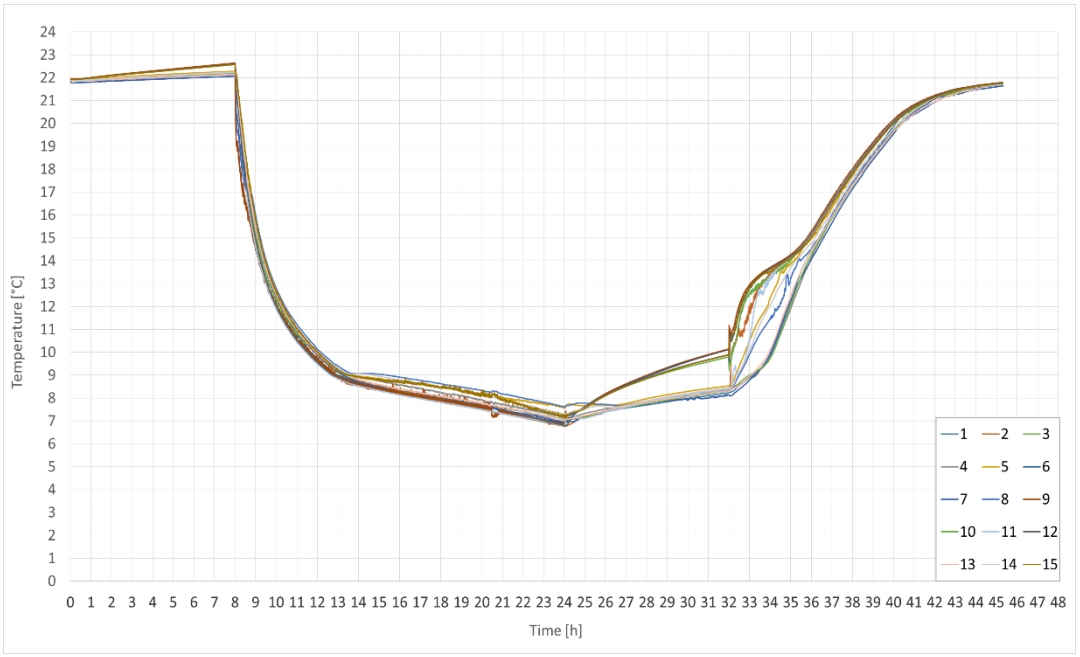

Figure 5. 21 – Water temperature recorded by all the sensors put in the tank 2 in the scenario 4 (two plastic cases, flow rate: 1.5 l/min).

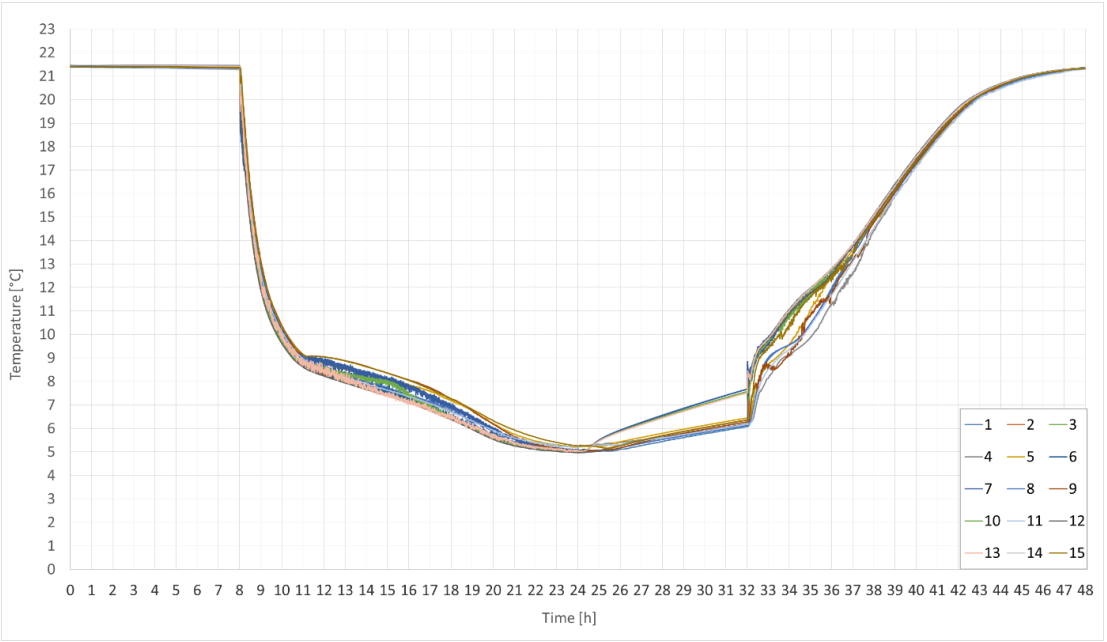

Figure 5. 22 – Water temperature recorded by all the sensors put in the tank 2 in the scenario 5 (two plastic cases, flow rate: 3 l/min).

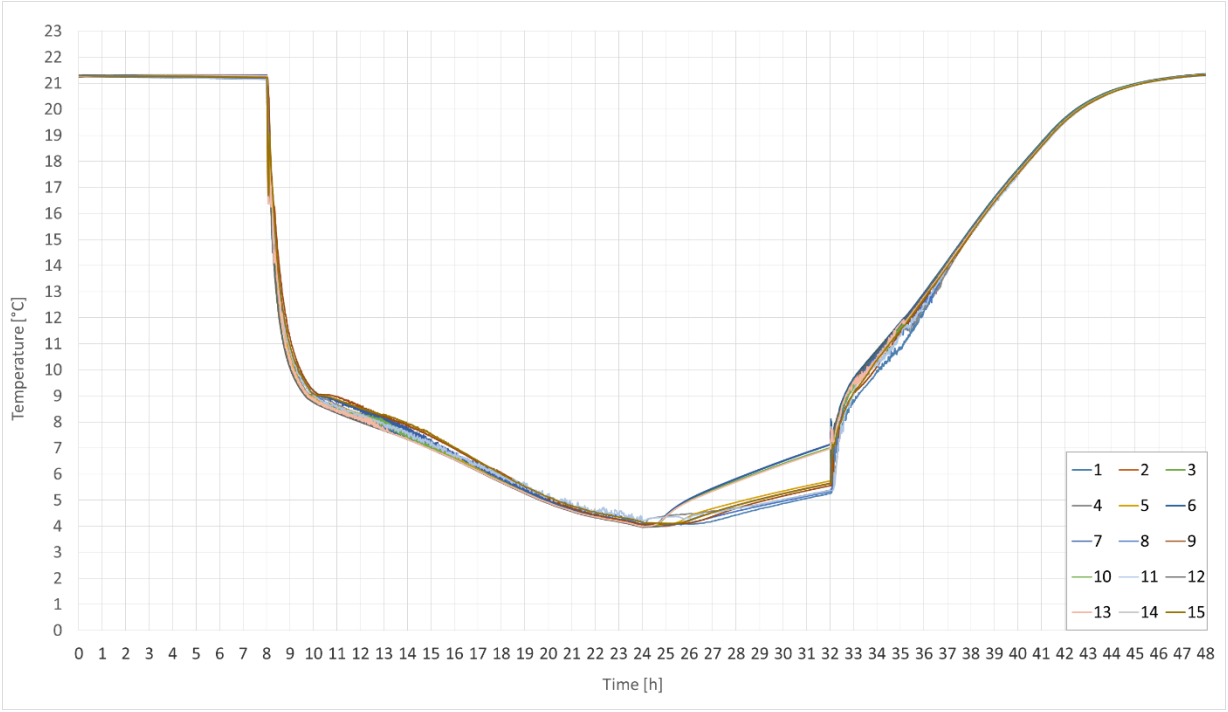

Figure 5. 23 - Water temperature recorded by all the sensors put in the tank 2 in the scenario 6 (two plastic cases, flow rate: 4.5 l/min).

As the numerical model will simulate the heat exchange between a single PCM stick and the water flow around it, it will be necessary to have single inlet, intermediate and outlet values. For this reason, we thought to use the arithmetical mean value of the temperatures registered by all the sensors placed at the same height (3-6-9-12-15, 2-5-8-11-14 and 1-4-7-10-13), but this option could be invalid if there was an excessive difference between the temperature values registered by the sensors of each group, for example due to the effect of the proximity of the sensors at the tank walls.

For this reason, the standard deviation (σ) was calculated for the difference between the temperatures registered by the 5 sensors placed at the top (inlet level), in the middle (intermediate level) and at the end of the plastic cases (outlet level) for each scenario.

The results are showed in the table below:

Table 5. 3 - Standard deviation study of the differences between the temperatures registered by the sensors placed at different levels of the plastic cases.

Scenario	Level	Standard deviation (σ) [°C]
1	INLET	0,16
	INTERMEDIATE	0,14
	OUTLET	0,12
2	INLET	0,12
	INTERMEDIATE	0,17
	OUTLET	0,18
3	INLET	0,11
	INTERMEDIATE	0,22
	OUTLET	0,25
4	INLET	0,18
	INTERMEDIATE	0,29
	OUTLET	0,10
5	INLET	0,14
	INTERMEDIATE	0,29
	OUTLET	0,11
6	INLET	0,12
	INTERMEDIATE	0,19
	OUTLET	0,14

As it can be observed, the standard deviation results less than 0,3 °C in every scenario, so it is possible to group the data in 3 outputs:

Inlet (Arithmetical mean of the temperatures registered by the 5 sensors placed at the top of the plastic cases)

Intermediate (Arithmetical mean of the temperatures registered by the 5 sensors placed in the middle of the plastic cases)

Outlet (Arithmetical mean of the temperatures registered by the 5 sensors placed at the bottom of the plastic cases).

Using these pooled data it will be possible to validate the numerical model comparing the water temperature evolution along the stick length during the heat exchange.

In the figures below, the inlet, intermediate and outlet temperature evolution is shown for the scenarios 2 and 5 (when the water flow rate is 3 l/m):

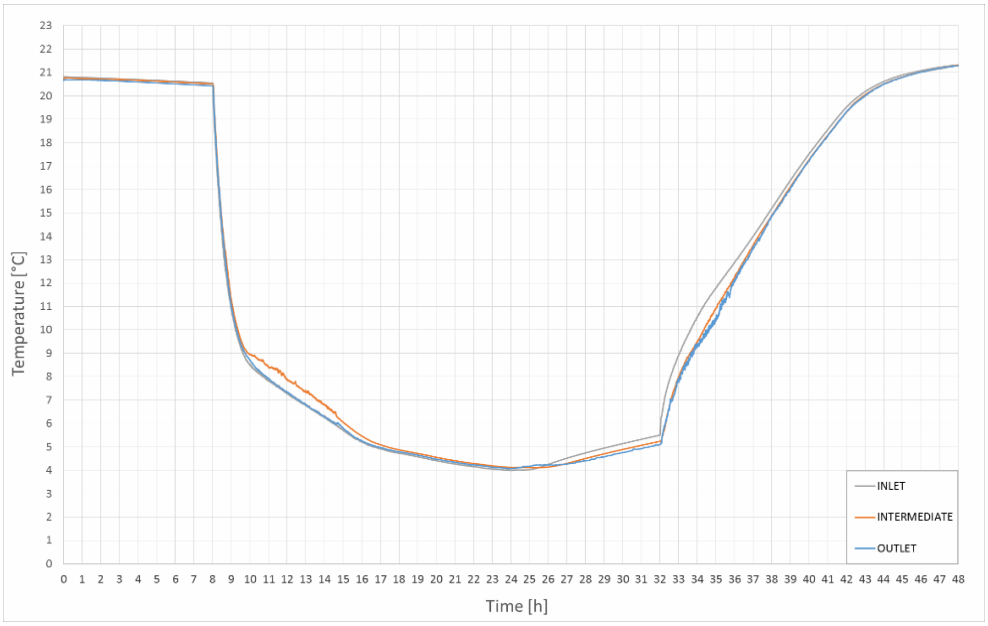

Figure 5. 24 - Inlet, Intermediate and Outlet mean water temperature values recorded by the sensors in the scenario 2 (one plastic case, flow rate: 3 l/min).

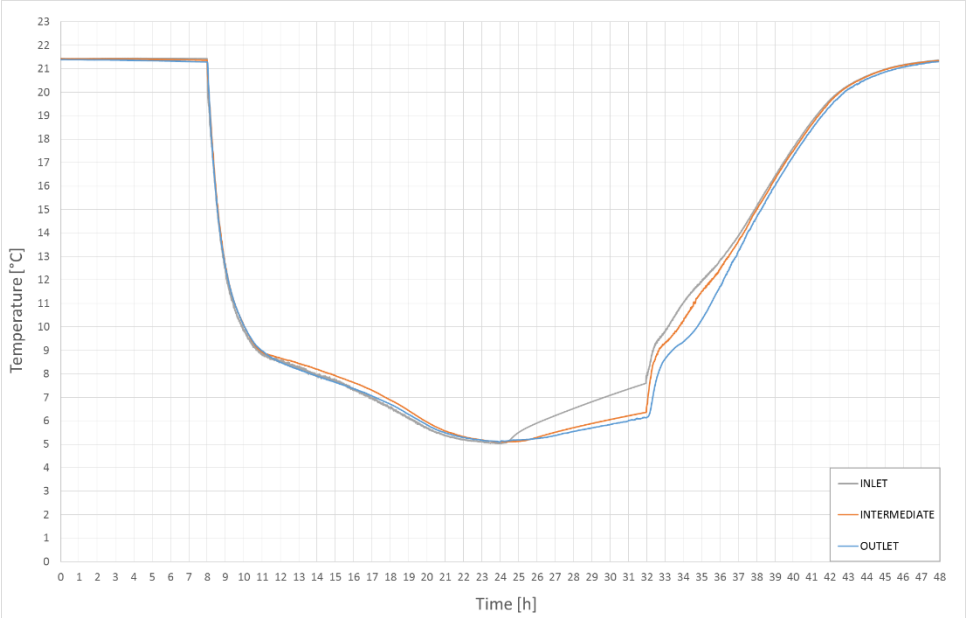

Figure 5. 25 - Inlet, Intermediate and Outlet mean water temperature values recorded by the sensors in the scenario 5 (two plastic cases, flow rate: 3 l/min).

It is interesting to observe that, in both cases, the "intermediate" curve has a particular behavior during the chilling phase of the water. In fact, according to thermodynamics, during this time the temperature variation of the intermediate curve should show lower values than those of the outlet curve and greater values than those of the inlet curve. On the contrary, the temperature values of the intermediate curve are greater than the others in every scenario, as it can be noticed in the figures below:

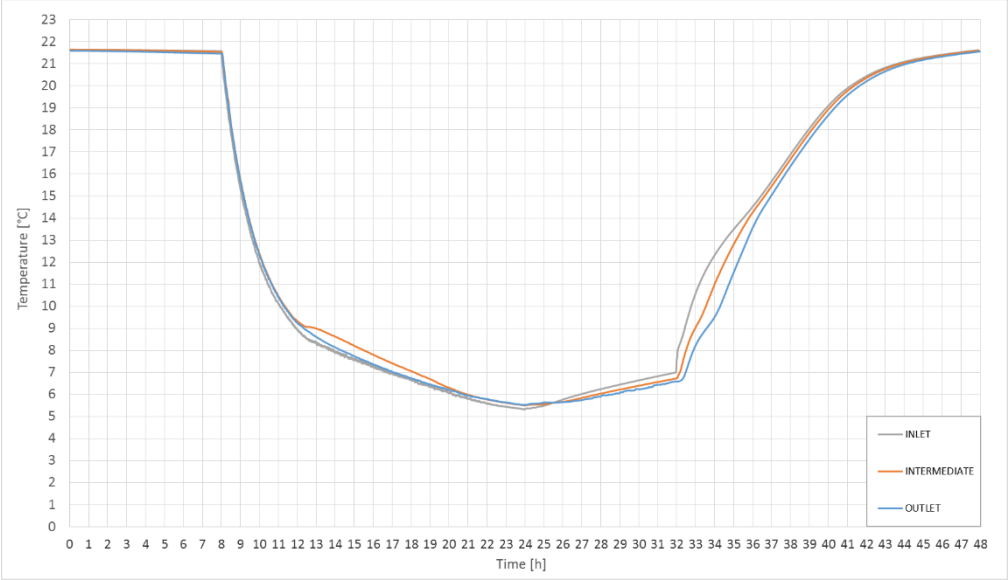

Figure 5. 26 – Inlet, Intermediate and Outlet mean water temperature values recorded by the sensors in the scenario 1 (one plastic case, flow rate: 1.5 l/min).

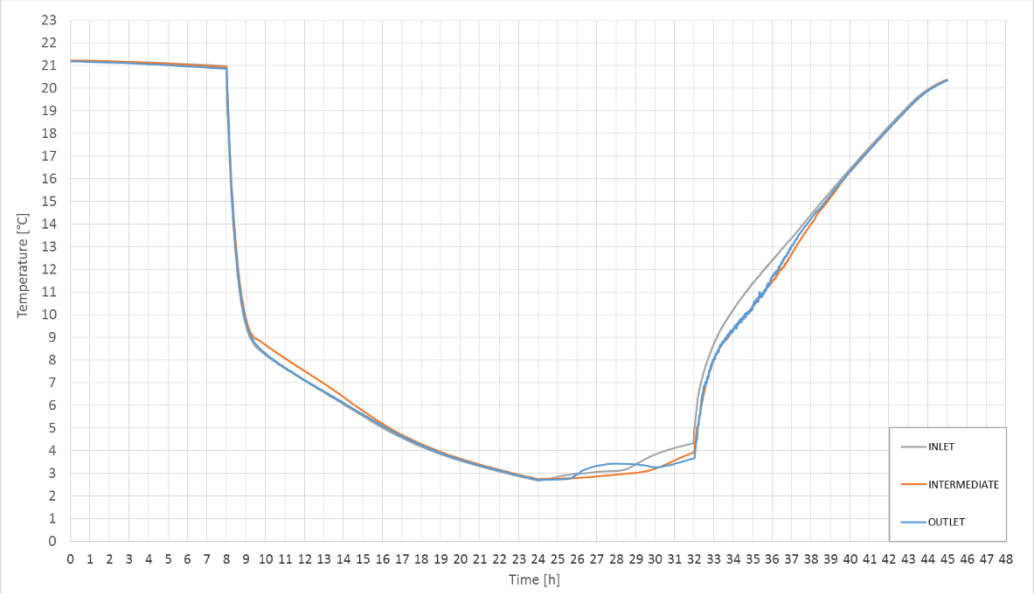

Figure 5. 27 – Inlet, Intermediate and Outlet mean water temperature values recorded by the sensors in the scenario 3 (one plastic case, flow rate: 4.5 l/min).

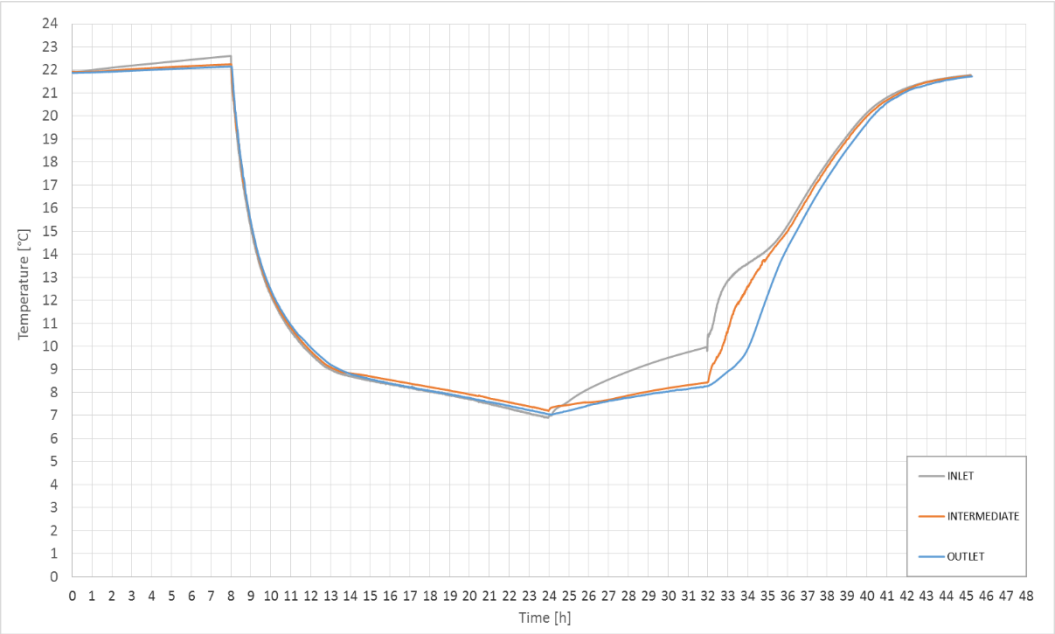

Figure 5. 28 – Inlet, Intermediate and Outlet mean water temperature values recorded by the sensors in the scenario 4 (two plastic cases, flow rate: 1.5 l/min).

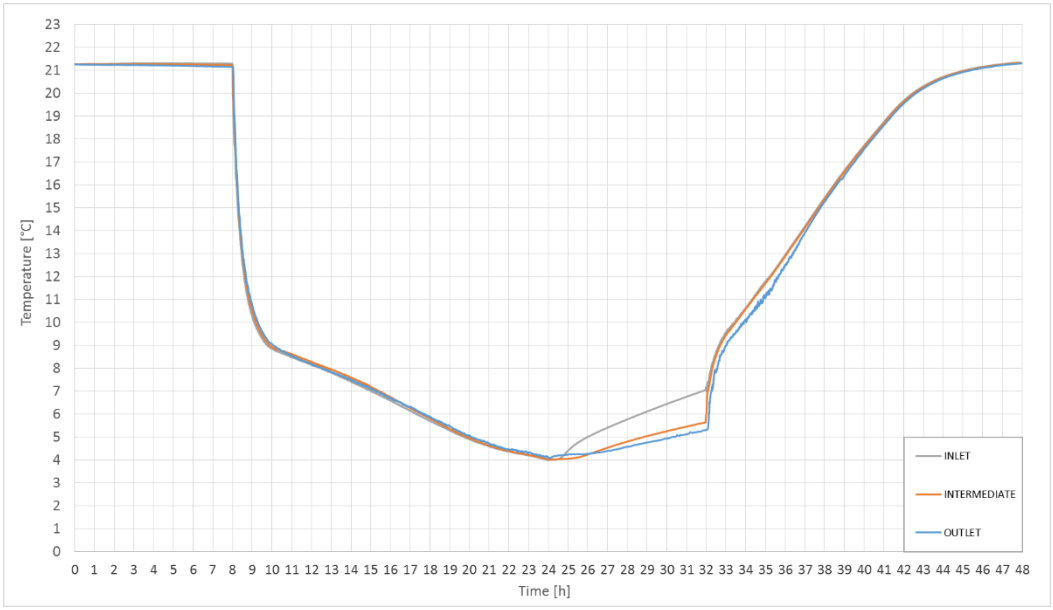

Figure 5. 29 – Inlet, Intermediate and Outlet mean water temperature values recorded by the sensors in the scenario 62 (two plastic cases, flow rate: 4.5 l/min).

The reason of this particular behavior could be that the intermediate temperature sensors were in proximity to the PCM sticks, while the others were just in contact with water. Another reason could be that, as the gel sticks increase in volume during their freezing phase, they could reduce the flow rate when it crosses the middle of the plastic case. This thesis is reinforced by the fact that this phenomenon is clearer when the flow rate is lower.

5.8 EXPERIMENTAL VALIDATION

In order to make the experimental validation of the numerical model described in chapter 3, we compared its results with the values shown in the previous paragraph.

The output that interested us was the "outlet" one, as this would be the value useful in the optimization phase of this work. Two examples of comparison between the prototype data and the model outlet results are shown in figures 5.30 and 5.31:

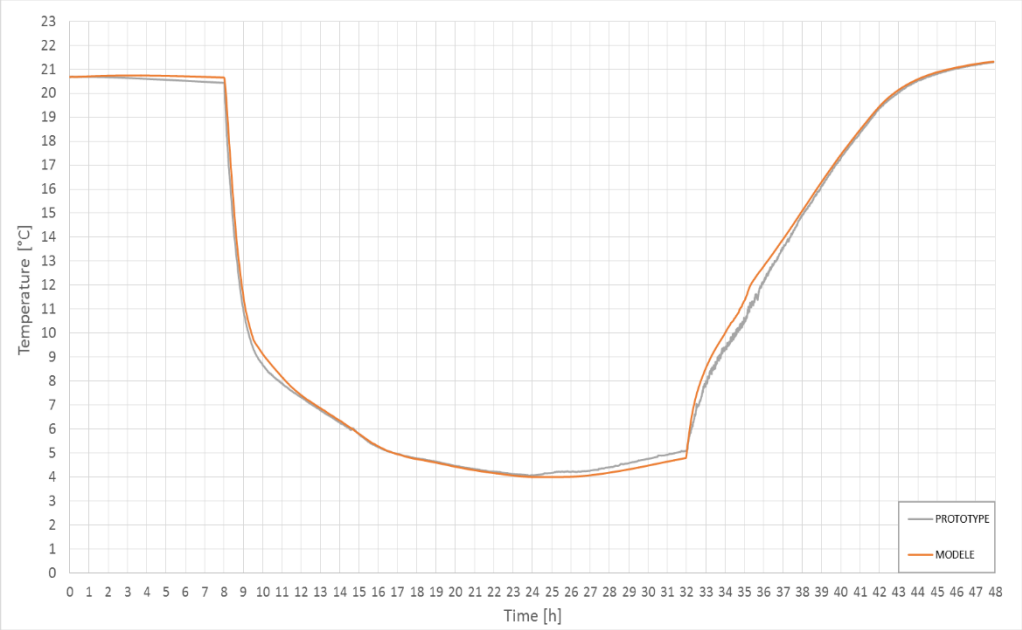

Figure 5. 30 - Comparison of the temperature curves for the same point between the experimental and the model results for scenario 2.

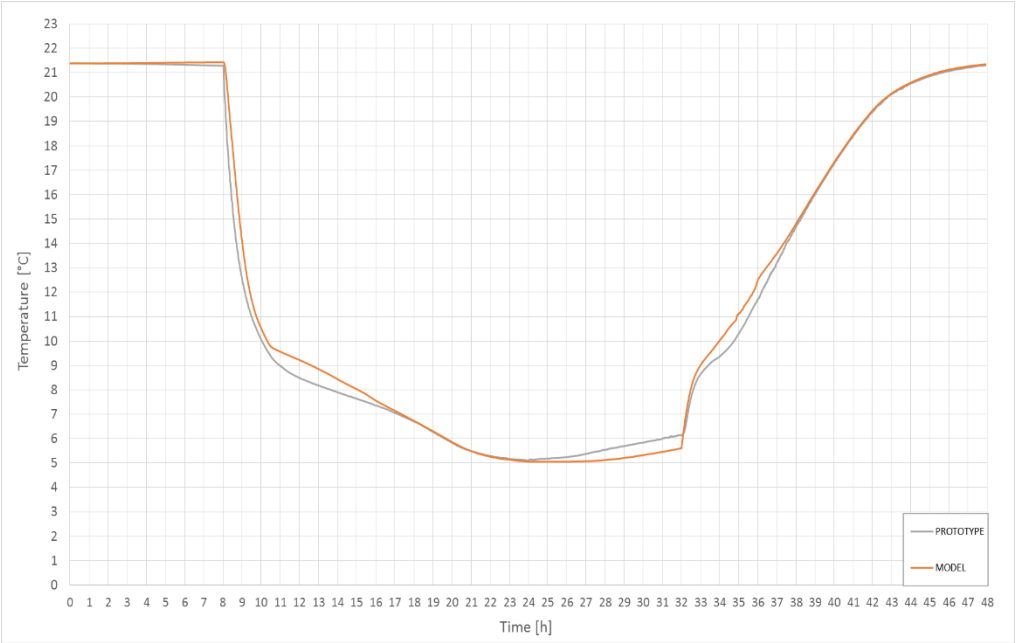

Figure 5. 31 – Comparison of the temperature curves for the same point between the experimental and the model results for scenario 5.

We considered this validation as the most precise we did, as it was conducted using the same PCM of the reference system (unlike the numerical model described in chapter 4) and it gave us the opportunity to test our model in different scenarios (unlike the comparison with the in situ data). Annex B shows all the recorded measures compared to the model results.

As in the other cases, we used the Normalized Mean Bias Error (NMBE) and the Coefficient of Variation of the Root Mean Squared Error (CV(RMSE)) as validation criteria, considering the prototype data as the reference values. The results for each scenario are shown in table 5.4:

Table 5. 4 – NMBE and the CV(RMSE) values for the comparison between the results obtained through the test bed monitoring and the discretization (m = 7, n = 3) of the MATLAB Simulink model.

Scenario	Statistical Index	Values [%]
1) 1 Plastic case Flow rate : 1,5 l/min	MBE	1,07
	CV(RMSE)	3,21
2) 1 Plastic case Flow rate : 3 l/min	MBE	0,97
	CV(RMSE)	2,57
3) 1 Plastic case Flow rate : 4,5 l/min	MBE	0,56
	CV(RMSE)	2,72
4) 2 Plastic cases Flow rate : 1,5 l/min	MBE	2,08
	CV(RMSE)	5,79
5) 2 Plastic cases Flow rate : 3 l/min	MBE	1,23
	CV(RMSE)	3,72
6) 2 Plastic cases Flow rate : 4,5 l/min	MBE	-0,05
	CV(RMSE)	2,81

5.8.1 Effect of a different convective heat transfer coefficient

Even if the results show that the model is experimentally validated, we preferred to test one of the assumptions that we made during the model design phase (see paragraph 3.3.6.1): the calculation approach of the convective heat transfer coefficient (h) .

We tried, in fact, to calculate it using another approach (Welty et al., 2008), based on the formula:

$$h = \frac{Nu \cdot \lambda}{L}$$

Equation 5.1

Where Nu is the Nusselt number, that is calculate as follows:

$$Nu = 0.664 \cdot Pr^{1/3} \cdot Re^{1/2}$$

Equation 5.2

Where Pr is the Prandtl number and Re is the Reynolds number, that depend on the properties of the materials, the water flow rate and the geometry of the system.

The result that we obtained for the convective heat transfer coefficient (h) using this formula was h = 71.37 W/m² ·K.

Nevertheless, we found out that the results obtained using this value change less than the 1% respect to the results obtained through the method shown in chapter 3. For this reason, we kept using the value previously calculated.

5.9 CONCLUSIONS

The first part of this chapter presents the HIKARI monitoring system and show how the data obtained through the monitoring of the reference system provided a first experimental validation of our numerical model. Nevertheless, this validation was not considered complete, and for this reason an original test bed based on a water-PCM exchanger was designed and developed at ENTPE-LTDS laboratory.

The objective of this experimental prototype construction was, on the one hand, to reproduce the behaviour of the reference storage system in a small-scale and with the opportunity to modify the boundary conditions, changing for example the inlet water flow rate or the type of PCM, and on the other hand to provide coherent and accurate measurement of water temperature evolution during the heat exchange between water and PCM.

Particular focus was given to the experimental protocol definition, necessary for the experimental validation of the model, because we had to find out which values of the real functioning of the system we wanted to avoid ; at the end, two data were chosen: the water flow rate and the temperature range.

The effect of the proximity of the sensors at the tank walls on the measures was analysed, in order to decree if the data could be group in 3 outputs (inlet, intermediate and outlet values),

necessary condition for a valid comparison with the numerical data. As it was found out that the grouping was possible while there is no deviation in case of horizontal distribution of the sensors, it has been possible to validate the numerical model comparing the water temperature evolution along the stick length during the heat exchange.

The validation results showed that the numerical model produces the same behaviours as the prototype and in-situ ones. The Normalized Mean Bias Error (NMBE) and the Coefficient of Variation of the Root Mean Squared Error (CV(RMSE)) used to analyse the validation results shows that our model is very accurate and fits largely the ASHRAE specifications for all tested configurations.

Due to its versatility the prototype will be able to be used in order to test other scenarios or other types of Phase Change Materials.

The next step of this work will focus on the utilization of the validated model in order to perform the optimization of the reference system when it is coupled to other energy architectures.

CHAPTER 6

WATER-PCM EXCHANGER INTEGRATION TO HIKARI'S HVAC SYSTEM: OPTIMIZATION PROCESS

6) WATER-PCM EXCHANGER INTEGRATION TO HIKARI'S HVAC SYSTEM: OPTIMIZATION PROCESS

6.1 INTRODUCTION

As explained in the previous chapters, a numerical model based on the formulation of heat balance equations and the apparent heat capacity method has been developed using the MATLAB Simulink environment in order to simulate the heat exchange between the PCM and the water flow.

Once numerically calibrated and experimentally validated, it has been coupled to the numerical model of the set of cooling systems of the HIKARI district, in order to reproduce the mutual interaction between all these systems (including the absorption chiller connected to the storage system). This coupling is explained in the introduction part of this chapter.

After that, the Genetic Algorithms method has been used in order to optimize the functioning of the HIKARI thermal energy storage system at low temperature, as it is explained in the final part of this chapter.

This part aims to demonstrate that it is possible to solve a Multi-Objective optimization problem using the Genetic Algorithms applied to a low temperature heat storage integrated to a complex multi energy system. After several attempts, due to luck of guidelines about the correct and optimal adaptation of the Genetic Algorithms to building issues, we have been able to find the best values to allocate to four parameters of an innovative cold storage system using PCM, in order to minimize two or three predefined objective functions linked to its functioning.

Given the novelty of this technology, it was necessary to optimize the technical characteristics of its storage system defining optimized designing and operating parameters in order to improve its productivity and reduce the losses of the building.

6.2 COUPLING WITH THE HIKARI'S HVAC SYSTEM MODEL

Once the numerical model realized and validated, we coupled it to the HIKARI HVAC system model.

It was necessary in order to proceed with the optimization of the HIKARI thermal energy storage system technology, as it allowed us to see the effect of any change of the reference system on the HIKARI's HVEC system functioning.

6.2.1 The HIKARI's HVAC system model

MANASLU ING, the enterprise that handles the monitoring of the HIKARI complex and checks its energetic performance, has developed the numerical model of the HIKARI's HVAC systems within which we integrated our water-Heat exchanger model.

This model was realized in the MATLAB Simulink environment (the existence of this model was also one of the reasons that justified our environment development choice, as it is explained in paragraph 3.3.4.1.) during the design phase of the HIKARI project, in order to test the mutual work of all the HVEC systems face to the HIKARI energy needs (simulated through the software EnergyPlus) and it has been changed gradually using the in situ data, in order to reproduce the real behaviour of the systems. In our case, as we analysed the thermal energy storage system at low temperature, only the numerical model concerning the thermal energy production at low temperatures was considered. It represents the mutual work between the cold water storage, the absorption chiller, the refrigeration unit and the adiabatic dry cooler, as it is shown in the HIKARI HVAC system scheme below:

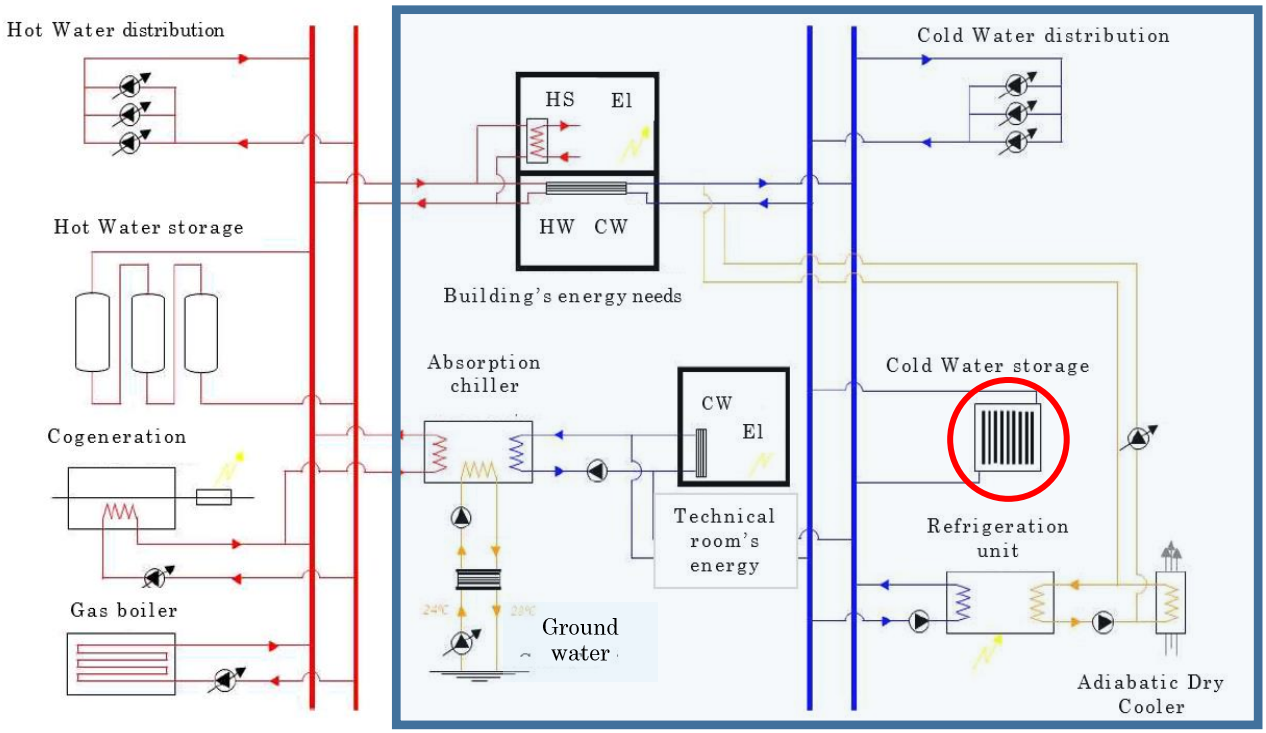

Figure 6. 1 - Scheme of the HVAC system of HIKARI .The HIKARI cooling systems set is indicated into the blue square, in particular the thermal energy storage system analysed in this work in indicated in the red circle.

6.2.2 HIKARI HVAC system an water-PCM exchanger models coupling

The model that we developed was integrated to the cooling systems model taking the place of an existing simplified water-PCM exchanger developed by MANASLU during the design phase of the project. Indeed, it was necessary for MANASLU to have such model for load calculation reasons in order to establish HVAC and storage system specifications and sizing. One of the aims of this PhD study is also to stress the lack of design tools related to latent heat storage systems designing. MANASLU's water-PCM heat exchanger model is described in annex.

However, before making this change we tested the results obtained through its use, in order to demonstrate that our model was effectively more accurate and could lead to better specification and more adapted design parameters: to do so, we set the same input values for both the models and we compared the output that they produced with the in situ monitoring results.

The input values that we took into account were the water flow rate and the inlet temperature of the water that crosses the tank 1 (one of the 4 tanks composing the reference system, as described in paragraph 3.2) during two charging-discharging phases, while the output values that we compared were the outlet temperature of the water at the bottom of the tank.

We carried out an error analysis between the results obtained through the two models by calculating the Normalized Mean Bias Error (NMBE) and the Coefficient of Variation of the Root Mean Squared Error (CV(RMSE)), already presented in paragraph 4.4. We considered the HIKARI monitoring data as the reference values, and we calculated the variation of our model and the MANASLU's one.

The NMBE and the CV(RMSE) values for the comparison are shown in table 6.1, while in figure 6.2 are shown the outlet temperatures and the error values between the HIKARI monitoring data and the model's results.

Table 6. 1 - NMBE and CV(RMSE) calculated between the results obtained using the MANASLU's model and our model ("Model").

	MANASLU's model	Model
Normalized Mean Bias Error	9,37%	3,86%
Coefficient of Variance of Root Mean Square Error	10.45 %	4.22 %

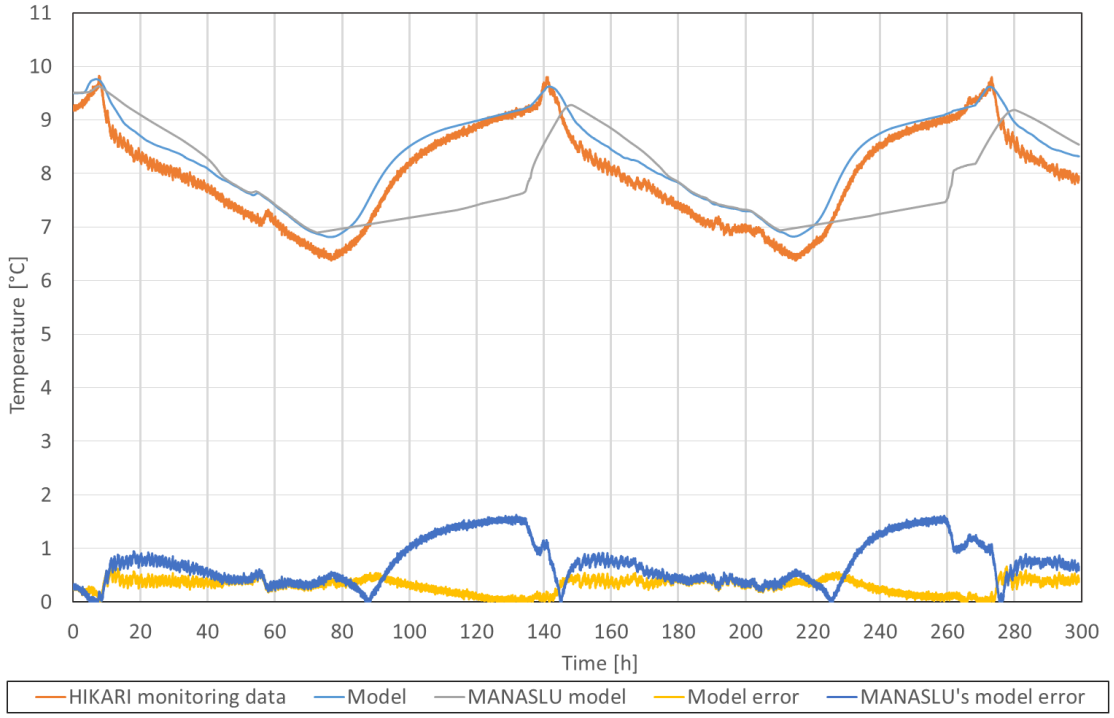

Figure 6. 2 - Tank 1 outlet temperature comparison using in situ monitoring and simulation results using both MANASLU's model and our model ("Model") and error between the simulated and the reference data.

As it can be noticed, our model reproduces the behaviour (charging and discharging phenomena) of the thermal exchanger with much better accuracy, especially during the charging phase. This comparison demonstrated that the MANASLU's model could be interesting for mandatory regulation loads calculations but not adequate for sizing and optimizing the HIKARI's system. For this reason, we substituted the pre-existent model with ours and we continued with the optimization of the thermal energy storage technology (figure 6.3).

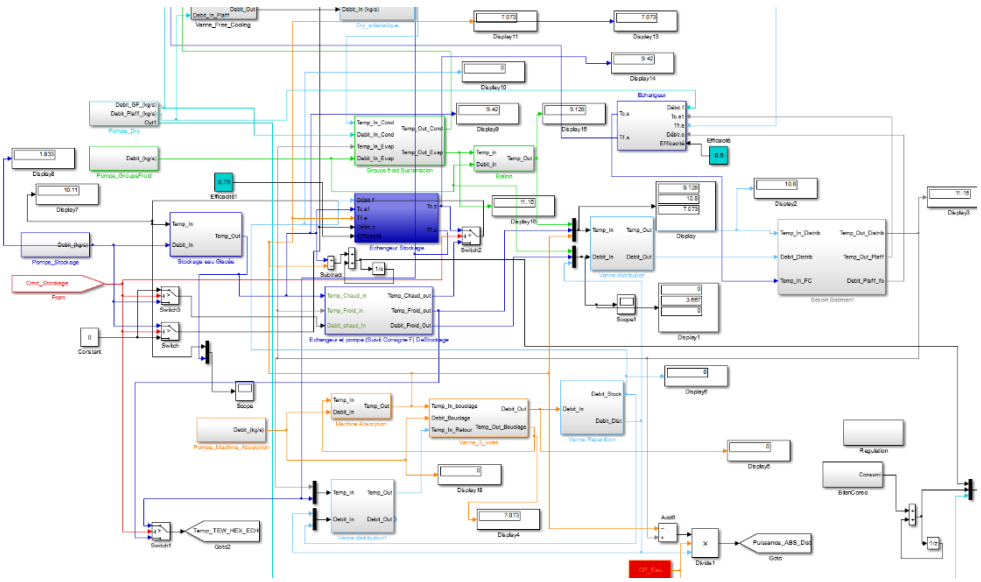

Figure 6. 3 - Integration of the model (blue square) to the HIKARI's HVAC systems model.

6.3 GENETIC ALGORITHMS AS SELECTED OPTIMIZATION TECHNIQUE

In order to achieve the optimisation of the HIKARI's cold storage system technology, Genetic Algorithms (GAs) were chosen: GA is a multi-dimensional and stochastic search method used for minimizing or maximizing a given function and if possible finding its most suitable solution. Their operating is based on the evolution of a population of individual objects, each with an associated fitness value, into a new generation of this population using the Darwinian principle of natural evolution, where the fittest individual in a pool of individuals has the highest chance of survival ; in the same way, genetic algorithms attempt to find the best solution to the problem by genetically breeding the population of individuals over a series of generations (Stojanovska and Dika 2010).

6.3.1 Non-dominated Sorting Genetic Algorithms II (NSGAs II)

In our case a specific kind of GA, the Non-dominated Sorting Genetic Algorithms II (NSGAs II) was chosen due to its capacity to reach more easily non-dominated solutions (also called "Pareto-Optimal" solutions - when no other feasible solution exists that decreases one objective without causing simultaneously an increase in at least one other objective) compared to other types of Multi-Objective Evolutionary Algorithms (MOEAs) (Deb et al. 2002).

Through the software MATLAB Simulink, it has been possible to apply the GAs to the numerical model described in chapter 3 using the NSGAs II toolbox (Lin, 2011), obtaining the best values to allocate to four parameters (described below) of the cold storage system in order to minimize two or three objective functions based on the functioning of the HIKARI cooling systems.

6.3.2 Selected optimization parameters and defined objective functions

The optimization parameters we selected and their variation domain, were:

- The diameter of every gel stick package (m) [0,013 ; 0.015] ;
- The length of every gel stick package (m) [0.2 ; 0.3]
- The melting point of the PCM (°C) [8 ; 12]
- The freezing point of the PCM (°C) [9 ; 13]

Changing the diameter or the length of the PCM sticks, allows us to test the effect of their geometry on the system functioning. In fact, in this way the contact surface between them and the water flow would change, just like the packing density of the gel sticks into the water tanks (see paragraph 3.3.6.2). These changes would affect the PCM thermal conductivity and would have a deep influence on the system's PCM-water heat exchange.

Instead, changing the melting and the freezing point of the PCM it was possible to test the performance of different kinds of PCMs that could be available on the market, in order to find the best one that could make the exchanger more energy-effective. This parameter allows also the selection of the most adequate rang meting rang that enhances the HIKARI's HVAC system

6.3.2.1 Two-objectives optimization case

Running the GAs for a simulation period of one week, we wanted to minimize two objectives functions:

- OBJ 1: The sum of the difference between the chiller's cold and hot inlet water temperature at each time step (°C)
- OBJ 2: Energy needs of the building (kWh)

The first objective was chosen because of its effect on the efficiency of the absorption chiller. In fact, one of the most important approaches followed in order to improve the efficiency of heat exchangers is the closer temperature one (Lunsford, 1998). It consists in reducing the difference between the exchanger's cold and hot medium temperatures, so that the minimum driving force for carrying out the necessary heat exchanging between hot fluid and cold fluid is required in the heat exchanging network.

The second objective was chosen because of the environmental and economic impact of energy needs of buildings.

6.3.2.2 Three-objectives optimization case

In a second time, we decided to introduce a third objective function to be minimized. As it is shown in paragraph 3.2.1, when the storage system is in its "discharged" phase (the temperature of the water in the four tanks is equal or greater than 10°C) a vapour compression refrigeration system (VCRS) does enters in operation, improving the performance of the absorption chiller and reducing the difference between the chiller's cold and hot inlet water temperature.

The third objection function (OBJ 3) that we wanted to reduce was the number of short cycles of this VCRS, which is the number of times when it turns off less than 5 minutes after it turned on. Improper cycling, in fact, could lead to a host of problems with the cooling device and to a big increase in energy needs.

6.3.3. Genetic Algorithms functioning

Thanks to these objective functions, we could assess the initial population and determine the best solutions in order to minimize them. The best solutions are the "parents" of the following

generation. The "children" are defined by recombination of the parents' chromosomes and are obtained through crossover and mutation operations. Crossover and mutation perform two different roles: the first one is a convergence operation which is intended to pull the population towards a local minimum/maximum, while the second one is a divergence operation that occasionally breaks one or more members of a population out of a local minimum/maximum space and potentially discovers a better minimum/maximum space.

Since the goal is to bring the population to convergence, crossover happens more frequently (typically every generation), while mutation, should happen less frequently and typically only effects a few members of a population (if any) in any given generation, being a divergence operation.

After the chromosomal recombination, we obtain "children" solutions that form a new generation, which is assessed. Individuals with the highest fitness are selected as parents for the next round of recombination. This process is iterative and stops after a fixed number of generations. The final population contains optimized solutions (Pernodet et al. 2009).

A scheme of these iterations is shown in figure 6.4:

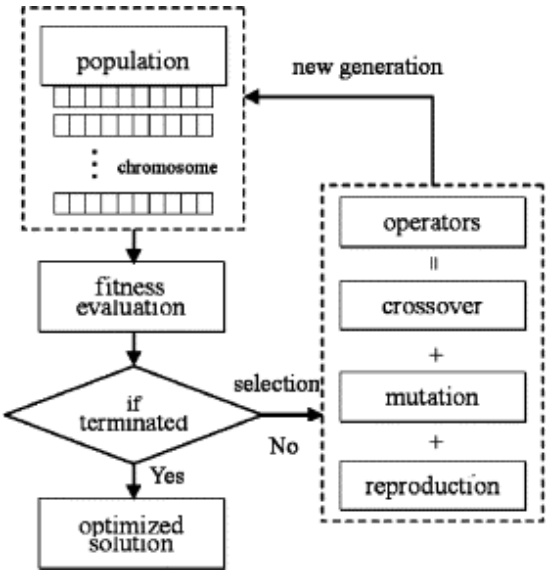

Figure 6. 4 - Evolution flow in a genetic algorithm (Chang-Hsu and Zsay-Shing 2006).

6.4 OPTIMIZATION RESULTS

6.4.1 Two objectives optimization

As a first approach, we tried to minimize the first two objective functions. We ran a first Genetic Algorithm choosing a number of individual for each population equal to 25 and we stopped the algorithm after 40 simulations.

When the problem treats two objectives, as in this case, the result of the optimization must be a curve of non-dominated solutions, called the Pareto curve (Wang et al. 2005). An example of Pareto curve is shown in figure 6.5.

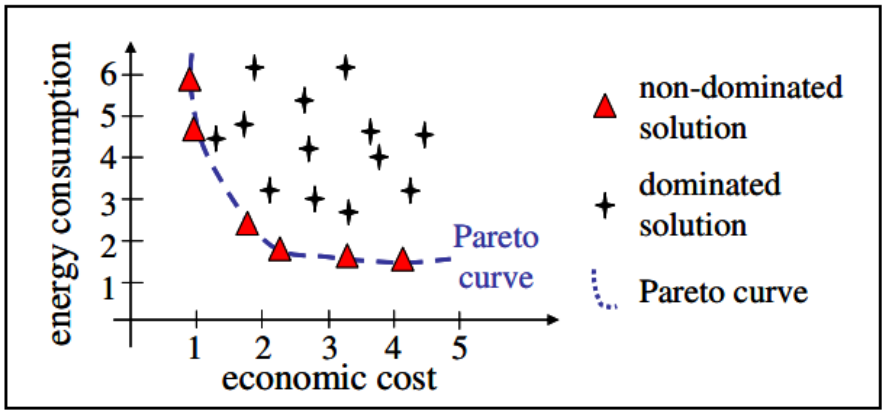

Figure 6. 5 - Example of Pareto curve (Pernodet et al. 2009).

The first optimization provided us 1000 solutions, that represent the combination between different "sums of difference between the chiller's cold and hot inlet water temperature at each time step" (Obj 1) and "energy needs of the building" (Obj 2). The objective of the GAs application was to find a solution that could minimize both these objective functions. However, the first optimization results didn't show a single Pareto curve with non-dominated solutions (Figure 6.6).

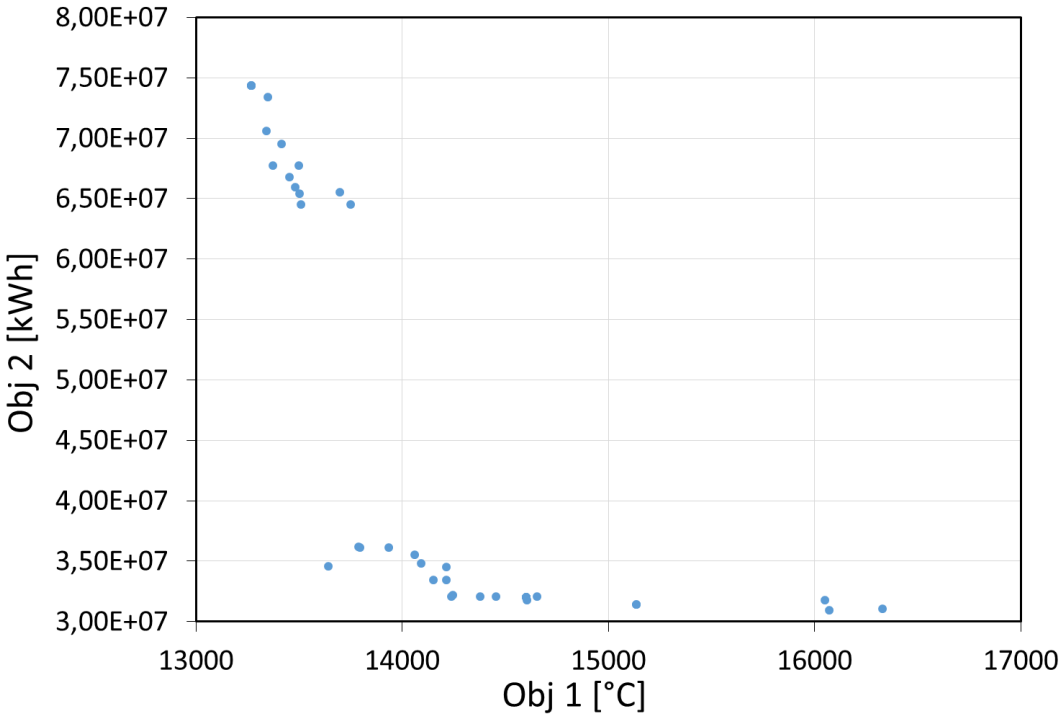

Figure 6. 6 - Results of the first application of the Genetic Algorithm.

This is due to the size of the initial population or the number of generations adopted. Indeed, the process of defining the number of generations and the population size is not clearly defined in the literature and remains very complex for building applications.

For this reason we tried to run another Genetic Algorithm choosing a number of 100 elements for each population and to stop after 10 generations. The result is shown in figure 6.7:

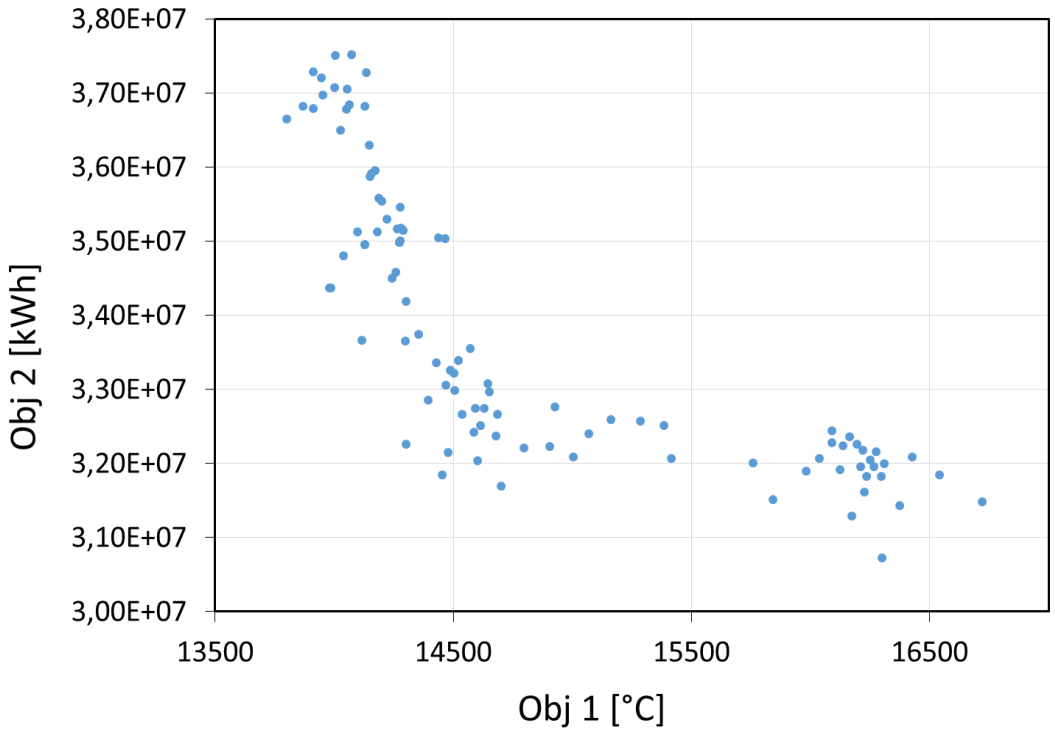

Figure 6. 7 - Results of the second application of the Genetic Algorithm.

In this case, the curve obtained was clearly more akin to the Pareto one. We tried, anyway, to run another Genetic Algorithm stopping after 20 generations, attempting to improve the quality of the final population.

The result is shown in figure 6.8:

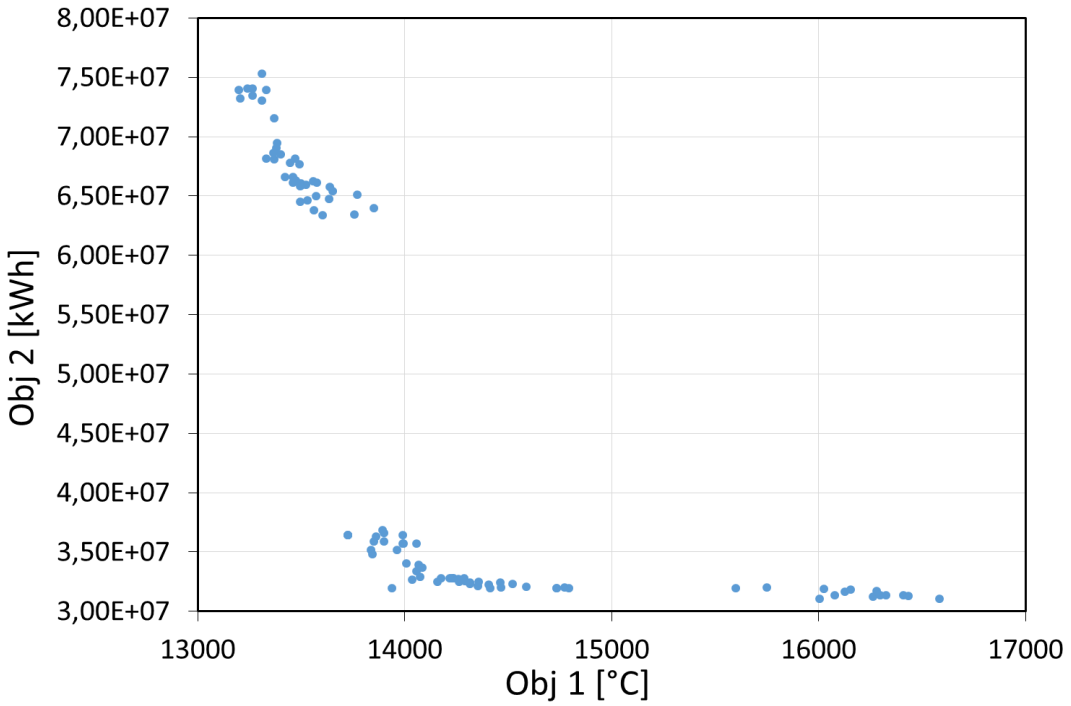

Figure 6. 8 - Results of the third application of the Genetic Algorithm.

The result obtained through this third application was not better than that obtained through the second application, as it can be noticed that we did not obtain a single curve of non-dominated solutions.

The difference between the three simulations can be observed more clearly in figure 6.9:

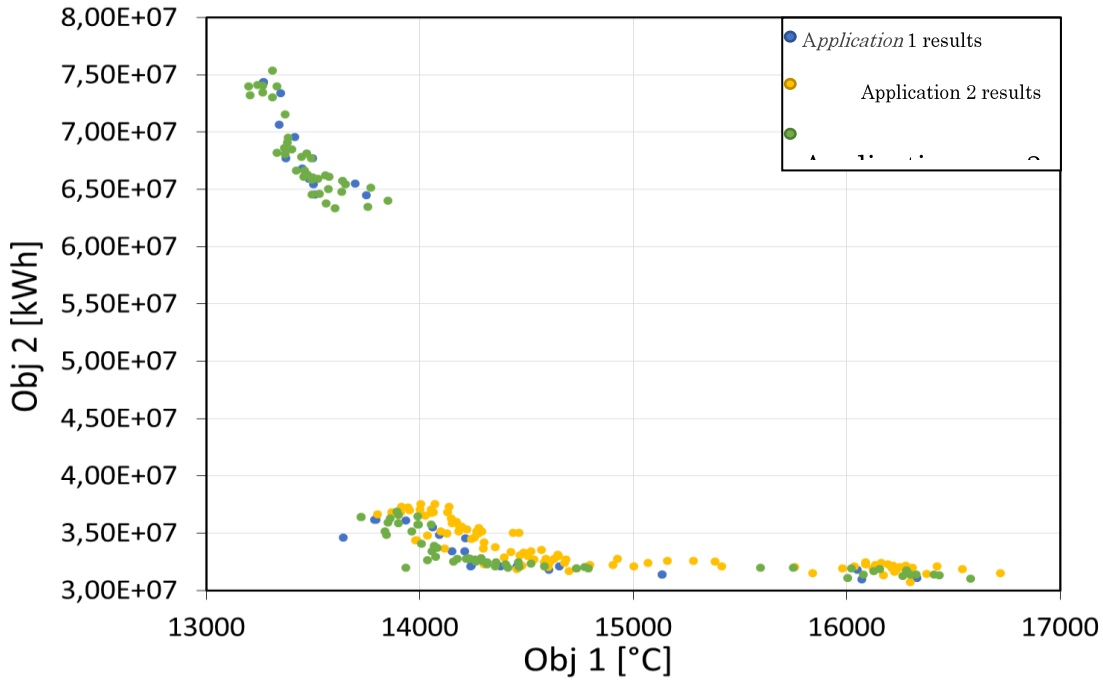

Figure 6. 9 - Comparison between the results obtained through the three different applications of the Genetic Algorithms.

For this reason, we decided to consider the data obtained through the second application for the optimization of the thermal energy storage system technology.

The last attempt that we made, however, was to run another Genetic Algorithm choosing a number of 100 elements for each population and stopping after 100 generations. The result is shown in figure 6.10:

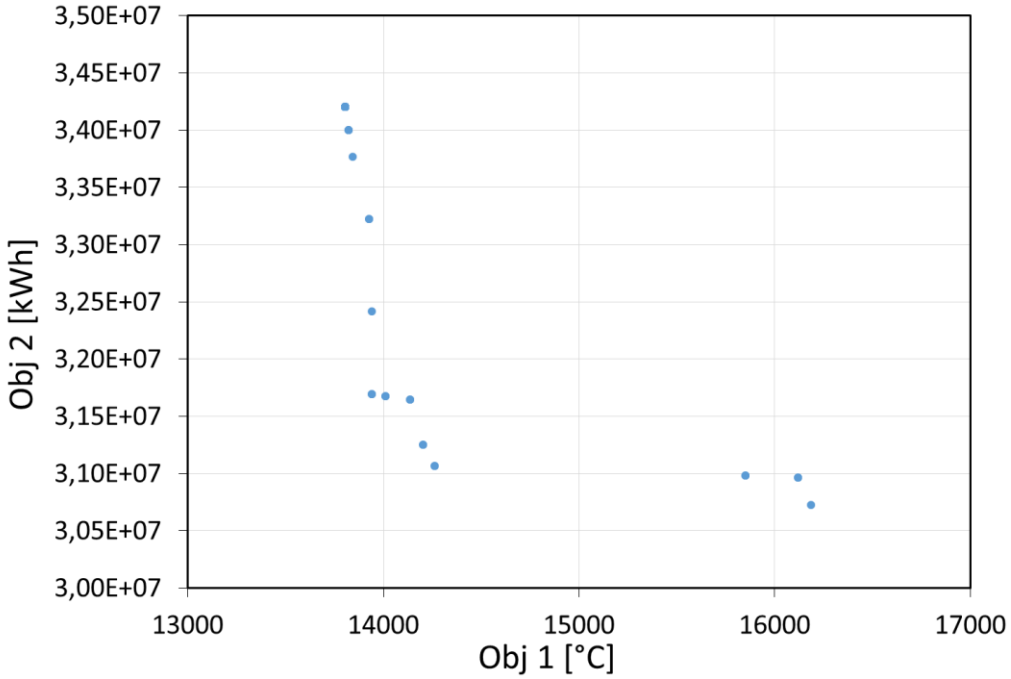

Figure 6. 10 - Results of the fourth application of the Genetic Algorithm.

In this last case, the curve obtained was akin to the Pareto one, so we compared it to the one obtained through the second application of the GAs. The comparison between the results obtained through the second and the fourth application is shown in figure 6.11:

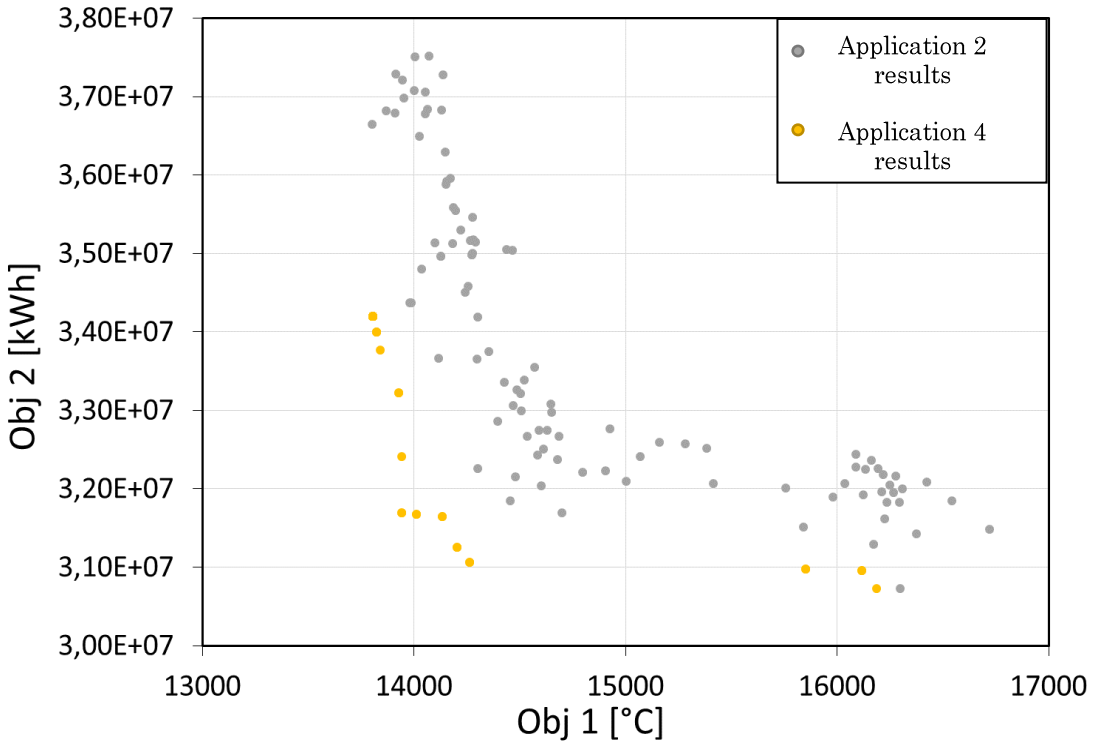

Figure 6. 11 - Comparison between the results obtained through the second and the fourth applications of the Genetic Algorithms.

As our objective was to choose the values that attributed to the storage system characteristics indicated above minimize the two objectives' values, we calculated the norm for every couple of the objectives obtained through each elements of the last population for both the second and the fourth GAs applications. We can define the norm $|x|$ of a vector $x = (x_1, x_2) \in R^2$ *as*

$$|x| = \sqrt{x_1^2 + x_2^2}$$

By Pythagoras theorem, the norm $|x|$ of the vector $x = (x_1, x_2)$ is equal to the length of the hypotenuse of the right angled triangle with sides x_1 and x_2, in other words, it is the distance from the origin to the point $x = (x_1, x_2)$ (figure 6.12).

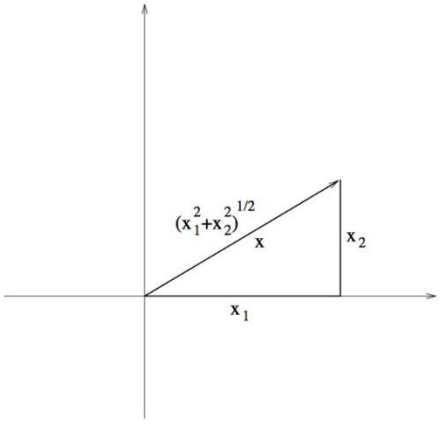

Figure 6. 12 - Graphic representation of the norm.

Considering that the origin corresponds to the best possible solution, the couple of the objectives whose norm was the smallest was considered the best solution.

Once all the norms calculated, we found that the best values that could be attributed to the low temperature heat storage system characteristics were obtained through the fourth round of optimization, and they were:

- Diameter of the gel stick packages: 0.0135 m
- Length of the gel stick packages: 0.23 m
- Freezing point of the PCM: 8 °C
- Melting point of the PCM: 13 °C

It is very important to mention that this optimization process is time-consuming with no defined rules for generation number and population size. As an example the simulation process for the first two calculation rounds showed in this chapter takes 24 hours, for the third one was calculation tame is 48 hours while for the last one it was of 240 hours.

Due to the big difference in term of necessary calculation for obtaining these results, we decided to compare the difference between the best solution selected for both the second and the fourth GAs round application and we found out that it was less than 1%.

It means that, in terms of time, it would be more convenient to choose a population size of 100 individuals and 10 generations. It takes 10 days calculation time and the convergence in term of Pareto front is reached.

The best values calculated for o the low temperature heat storage system characteristics obtained through the second round are:

- Diameter of the gel stick packages: 0.0136 m
- Length of the gel stick packages: 0.26 m
- Freezing point of the PCM: 7.5 °C
- Melting point of the PCM: 13 °C

6.4.2 Three objectives functions optimization

In the second stage of the work, we decided to introduce a third objective function described in the previous chapter: the number of short cycles of the VCRS.

Contrary to the two first objectives functions, the result of the three objectives problems optimization must be a surface of non-dominated solutions, as the example shown in figure 6.13.

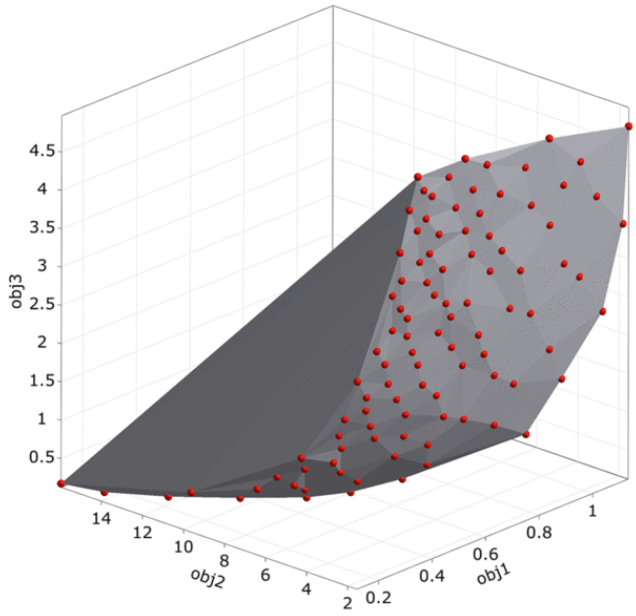

Figure 6. 13 - Example of Pareto surface (Ozen Engineering, Inc).

For this reason, it was more difficult to immediately distinguish between dominated and no-dominated solutions, but we still applied the norm selection method to identify the best solution.

Thanks to the learned lessons from the first stage of optimization, we ran a Genetic Algorithm choosing a number of 100 elements for each population and stopping after 100 generations, as we considered that this was the most precise combination, even if it was not really effective in terms of calculation time.

However, it was possible to show the results obtained considering the objectives two by two, as it is shown in figures 6.14, 6.15 and 6.16:

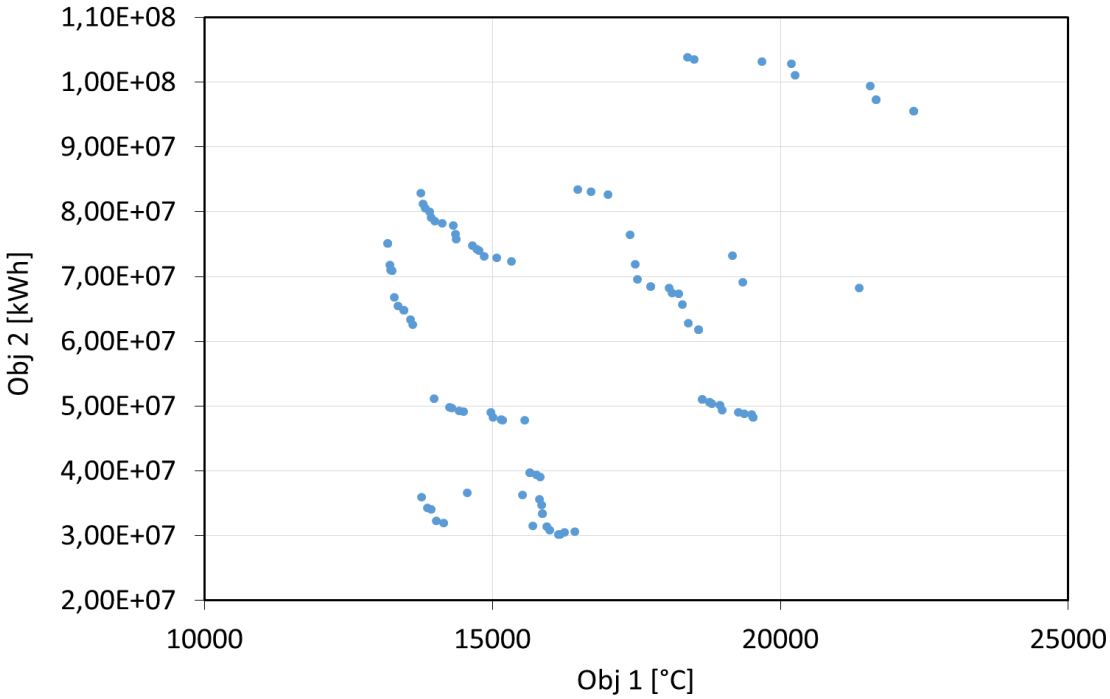

Figure 6. 14 – Result of the three objectives application of the Genetic Algorithm considering only objective 1 and 2.

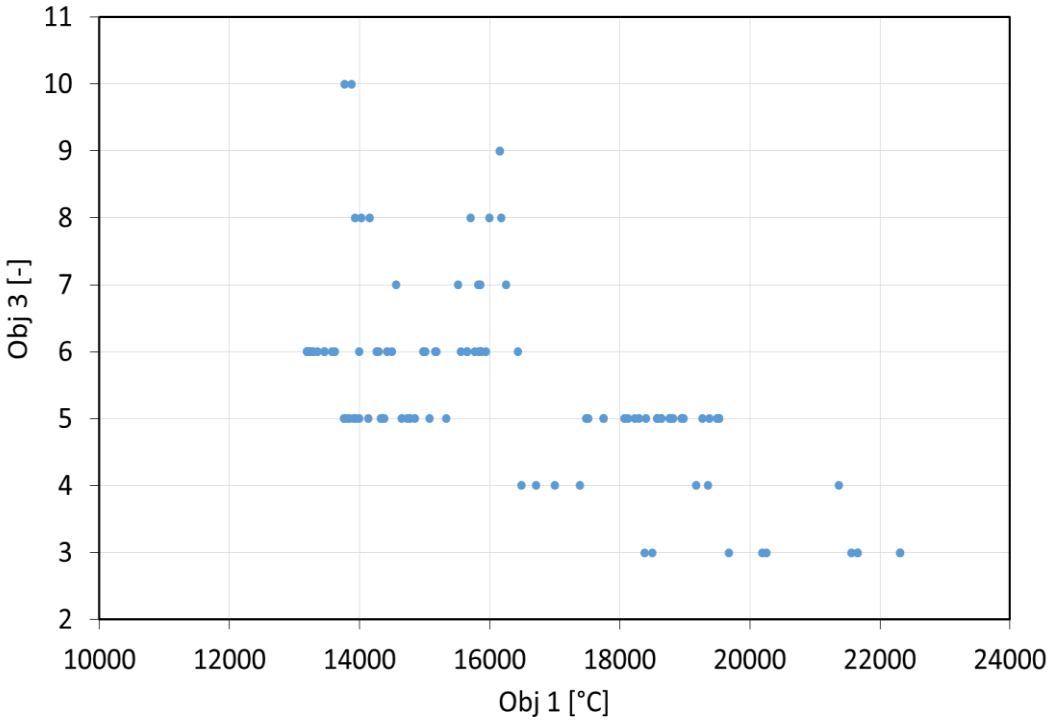

Figure 6. 15 – Result of the three objectives application of the Genetic Algorithm considering only objective 1 and 3.

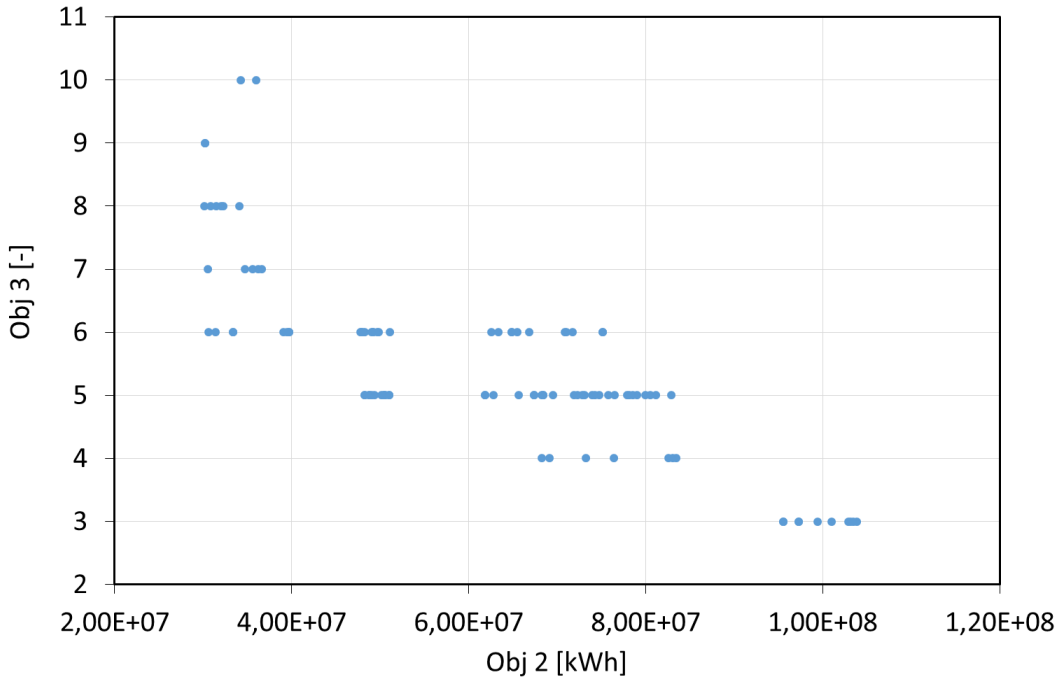

Figure 6. 16 - Result of the three objectives application of the Genetic Algorithm considering only objective 2 and 3.

Once again, as we considered that the best values attributed to the storage system characteristics indicated above should minimize the objectives' values, we calculated the norm for all the trio of objectives obtained at the last generation.

In this case, the best values attributed to the cold storage system characteristics obtained through the second applications were:

- Diameter of the gel stick packages: 0.014 m
- Length of the gel stick packages: 0.2 m
- Freezing point of the PCM: 8 °C
- Melting point of the PCM: 13 °C

As it can be noticed, all the combinations that furnish the best results indicate the best melting point for the PCM at 13°C (3 degrees more than the real one). This is caused by the fact that, melting at a higher temperature, the PCM could extend its discharge period, so it could furnish cold water at the absorption chiller during more time.

Another result in common is that in all cases the length of the gel stick packages is lower than the real one. This can be explained with the fact that during the charging phase, a shorter stick

allows the water arriving at the inferior stick at a lower temperature, as the heat exchange between the water flow and its surface lasts less.

This situation makes it necessary to run many other simulations in the future, with totally different combinations of number of elements for each populations and number of generations, in order to find the best solutions.

It could be interesting to create a guideline for the Genetic Algorithms users, in the future, that could help them in the choice of the number of elements for each population and the number of total populations to generate.

6.5 CONCLUSIONS

This study part presents the optimization of an innovative thermal energy storage technology at low temperatures obtained through the application of a Genetic Algorithm.

The first difficulty that we encountered was the choice of the best system parameters that we had to change in order to minimize three objective functions that could affect the HIKARI's cooling systems efficiency. We had to consider the effects of geometrical and technologic changes on the system behaviour and to choose the more influential ones.

Another difficulty that we faced was the definition of the number of generations and the population sizes at each GA application, as it is not clearly defined in the literature. It is interesting to note that there is not a linear relationship between the generation number and population size and the result accuracy ; in fact, even if in the third application of the GA we increased the number of generations, considering to make the choice of the best solution more accurate, the solutions didn't converge in a Pareto curve. On the contrary, the results that we obtained in the second application were more akin to the Pareto curve even if we stopped calculating after 10 generations.

Finally, we had to choice the approach to be adopted to define the best values that, attributed to the storage system characteristics indicated above, minimized the objectives' values. We solved this problem by calculating the norm for every couple of the objectives obtained through each elements of the last population for the best GAs applications.

The obtained results showed that, thanks to this method, it is possible to solve Multi-Objective problems linked to the optimization of this and other innovative experimental technologies.

Due to the expanding research of solution to adopt in nearly Zero Energy Buildings (nZEBs), it appears important, nowadays, to find valid optimization methods that we can universally apply to all the cases, just like the approach that was explained in this chapter due to its versatility. Anyway, because of the deficiency of guidelines about the use of the Genetic Algorithms, it would be still necessary to make some assumptions and to proceed by attempting possible solutions.

CONCLUSIONS AND OUTLOOK

CONCLUSIONS AND OUTLOOK

Conclusive summary

In view of the entry into force of the Paris Agreement in November 2016, new technologies able to replace conventional energy sources with renewable and waste ones entered the market. However, the lack of universal analytical and simulation methods useful for the optimization of these innovative energy-effective technologies motivated the research performed in this PhD dissertation. The objective of our work, in fact, was to optimize a new thermal energy storage technology particularly created for HIKARI, the first positive energy, mixed use building group in Europe. A numerical and multiscale experimental approach has then been established and carried out.

The first part of the approach consisted in developing a fast, accurate and re-utilizable numerical model able to reproduce the heat exchange between the Phase Change Material (PCM) contained in the reference system and a water flow.

This model has been developed in the MATLAB Simulink environment using the heat balance approach and the apparent heat capacity method.

Once developed, the model was firstly calibrated using the results obtained through a second numerical model that we developed using the Computational Fluid Dynamics method. The results of this calibration showed that our model was accurate and faster in long duration simulation studies when compared to ANSYS Fluent results.

A second calibration was realized once the HIKARI in situ data obtained thanks to in-situ monitoring. This comparison allowed us to make a first experimental validation of the model, but even if it proved the accuracy of our model, it was considered incomplete. Indeed, this in situ validation could be only considered for the given HIKARI control strategy in operation, so it was impossible to recreate different conditions and establish a multi conditions protocol while buildings were occupied, such as different inlet water flow rates or quantity of PCM sticks.

For this reason, an original experimental prototype reproducing the HIKARI's cold storage system was designed and developed, in order to obtain valid experimental data useful for a complete experimental validation of the numerical model and for the validation of other kinds of phase change materials in the future. For this reason, the prototype has the advantage to be easy to dissemble and reassemble (in case of transport) but at the same time able to make the PCM changing quickly its phase and to record all the temperature changes with a very good precision.

The results obtained through its construction showed that our model was able to reproduce the PCM-water heat exchange with a high accuracy. The Normalized Mean Bias Error (NMBE) and the Coefficient of Variation of the Root Mean Squared Error (CV(RMSE)) used to analyse

the validation results shows that our model was very accurate and fitted largely the ASHRAE specifications for all tested configurations.

Once numerically calibrated and experimentally validated, the model was coupled to the HIKARI's HVAC systems model, replacing an existing simplified and less accurate model of the reference system that was developed during the HIKARI design phase.

The Genetic Algorithms method was finally applied to the global model in order to test the effects of geometry and thermo-physical changes of the reference system on the efficiency of some other systems and on HIKARI energy needs. The obtained results showed that it is possible to solve Multi-Objective problems through our optimization approach applying it to innovative HVAC and energy storage management systems.

Indeed, this PhD produced valid, accurate and fast numerical models, a laboratory experimental test bed and an optimization approach that can be used for further breakthrough systems development.

Perspectives and outlook

In this dissertation, the optimization of an innovative thermal energy storage technology was realized through the development of original numerical and experimental tools and the application of genetic algorithms. Several fields can be investigated as a continuity of this work.

First of all, try to convince HIKARI's builder (Bouygues Immobilier) to take our optimization results into account in its future projects.

New simulation assumptions can be made during the numerical modelling phase, in order to study other configurations and help improve the behaviour of Phase Change Materials. Applying the calibration and validation techniques shown in this work, new geometries and solving methods can be tested as well for this and other systems in the future.

The robustness of the developed experimental prototype can be tested using different PCMs, temperatures ranges and water flow rates, due to its versatility. For example, it would be interesting to see if it is able to adequately test PCMs working at high temperatures. Indeed, a visiting PhD student from Hunan University (China) and a H2020 project team are already interested in its use.

New assumptions and objective functions could be used for the optimization of this thermal energy storage technology, studying how and how much the populations and generations size affect the results obtained through the use of Genetic Algorithms.

Finally, the optimization of the technology analyzed in this work can be made testing its efficiency when it is part of different buildings' HVAC systems or it is coupled to different energy architectures. It would be interesting to see whether these results can contribute to this field and verify the efficiency of new proposed technology with the tools we developed.

REFERENCES

Abedin A., Rosen M. (2011) "A Critical Review of Thermochemical Energy Storage Systems". The Open Renewable Energy Journal, Vol. 4, pp 42-46.

Abhat A. (1983) "Low Temperature Latent Heat Thermal Energy Storage: Heat Storage Materials". *Solar Energy*, Vol. 30, pp 313-332.

ADEME (2017) "Actualisation du scénario énergie-climat ADEME 2035-2050".

Alva G., Liu L., Huang X., Fang G. (2017) "Thermal energy storage materials and systems for solar energy applications". *Renewable and Sustainable Energy Reviews.* Vol. 68, Part 1, pp 693–706.

AL-Saadi S. N., Zhai Z. (2013) "Modeling phase change materials embedded in building enclosure: A review". *Renewable and Sustainable Energy Reviews.*

Alexiades V., Solomon A. D. (1993) "Mathematical modeling of melting and freezing processes". *Hemisphere Publishing Corporation.*

Ashgriz N., Mostaghimi J. (2000) "An Introduction to Computational Fluid Dynamics". *Fluid Flow Handbook*, Chapter 20.

ASHRAE (2002) Guideline 14 - Measurement of Energy and Demand Saving.

Baetens R., Jelle B. P., Gustavsen A. (2010) "Phase change materials for building applications: A state-of-the-art review." *Energy and Buildings*, Vol. 42, pp 1361-1368.

Bony J., Citherlet. S. (2008) "Simulation model of PCM modules plunged in a water tank (type 860)". Simulation models of PCM Storage Units, Report C5 of Subtask C of IEA Solar Heating

and Cooling programme - Task 32 (Advanced storage concepts for solar and low energy buildings).

Bubbico R., Loreti B., Menale C. (2014) "Analisi teorica delle modalità di scambio termico tra acqua e PCM: studio parametrico delle principali variabili in gioco", *Report Ricerca di Sistema Elettrico, Accordo di Programma Ministero dello Sviluppo Economico – ENEA.*

Cabeza L. F., Mehling H. (2008) "Heat and cold storage with PCM: An up to date introduction into basics and applications". Springer , Handbook.

Cabeza L. F., Castell A., Barreneche C., de Gracia A., Fernández A. I. (2011) "Materials used as PCM in thermal energy storage in buildings: A review". *Renewable and Sustainable Energy Reviews,* Vol. 15, pp 1675-1695.

Cao X., Dai X., Liu J. (2016) "Building energy-consumption status worldwide and the state-of-the-art technologies for zero-energy buildings during the past decade". *Energy and Buildings.* Vol. 128, pp 198-213.

Cascone Y., Perino M. (2015) "Estimation of the Thermal Properties of PCMs through Inverse Modelling". *Energy Procedia*, Vol. 78, pp 1714-1719.

Catalina T., Virgone J., Blanco E. (2011) "Multi-source energy systems analysis using a multi-criteria decision aid methodology". *Renewable Energy*, Vol. 36, Issue 8, pp 2245-2252.

Cellat K., Beyhan B., Güngör C., Konuklu Y., Karahan O., Dündar C., Paksoy H. (2015) "Thermal enhancement of concrete by adding bio-based fatty acids as phase change materials". *Energy and Buildings*, Vol. 106, pp 156-163.

Chang-Hsu C., Zsay-Shing L. (2006) "A committee machine with empirical formulas for permeability prediction". *Computers & Geosciences,* Vol. 32, Issue 4, pp 485-496

Deb K., Pratap A., Agarwal S. and Meyarivan T (2002) "A fast and elitist multiobjective genetic algorithm: NSGA- II", *IEEE Transactions on Evolutionary Computation*, Vol. 6, Issue 2, pp 182 – 197.

El Mankibi M., Stathopoulos N., Rezaï N., Zoubir A. (2015) "Optimization of an Air-PCM heat exchanger and elaboration of peak power reduction strategies". *Energy and Buildings*, Vol. 106, pp 74-86.

Fabrizio E., Corrado V., Filippi M. (2010) "A model to design and optimize multi-energy systems in buildings at the design concept stage". *Renewable Energy*, Vol. 35, pp 644-665.

Fernandez A. I. , Martínez M., Segarra M., Martorell I., Cabeza L. F. (2010) "Selection of materials with potential in sensible thermal energy storage". *Solar Energy Materials & Solar Cells.*

Ferreira M., Almeida M. (2015) "Benefits from Energy Related Building Renovation Beyond Costs, Energy and Emissions". *Energy Procedia.* Vol. 78, pp 2397-2402.

Ghorbani B., Kowsary F., Ebrahimi S., Vijayaraghavan K. (2017) "CFD Modeling and optimization of a latent heat storage unit for running a solar assisted single effect Li-Br absorption chiller using multi-objective genetic algorithm". *Sustainable Cities and Society.*

Goia F., Perino M., Serra V. (2013) "Improving thermal comfort conditions by means of PCM glazing systems". Energy and Buildings, Vol. 60, pp 442-452.

Hachem-Vermette C., Cubi E., Bergerson J. (2016) "Energy performance of a solar mixed-use community". *Sustainable Cities and Society.* Vol. 27, pp 145-151.

Hadjieva, M., Kanev S., Argirov J. (1992) "Thermophysical properties of some paraffins applicable to thermal energy storage". *Solar Energy Materials and Solar Cells*, Vol. 27, pp 181-187.

IEA-ETSAP and IRENA (2013) "Thermal Energy Storage. Technology Brief."

IEA (2014) “Applying Energy Storage in Ultra-low Energy Buildings”. Final report of Annex 23: Applying energy storage in buildings of the future.

IEA (2016) “World Energy Outlook”.

INSEE (2012) “Bilan énergétique 2012”.

Iten M., Liu S., Shukla A. (2016) “A review on the air-PCM-TES application for free cooling and heating in the buildings”. *Renewable and Sustainable Energy Reviews*, Vol. 61, pp 175-186.

Kenisarin M., Mahkamov K. (2007) “Solar energy storage using phase change materials”. *Renewable and Sustainable Energy Reviews*, Vol. 11, Issue 9, pp 1913-1965.

Kheradmand M., Azenha M., L. B. de Aguiar J., Castro-Gomes J. (2015) “Experimental and numerical studies of hybrid PCM embedded in plastering mortar for enhanced thermal behaviour of buildings”. *Energy.*

Khudhair A. M., Farid M. M. (2004) “A review on energy conservation in building applications with thermal storage by latent heat using phase change materials”. *Energy Conversion and Management*, Vol. 45 pp 263–275.

Konuklu Y., Ostry M., Paksoy H. O., Charvat P. (2015) “Review on using microencapsulated phase change materials (PCM) in building applications”. *Energy and Buildings*, Volu. 106, pp 134-155.

Kuznik F., David D., Johannes K., Roux J. J. (2010) “A review on phase change materials integrated in building walls”. *Renewable and Sustainable Energy Reviews.*

Lane G. A. (1981) “Adding strontium chloride or calcium hydroxide to calcium chloride hexahydrate heat storage material”. *Solar Energy*, Vol. 27, pp 73-75.

Lee K. H., Lee D. W., Baek N. C., Kwon H. M., Lee C. J. (2012) "Preliminary determination of optimal size for renewable energy resources in building using RETScreen". *Energy*, Vol. 47, pp 83-96.

Lin S. (2011) "NGPM -- A NSGA-II Program in Matlab. Version 1.4". College of Astronautics, Northwestern Polytechnical University, China.

Liu S., Li Y., Zhang Y. (2014) "Mathematical solutions and numerical models employed for the investigations of PCMs' phase transformations". *Renewable and Sustainable Energy Reviews.*

L≈pez-Navarro A., Biosca-Taronger J., Corberán J. M., Pe⇔alosa C., Lázaro A., Dolado P., Payá J. (2014). "Performance characterization of a PCM storage tank". *Applied Energy.* Volume 119, April 2014, pp 151-162.

Lunsford K. M. (1998)"Increasing Heat Exchanger Performance". *Hydrocarbon Engineering.*

Ministère de la Transition écologique et solidaire (2006) "Actualisation 2006 du Plan Climat 2004-2012".

Ministère de la Transition écologique et solidaire (2009) "La première loi du Grenelle".

Ministère de la Transition écologique et solidaire (2012) "Loi Grenelle 2".

Ministère de la Transition écologique et solidaire (2015) " Loi de Transition Energétique relative à la Croissance Verte".

Nagano K., Takeda S., Mochida T., Shimakura K., Nakamura T. (2006) "Study of a floor supply air conditioning system using granular phase change material to augment building mass thermal storage—Heat response in small scale experiments". *Energy and Buildings.* Vol. 38, Issue 5, pp 436-446.

Nchelatebe Nkwetta D., Haghighat F. (2014) "Thermal energy storage with phase change material— A state-of-the art review". *Sustainable Cities and Society.* Vol. 10, pp 87-100.

Nchelatebe Nkwetta D., Vouillamoz P. E., Haghighat F., El-Mankibi M., Moreau A., Daoud A. (2014). "Impact of phase change materials types and positioning on hot water tank thermal performance: Using measured water demand profile". *Applied Thermal Engineering.* Vol. 67, Issues 1–2, pp 460-468.

Observatoire BBC. Rechercher des bâtiments Bepos. Available at: http://www.observatoirebbc.org/bepos

Ozen Engineering, Inc. Vizualization of the Pareto front designs. Available at: http://www.ozeninc.com/optislang-multi-objective-optimication/

Palomba V., Brancato V., Frazzica A. (2017) "Experimental investigation of a latent heat storage for solar cooling applications". *Applied Energy*, Vol.199, pp 347-358.

Pernodet F., Lahmidi H., Michel P (2009) "Use of Genetic Algorithms for multicriteria optimization of building refurbishment". *11th International Building Performance Simulation Association (IBPSA) Conference. Glasgow, Scotland.*

Saffari M., de Gracia A., Fernández C., Cabeza L. F. (2017) "Simulation-based optimization of PCM melting temperature to improve the energy performance in buildings". *Applied Energy*, Vol. 202, pp 420-434.

Salunkhea P. B., Krishna D. J. (2017) "Investigations on latent heat storage materials for solar water and space heating applications". *Journal of Energy Storage*, Vol. 12, pp 243-260.

savENRG™. Sensible Heat vs Latent Heat. Available at: http://www.rgees.com/technology.php

Shamsi H., Boroushaki M., Geraeib H. (2017) "Performance evaluation and optimization of encapsulated cascade PCM thermal storage". *Journal of Energy Storage,* Vol. 11, pp 64–75.

Soares N., Costa J. J., Gaspar A. R., Santos P. (2013) "Review of passive PCM latent heat thermal energy storage systems towards buildings' energy efficiency". *Energy and Buildings*, Vol. 59, pp 82–103.

Sontag R., Lange A. (2003) "Cost effectiveness of decentralized energy supply systems taking solar and wind utilization plants into account". *Renewable Energy*, Vol. 28, pp 1865–1880.

Stathopoulos N. (2015) "Optimisation numérique et expérimentale de stratégies d'effacement énergétique".

Stathopoulos N., El Mankibi M., Issoglio R., Michel P., Haghighat H. (2016) "Air–PCM heat exchanger for peak load management: Experimental and simulation." *Solar Energy.* Vol. 132, pp 453–466.

Stojanovska I. and Dika A. (2010) "Impact of the number of generations on the fitness value and the time required to find the optimal solution in standard GA applications" *Proceedings of the 3rd International Conference on Computer Science and Information Technology (IEEE ICCSIT 2010), Chengdu, China*, Vol. 1.

Tannehill J. C., Anderson D. A., Pletcher R. H. (1997) "Computational fluid mechanics and heat transfer". Series in Computational and Physical Processes in Mechanics and Thermal Sciences. Taylor & Francis Publishing Office.

Telkes M., "Remarks on "Thermal energy storage using sodium sulfate decahydrate and water"". *Solar Energy*, Vol. 20, p. 107.

Trillat-Berdal V., Souyri B., Fraisse G. (2006) "Experimental study of a ground-coupled heat pump combined with thermal solar collectors". *Energy and Buildings*, Vol. 38, pp 1477–1484.

Turner W. J. N., Staino A., Basu B. (2017) "Residential HVAC Fault Detection Using a System Identification Approach". *Energy and Buildings.*

Tyagi V. V., Buddhi D. (2005) "PCM thermal storage in buildings: A state of art". *Renewable and Sustainable Energy Reviews.*

Tyagi V.V., Kaushik S. C., Tyagi S. K., Akiyama T. (2010) "Development of phase change materials based microencapsulated technology for buildings: A review". *Renewable and Sustainable Energy Reviews.*

Verma P., Varun, Singal S.K. (2008) "Review of mathematical modeling on latent heat thermal energy storage systems using phase-change material". *Renewable and Sustainable Energy Reviews*, Vol. 12, pp 999–1031.

Voller V. R. and Swaminathan C. R. (1990) "Fixed grid techniques for phase change problems: A review". *International journal for numerical methods in engineering*, vol. 30, pp 875–898.

Voller V. R., Swenson J. B., Kim W., Paola C. (2006). "An enthalpy method for moving boundary problems on the earth's surface*". International Journal of Numerical Methods for Heat & Fluid Flow*, vol. 16, pp 641 - 654.

Wang W., Zmeureanu R., Rivard H. (2005) "Applying multi- objective genetic algorithms in green building design optimization" *Building and Environment*, Vol. 40, Issue 11, pp 1512–1525.

Welty J. R., Wicks C. E., Wilson R. E., Rorrer G. L. "Fundamentals of Momentum, Heat, and Mass Transfer". *John Wiley & Sons, Inc.*

Yan T., Wang R. Z., Li T. X., Wang L. W., Fred I. T. (2015) "A review of promising candidate reactions for chemical heat storage". *Renewable and Sustainable Energy Reviews,* Vol. 43, pp 13–31.

Zalba B., Marín J. M., Cabeza L. F., Mehling H. (2003*)"*Review on thermal energy storage with phase change: materials, heat transfer analysis and applications". *Applied Thermal Engineering*, Vol. 23, pp 251–283.

Zalba B., Marín J. M., Cabeza L. F., Melhing H. (2004) "Free-cooling of buildings with phase change materials". *International Journal of Refrigeration*, Vol. 27, pp 839–849.

Zhu N., Ma Z., Wang S. (2009) "Dynamic characteristics and energy performance of buildings using phase change materials: A review". *Energy Conversion and Management.*

ANNEX A

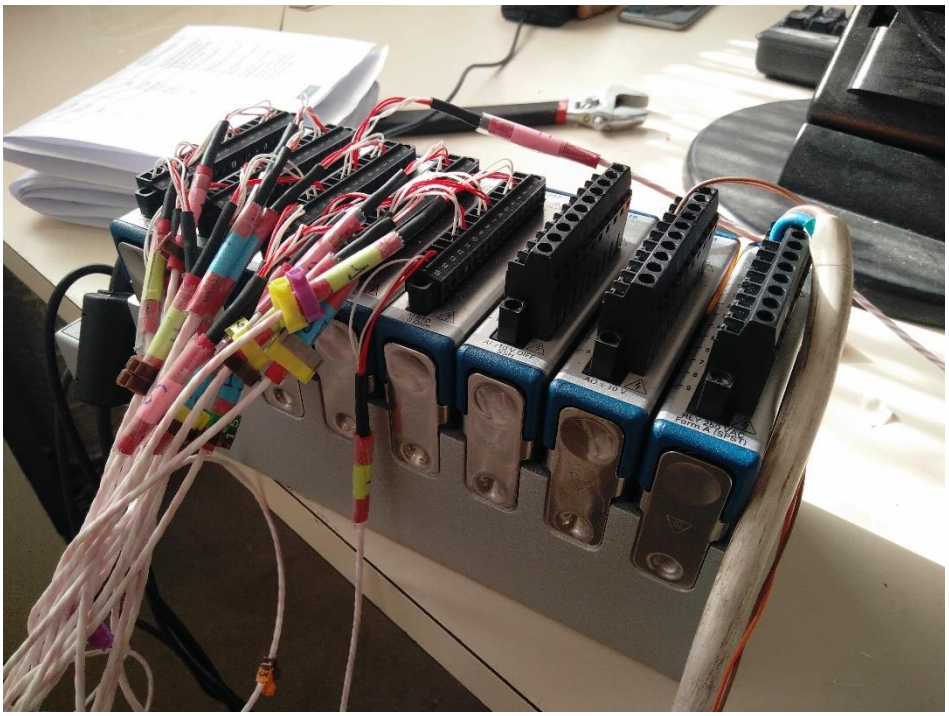

Annex A. 1 – Sensors' cables inserted in the Compact Daq modular system.

Annex A. 2 – Comparison between a two sticks with PCM in solid and liquid phase.

Annex A. 3 – Submersible pump

Annex A. 4 – Water flow rate controller

Annex A. 5 – Tank 1 and 2

Annex A. 6 – The prototype

ANNEX B

- Scenario 1

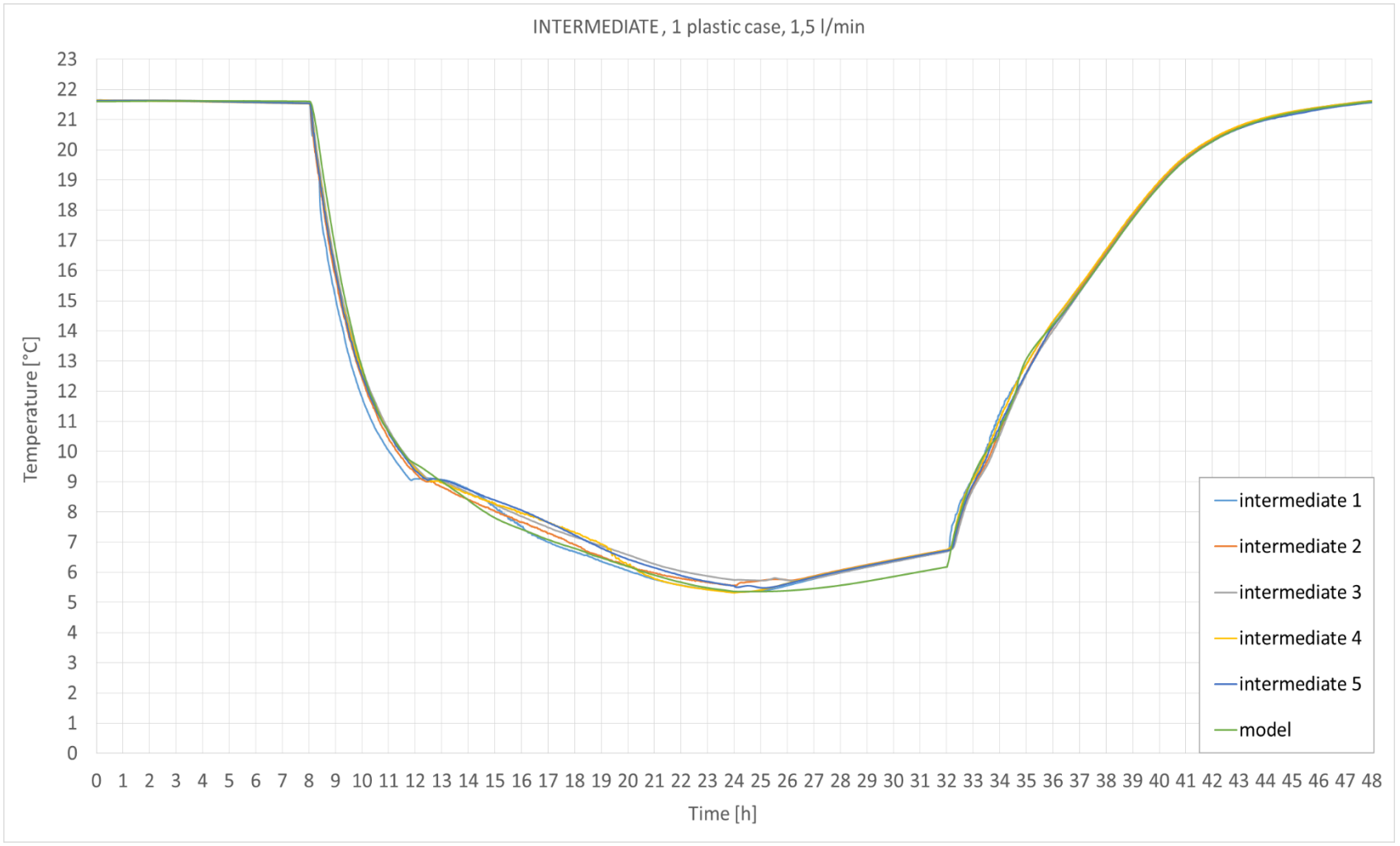
INTERMEDIATE , 1 plastic case, 1,5 l/min
Temperature [°C]
Time [h]
intermediate 1
intermediate 2
intermediate 3
intermediate 4
intermediate 5
model

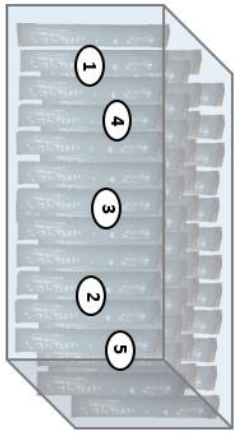
1
4
3
2
5

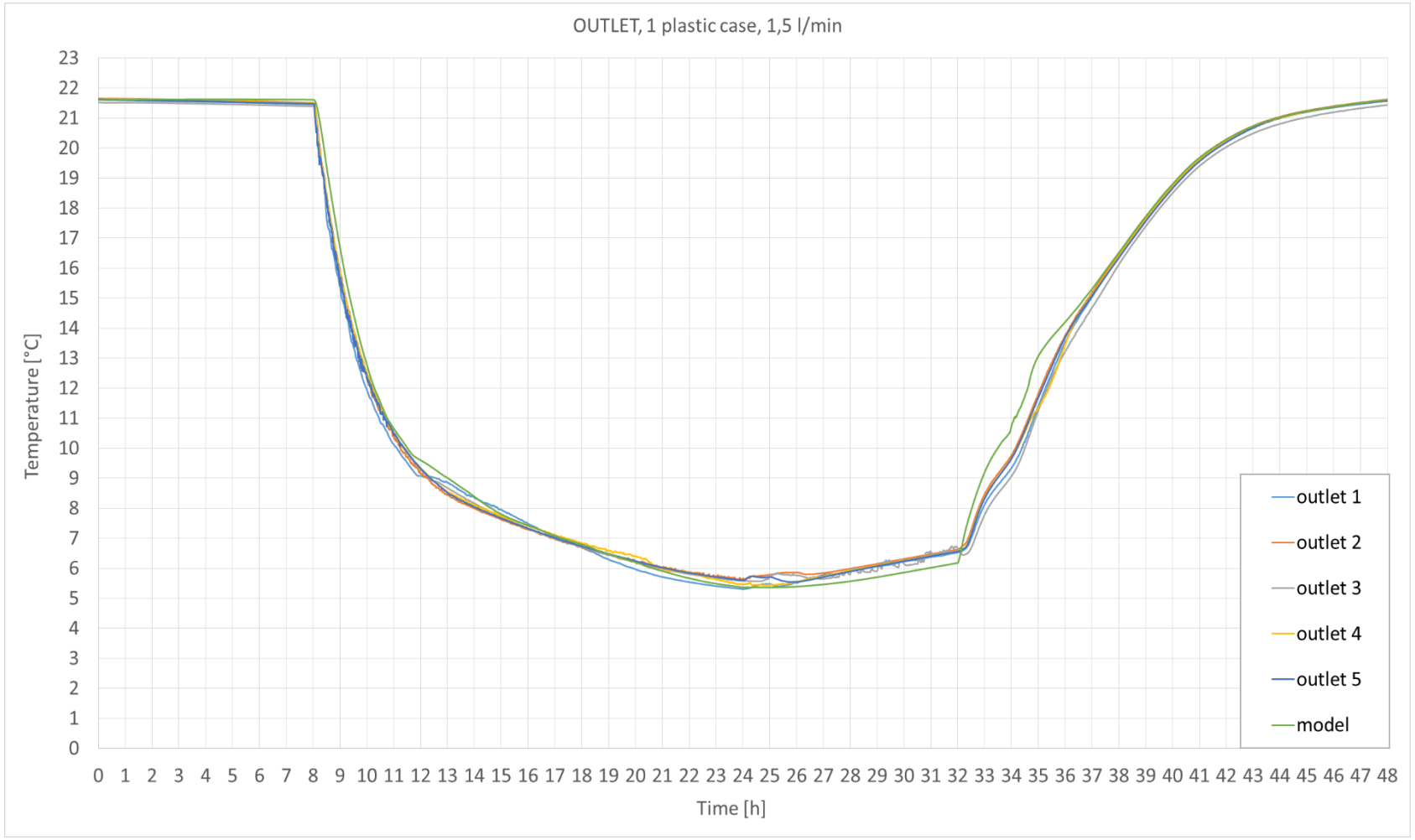
OUTLET, 1 plastic case, 1,5 l/min
Temperature [°C]
Time [h]
outlet 1
outlet 2
outlet 3
outlet 4
outlet 5
model

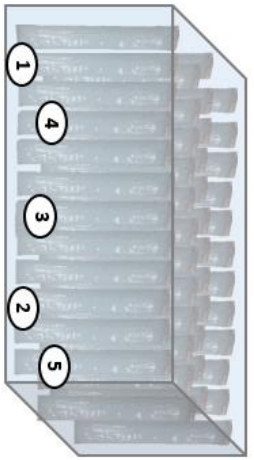
1
4
3
2
5

- Scenario 2

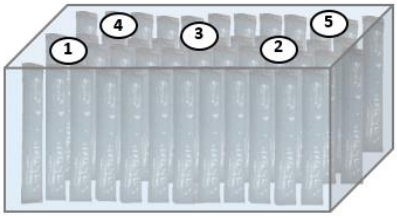
1
4
3
2
5

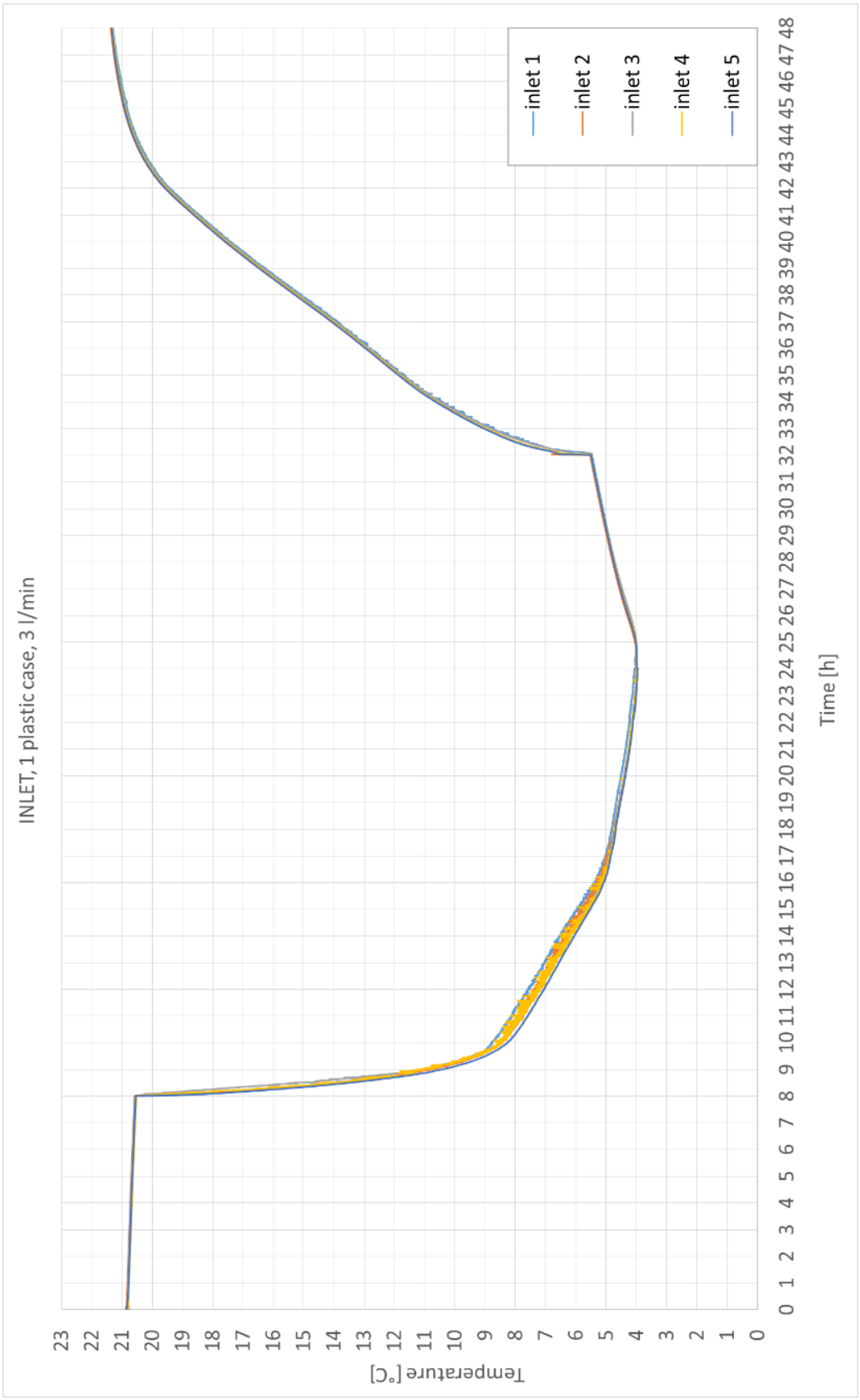
INLET, 1 plastic case, 3 l/min
inlet 1
inlet 2
inlet 3
inlet 4
inlet 5
Temperature [°C]
Time [h]

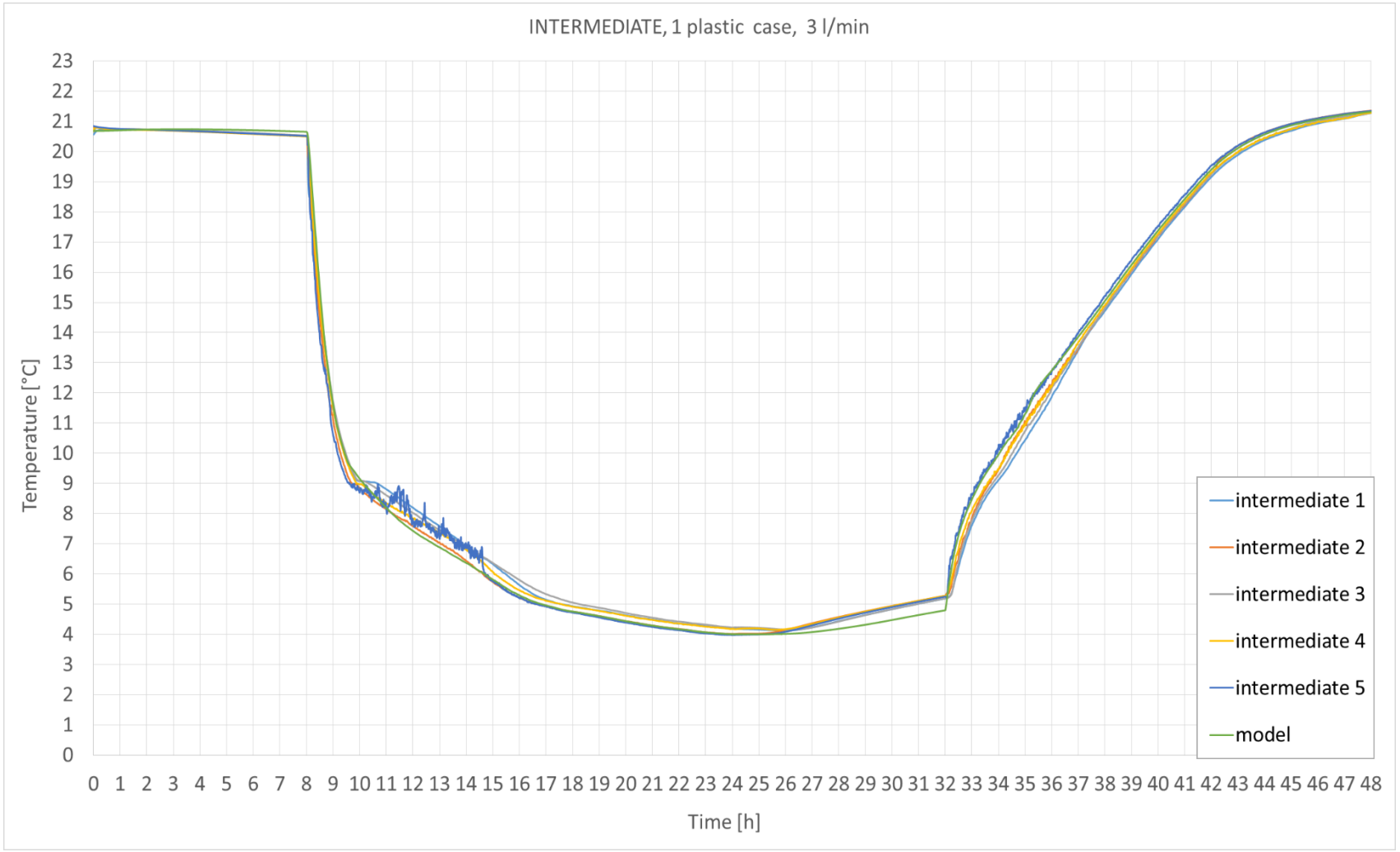
INTERMEDIATE, 1 plastic case, 3 l/min
Temperature [°C]
Time [h]
intermediate 1
intermediate 2
intermediate 3
intermediate 4
intermediate 5
model

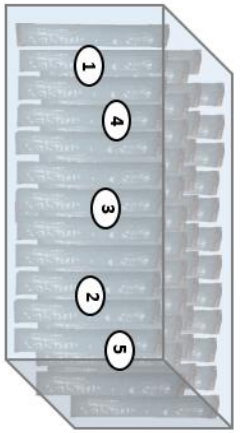
1
4
3
2
5


OUTLET, 1 plastic case, 3 l/min
Temperature [°C]
Time [h]
outlet 1
outlet 2
outlet 3
outlet 4
outlet 5
model

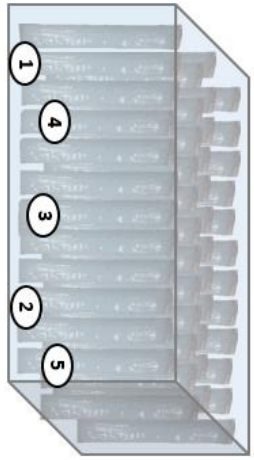
1
4
3
2
5

- Scenario 3

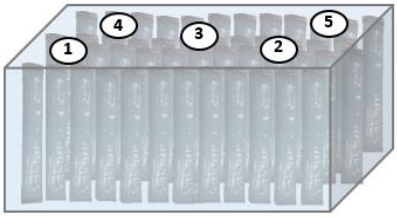
1
2
3
4
5

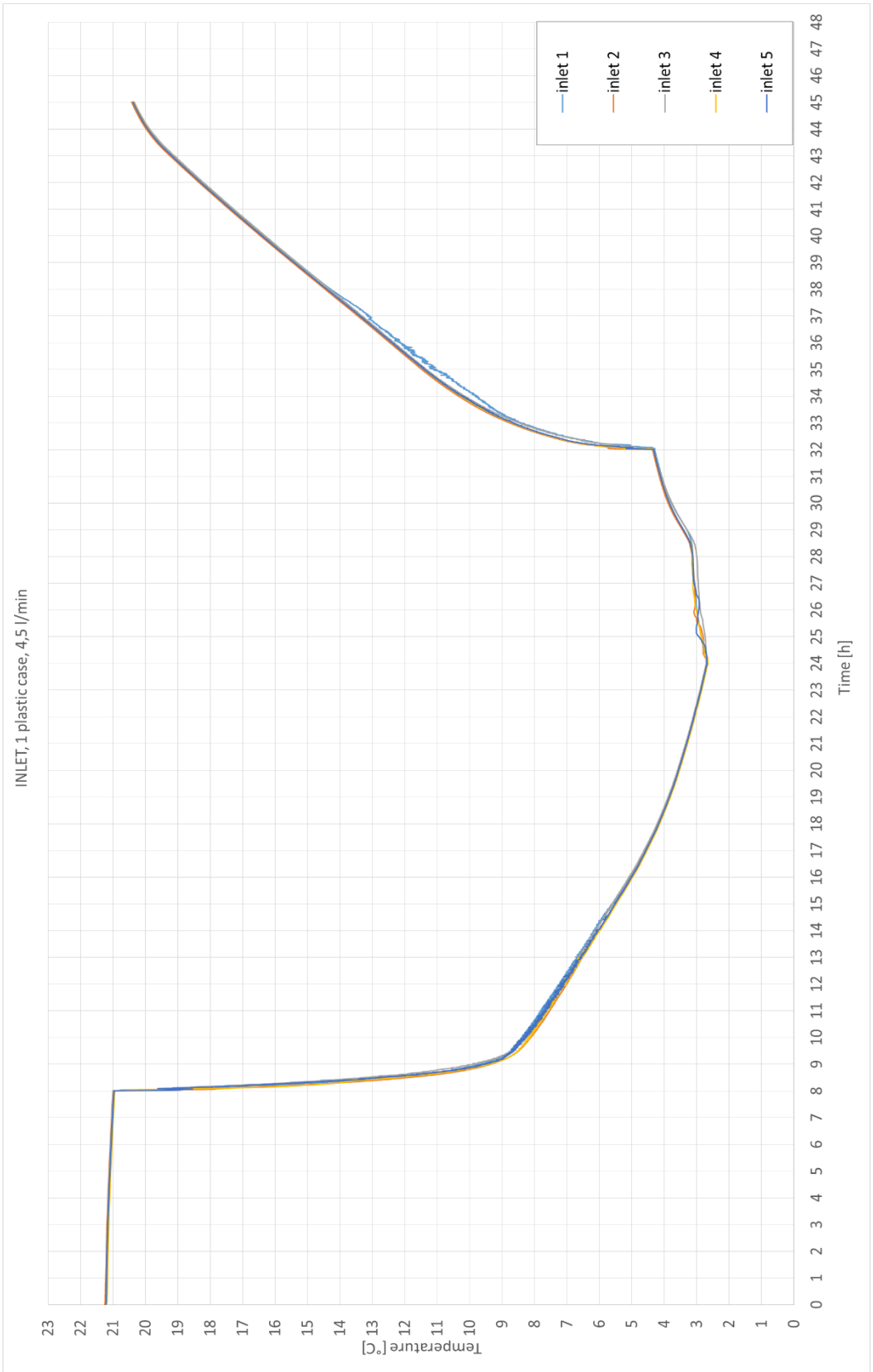
INLET, 1 plastic case, 4,5 l/min
inlet 1
inlet 2
inlet 3
inlet 4
inlet 5
Temperature [°C]
Time [h]
0 1 2 3 4 5 6 7 8 9 10 11 12 13 14 15 16 17 18 19 20 21 22 23
0 1 2 3 4 5 6 7 8 9 10 11 12 13 14 15 16 17 18 19 20 21 22 23 24 25 26 27 28 29 30 31 32 33 34 35 36 37 38 39 40 41 42 43 44 45 46 47 48


1
4
3
2
5

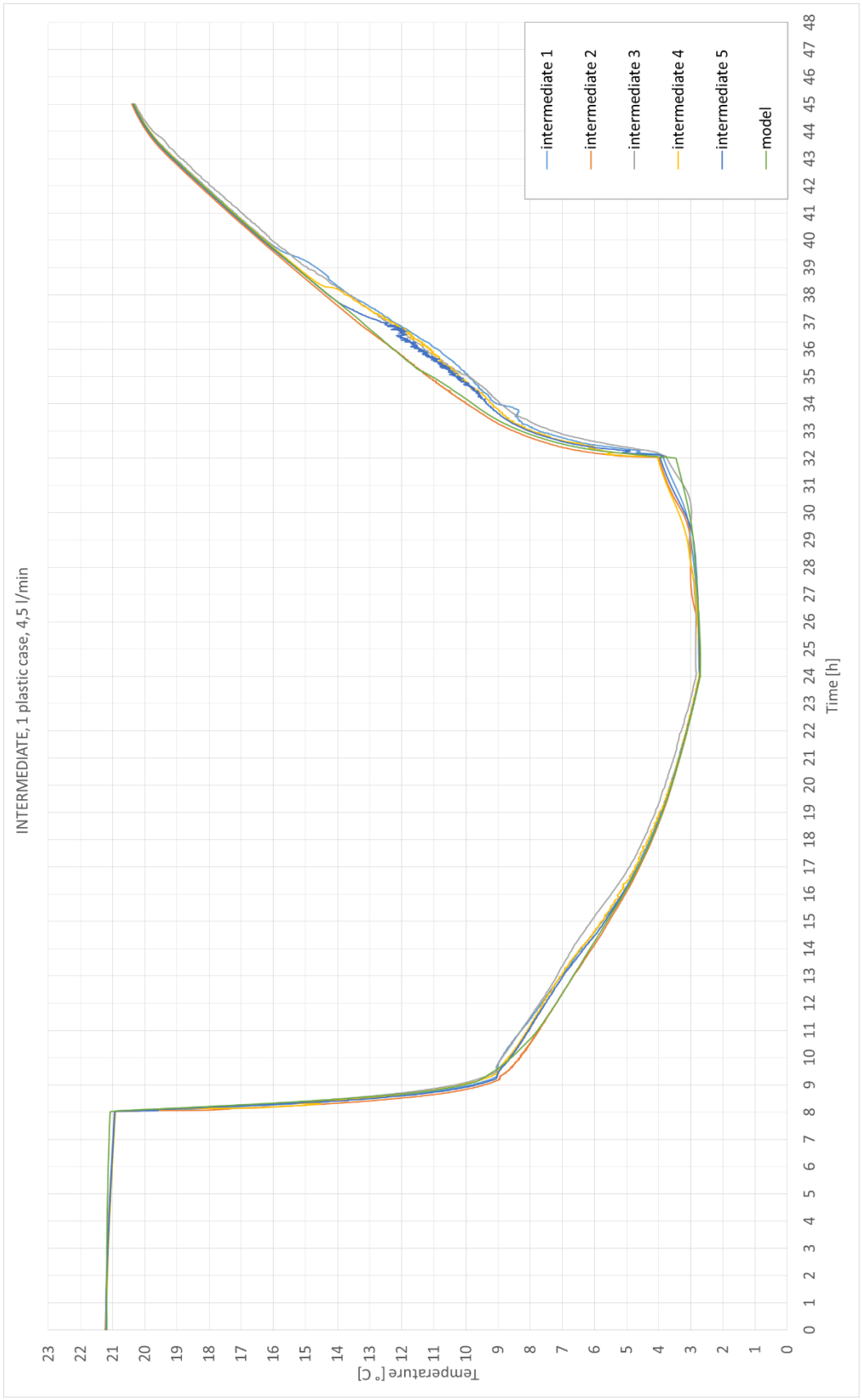
INTERMEDIATE, 1 plastic case, 4,5 l/min
intermediate 1
intermediate 2
intermediate 3
intermediate 4
intermediate 5
model
Temperature [°C]
Time [h]

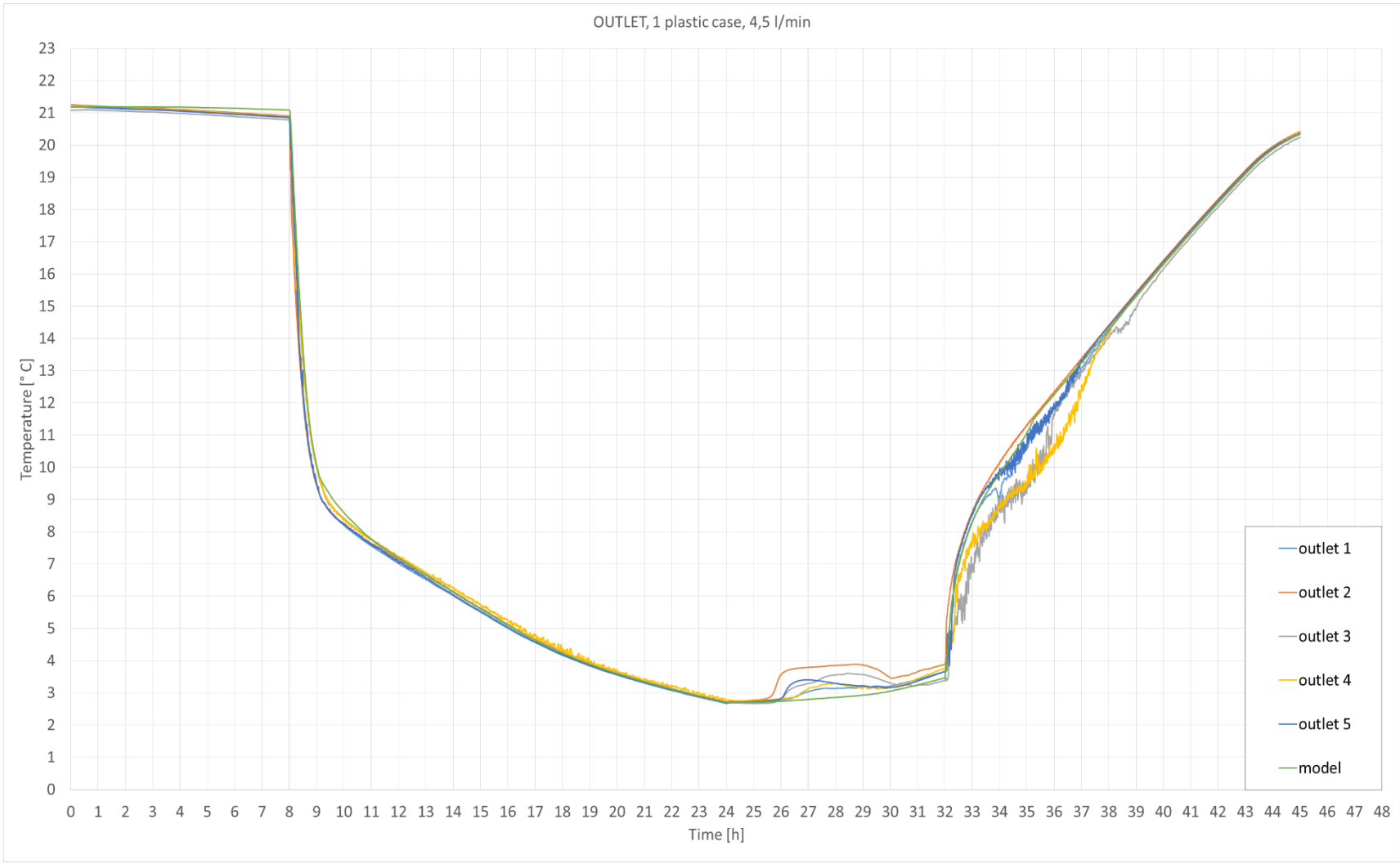
OUTLET, 1 plastic case, 4,5 l/min
Temperature [° C]
Time [h]
outlet 1
outlet 2
outlet 3
outlet 4
outlet 5
model

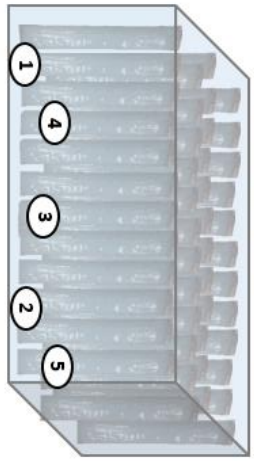
1
4
3
2
5

- Scenario 4

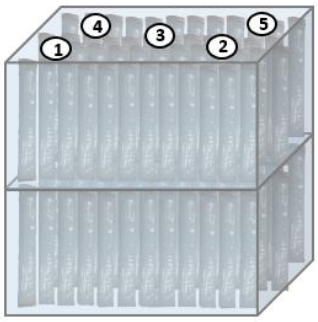
1
2
3
4
5

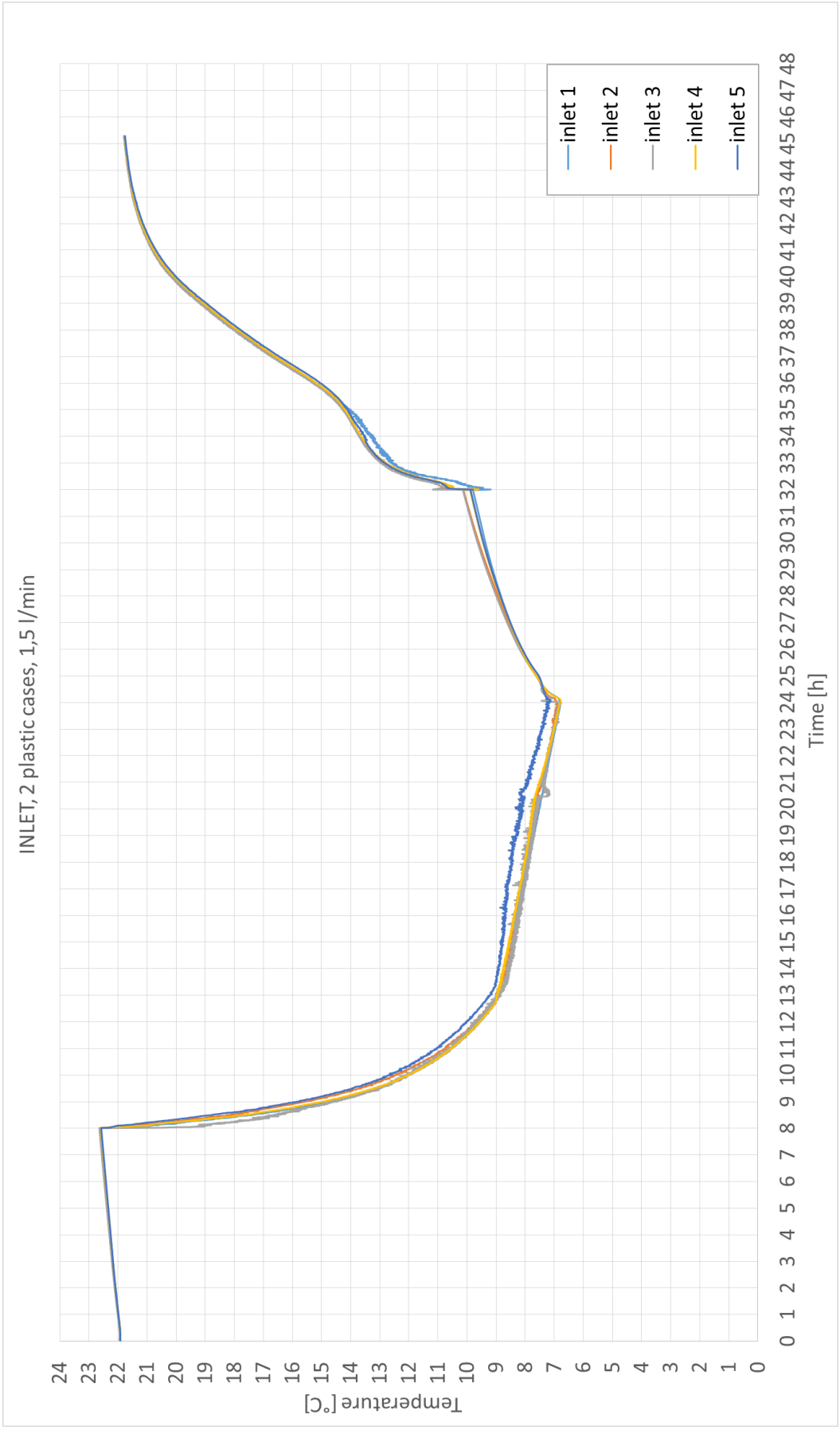
INLET, 2 plastic cases, 1,5 l/min
Temperature [°C]
Time [h]
inlet 1
inlet 2
inlet 3
inlet 4
inlet 5
0 1 2 3 4 5 6 7 8 9 10 11 12 13 14 15 16 17 18 19 20 21 22 23 24 25 26 27 28 29 30 31 32 33 34 35 36 37 38 39 40 41 42 43 44 45 46 47 48
0 1 2 3 4 5 6 7 8 9 10 11 12 13 14 15 16 17 18 19 20 21 22 23 24

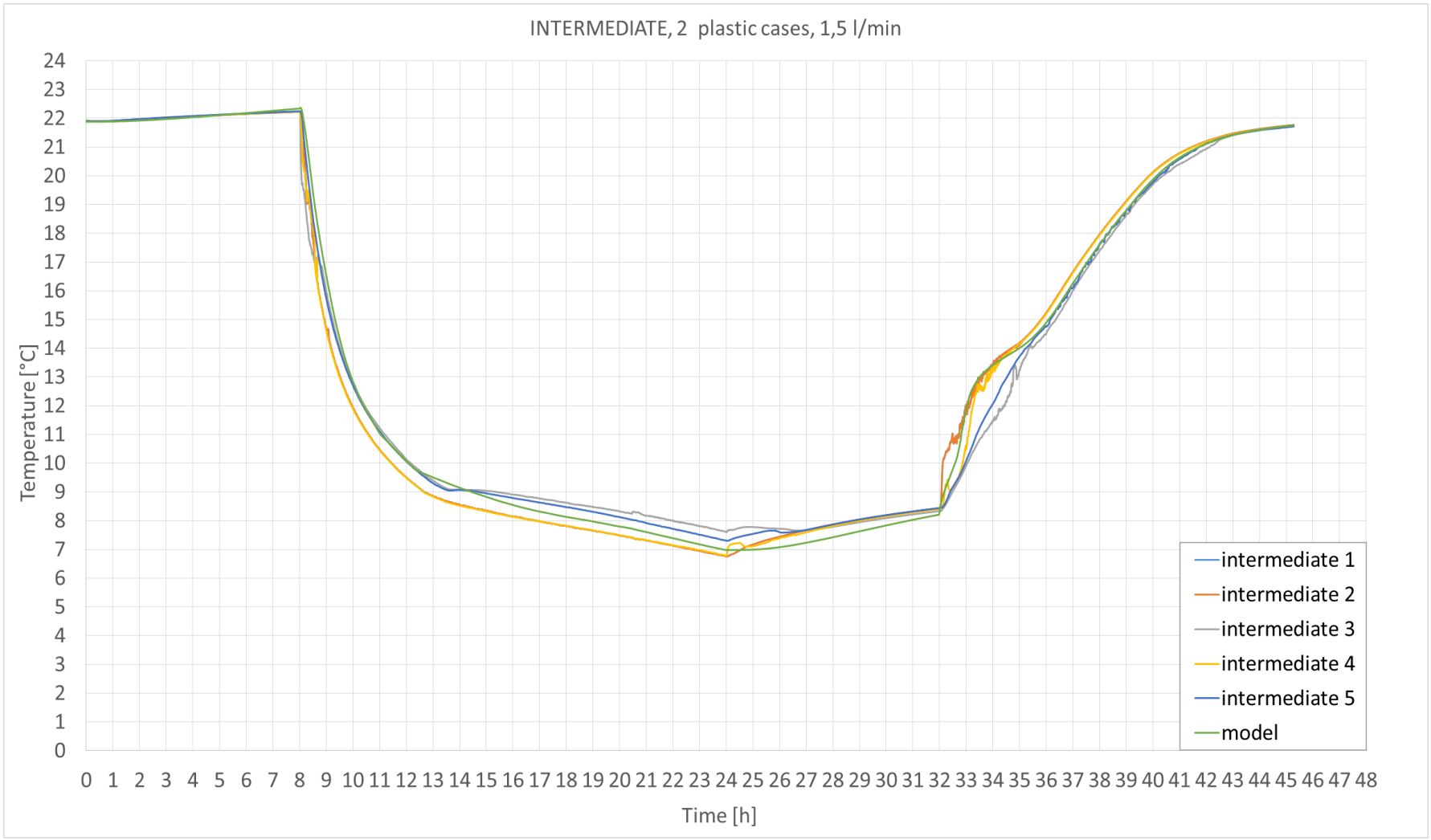
INTERMEDIATE, 2 plastic cases, 1,5 l/min
Temperature [°C]
Time [h]
intermediate 1
intermediate 2
intermediate 3
intermediate 4
intermediate 5
model

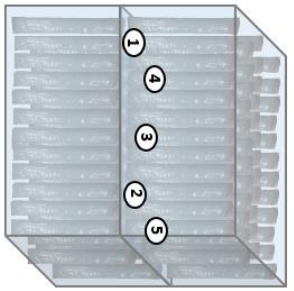
1
4
3
2
5


OUTLET, 2 plastic cases, 1,5 l/min
Temperature [°C]
Time [h]
outlet 1
outlet 2
outlet 3
outlet 4
outlet 5
model

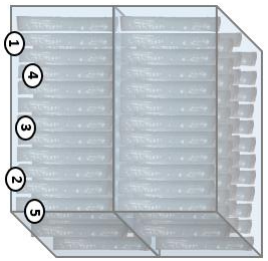
1
4
3
2
5

- Scenario 5

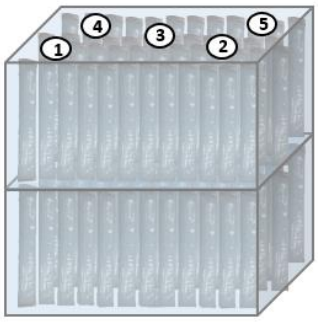
1
2
3
4
5

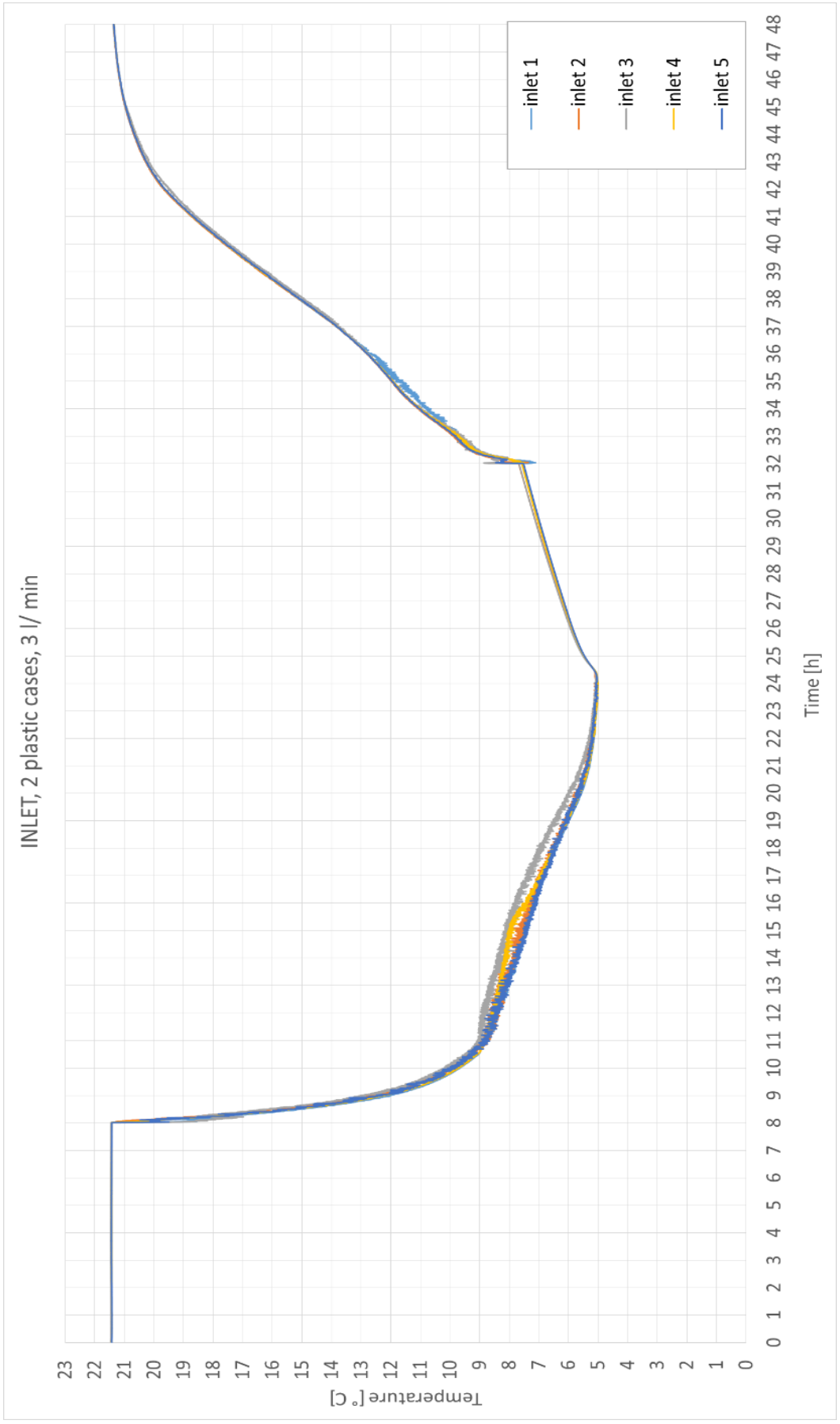
INLET, 2 plastic cases, 3 l/ min
inlet 1
inlet 2
inlet 3
inlet 4
inlet 5
Temperature [° C]
Time [h]
0 1 2 3 4 5 6 7 8 9 10 11 12 13 14 15 16 17 18 19 20 21 22 23
0 1 2 3 4 5 6 7 8 9 10 11 12 13 14 15 16 17 18 19 20 21 22 23 24 25 26 27 28 29 30 31 32 33 34 35 36 37 38 39 40 41 42 43 44 45 46 47 48


INTERMEDIATE , 2 plastic cases, 3 l/ min
Temperature [°C]
Time [h]
intermediate 1
intermediate 2
intermediate 3
intermediate 4
intermediate 5
model

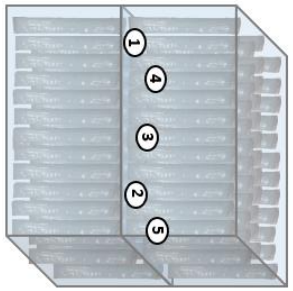
1
4
3
2
5


OUTLET , 2 plastic cases, 3 l/ min
Temperature [°C]
Time [h]
outlet 1
outlet 2
outlet 3
outlet 4
outlet 5
model

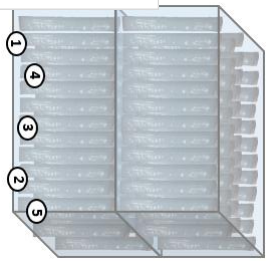
1
4
3
2
5

- Scenario 6

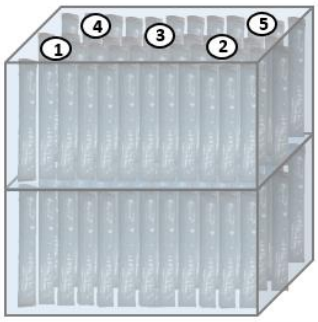
1
2
3
4
5

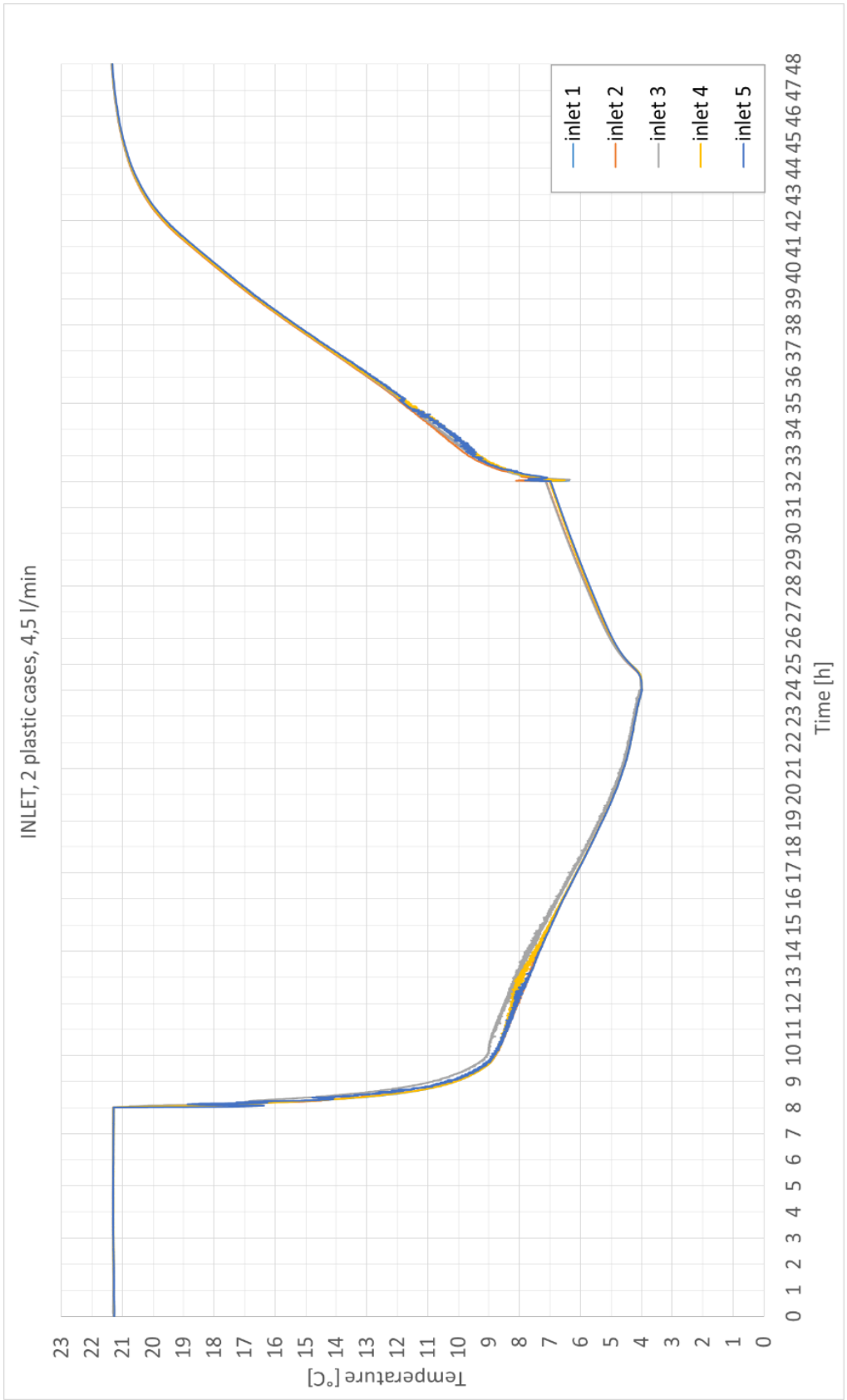
INLET, 2 plastic cases, 4,5 l/min
Temperature [°C]
Time [h]
inlet 1
inlet 2
inlet 3
inlet 4
inlet 5
0 1 2 3 4 5 6 7 8 9 10 11 12 13 14 15 16 17 18 19 20 21 22 23 24 25 26 27 28 29 30 31 32 33 34 35 36 37 38 39 40 41 42 43 44 45 46 47 48
23 22 21 20 19 18 17 16 15 14 13 12 11 10 9 8 7 6 5 4 3 2 1 0

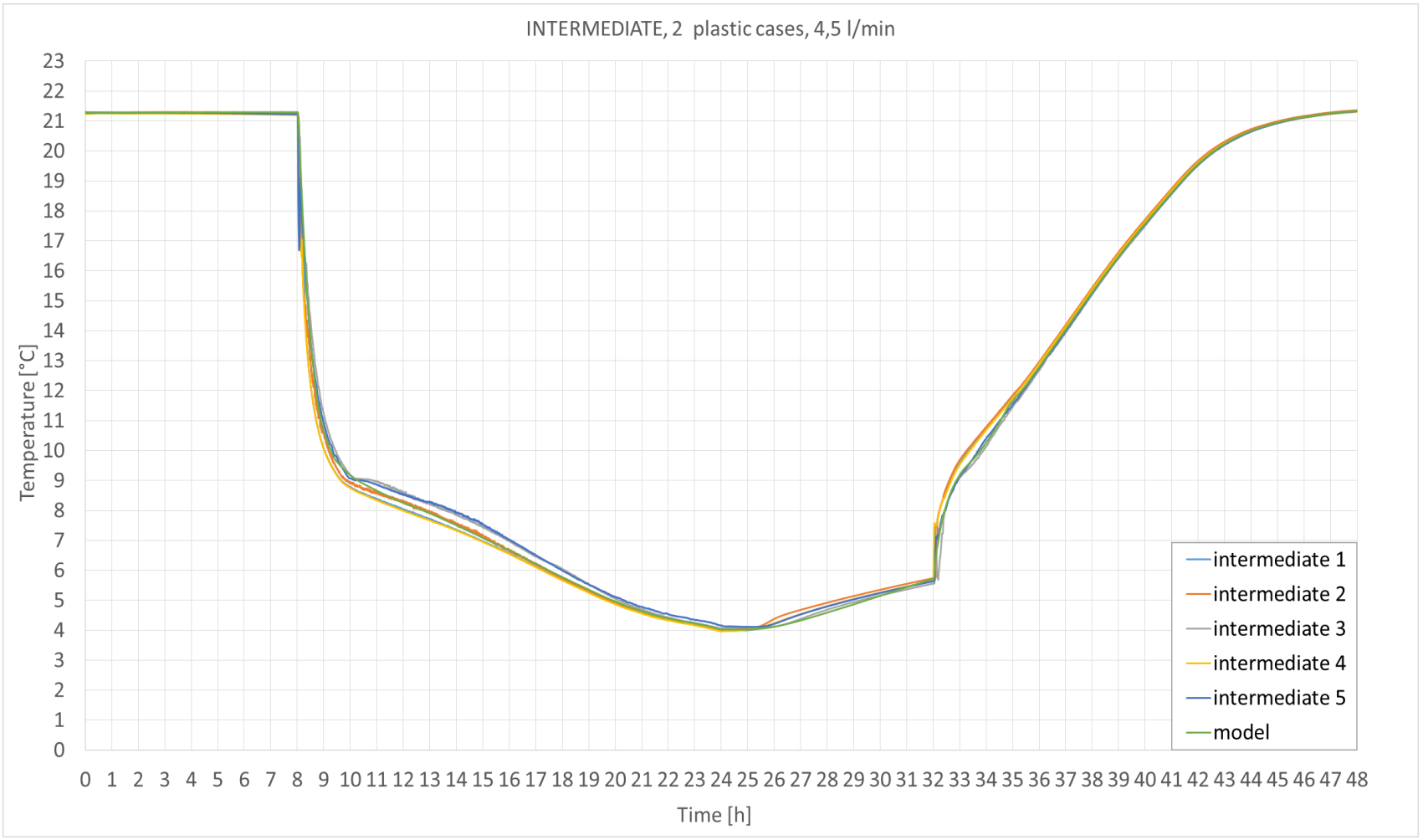
INTERMEDIATE, 2 plastic cases, 4,5 l/min
Temperature [°C]
Time [h]
intermediate 1
intermediate 2
intermediate 3
intermediate 4
intermediate 5
model

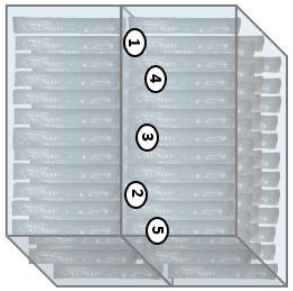
1
4
3
2
5

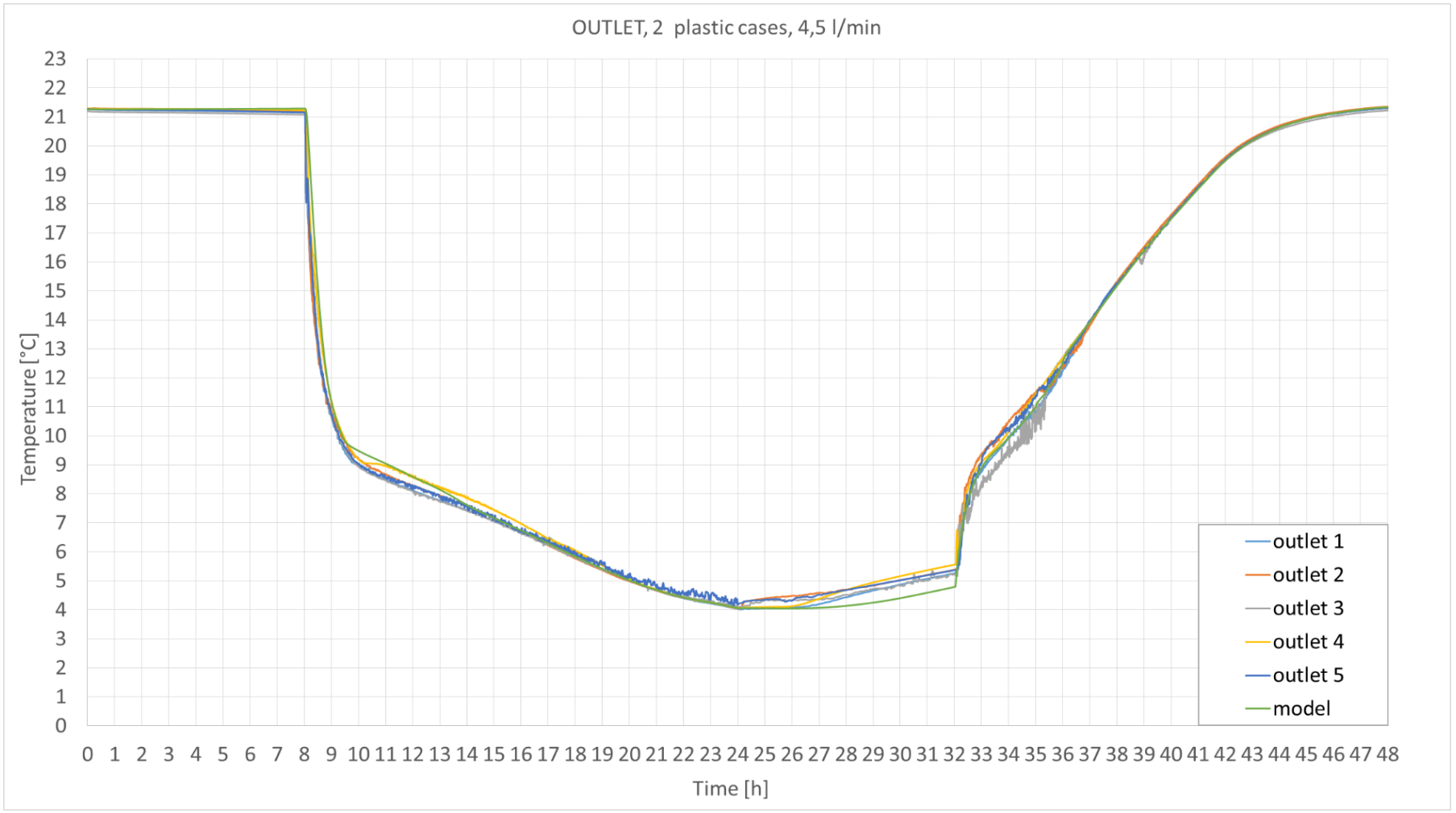
OUTLET, 2 plastic cases, 4,5 l/min
Temperature [°C]
Time [h]
outlet 1
outlet 2
outlet 3
outlet 4
outlet 5
model

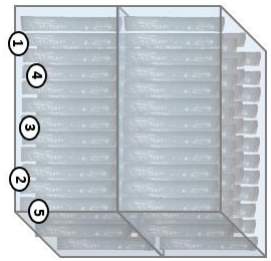
1
4
3
2
5